Fraunhofer IGB

FRAUNHOFER-INSTITUT FÜR GRENZFLÄCHEN- UND BIOVERFAHRENSTECHNIK IGB

BERICHTE AUS FORSCHUNG UND ENTWICKLUNG NR. 036

Kimball Sebastiaan Roelofs

Sulfonated Poly(Ether Ether Ketone) Based Membranes For Direct Ethanol Fuel Cells

FRAUNHOFER VERLAG

Fraunhofer Institute for
Interfacial Engineering and Biotechnology IGB

Berichte aus Forschung und Entwicklung Nr. 036

Sulfonated Poly(Ether Ether Ketone) Based Membranes For Direct Ethanol Fuel Cells

Kimball Sebastiaan Roelofs

FRAUNHOFER VERLAG

Contact:
Fraunhofer Institute for Interfacial Engineering
and Biotechnology IGB
Nobelstr. 12
70569 Stuttgart
Phone +49 (0) 711 970-4000
Fax +49 (0) 711 970-4200
E-Mail info@igb.fraunhofer.de
URL www.igb.fraunhofer.de

Bibliographic information published by Die Deutsche Bibliothek
Die Deutsche Bibliothek lists this publication in the Deutsche Nationalbibliografie; detailed bibliografic data is available in the Internet at <http://dnb.d-nb.de>.
ISBN: 978-3-8396-0122-8

D 93

Zugl.: Stuttgart, Univ., Diss., 2010

Printing and Bindery:
Mediendienstleistungen des
Fraunhofer-Informationszentrum Raum und Bau IRB, Stuttgart

Printed on acid-free and chlorine-free bleached paper.

Fraunhofer Information-Centre for Regional Planning and Building Construction IRB
P.O. Box 80 04 69, D-70504 Stuttgart
Nobelstrasse 12, D-70569 Stuttgart
Phone +49 (0) 711 970-2500
Fax +49 (0) 711 970-2508
E-Mail verlag@fraunhofer.de
URL http://verlag.fraunhofer.de

Sulfonated Poly(Ether Ether Ketone) Based Membranes For Direct Ethanol Fuel Cells

Von der Fakultät Energie-, Verfahrens- und Biotechnik der Universität Stuttgart
zur Erlangung der Würde eines Doktors der Ingenieurwissenschaften (Dr.-Ing.)
genehmigte Abhandlung

vorgelegt von

Kimball Sebastiaan Roelofs

aus Zevenaar (NL)

Hauptberichter:	**Prof. Dr. rer. nat. Thomas Hirth**
Mitberichter:	**Prof. Dr. -Ing. Matthias Wessling**
Vorsitzender:	**Prof. Dr. -Ing. Ulrich Nieken**

Tag der mündlichen Prüfung: 22. März 2010

Institut für Grenzflächenverfahrenstechnik, Universität Stuttgart

Stuttgart, 2010

Eidesstattliche Erklärung

Hiermit erkläre ich, dass ich diese Arbeit unter Anleitung meiner wissenschaftlichen Lehrer Prof. Dr. Thomas Hirth und Dr. Thomas Schiestel und nur mit den angegebenen Hilfsmitteln selbständig angefertigt habe.

Stuttgart, im November 2009

Summary

The decreasing availability of fossil fuels and the increasing impact of greenhouse gases on the environment lead to an extensive development of more efficient or renewable energy sources. The direct alcohol fuel cell is an electrochemical cell that exhibits the feature to convert chemical energy directly into electrical energy with high efficiency and is a promising technology for future portable appliances. Nowadays, the focus lies on applying methanol, whereas ethanol has some evident advantages. Ethanol is a generally known and accepted substance and is environmentally compatible, not toxic, contains a high energy density, and the infrastructure for distribution already exists.

This thesis reports on the development and characterization of proton conductive membranes for the usage as electrolyte in Direct Ethanol Fuel Cells (DEFC). These membranes consist of an inorganic-organic mixed-matrix whereby the inorganic matrix can be modified by means of functional silanes. The polymeric phase is sulfonated poly(ether ether ketone) (sPEEK). The inorganic phase consists of hydrophilic fumed silica particles (Aerosil®380) which is interconnected by partially condensed tetraethoxysilane (TEOS). Characterization of the developed materials and membranes is subdivided in the following domains: i) material analysis; ii) membrane characterization and iii) fuel cell tests. The main focus within the characterization lies on proton conductivity and membrane behavior in ethanol-water mixtures.

The sulfonation of poly(ether ether ketone) (PEEK) and preparation and characterization of polymeric sPEEK membranes is accomplished to test the applicability in DEFC. The sulfonation of PEEK is reproducible and can be controlled by sulfonation time and temperature. The membrane properties, e.g., swelling, proton conductivity and permeability of ethanol and water, are studied as a function of ion exchange capacity (*IEC*). The *IEC* of the sPEEK membranes ranges from 1.15 to

2.30 mmol g^{-1}. The main problem of sPEEK membranes is their stability features in aqueous-ethanolic environments in relation to their proton conductivity. Low sulfonated membranes (*IEC* < 1.4 mmol g^{-1}) are stable and low water and ethanol permeability is obtained, whereas the proton conductivity is too low. Membrane properties change exponentially when the *IEC* exceeds 1.8 mmol g^{-1}. Due to its uncontrollable swelling properties in this *IEC* range, pure polymeric membrane cannot be applied. The most appropriate *IEC* range for applying sPEEK in DEFC applications is between 1.4 and 1.8 mmol g^{-1}. In comparison to Nafion®, improved fuel cell performance is predicted based on the ratio of proton diffusion coefficient to ethanol permeability. This makes sPEEK a promising polymer type for application in DEFCs.

The approach to further reduce the ethanol permeability, while maintaining the proton conductive features of the membrane, is by adding an inorganic phase in the polymer matrix to obtain mixed-matrix membranes (MMMs). Unmodified inorganic-organic MMMs with various compositions and inorganic loadings (between 11% and 50%) are investigated. Addition of TEOS as a crosslinker between Aerosil®380 particles results in interconnected MMMs. The inorganic particles are homogeneously distributed and TEOS is completely converted in the preparation of inorganic-organic mixed-matrix membranes. Proton conductivity is dependent on water content in the membrane, but the proton diffusion coefficients are similar for all Aerosil®380-TEOS combined systems. Membranes with an Aerosil®380-TEOS based inorganic phase exhibit in all cases remarkable permeation reduction in the liquid-liquid diffusion system. The ideal water to ethanol membrane selectivity, determined with pervaporation, is in all cases between 10 and 12, indicating that separation is not affected by the composition of the inorganic phase.

To improve the membrane properties, the MMMs have been modified with various functional silanes bearing basic groups. This is done to obtain an interaction between the organic and the inorganic phase resulting in better membrane stability and lower

ethanol permeability. Basic group type, amount of basic groups, basicity, hydrophilicity and spacer lengths have an impact on the mixed-matrix system. The MMM modified with N-[3-(triethoxysilyl)propyl]-4,5-dihydroimidazole (DHIM) exhibits highest water to ethanol selectivity coefficient as well as highest proton diffusion to ethanol permeation selectivity coefficient. Modified MMMs with an inorganic loading of 27.3% and DHIM concentrations up to 1.0 mmol modifier respective to the mass of inorganic content are studied more profoundly.

Reduction in ethanol permeability is more pronounced than the decrease in proton conductivity within the range of studied DHIM modified MMMs. High proton diffusion to ethanol permeability selectivity coefficients are obtained with high modifier concentrations. At low modifier concentrations this selectivity is mainly determined by ethanol permeation and at high modifier concentrations by proton diffusion. The modified MMMs clearly demonstrate prosperous properties with respect to proton diffusion and ethanol permeability in comparison to Nafion®, pure sPEEK, and unmodified mixed-matrix membranes.

DEFC tests show that the presence of modifier in the MMM has a significant influence on the fast activation and immediate functioning of the DEFC. The highest power density at 40 °C and 50 °C is obtained with the modified MMM with the lowest modifier concentration. The most constant development in fuel cell characteristics in time at all measuring temperatures is obtained with the modified MMM with the highest modifier concentration. Higher ethanol concentration in the anode feed stock results in improved fuel cell performance. Nafion®115 exhibits highest increase in DEFC performance as a function of temperature, but is clearly inferior to the modified MMMs at 30 °C and 40 °C. The target of 10 mW cm^{-2} at 40 °C is not reached within the measuring conditions, but is predicted at a higher ethanol concentration (2 M or 3 M) in the anode feed stock.

Zusammenfassung

Die abnehmenden Vorräte an fossilen Brennstoffen und die zunehmende Auswirkung von Treibhausgasen führen zu einer intensiven Entwicklung effizienter oder erneuerbarer Energiequellen. Die Direkt-Alkohol-Brennstoffzelle ist eine elektrochemische Zelle, die die Fähigkeit besitzt chemische Energie direkt und mit hohem Wirkungsgrad in elektrische Energie umzuwandeln. Damit ist sie eine vielversprechende Technologie für zukünftige portable Anwendungen. Heutzutage liegt der Fokus vor allem auf der Verwendung von Methanol, obwohl Ethanol deutliche Vorteile bietet. Ethanol ist eine allgemein bekannte und akzeptierte Substanz. Es ist umweltverträglich, nicht giftig, enthält eine hohe Energiedichte und die Infrastruktur für den Vertrieb ist bereits vorhanden.

Diese Dissertation beschäftigt sich mit der Entwicklung und Charakterisierung von protonenleitenden Membranen für die Direkt-Ethanol-Brennstoffzelle (DEFC). Diese Membranen sind aus einer anorganisch-organischen Mixed-Matrix aufgebaut, wobei die anorganische Matrix mittels funktioneller Silane modifiziert werden kann. Sulfoniertes poly(ether ether keton) (sPEEK) bildet die polymere Phase. Die anorganische Phase besteht aus pyrogener Kieselsäure (Aerosil®380), welche durch partiell-kondensiertes Tetraethoxysilan (TEOS) vernetzt ist. Die Charakterisierung der entwickelten Materialien und Membranen ist in die folgenden Bereiche unterteilt: i) Materialanalyse; ii) Membrancharakterisierung und iii) Brennstoffzellentests. Die Schwerpunkte im Rahmen dieser Charakterisierungen liegen auf der Protonenleitfähigkeit und dem Membranverhalten in Ethanol-Wasser-Misschungen.

Die Sulfonierung des Poly(ether ether keton)s und die Herstellung und Charakterisierung der polymeren sPEEK-Membranen wurde durchgeführt, um deren prinzipielle Anwendbarkeit in der DEFC zu beurteilen. Die Sulfonierung des PEEKs ist reproduzierbar und kann durch Sulfonierungszeit und -Temperatur gesteuert werden. Die Membraneigenschaften, wie z.B. Quellung, Protonenleitfähigkeit,

Ethanol- und Wasserpermeabilität, werden in Bezug zur Ionenaustauchkapazität (*IAK*) gesetzt. Die *IAK* der sPEEK-Membranen reichen von 1.15 bis 2.30 mmol g^{-1}. Das Hauptproblem der sPEEK-Membranen ist die Stabilität in ethanolischen Lösungen in Verbindung mit einer ausreichenden Protonenleitfähigkeit. Niedrig-sulfonierte Membranen (*IAK* < 1.4 mmol g^{-1}) weisen eine geringfügige Ethanol- und Wasserpermeabilität auf und sind stabil, jedoch ist ihre Protonenleitfähigkeit zu niedrig. Die Membraneigenschaften ändern sich exponentiell wenn die *IAK* größer als 1.8 mmol g^{-1} ist. Hier können infolge von unkontrollierbaren Quellungseigenschaften die reinen sPEEK Membranen nicht angewendet werden. Der Bereich, der am besten für die Anwendung des sPEEKs geeignet ist, liegt zwischen 1.4 and 1.8 mmol g^{-1}. Eine verbesserte Leistung der Brennstoffzelle im Vergleich zu Nafion® kann basierend auf dem Verhältnis von Protonendiffusionskoeffizient zu Ethanol-permeabilität prognostiziert werden. Dies macht sPEEK zu einem vielversprechenden Polymer-Typ für den Einsatz in der DEFC.

Zur Reduzierung der Ethanolpermeabilität und Aufrechterhaltung der Protonenleitfähigkeit wird eine anorganische Phase der polymeren Matrix zugegeben. Anorganisch-organische Mixed-Matrix-Membranen (MMM) mit unterschiedlichen Zusammensetzungen und anorganischen Beladungen zwischen 11% und 50% wurden untersucht. Das Zusetzen von TEOS als Vernetzer zwischen den Aerosil®380 Partikeln erfolgt in vernetzten MMM. Die anorganischen Partikel sind homogen verteilt und TEOS wird während der Aufbereitung der anorganisch-organischen MMM vollständig umgesetzt. Die Protonenleitfähigkeit ist von dem Wassergehalt in der Membran abhängig, aber die Protonendiffusionskoeffizienten sind für alle Aerosil®380-TEOS kombinierten Systeme ähnlich. Die Membranen mit einer Aerosil®380-TEOS gemischten anorganischen Phase weisen in allen Fällen beachtenswerte Permeationsreduktion in dem Flüssig-Flüssig Diffusionssystem auf. Die ideale Wasser-zu-Ethanol Membranselektivität, bestimmt mittels Pervaporation, liegt in allen Fällen zwischen 10 und 12. Dies deutet daraufhin, dass die Separation nicht durch die Komposition dieser anorganischen Phase beeinflusst wird.

Um die Membraneigenschaften weiter zu verbessern, wurden die MMM mit unterschiedlichen Silanen mit basischen Gruppen modifiziert. So wird die Interaktion zwischen der organischen und der anorganischen Phase gefördert, was zu einer besseren Membranstabilität und einer niedrigen Ethanolpermeabilität führt. Unterschiedliche basische Gruppen, Zahl der basischen Gruppen, Basizität, Hydrophilizität und Spacerlänge zeigen eine große Wirkung auf das Mixed-Matrix System. Die MMM modifiziert mit N-[3-(triethoxysilyl)propyl]-4,5-dihydroimidazole (DHIM) zeigen sowohl den höchsten Wasser-zu-Ethanol Selektivitätskoeffizient als auch den höchsten Protonendiffusion-zu-Ethanolpermeations-Selektivitätskoeffizient. Modifizierte MMM mit einer anorganischen Beladung von 27.3% und DHIM-Konzentrationen von bis zu 1.0 mmol Modifikator bezogen auf den totalen anorganischen Gehalt sind ausführlich untersucht.

Innerhalb der Datenreihe der DHIM-modifizierten Membranen ist die Abnahme in der Ethanolpermeabilität stärker ausgeprägt als die Abnahme in der Protonenleitfähigkeit. Hohe Protonendiffusion-zu-Ethanolpermeations-Selektivitäts-koeffizienten werden mit hohen Modifikatorkonzentrationen erreicht. Bei niedrigen Modifikatorkonzentrationen wird diese Selektivität hauptsächlich durch die Ethanolpermeabilität bestimmt und bei hohen Modifikatorkonzentrationen durch die Protonendiffusion. Hinsichtlich der Protonendiffusion und der Ethanolpermeabilität zeigen die modifizierten MMM eindeutig vielversprechende Eigenschaften in Vergleich zu Nafion®, reinen sPEEK und unmodifizierten Mixed-Matrix Membranen.

Die DEFC-Tests zeigen, dass die Anwesendheit des Modifikators in der Membran einen signifikanten Einfluss auf die schnelle Aktivierung und das sofortige Funktionieren der Brennstoffzelle hat. Die höchste Leistungsdichte bei 40 °C und 50 °C wird mit der modifizierten MMM mit der niedrigsten DHIM-Konzentration erzeugt. Die modifizierten MMM mit der höchsten DHIM-Konzentration zeigt eine meist konstante Entwicklung der Brennstoffzelleneigenschaften als Funktion der Zeit bei allen Messtemperaturen. Höhere Ethanolkonzentrationen in der Anode führen zu

einer verbesserten Brennstoffzellenleistung. Die schnellste Zunahme in der Leistung als Funktion der Messtemperatur ist mit Nafion®115 festgestellt. Dabei liegt die Leistung bei 30 °C and 40 °C deutlich unter der Leistung aller modifizierten MMM. Die Zielsetzung von 10 mW cm^{-2} bei 40 °C wurde bei den verwendeten Messbedingungen nicht erreicht, wobei diese Leistung bei höheren Ethanolkonzentrationen (2 M und 3 M) in der Anode prognostiziert werden kann.

Table of contents

List of symbols

A	Membrane surface area	[m^2]
C	Concentration	[mol dm^{-3}]
C_P	Heat capacity	[J mol^{-1} K^{-1}]
DS	Degree of sulfonation	[-]
D_σ	Proton diffusion coefficient	[cm^2 s^{-1}]
E	Cell voltage	[V]
E_a	Activation energy	[kJ mol^{-1}]
E_{eq}	Equilibrium cell voltage	[V]
f	Impedance correction factor	[-]
F_i	Permeability of component i (L-G system)	[kg µm m^{-2} h^{-1} bar^{-1}]
I	Current	[A]
IEC	Ion exchange capacity	[mmol g^{-1}]
j	Current density	[A cm^{-2}]
J_i^{L-G}	Flux of component i (L-G system)	[kg m^{-2} s^{-1}]
J_i^{L-L}	Flux of component i (L-L system)	[mol m^{-2} s^{-1}]
k	Reaction rate coefficient	[L mol^{-1} h^{-1}]
k_0	Pre-exponential factor	[L mol^{-1} h^{-1}]
L	Inorganic loading	[-]
$L_{catalyst,total}$	Total catalyst loading per surface area	[mg cm^{-2}]
m	Mass	[g]
M_n	Number-average molar mass	[g mol^{-1}]
M_w	Weight-average molar mass	[g mol^{-1}]
n	Molar amount	[mol]
n	Number of electrons	[-]
P	Power density	[W cm^{-2}]
P_i	Permeability of component i (L-L system)	[cm^2 s^{-1}]

pK_b	Base dissociation constant	[-]
p^p	Permeate pressure	[Pa]
p^{sat}	Saturation pressure	[Pa]
R_e	Electrolyte resistance	[Ω]
RT	Room temperature	[°C]
s	Distance between inner electrodes	[cm]
$S_m(J)$	Standard molar entropy of reaction component J	[J mol^{-1} K^{-1}]
SD	Swelling degree	[-]
$S_{i/j}$	(ideal) membrane selectivity of component i over j	[-]
t	Time	[s]
T	Temperature	[K]
W	Width of the membrane sample	[cm]
$w_{e,max}$	Maximum electrical work	[J mol^{-1}]
w_i	Weight fraction of component i	[-]
x_i	Molar fraction of component i in liquid phase	[-]
y_i	Molar fraction of component i in gas phase	[-]
|Z|	Impedance (Ohm)	[Ω]

Greek symbols:

$\alpha_{i/j}$	Separation factor of component i over j (-)	[-]
$\Delta_r G_m$	Standard molar Gibbs free energy of reaction	[J mol^{-1}]
$\Delta_f H_m$	Standard molar enthalpy of formation	[J mol^{-1}]
$\Delta_r H_m$	Standard molar enthalpy change of reaction	[J mol^{-1}]
$\Delta_r S_m$	Standard molar entropy change of reaction	[J mol^{-1} K^{-1}]
Δt	Time interval (s)	[s]

ε_{cell}	Fuel cell efficiency	[-]
ε_{E}	Electrochemical efficiency	[-]
ε_{F}	Faradaic efficiency	[-]
ε_{rev}	Ideal or reversible efficiency	[-]
γ_{i}	Activity coefficient of component i	[-]
η	Overpotential	[V]
φ	Phase (impedance)	[°]
$\lambda_{ethanol}$	Ethanol number	[-]
λ_{water}	Water number	[-]
ρ	Density	[g cm^{-3}]
σ_{H+}	Proton conductivity	[mS cm^{-1}]
υ_{J}	stoichiometric number of the reaction component J	[-]

Other symbols:

ℓ	Membrane thickness	[µm]

Constants:

F	Faraday constant	[C mol^{-1}]
R	Gas constant	[J mol^{-1} K^{-1}]

List of abbreviations

AEAPTMS	N-(2-aminoethyl)-3-aminopropyltrimethoxysilane
AHAPTMS	N-(6-aminohexyl)aminopropyltrimethoxy- silane
APTES	3-Aminopropyltriethoxysilane
APU	Auxiliary power unit
DBFC	Direct borohydride fuel cell
DEFC	Direct ethanol fuel cell
DHIM	N-[3-(triethoxysilyl)propyl]-4,5-dihydroimidazole
DI	Deionized
DMAc	Dimethylacetamide
DMFC	Direct methanol fuel cell
DMSO	Dimethylsulfoxide
DSC	Differential scanning calorimetry
e.g.	For example (latin: exempli gratia)
EP	Equivalence point
et al.	And others (latin: et alii)
EtOH	Ethanol
GDL	Gas diffusion layer
GPC	Gel permeation chromatography
HPA	Heteropolyacids
i.e.	That is (latin: id est)
L-G	Liquid-Gas
L-L	Liquid-Liquid
MCM	Mobile composition of matter

MEA	Membrane electrode assembly
MeOH	Methanol
MMM	Mixed-matrix membrane
MMT	Montmorillonite
MoPA	Molybdophosphoric acid
N/A	Not applicable
NMP	N-methyl-2-pyrrolidone
NMR	Nuclear magnetic resonance
PAI	Poly(amide imide)
PBI	Poly(benzimidazole)
PECVD	Plasma enhanced chemical vapor deposition technique
PEEK	Poly(ether ether ketone)
PEEKK	Poly(ether ether ketone ketone)
PEG	Poly(ethylene glycol)
PEK	Poly(ether ketone)
PEKEKK	Poly(ether ketone ether ketone ketone)
PEKK	Poly(ether ketone ketone)
PEM	Polymer electrolyte membrane
PEMFC	Polymer electrolyte membrane fuel cell
PES	Poly(ethersulfone)
PFSA	Perfluorosulfonic acid
PS	Polystyrene
PTFE	Poly(tetrafluoroethylene)
PVA	Poly(vinyl alcohol)
PVP	Poly(vinylpyrrolidone)

PWC	Platinum wire configuration
RT	Room temperature
SAXS	Small-angle X-ray scattering
sDDS	Sulfonated diphenyldimethoxysilane
SEM	Scanning electron microscopy
sMMT	Sulfonated montmorillonite
sPAEK	Sulfonated poly(aryl ether ketone)
sPEEK	Sulfonated poly(ether ether ketone)
sPEEKK	Sulfonated poly(ether ether ketone ketone)
sPEK	Sulfonated poly(ether ketone)
sPPO	Sulfonated poly(2,6-dimethyl-1,4-phenylene oxide)
STC	Spring tips configuration
TEOS	Tetraethoxysilane
$TEOS_{H/C}$	Hydrolyzed and condensed tetraethoxysilane
TGA	Thermogravimetric analysis
TMS	Tetramethylsilane
TMSPA	Bis(trimethoxysilylpropyl)amine
TPA	Tungstophosphoric acid
TRL	Technology readiness level
WAXD	Wide-angle X-ray diffraction
WDXRF	Wavelength dispersive X-ray fluorescence
ZrP	Zirconium phosphate

Chapter 1

Introduction

1.1. Fuel cells

Decreasing availability of fossil fuels, their environmental consequences, e.g., greenhouse effect, global warming and increasing energy demand due to the increasing world population led to extensive research and development in the field of renewable or more efficient energy sources over the past decades.[1] Fuel cells exhibit the feature to convert chemical energy directly to electrical energy with high efficiencies and low or zero levels of pollutant emissions. Not only the prospect of high efficiencies, but also the relative simplicity of a fuel cell and the absence of moving parts led to the conclusion that a real alternative for internal combustion engines was at hand. Research activities in industry and universities have reached enormous extents and fuel cell related sessions have become a regular part of many international conferences and fairs. Possible applications of fuel cells reach from stationary power production in Megawatt dimensions down to portable systems to supply mobile consumer electronics with below one Watt. Though, some barriers arose that hampered the commercial breakthrough of fuel cells.[2] They can be found on component level (e.g., catalysts and electrolytes), on system level (e.g., water management), and in fuel management (e.g., hydrogen and methanol). Up to now, electricity supplied with this technology cannot compete with those of the existing technologies with respect to availability and costs.

1.1.1. Brief historical overview

The principle and application of fuel cells are not new. In the beginning of the 19th century Johann Wilhelm Ritter, William Nicholson and Anthony Carlisle discovered electrolysis, the process of using electricity to break water into hydrogen and oxygen. Christian Friedrich Schönbein introduced the fuel cell concept in his publication in 1839.[3] In the same period Sir William Grove invented the *gas battery* based on the thought that recombination of hydrogen and oxygen could produce electricity.[4] The chemists Ludwig Mond and Charles Langer built the first practical device based on the *gas battery* and they introduced the term *fuel cell* in 1889.[5] Further development in that time lacked a drive because primary energy sources were unrestricted and inexpensive. In the 20th century, the conversion of chemical energy to electricity became more important because of the increasing use of electricity. Francis Thomas Bacon improved the machine of Mond and Langer by changing the electrode material (nickel instead of platinum) and electrolyte (alkaline instead of acidic) resulting in the first alkali electrolyte fuel cells in the late 1930s. He presented the first truly workable fuel cell in 1959.[6] Other important fuel cell activities took place at General Electric, GE. Thomas Grubb modified the fuel cell concept in 1955 by using a sulfonated polystyrene membrane as electrolyte resulting in the first polymer electrolyte membrane fuel cell (PEMFC).[7] The PEMFC was further improved together with his colleague Leonard Niedrach who devised a way of depositing the platinum catalyst onto the membrane.[8] This technology was further developed by GE and NASA resulting in the first application of fuel cells in the early 1960s.[9] An excellent historical overview is given by Schaeffer.[10] Fuel cells have been researched and developed from that point for general use in transportation, stationary systems, and portable applications or as auxiliary power units (APUs). Nowadays, various types of fuel cells have been developed. They mainly differ in electrolyte, application temperature and fuel.[11,12]

The focus in this thesis lies on the polymer electrolyte membrane fuel cells.

1.1.2. Polymer electrolyte membrane fuel cell (PEMFC)

The polymer electrolyte membrane fuel cell is an electrochemical cell where the anode and cathode are separated by a polymeric electrolyte. The configuration and principle of a single fuel cell is given in **Figure 1.1**. On the anode side, fuel is catalytically oxidized into protons and electrons. The electrons follow an external circuit where they are utilized as electricity. Meanwhile, protons diffuse through the proton conductive membrane (1) to the cathode side. This membrane is a barrier for all other substances, e.g., fuel and oxidant. At the cathode, the catalytic reduction reaction takes place with oxygen as oxidant. The recombination of protons, electrons and oxygen results in water as the reaction product.

The electrodes (2) consist of electrical conductive material, typically carbon, with catalyst deposited on it. Also proton conductive polymer is present in the layer for proton transfer i) from the catalyst surface to the membrane on the anode side and ii) from the membrane to the catalyst surface on the cathode side. The sandwich of the two electrode layers with the membrane in the middle is called the membrane electrode assembly (MEA). It forms the heart of the fuel cell.

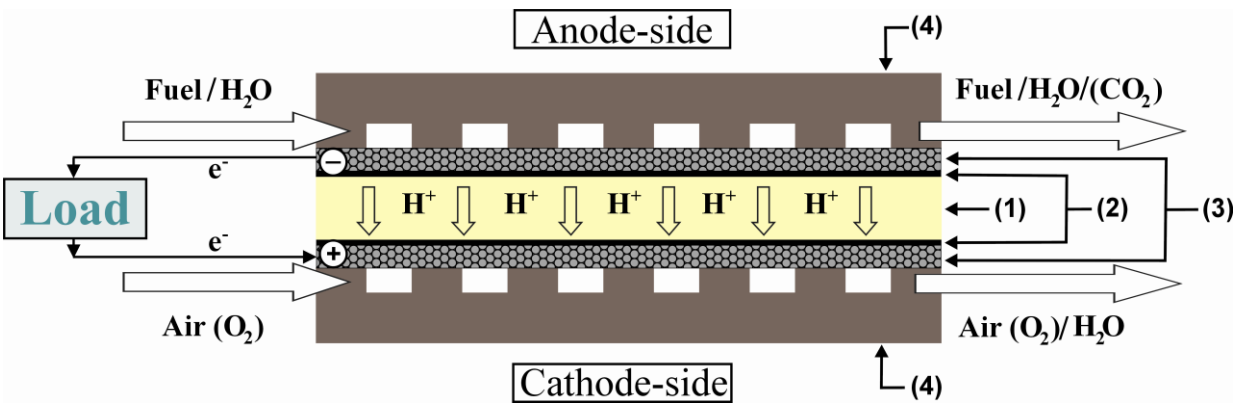

Figure 1.1: Schematic representation of a polymer electrolyte membrane single cell, (1) proton electrolyte membrane; (2) electrodes; (3) gas diffusion layers; (4) current collectors.

Porous electrical conductive layers, the gas diffusion layer (GDL) (3), are attached on both sides of the MEA. These layers account for optimal distribution of the reactants and removal of the reaction products.

Finally, the MEA and GDLs are pressed between the endplates or current collectors (4) having a certain flow field to ensure a uniform distribution of fuel and air across both sides of the membrane. The voltage of a single fuel cell is often too low for most applications. Therefore, individual cells are stacked to achieve higher voltages. The assembly is called a fuel cell stack and bipolar plates with flow fields on both sides are positioned between the MEAs. For the actual application of the fuel cell, a whole system containing fuel tanks, pumps, valves, controllers etc. is necessary.

The focus in this thesis lies on the polymer electrolyte membrane.

1.1.3. Basic thermodynamics of fuel cells

PEMFCs are galvanic cells in which chemical energy is electrochemically converted into electrical energy. The maximum electrical work ($w_{e,max}$) obtainable in a fuel cell operating at constant temperature and pressure is given by the change in free energy of the electrochemical reaction ($\Delta_r G_m$) which is related to equilibrium cell voltage (E_{eq}) via:[13]

$$w_{e,\max} = \Delta_r G_m = -nFE_{eq} \qquad \textit{Eq. 1.1}$$

n is the number of electrons participating in the reaction and F is Faraday's constant (96487 C mol^{-1}). The standard molar Gibbs free energy of reaction is given by:

$$\Delta_r G_m = \Delta_r H_m - T\Delta_r S_m \qquad \textit{Eq. 1.2}$$

where $\Delta_r H_m$ is the standard molar enthalpy change, the total thermal energy available, and $\Delta_r S_m$ is the isothermal molar entropy change. The available free energy is equal to the enthalpy change subtracted by the product of temperature and entropy change. The enthalpy and entropy change of a reaction are determined from the standard molar enthalpy of formation ($\Delta_f H_m$) and the standard molar entropy of the reaction components J:

$$\Delta_r H_m = \sum_J \nu_J \Delta_f H_m(J) \quad \text{and} \quad \Delta_r S_m = \sum_J \nu_J S_m(J) \qquad \textit{Eq. 1.3}$$

The stoichiometric numbers of the reaction components in these equations are denoted as ν_J. The heat capacity (C_p) relates the enthalpy and entropy to temperature at constant pressure and is defined as:

$$C_p = \left(\frac{\partial H}{\partial T}\right)_p = T\left(\frac{\partial S}{\partial T}\right)_p \qquad \textit{Eq. 1.4}$$

Integration from T_1 to T_2 results in the enthalpy or entropy at a temperature T_2:

$$\Delta_f H_m(T_2) = \Delta_f H_m(T_1) + \int_{T_1}^{T_2} C_p dT \quad \text{and} \quad S_m(T_2) = S_m(T_1) + \int_{T_1}^{T_2} \frac{C_p}{T} dT \qquad \textit{Eq. 1.5}$$

The standard enthalpy and standard entropy are generally given at 298 K (normally T_1).[13] The ideal efficiency or reversible efficiency (ε_{rev}) under standard conditions of the fuel cell is calculated from the thermodynamic data and is defined as:

$$\varepsilon_{rev} = \frac{\Delta_r G_m}{\Delta_r H_m} \qquad \textit{Eq. 1.6}$$

The practical fuel cell efficiency is generally lower than the reversible efficiency. Lowering of the efficiency is mainly caused by two phenomena.[14,15] Firstly, the electrochemical efficiency (ε_E), which is determined by electrode overpotentials and electrolyte resistance of the cell. The experimental cell voltage is defined as:

$$E(j) = E_{eq} - \left(|\eta_a(j)| + |\eta_c(j)| + R_e j\right) \qquad \textit{Eq. 1.7}$$

The anode and cathode overpotentials are $\eta_a(j)$ and $\eta_c(j)$ respectively, R_e is the electrolyte resistance, and j is the current density. Secondly, the Faradaic efficiency (ε_F) lowers the fuel cell efficiency. The Faradaic efficiency is defined as the ratio of the experimental current to the maximal possible current. Parallel reactions lead to lower current yield than theoretically possible. The practical fuel cell efficiency (ε_{cell}) can therefore be written as:[15]

$$\varepsilon_{cell} = \frac{-nFE_{eq}}{\Delta_r H_m} \cdot \frac{E(j)}{E_{eq}} \cdot \frac{n_{\exp}}{n} = \varepsilon_{rev} \cdot \varepsilon_E \cdot \varepsilon_F \qquad \textit{Eq. 1.8}$$

1.1.4. Types of fuel

The most investigated and applied fuel for PEMFC is *hydrogen*.[16] This fuel can be obtained from a variety of feedstocks, e.g., fossil fuels, electrolysis of water with renewable or nuclear energy.[17] Hydrogen fuel cells produce only pure water as direct exhaust and the overall equation is $H_2 + {}^1/_2\ O_2 \rightarrow H_2O$. These systems are highly efficient due to the relatively easy oxidation of hydrogen and this technology is developed to a large extent.[12] Also the flexible system design due to the connecting of fuel cell stacks is worth mentioning. These systems however remain expensive due to the noble metal catalyst and the high membrane costs. Other drawbacks can be found in, for instance, the hydrogen production. Ways of producing hydrogen results in high energy demands (electrolysis of water) or coherent emissions like

CO_2, NO_x and SO_x (e.g., natural gas-steam reforming, partial oxidation). Promising hydrogen sources to make PEMFC profitable are electrolysis of water by means of renewable energy sources or direct hydrogen production out of water with for example photoelectrolysis.[18] Other drawbacks are that hydrogen is a gas, and storage and distribution lead to severe problems due to high pressures or low temperatures needed for liquidization. Leakage can result in explosion danger when hydrogen is mixed with oxygen. In spite of these (to overcome) disadvantages, hydrogen is used in PEMFC technology mainly for stationary applications and transportation.[12,17] It is widely accepted that hydrogen is not appropriate for the use in portable applications due to handling drawbacks of this fuel and low volume energy density.

In fact, *methanol* is chosen in the fuel cell community because it is a liquid with the advantages of easy storage and transportation. Methanol has a high carbon to oxygen ratio and an acceptable energy density. This type of PEMFC is called the direct methanol fuel cell (DMFC) and the overall reaction in this fuel cell type is $CH_3OH + {}^3/_2\ O_2 \rightarrow 2\ H_2O + CO_2$. Portable application of fuel cells already penetrated the market and this market will grow extensively in the coming decade.[19] Significant drawbacks of methanol are the low boiling point, the inflammability and toxicity. Leakage during application could lead to severe health problems.[20]

Therefore, the use of *ethanol* as a fuel for portable applications is becoming more and more of interest.[20] This PEMFC is called the direct ethanol fuel cell (DEFC). Ethanol is a generally accepted substance, non-toxic, and the infrastructure for ethanol distribution already exists to a large extent. It has a higher energy density than methanol as well as a higher boiling point. Next to the normal industrial ethanol production, ethanol can be produced out of bioprocesses (e.g., fermentation of sugar-containing raw materials) as well and is therefore a potential renewable fuel source. The main disadvantages are the catalytic cracking of the C-C bond at low temperatures,[21] and that this technology is behind on the DMFC technology. An overview of the differences between thermodynamic and physical properties as well

as the risks of hydrogen, methanol and ethanol is given in **Table 1.1**. The development status is classified according the technology readiness level (TRL) which assesses the maturity of evolving technologies.[22]

Table 1.1: Differences between hydrogen, methanol and ethanol as a fuel in polymer electrolyte membrane fuel cells.[13,22,23]

		Hydrogen	Methanol	Ethanol
$\Delta_r H_m^0$	[kJ mol^{-1}]	-285.8	-726.3	-1366.9
$\Delta_r S_m^0$	[J mol^{-1} K^{-1}]	-163.3	-81.1	-139.0
$\Delta_r G_m^0$	[kJ mol^{-1}]	-237.2	-702.1	-1325.5
Energy density	[kWh kg^{-1}]	32.9	6.1	8.0
	[kWh dm^{-3}]	0.0030	4.8	6.3
Equilibrium cell voltage	[V]	1.23	1.21	1.14
Maximum efficiency	[%]	83.0	96.7	97.0
Boiling point	[°C]	-252.9	64.6	78.4
Vapor pressure at 20 °C	[mbar]	-	129	58
Potential risks:				
Toxic		no	yes	no
Explosive		yes	no	no
Inflammable		yes	yes	yes
Development status		TRL 7-9	TRL 7-9	TRL 3-4

Many other fuels have been proposed in literature for application in direct liquid fuel cells. Most of them are hydrocarbons bearing oxygen-groups in the form of *alcohols*, *ethers*, and *acids*. These substances are reviewed by Demirci by means of comparing thermodynamic and environmental data as well as the hazards of the fuel

and its by-products.[24] Higher alcohols than ethanol, e.g., 1-propanol and 2-propanol, contain high energy densities, but the electrochemical activity is very low.[25] On the other hand, the simplest carboxylic acid, formic acid, has a relatively high electrochemical activity. The energy density is very low and the corrosive and toxic nature of formic acid are significant drawbacks for portable applications.[24] Attention should be paid to the health effects, environmental hazards and inflammability of the fuels and their by-products when fuels are compared. These carbon containing liquid fuels are ideally oxidized to CO_2, but the efficient conversion in fuel cells leads to CO_2 reduction in comparison with, e.g., combustion.

A non-carbon containing fuel is *hydrazine* (N_2H_4) and is investigated and applied as fuel for PEMFC.[26] Hydrazine is a zero emission fuel like hydrogen, but it is highly toxic, dangerously unstable, and the by-product ammonia make hydrazine undesirable for portable applications.[24]

A promising non-carbon fuel for PEMFC is *sodium borohydride* ($NaBH_4$) and is called the direct borohydride fuel cell (DBFC).[27,28] This fuel cell only functions in alkaline mode. Borohydride has a high overall cell voltage (1.64 V), but low maximum efficiency (91%). No harmful by-products are formed during operation. Borohydride is not a renewable fuel source and the fuel itself is toxic, corrosive and highly flammable. To date, the DBFC is like the DEFC still in the development phase. Next to the DMFC, these are the most promising fuel cells for application as portable direct liquid fuel cell.[24]

The focus in this thesis lies on the use of ethanol as a fuel for portable applications.

1.1.5. Direct ethanol fuel cells

In direct ethanol fuel cells (**Figure 1.2**), an ethanol-water mixture is fed to the anode compartment and air or oxygen to the cathode compartment. The theoretical electrochemical reactions are:

Oxidation (anode): $C_2H_5OH + 3\ H_2O \rightarrow 2\ CO_2 + 12\ H^+ + 12\ e^-$ *R. 1.1*

Reduction (cathode): $3\ O_2 + 12\ H^+ + 12\ e^- \rightarrow 6\ H_2O$ *R. 1.2*

The overall reaction: $C_2H_5OH + 3\ O_2 \rightarrow 2\ CO_2 + 3\ H_2O$ *R. 1.3*

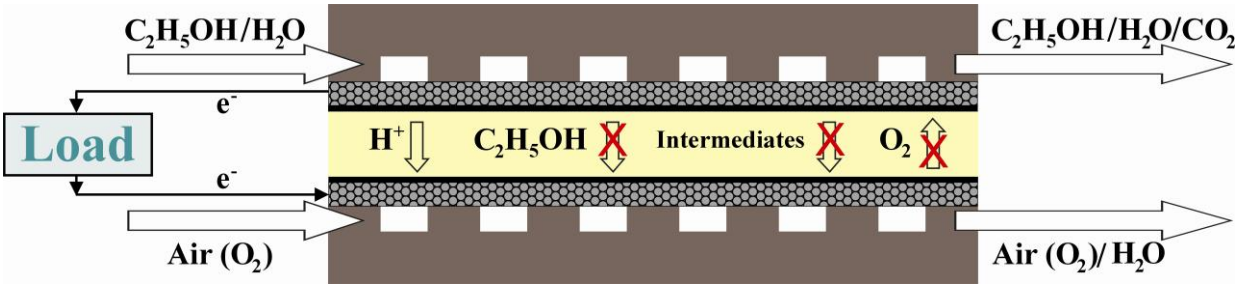

Figure 1.2: Schematic representation of a direct ethanol (single) fuel cell.

The reaction mechanism for the oxidation of ethanol involves several absorbed intermediates and by-products. The global oxidation mechanism of ethanol in acid solution can be summarized by means of the scheme presented in **Figure 1.3**.[21,29]

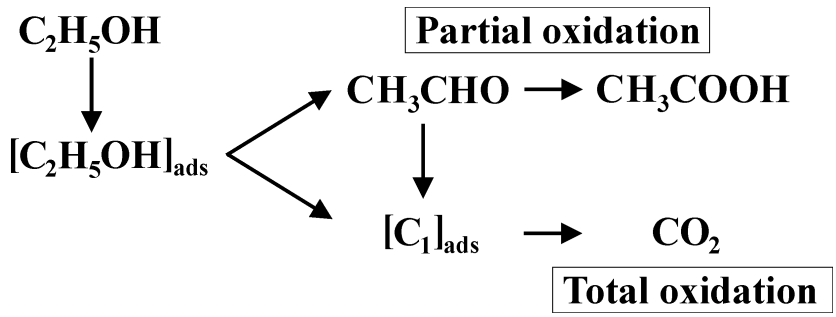

Figure 1.3: Simplified schematic representation of the oxidation pathways of ethanol.

Next to the full oxidation of ethanol, the fuel cell efficiency is severely limited by the formation of partial oxidation products containing an intact carbon-carbon bond. The unwanted partial oxidation half reactions for the formation of acetaldehyde and acetic acid are:[20]

Oxidation (anode): $C_2H_5OH \rightarrow CH_3CHO + 2\,H^+ + 2\,e^-$ *R. 1.4*

Oxidation (anode): $C_2H_5OH + H_2O \rightarrow CH_3COOH + 4\,H^+ + 4\,e^-$ *R. 1.5*

The transferring of 2 and 4 electrons, instead of 12 electrons in case of the total oxidation of ethanol, leads to a significant decrease in Faradaic efficiency. Next to the negative effect on fuel cell efficiency, these products are also unwanted due to their polluting nature.

Besides partial oxidation, dissociative adsorption of ethanol and acetaldehyde leads to C_1 species (**Figure 1.3**). The DEFC efficiency is also reduced by the formation of strongly adsorbed intermediates. The main surface poisoning species are CO and CH_x. The latter species originates from the $-CH_3$ group of the ethanol molecule and can be reduced to methane at low potentials or oxidized to CO-intermediate before subsequent oxidation to CO_2 at high potentials.[30]

A more detailed description of the ethanol oxidation mechanism is described below. Reactions are mainly taken from references [23,29,30]. Initially, ethanol adsorbs (molecular adsorption) weakly to the platinum surface through the lone pair electrons on the oxygen. Once adsorbed, ethanol can be oxidized to (weakly) adsorbed acetaldehyde, a reaction requiring two dehydrogenation steps:

$CH_3CH_2OH + Pt \rightarrow Pt(O\text{-}CH_2CH_3) + H^+ + e^-$ *R. 1.6*

$Pt(O\text{-}CH_2CH_3) + Pt \rightarrow 2Pt + CH_3CHO + H^+ + e^-$ *R. 1.7*

The main ethanol oxidation product is acetaldehyde, especially at higher ethanol concentrations.[31] The C-C bond primarily breaks after dehydrogenation to acetaldehyde. Dissociative adsorption of ethanol, leading to adsorbed CH_x and adsorbed CO, is not favoured, because this reaction is very sluggish in comparison to acetaldehyde. The reaction path to decompose acetaldehyde to form these adsorbed C_1 species occur via an additional dehydrogenation step:

$CH_3CHO + Pt \rightarrow Pt(OC\text{-}CH_3) + H^+ + e^-$ *R. 1.8*

$Pt(CO\text{-}CH_3) + Pt \rightarrow Pt(CO) + Pt(CH_3)$ *R. 1.9*

Surface oxygenated species like adsorbed hydroxyl groups can be formed by oxidation of water. These species are necessary to accomplish the oxidation of adsorbed CO to CO_2:

$H_2O + Pt \rightarrow Pt(OH) + H^+ + e^-$ *R. 1.10*

$Pt(CO) + Pt(OH) \rightarrow 2Pt + CO_2 + H^+ + e^-$ *R. 1.11*

The mechanism of the oxidation of acetaldehyde to acetic acid is not fully understood. Acetic acid can be formed via the intermediate 1,1-ethane-diol or direct oxidation of acetaldehyde. The possible reaction for this direct oxidation is:

$CH_3CHO + Pt(OH) \rightarrow Pt + CH_3COOH + H^+ + e^-$ *R. 1.12*

A detailed study of the oxidation mechanism of ethanol and acetaldehyde on platinum is investigated and discussed by Lai and Koper.[29,30] These works are highly recommended for further reading. It can be stated that the development of selective catalysts is a major challenge in the development of DEFCs. Various binary and tertiary catalyst systems have been explored for possible application in DEFC and these investigations are reviewed by Antolini.[21] Up to now, a combined catalyst system with platinum, ruthenium, and tin shows promising results.[32]

1.1.6. Polymer electrolyte membrane for DEFC

An important component in the direct ethanol fuel cell is the electrolyte membrane. This membrane should provide the transport of protons (electrolyte function) and retain substances like fuel and intermediates at the anode side and oxidant at the cathode side (barrier function). In the case of direct alcohol fuel cells, many studies

have been carried out on methanol as a fuel in the direct methanol fuel cell.[33-35] Only a couple of studies are known for the direct ethanol fuel cell.[36-38] The demands for electrolyte membranes for both direct alcohol fuel cells are similar and can be summarized by:[35,39]

- High proton conductivity, but low electron conductivity
- Low oxidant and fuel crossover
- Long-term chemical stability
- Good mechanical stability
- Compatibility with the catalyst layers
- Easy assembly of the fuel cell
- Low costs

The polymer electrolyte membranes or proton exchange membranes generally consist of polymers. These polymers can roughly be subdivided in perfluorinated and non-fluorinated polymers. Various modifications are studied to improve the properties of these polymer membranes like fuel crossover, proton conductivity or stability. Some types of modification are: fabric supporting, blending polymers, crosslinking, doping with heteropolyacids, or adding an inorganic phase. A detailed review of these polymers and their modification is given in Chapter 2.

1.2. Objectives of this thesis

The focus of this thesis lies on the development and characterization of proton conductive membranes for application in direct ethanol fuel cells. The drawback of the membranes presently used in direct alcohol fuel cells are the proton conductivity in relation to the fuel crossover. The latter one is mainly caused by excessive swelling of the membrane material and will be investigated with pure polymeric membranes. The strategy to reduce fuel crossover is to develop particle loaded inorganic-organic hybrid membranes and fill the free volume of the membrane to inhibit the fuel

transport. To further improve the stability of these particular nanocomposite systems, the particles will be interconnected leading to inorganic-organic mixed-matrix membranes. In addition, the large inorganic inner surface offers the potential to be modified by means of functional groups to further control the membrane structure and to regulate the membrane properties.

Characterization of the material and membrane will be carried out in the following domains: i) material analysis and ii) membrane characterization. In case of membrane characterization the main parameters to study are proton conductivity and membrane behavior in ethanol-water systems (e.g., swelling, permeation, selectivity). Direct ethanol fuel tests are performed by the project partners and are presented in addition to the membrane investigation. These data will be included and discussed, but will not form the basis of this work. In this work, the main focus will lie on the combination of polymer modification, inorganic materials, and silane chemistry with membrane technology and surface engineering.

1.3. Thesis outline

In **Chapter 2** a literature overview of polymer electrolyte membranes is presented. The focus lies on fluorinated and non-fluorinated based membranes. Polymer types, functioning of the membrane and membrane modifications are discussed. A more profound overview is given of the inorganic-organic hybrid membrane systems.

Chapter 3 describes the methodology which is used to characterize the developed membranes. The used and developed methods in material analysis and membrane characterization are presented. Membrane characterization is subdivided in two sections, namely proton conductivity and membrane behavior in water-ethanol systems. Finally fuel cell tests are described.

An in-depth study of the sulfonation of poly(ether ether ketone) and preparation and characterization of polymeric membranes is given in **Chapter 4**. Two different sulfonation methods are compared. The influence on the degree of sulfonation on membrane properties as liquid uptake, permeation and proton conductivity is studied.

In **Chapter 5**, inorganic-organic composite membranes with various compositions and inorganic loading are presented. Next to particle loaded membranes, membranes are prepared with crosslinked inorganic particles to obtain an interconnected inorganic network.

Chapter 6 focuses on modification of the inorganic network by means of functional silanes to obtain modified mixed-matrix membranes. The first part of this chapter deals with testing various modifiers with different properties. A modifier is selected for further investigation, which is profoundly described in the second part of this chapter. Finally, these developed membranes are compared with non-fluorinated and fluorinated membranes.

Finally, in **Chapter 7** conclusions are presented of the developed and investigated membranes. Recommendations for further research are given as well as other directions for the use of these kinds of membranes.

Chapter 2

Background – a literature review

In the polymeric membrane development for direct alcohol fuel cells, polymers are often discriminated between fluorinated and non-fluorinated ionomers.[35,40] On the one hand, fluorinated ionomers possess high proton conductivity but also considerable high fuel cross-over. Significant drawbacks are the costs and disposal of these materials. On the other hand, non-fluorinated ionomers, which have similar stability properties as fluorinated ionomers, are of interest because of the low costs. Generally, these materials provide a good barrier function but exhibit relatively low proton transport resulting in opposite fuel cell characteristics in comparison to fluorinated ionomers. A third type, belonging to the more recent membrane developments, are the partially fluorinated ionomers. These polymers consist of fluorinated monomers bearing sulfonic acids groups and non-fluorinated, often arylene based, monomers. These polymer types are out of the scope of this thesis, because they are not commercially available and they exhibit possible thermal and oxidative instability due to their aliphatic nature.[41]

In this chapter, the focus lies on fluorinated and non-fluorinated ionomers. Both polymer classes will be discussed in detail with respect to structure, functionalization, properties, and their modifications. Various modification possibilities have been reported in literature to improve the polymer electrolyte membrane properties. These modifications are, e.g., radiation grafting, polymer blending, fabric supporting, and crosslinking. Also organic-inorganic hybrid materials, often called nanocomposites or mixed-matrix materials, are a widely studied approach. Various inorganic materials are possible ranging from amorphous silica to structured inorganic particle systems

loaded with heteropolyacids. These proton conductive membranes are often described and characterized for the application in hydrogen-PEMFC and DMFC. The review will basically focus on PEMs for both systems, but particularly on DMFC. This kind of fuel cell functions similar to DEFC and much knowledge can be transferred.

2.1. Perfluorinated membranes

Fluorinated ionomers consist of a chemically, mechanically and thermally stable backbone, known as poly(tetrafluoroethylene) (PTFE). This backbone contains pendant side chains that terminate in ion exchangeable groups. The functional group is generally a sulfonic acid group, but also carboxylic acid groups are possible. In case of sulfonic acid proton exchange groups the ionomer is called perfluorosulfonic acid (PFSA). These materials show higher proton conductivity then the polymers containing carboxylic acid groups. High proton conductivity is significant in case of fuel cell membranes, and therefore, PSFA membranes are further discussed. Nafion® of Dupont de Nemours is the oldest and best known commercially available PFSA. Various PFSA polymers have been developed based on the structure of Nafion®. These structures vary mainly in monomer repeatability, side chain composition, and length. A detailed review about the synthesis of PSFA polymers is given by Souzy and Ameduri.[42] The general chemical structure of PFSA is given in **Figure 2.1**. The commercial membranes are listed together with the structure parameters, equivalence weight, and the thickness range in **Table 2.1**.

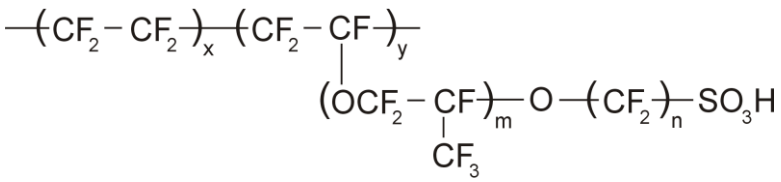

Figure 2.1: General chemical structure of perfluorosulfonic acid.

Table 2.1: Commercial perfluorosulfonic acid membranes.[42,43]

Structure parameters	Company	Type	Equivalence weight [g mol^{-1}]	Thickness [µm]
m = 1, n = 2 x = 5 - 13.5, y = 1	Dupont	Nafion®	1100	80 - 175
m = 0 - 1, n = 1 - 5	Asahi Glass	Flemion®	1000	50 - 120
m = 0, n = 2 - 5 x = 1.5 - 14	Asahi Kasei Chemicals	Aciplex®	1000-1200	25 - 100
m = 0, n = 2 x = 3.6 - 10	Dow Chemical	Dow®	800	125

Other companies developed PFSA membranes based on modifications on the polymers presented in **Table 2.1**. Examples are Gore with the development of a PTFE stabilized ionomer membrane, also known as the Gore-Select® membrane.[44] Solvay Solexis introduced Hyflon® based on the technology developed by Dow Chemical.[45] The company 3M developed a new polymer with a similar structure but a longer side chain (n = 4). Fumatec introduced the perfluorinated fumapem®F membrane based on the fumion® ionomer.[46] Besides all new developments and new products, Nafion® is still the most described PFSA in case of fuel cell application and characterization and is generally taken as reference material in case of PEM development. Further discussion of PSFA will be based on Nafion®.

As mentioned the fluorinated backbone account for a high mechanical, thermal and chemical stability. The small size and high electronegativity of the fluorine atom result in a strong C-F bond. These hydrophobic chains show low intra- and intermolecular interaction resulting in low surface energy.[42] The sulfonic acid group is highly ionic and hydrophilic. When the membrane is hydrated, water clusters are formed around the acidic sides and the hydrophobic backbone tend to segregate from the water

domains resulting in a unique nanostructure due to the hydrophilic/hydrophobic nanoseparation.[34,47] Over the years various models have been developed to describe these remarkable properties of Nafion®. They can be subdivided in spheroidal-cluster or network models, thin water layers in sheet-like models or more recently the parallel water-channel model.[47,48] The first model to describe the structure of Nafion® was presented by Hsu and Gierke.[49] The morphology features of Nafion® were examined by means of small-angle X-ray scattering and wide-angle X-ray diffraction (SAXS and WAXD respectively). The hydrated morphology was best described by a model of ionic clusters that were approximately spherically shaped with an inverted micellar structure. It was proposed that these spherical ionic clusters were interconnected by narrow channels. This morphology is also referred to as the cluster-network model (**Figure 2.2**).

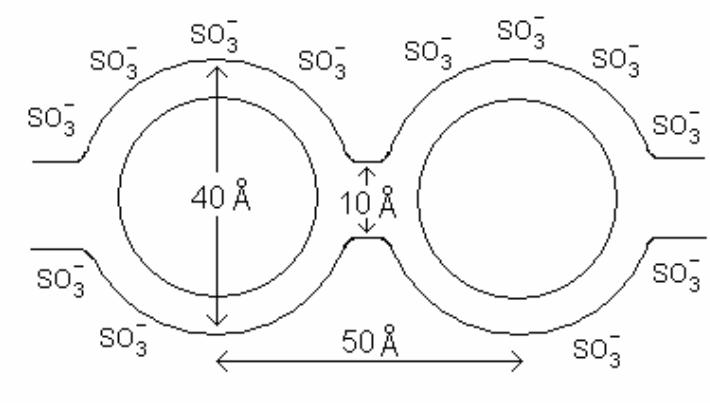

Figure 2.2: Cluster-network model for the morphology of hydrated Nafion®.[49]

A modification of the cluster-network model is the random-network model proposed by Eikerling et al.[50] This model includes an intermediate region wherein the side chains ending with pendant sulfonic acid groups. These groups show hydrophobic-hydrophilic repulsion with the perfluorinated backbone and tend to cluster within the overall structure of the material. The distribution of hydrated regions in the polymer matrix is, therefore, more random than in the cluster-network model. Proton mobility is enhanced through the rotation of the polymer side chains.

Haubolt et al.[51] investigated Nafion® in methanol-water systems and proposed a three-phase sandwich structure in a layer-model. The shell-core sandwich structure consists of i) an hydrophobic region, ii) a shell region with the side-chains, and iii) an embedded core region, either empty or filled with methanol-water mixture.

Schmidt-Rohr and Chen critically discussed the existent Nafion® models and they recently proposed the water-channel model.[48] The stiffness of the helical backbone can stabilize long cylindrical structures. The parallel-pore structure consists of an inverted-micelle cylinder, with polymer backbones on the outside and ionic side groups lining the water channel. The water-channel model accounts for many of the outstanding properties of Nafion®, in particular its high proton conductivity and water permeability. The high water self-diffusion is explained by a larger channel diameter (~2.4 nm) in comparison to the existing models (typically < 1.2 nm). These diameters are based on a water volume fraction in Nafion® of 20%.

These presented models are given as an example for better understanding of the functioning of the perfluorinated material. These materials form the basis for the development of other non-fluorinated membranes. A further detailed description of transport of water, protons, and other substances in Nafion® is beyond the scope of this thesis. For more details, other review articles are recommended.[47,52,53]

Besides the remarkable properties of Nafion®, the material exhibits some shortcomings that led to studies of Nafion® membrane modifications or the development of non-fluorinated materials. Drawbacks of Nafion® membranes are that they are expensive (600 – 1200 \$ m^{-2}) and suffer from low conductivity at low water contents and moderate glass transition temperatures.[43] Next to that, these membranes exhibit high fuel crossover in case of direct liquid fuel cells and high ruthenium crossover in case that the anode catalyst contains ruthenium.[35] Also the environmental issues with respect to manufacturing and recycling or disposal of PFSA are worth mentioning.[39]

2.1.1. Modified perfluorinated membranes

The main reasons to modify Nafion® membranes for application in direct liquid fuel cells are the costs and fuel crossover. Two types of modification are most described: i) surface modification and ii) reinforcement of the membrane. A method to modify PFSA membranes is surface grafting.[42] To this, the polymer must be activated. Typical activation techniques are thermal, ozone, plasma electron beam, or X-ray activation. Due to this activation, radical (co)polymerization is initiated of various monomers leading to graft copolymers. Bae et al.[54] studied the plasma induced polymerization technique to graft polystyrene and polystyrene sulfonic acid onto Nafion®. Both methanol crossover and proton conductivity were reduced. Lowest values were 70% and 10% respectively to the value of pristine Nafion®, dependent on the crosslinker agent concentration and the grafting time. Another technique to deposit films on Nafion® is chemical vapor deposition. Kim et al.[55] employed the plasma enhanced chemical vapor deposition technique (PECVD) to deposit nano-scaled films of silica on Nafion® membrane. A reduction in methanol permeability as well as in proton conductivity was found. Also the power density was significantly low when the silica layers were thicker as 10 nm. Another kind of surface modification is sandwiching the Nafion® membrane between layers with low methanol permeating characteristics. Shao et al.[56] sandwiched Nafion® membranes between poly(vinylalcohol) (PVA)/Nafion® blend layers with different compositions. Better relative selectivity (MeOH permeation resistance to membrane area resistance) resulted in better fuel cell performance than pristine Nafion®. Lin et al.[57] reported data about hybrid-laminated Nafion®115 membranes. The membrane was soaked in a lamination solution consisting of an alkoxysilane-endcapped PEG precursor. The PEG-silica based layers were modified with phenyl-groups to improve stability and with 4-dodecylbenzene sulfonic acid to improve proton conductivity. In both cases, a simultaneous decrease in methanol permeability and proton conductivity was obtained. A similar dip-coating procedure to obtain mesoporous silica on a Nafion® membrane was followed by Lin et al.[58] This surface modification resulted in higher

water uptake, but lower dimensional swelling in comparison to the unmodified membrane. This higher uptake resulted in higher proton conductivity. The drawback of surface modification is that the membrane costs are not reduced. In contradiction to this, with the other type of membrane modification, membrane reinforcement, fuel crossover, and concomitant reduction in membrane costs is enabled.

Many strategies of membrane reinforcement are described in literature. An approach, which is also commercialized, is the PSFA reinforced membrane with a PTFE porous sheet, also known as the Gore-Select® membrane.[44] Other PTFE supported membranes are based on embedded PTFE-yarn and dispersed PTFE-fibril.[59] This hydrophobic support makes the membrane more hydrophobic and, therefore, significantly influences the water management in the membrane. Other supporting materials, like poly(ethylene terephthalate)[60] and microporous poly(ethylene)[61] were also successfully impregnated with Nafion®. This type of modified Nafion® membrane normally exhibits lower methanol crossover and proton conductivity and shows better fuel cell performance than the pure Nafion® due to its stability.

Polymer blending for polymer electrolyte membrane systems has been studied by various groups and is reviewed by Kerres.[62] Interaction between polymers is established by Van der Waals forces, dipole-dipole interactions, H-bridges, ionic, or covalent bonding. Some examples of blend membrane systems of Nafion® with other, typically non-fluorinated, polymers are given. The influence of blending 5, 10 and 20 wt-% of PVA in Nafion® on DMFC performance was studied by DeLuca and Elabd.[63] The blend membrane with the lowest amount of PVA showed an improvement. Kim et al.[64] blended sulfonated poly(aryl ether ketone) (sPAEK) with Nafion® with various compositions. The blend membranes showed phase separated morphology since they became immiscible during the solvent evaporation process. An example of an acid-base polymer blend is a poly(benzimidazole) (PBI)-Nafion® blend-system as investigated by Wycisk.[65] DMFC tests of these polymer blends showed results inferior to pristine Nafion® membranes except for high methanol

concentrations. Under these conditions the membrane stability was decisive for better DMFC results.

Another approach which is frequently studied in literature is perfluorinated ionomer-inorganic hybrid materials. Because this approach corresponds to the approach which is chosen for this thesis, a separate section is dedicated to this topic (**Section 2.1.2**).

2.1.2. Perfluorinated ionomer based composite membranes

Perfluorinated ionomer-inorganic hybrid materials are reviewed in this section. These materials are also called nanocomposite membranes or mixed-matrix membranes. Various inorganic materials and various preparation routes have been described. Mostly membrane systems for DMFC will be described, because this technology is further developed than DEFC and the functioning is similar.

Inorganic phase prepared by sol-gel processing

For the preparation of a sol-gel based inorganic phase into the membranes, roughly two different approaches are described. Firstly, the precursor solution is mixed with a polymer solution followed by preparing the membrane. Secondly, a membrane is soaked in a precursor solution and the preparation of the inorganic phase occurs *in situ*. A review of perfluorinated ionomers as sol-gel polymerization templates for inorganic alkoxides is given by Mauritz.[66] Silicon based inorganic materials are studied to a large extent because of the large variety of silanes. Tetraethoxysilane (TEOS) is often used for building inorganic networks or particles, because it is widely studied and the reactions are relatively slow and controllable.[67]

Jiang et al.[68] prepared Nafion®-silica mixed-matrix membranes with an inorganic loading varying between 3% and 15%. The silica was prepared in methanol by hydrolyzing and condensing tetraethoxysilane. Nafion® solution was added to this mixture. The water uptake increased with increasing loading, exceeding the uptake of

Nafion®. They suggested that this was due to the hydrophilic property of silica. They found a minimum methanol permeability with 5% loading. The proton conductivity decreased with increasing loading. Ren et al.[69] described the formation of nanocomposite membranes by mixing a silica sol with a Nafion® solution to obtain 5% inorganic loading. The precursors used were TEOS, mercaptopropylmethyl-dimethoxysilane (SH), or a mixture of them. The thiol-groups (-SH) were afterwards oxidized with hydrogen peroxide to sulfonic acid groups. The proton conductivity and fuel cell performance with 1 M methanol were inferior to Nafion® and dropped in the following order:

SH / Nafion® < TEOS / Nafion® < TEOS-SH / Nafion® < Nafion®117

The fuel cell performance of the TEOS-SH / Nafion® composite membrane showed better performance in 5 M methanol than the pure polymer membrane, which was due to the lower methanol permeability. Li et al.[70] used a sol-gel derived sulfonated diphenyldimethoxysilane (sDDS) solution and mixed it with Nafion® solution to obtain inorganic loading varying from 5 to 25%. The addition of an inorganic phase resulted in all cases in lower methanol permeability and coherent proton conductivity. The proton conductivity of a sDDS inorganic phase was four times as high as the unsulfonated inorganic phase. Composite membranes with an sDDS inorganic phase showed similar performance with DMFC tests. Kim et al.[71] prepared organically modified silane based composite membranes by soaking Nafion®117 membranes in a reaction medium consisting of various precursors with different functionalities. TEOS was used for networking and triethoxyvinylsilane with three alkoxy-groups had a crosslinking function. Diethoxydimethylsilane and diethoxydiphenylsilane, both having two alkoxy-groups, had a bridging function. The inorganic loading in the composite membranes varied between 0 to 50%. These precursors affected the hydrophilicity and morphology of the composite membrane. Homogeneous structures were observed with SEM, except for precursors with a bridging function. Here large particles (~1 µm) were obtained. A decrease in methanol permeation was observed

over the whole range of loading with a coherent decrease in proton conductivity. Lavorgna et al.[72] applied a similar method and used a mixture of TEOS and mercaptopropyltrimethoxysilane with two different compositions. The thiol-groups were oxidized again with hydrogen peroxide to sulfonic acid groups. The inorganic loading for all composite membranes was approximately 10%. Instead of increasing the proton mobility with increasing the oxidized thiol-groups, the opposite effect was achieved.

Next to silica and their modifications, other metal oxides, e.g., zirconia and titania are studied as well. Advantages of these metal oxides are mainly the better stability in acidic or basic media in comparison to silica. Jalani et al.[73] studied the incorporation of silica, zirconia, and titania prepared by *in situ* formation. Therefore, Nafion® membranes were soaked in various precursor solutions. Unfortunately, the inorganic loading was not mentioned. Zirconia based composites exhibited higher water uptake resulting in higher proton conductivity in comparison to the other composite membranes. The fuel cell performance was for all membranes similar, except for the silica based composite membrane. This membrane showed poor DMFC behavior. Furthermore, no remarkable differences were observed between the composite membranes.

Commercial particles

Dimitrova et al.[74] studied Nafion® membranes and Aerosil®380 loaded nanocomposite membranes as a function of thickness and temperature. The inorganic loading was 4.3%. Methanol permeation was similar for the composite membranes and the commercial Nafion® membranes. Methanol permeation decreased with increasing membrane thickness. It was remarkable, that water permeation did not decrease as a function of membrane thickness. The composite membranes exhibited properties which were advantageous, especially at higher temperatures, like higher proton conductivity at 90 °C. A comparison study between the incorporation of commercial silica, alumina, and zirconia in Nafion® is given by

Arico et al.[75] Alumina particles were slightly basic and the proton conductivity was significantly lower than the more acidic silica and zirconia systems. The DMFC performance at 145 °C improved in order of the following filler material: silica > zirconia > alumina.

Silicates

Layered silicates

Among the broad variety of natural or synthetic layered silicates, montmorillonite, hectorite and saponite are most commonly used in nanocomposite materials.[76] In nanocomposite materials for DMFC, montmorillonite (MMT) is decribed most frequently. This material consists of two-dimensional layers, where a central octrahydral sheet of alumina, with partial substitution of Al with Mg, is fused to two external silica tetrahedra in the way that the oxygen atoms are shared (2:1 phyllosilicates). The chemical structure is described by $M_x(Al_{4-x}Mg_x)Si_8O_{20}(OH)_4$ where M is a monovalent cation, e.g., H^+, Na^+ or Li^+. Nanocomposite membranes consisting of Nafion® and MMT were prepared by Song et al.[77] The inorganic loading of MMT was varied up to 20%. Very low amounts of filler showed a large effect on methanol permeability. With 1% loading, a 90% reduction in methanol crossover was achieved. The fuel cell performance was significantly better especially with higher concentrated feed. Lee et al.[78] varied the MMT loading between 0% and 10% and functionalized MMT with 1,3-propane sultone. An optimum in selectivity of proton conductivity to methanol permeability was found at 5%. DMFC tests with the composite membrane showed better performance than with Nafion®, but the influence of the functionalization was rather modest. Lin et al.[79] described the modification of MMT with poly(propylene oxide)-backboned diamines functionalized with sulfonic acid groups, calling it MMT/POPD400-PS. They achieved a decrease in methanol permeability and an increase in proton conductivity. They suggested two mechanisms to the latter, i) hopping mechanism was promoted by the intercalating agent (POPD400-PS) with a long chain and (ii) the vehicle mechanism was

accelerated on the surface of the introduced clay network. The DMFC fuel cell tests also showed improved performance in comparison with Nafion®.

Zeolites

Other well known structured materials are zeolites. This type of inorganic filler is frequently studied as well because of its hydrophilic character. It is believed that the water sorption is increased with coherent exclusion of alcohols. Drawbacks are the possible structure breakdown in strong mineral acids and the poor interfacial compatibility between zeolite crystals and polymer matrix. These drawbacks led to various studies to improve the properties for DMFC. Li et al.[80] studied the incorporation of modified zeolite NaA in Nafion®. Zeolite particles with two different sizes were studied, 2-3 μm and 300 nm, and were modified with aminopropyl-trimethoxysilane. They demonstrated that silane-based coupling agents can be used to improve the interface compatibility between zeolite crystals and Nafion®. With increasing zeolite loading, decrease in proton conductivity and increase in methanol permeability was obtained. They suggested that this was due to the formation of pinholes. The incorporation of low cost natural zeolites, chabazite and clinoptilolite, with a loading of 40% was studied by Tricoli et al.[81] The membranes were inferior to Nafion®. The characteristic factor, selectivity of proton conductivity to methanol permeation, was nearly a factor of 5 lower than pristine Nafion®. Buyn et al.[82] obtained a characteristic factor twice as high as Nafion®115 with a composite membrane where the inorganic phase consisted of ZSM-5 zeolites. The zeolite was ball-milled to obtain particles between 100 and 200 nm and the zeolite content in the membrane was 5%.

Molecular sieves

Another type of silicate materials added to form nanocomposite materials is a mesoporous silica molecular sieve, MCM-41.[83] It possesses hexagonally packed arrays of channels with very high surface areas and narrow pore size distribution

compared to amorphous silica. MCM-41 has, like zeolites, a channel structure with a pore size in the range of 20 – 100 Å by varying the type of surfactant. Compared to zeolites, a significant disadvantage is the structure collapse during heating in boiling water and aqueous solutions, which leads to various kinds of modifications of MCM-41.[84] Various nanocomposite membranes containing MCM-41 and organo-functionalized MCM-41 up to 5% loading have been prepared and characterized by Park et al.[84] The addition of the organic groups, vinyl- and phenethylgroups, were catalyzed by NaF and these groups could be sulfonated with chlorosulfuric acid. The characteristic factor, defined as the ratio of proton conductivity and methanol permeability, was nearly in all cases inferior to Nafion®. The investigation of the incorporation of 1 and 3% MCM-41 in Nafion was done by Jin et al.[85] They found that these mesoporous nanospheres enhanced water retention properties, improved thermal stability, and reduced methanol crossover in comparison to pristine Nafion®.

Precipitation

Zirconium phosphate

Layered zirconium phosphates (ZrP) are interesting materials due to their high ionic conductivity. In case of α-zirconium layered phosphates, $Zr(HPO_4)_2{\cdot}H_2O$, the additional protons of the phosphate-moiety and bound crystal water have the potential to improve the high temperature conductivity of the Nafion® membrane. A material-based study was done by Bauer and Willert-Porada.[86] The incorporation of ZrP was based on ion exchange followed by precipitation. The protons on the sulfonic acid groups were exchanged by zirconium ions and after treating the membrane with phosphoric acid the ZrP precipitated in the membrane matrix. The ZrP loading was varied between 0% and 35%. The ZrP was present as monolayers rather than as multi-layers inside Nafion® and decreased the crystallinity of Nafion® significantly when more ZrP was present in the composite structure. The permeation experiments and the swelling kinetics showed that the methanol permeability is reduced by the inorganic compound and the phosphate layer has a preferred permeability for water

compared to methanol. A composite membrane with 25% ZrP loading in Nafion®115 was compared to an unmodified Nafion®115 by Yang et al.[87] The proton conductivity results, as a function of water content in the membrane, were compared to two models: i) the random-network model of Eikerling[50,88] and ii) a model analogous to the proton diffusion model for aqueous electrolyte described by Thampan.[89] The latter appeared to be the most appropriate model for the experimental data. Hou et al.[90] compared a ZrP based Nafion®115 composite membrane with 23% loading with Nafion®115. The influence of methanol concentration was studied, and liquid uptake and methanol permeability of the composite membrane was significantly lower in comparison to the Nafion®115 membrane. For both membranes, an increase in both parameters was observed as a function of methanol concentration. The improvement in fuel cell performance of the composite membrane measured with 5 M and 10 M methanol was more pronounced at the highest methanol concentration.

Sulfated zirconia

Various preparation routes to form proton conductive sulfated zirconia (S-ZrO_2) were investigated by Hara et al.[91] $ZrOCl_2 \cdot 8H_2O$ and ammonia were used to form ZrO_2-particles. These were sulfonated with sulfuric acid (S-ZrO_2). The incorporation of S-ZrO_2 in Nafion® membranes and their fuel cell characteristics were studied by Zhai et al.[92] These particles were mixed in a Nafion® solution, of which subsequently membranes were cast. The inorganic loading varied between 0 and 20%. The references were Nafion®112 and recast Nafion®. They found an increase of ion exchange capacity (*IEC*) and an optimum in water uptake with 10% inorganic loading. The crystallinity increased with addition of S-ZrO_2 in contradiction to the findings of Bauer and Willert-Porada, who found a decrease with ZrP loading. The best fuel cell performance was obtained with a composite membrane with 15% loading. The *in situ* preparation by means of ion exchange followed by precipitation in the Nafion®115 membrane was done by Ren et al.[93] The presence of this inorganic phase increased the amount of water uptake at temperatures above 70 °C. In addition, the acid sides

promote proton transportation, resulting in higher proton conductivity compared to Nafon®117 at higher temperatures.

Heteropolyacids

Another type of inorganic phase are heteropolyacids (HPAs). They have a well-defined local structure, of which the Keggin structure is best known. This structure is formed by a central atom (Si or P) tetrahedrally linked to oxygen and surrounded by oxygen-linked peripheral metal atoms (W, Mo, V, Nb, Ta). Some often used HPAs are tungstophosphoric acid (TPA) and molybdophosphoric acid (MoPA). The main feature of interest is the strong acidity of HPA. However, the HPA electrolyte dissolves in the liquid (alcohol fuel) during fuel cell operation. An approach to prevent the HPA to leach out of the membrane is to incorporate the HPA in an host material.[94] HPA are built in a Nafion® membrane to achieve proton conductivities at high temperatures. For lower temperature applications, this type of modification is more appropriate for polymers exhibiting low proton conductivities.

Shao et al.[95] investigated the influence of an inorganic phase and HPA-loaded inorganic phase in a Nafion® matrix. Therefore, a Nafion® solution was mixed with silica and TPA/silica mixtures, whereby the silica-gel and HPA were commercial. The composite membranes were prepared by the recasting procedure. Higher water uptake, especially at higher temperatures, was found for the Nafion®/TPA/silica-membrane, resulting in concomitant higher proton conductivity in comparison to recast Nafion®. A study to incorporate HPA in silica prepared by sol-gel was done by Kim et al.[96] They described the preparation of TPA-SiO_2 nanoparticles by a microemulsion technique. Sulfonic acid groups were introduced onto the surface of the silica by oxidizing the thiol-groups of the added 3-mercaptopropyltrimethoxysilane with hydrogen peroxide. This was done to improve the hydrophilic and proton-conducting properties. The sulfonic-functionalized heteropolyacid-SiO_2 nanoparticles could be conductive carriers for protons and also act as water reservoir in the composite membrane to make DMFC measurements up to 200 °C possible. Kim et

al.[97] prepared TPA on MCM-41 via two different routes: i) conventional impregnation and ii) directly synthesizing in the pores. The impregnated TPA existed in the pores on the MCM-41 surface and was more easily washed out, whereas the TPA was better distributed in the pores and remained in there during washing procedures. The effect on methanol permeation, proton conductivity, and DMFC test was rather modest.

2.1.3. Summary of perfluorinated membranes

Various perfluorinated sulfonic acid ionomeric membranes have been commercialized over the years. These polymer electrolyte membranes possess high mechanical, thermal, and chemical stability. These membranes exhibit high proton conductivity due to the highly ionic and hydrophilic sulfonic acid group. Therefore, proton conductivity is highly dependent on the water household in the membrane. Hydrophilic/hydrophobic nanoseparation results in a large, interconnected water channels with the consequence of high and non-selective crossover of liquid substances, e.g., fuel and intermediates. Other significant drawbacks are the high costs and environmental issues with respect to manufacturing and disposal of these membranes. Membrane modifications are mainly done to reduce fuel crossover and membrane costs. Two types of modification are most described: i) surface modification and ii) reinforcement of the membrane. The drawback of surface modification is that the membrane costs are not reduced. Fabric supported PFSA membranes and polymer blends with various kinds of interactions show promising results, mainly with respect to stabilization in higher concentrated fuel systems. Inorganic-organic hybrid systems are described more profoundly. Some materials used as inorganic phase are metal oxides prepared by sol-gel, layered silicates, molecular sieves, heteropolyacids, and inorganics obtained by precipitation like zirconium phosphate and sulfated zirconia. These inorganics affect the hydrophilicity and morphology of the composite membrane. A general observation is that these

composite materials show a reduction in methanol permeation and a coherent decrease in proton conductivity. Nevertheless, the positive effects on fuel cell performance are rather limited and therefore not commercialized, at least to the knowledge of the author.

2.2. Non-fluorinated membranes

The shortcomings of PSFA, especially fuel cross-over and membrane costs, for possible application in DMFC led to further polymer development. Many non-fluorinated specialty polymers have been functionalized, characterized, and tested for this application. These polymers should exhibit stability features comparable to PFSA, but the polymers should be less expensive. The functioning of these polymers is generally similar to that of PFSA. This means that these chemically, hydrolytically, mechanically, and thermally stabile polymers have to be functionalized. In case of proton electrolyte membranes, mainly sulfonic acids groups are introduced onto the polymer chains. Sulfonation reactions are common and profoundly described for many reaction systems.[98] The sulfonic acid groups exhibit high acidity and are therefore highly hydrophilic. Similar to PSFA systems, nanoseparation is induced under humid and wet conditions, resulting in hydrophilic regions in which protons can diffuse. In this section, a short review of sulfonated polymers is given of frequently mentioned non-fluorinated polymers in fuel cell literature. The emphasis of this fuel cell literature is, again, the literature concerning DMFC, because of the wide range of in-depth studies and the similarity to the DEFC system.

As mentioned in the introduction (**Chapter 1**), the first PEM was a sulfonated *polystyrene* membrane. It was soon discovered that these hydrocarbon polymers show insufficient chemical stability. Especially tertiary C-H bonds and benzylic bonds are easily attacked by oxygen.[40]

An alternative non-hydrocarbon polymer is *poly(phosphazene)* consisting of a -P=N- polymer backbone. Poly(phosphazene)s are of great synthetic and technological interest because of the wide range of side group structures providing tailored properties for various applications.[99] This means that various side chains for ion-exchange sites and polymer crosslinking onto the -P=N- polymer backbone can be attached. For example, Guo et al.[100,101] described the sulfonation of poly(bis(3-methylphenoxy)phosphazene) (**Figure 2.3a**) and obtained promising results for DMFC.

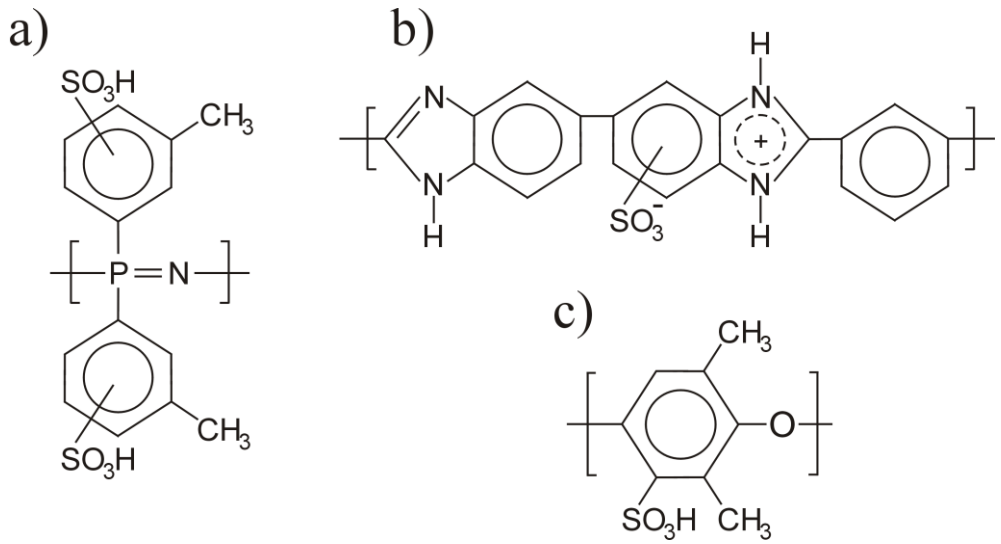

Figure 2.3: Sulfonated repeating units of a) poly(bis(3-methylphenoxy)phosphazene); b) polybenzimidazole (PBI); c) poly(2,6-dimethyl-1,4-phenylene oxide) (PPO).

Another frequently mentioned polymer for various types of fuel cell oparations is *poly(benzimidazole)*.[102] Sulfonation of this basic polymer for the preparation of proton conductive membranes and its characterization was done by Staiti et al.[103] Membranes consisting of sulfonated poly(benzimidazole) (sPBI, **Figure 2.3b**) showed low proton conductivity values, which is probably due to a strong interaction between protons and nitrogen atoms of the imidazolium ring in poly(benzimidazole). The strong interaction between the basic nitrogen and sulfonic acid groups in sPBI induced cristallinity, making the semi-crystalline polymer insoluble in common aprotic solvents. An extensive review of PBI membranes together with possible modifications for fuel cell applications is given by Li and Jensen.[104]

A number of hydrocarbon-based ionomeric membranes containing aryl-groups in the polymer backbone have been proposed for usage as proton exchange membranes. Their stability features and relatively low costs make them very attractive. *Poly(phenylene)s* and their derivatives are known to form rather non-flexible films, probably due to their rigid rod backbone. The inability of these polymers to form flexible films complicated MEA fabrication and PEM testing.[105] *Poly(phenylene oxide)* is a promising polymer type, because of the diversity in reactions to modify the polymer structure.[106] The best known sulfonated poly(substituted-phenylene oxide)s are sulfonated poly(2,6-dimethyl-1,4-phenylene oxide) (sPPO, **Figure 2.3c**) and poly(2,6-diphenyl-4-phenylene oxide) known as Ballard Advanced Materials, BAM2G membrane. Another polymer type in this series is *poly(phenylene sulfide)*, which becomes water soluble when the sulfonation degree is > 30%.[98] *Poly(imide)s* are of interest as well. These sulfonated polymers are often obtained via direct polymerization of sulfonated monomers, because they are commercially available.[107] Many different poly(imide) structures can be obtained due to a large variety of sulfonated and unsulfonated monomers.[108]

The class of high performance engineering thermoplastics, which have been known for their chemical resistance and physical and mechanical properties, are the *poly(arylene ether)*-type polymers. In the field of proton conductive membranes for fuel cells, *poly(arylene ether ketone)s* and *poly(arylene ether sulfones)* are the most intensively studied non-fluorinated polymers. In **Figure 2.4**, the chemical structures of a sulfonated poly(ether ether ketone) and sulfonated poly(ether sulfone) repeating unit are given.

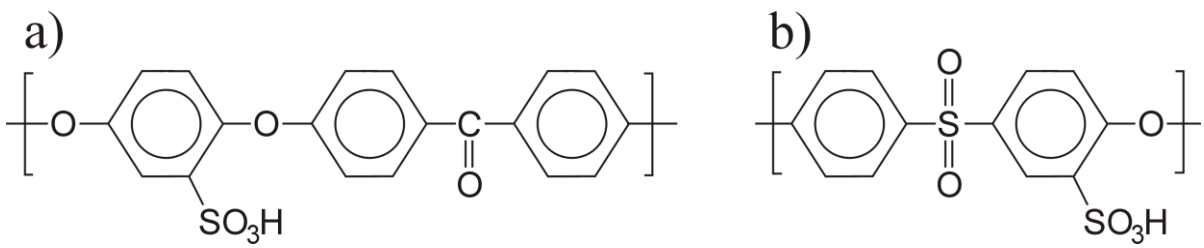

Figure 2.4: Sulfonated repeating units of a) poly(ether ether ketone) and b) poly(ether sulfone)

Probably the earliest publication on the sulfonation of *poly(arylene ether sulfone)s* was a patent of Quentin.[109] The sulfonation of polysulfone with chlorosulfonic acid was furthermore described by, amongst others, Johnson et al.[110] to make the polymer more hydrophilic for membrane applications. A fundamental study on partially sulfonated poly(arylene ether sulfone)s as proton conducting membrane material for energy conversion technologies was reported by Nolte et al.[111] From that point, alternative sulfonation routes and membrane modifications of sulfonated poly(arylene ether sulfone)s for possible replacement of PFSA are investigated. This is extensively reviewed by Kerres.[40] *Poly(arylene ether ketone)s*, the other type of poly(arylene ethers), is in the focus of this thesis and is, therefore, discussed separately and more profoundly in the following section.

Due to the volume of work in the field of polymeric fuel cell membranes, it will go too far to describe all (co)polymers which have been synthesized and functionalized and of which membranes were prepared for testing the fuel cell characteristics. Extensive reviews have been composed by various authors where non-fluorinated ionomers for fuel cells are described.[35,40,43,62,98,112-115] From this point, the focus of this thesis lies on the sulfonated poly(arylene ether ketone)s, its structure variations and their modifications.

2.2.1. Poly(arylene ether ketone)s

Poly(arylene ether ketone)s are known as aromatic polymers with excellent thermal stability, chemical resistance, and mechanical properties. These copolymers are attractive for the use as PEMs because of their oxidative and hydrolytic stability. Various types of poly(arylene ether ketone)s are commercially available, and they differ in arrangement of ether-groups and ketone-groups and their molar quantity per monomer. Examples are poly(ether ketone) (PEK), poly(ether ether ketone) (PEEK), poly(ether ketone ketone) (PEKK), poly(ether ether ketone ketone) (PEEKK), and poly(ether ketone ether ketone ketone) (PEKEKK). With increasing amount of ketone-

segments in the polymeric backbone, the sulfonation is hindered and the reaction conditions have to be stronger.[116] On the other hand, the oxidative and hydrolytic stability is increased.[98]

Among these various structures of poly(arylene ether ketone)s, the most reported structure with respect to sulfonation is PEEK, poly(oxy-1,4-phenylene-oxy-1,4-phenylene-carbonyl-1,4-phenylene). Two routes to obtain sulfonated PEEK (sPEEK) can be distinguished:[115] i) post sulfonation of PEEK and ii) direct copolymerization of sulfonated and unsulfonated segments. The most common way to sulfonate PEEK is to employ electrophilic aromatic substitution. This substitution readily takes place on the phenyl ring containing the highest electron density, typically the ortho-position between the ether segments, resulting in the structure given in **Figure 2.4**.

The first sulfonation procedure of PEEK was reported in 1985 by Jin et al.[117] Often described sulfonating agents are concentrated sulfuric acid, fuming sulfuric acid, and chlorosulfonic acid.[98] Fuming sulfuric acid and chlorosulfonic acid are much stronger sulfonating agents than concentrated sulfuric acid, resulting in less controllable sulfonation reactions accompanied by side reactions.[118] The degree of sulfonation (*DS*) is defined as the ratio of sulfonated segments to the total amount of segments present in the polymer. The *DS* of sPEEK in concentrated sulfuric acid mainly depends on the concentration of sulfuric acid, the sulfonation temperature, and sulfonation time. A kinetic study on these parameters was reported by Huang et al.,[119] who also reported that the sulfonation was a second-order reaction. The post-sulfonation can be subdivided into heterogeneous and homogeneous sulfonation.[120] In the case of heterogeneous sulfonation, the dissolving and sulfonation of PEEK occur simultaneously. Homogeneous sulfonation means that the PEEK is dissolved in a solvent, like methylsulfonic acid, and subsequently sulfonated by the addition of sulfuric acid. The *DS* of sPEEK prepared by heterogeneous sulfonation at room temperature was strongly dependant on sulfonation time up to 60 h. After that point, the *DS* increased slowly in time, indicating logarithmic dependency. Homogeneous sulfonation was time consuming, because of the lower concentration of sulfuric acid

in the reaction mixture. The sulfonation behavior as a function of time was linear. Membranes with ion exchange capacities varying from 1.4 to 2.4 mmol g^{-1} were prepared and characterized with respect to proton conductivity and methanol permeability. Results of sulfonated membranes up to 1.8 mmol g^{-1} were similar. The sulfonation of two types of commercially available PEEKs, Victrex® (Victrex PLC, England) and Gatone® (Gharda Chemicals Ltd., India), was studied by Xing et al.[121] sPEEK obtained with both PEEK types exhibited similar polymer and membrane characteristics. The *DS* has a strong influence on the processability and stability.[122] If the sulfonation degree is too high (> 90%), sPEEK is water soluble, and if the sulfonation degree is too low (< 40%), it is not soluble in standard solvents used for membrane formation.

Lack of control over the degree and location of functionalization, degradation of the polymer and unwanted side reaction are frequently mentioned drawbacks of post-sulfonation of PEEK. The main advantages of copolymerization of sulfonated and unsulfonated segments are the chain length regulation, the use of monomers containing two sulfonic acid groups, and controlling the *DS* and polymer structure without crosslinking reaction.[115,123] The first reported sulfonated monomer used in the direct copolymerization of sPEEK was 2-fluorobenzenesulfonate.[124] sPEEK prepared by copolymerization with improved membrane properties in comparison to post-sulfonated sPEEK were obtained by, amongst others, Gil et al.[123] and Muthu Lakshmi et al.[125]

Similar to Nafion®, the structure of sulfonated poly(arylene ether ketone) nanoseparates when material is humidified or wetted. Fundamental work was carried out by Kreuer,[34] who made a comparison between the morphology of Nafion® and sulfonated PEEKK (sPEEKK) based on a network model. It was found, that the transport properties and morphological stability between both systems are distinctly different. These differences were ascribed to the more hydrophobic and flexible backbone and the more acidic sulfonic acid groups of Nafion® in comparison to

sPEEKK. Therefore, Nafion® exhibit wide water channels, a good connected percolated hydration structure, and no dead-end channels. For sPEEKK on the other hand, the hydrophilic/hydrophobic regions are less separated. The highly branched hydration structure consists of small channels with many dead ends. This is schematically represented in **Figure 2.5**.

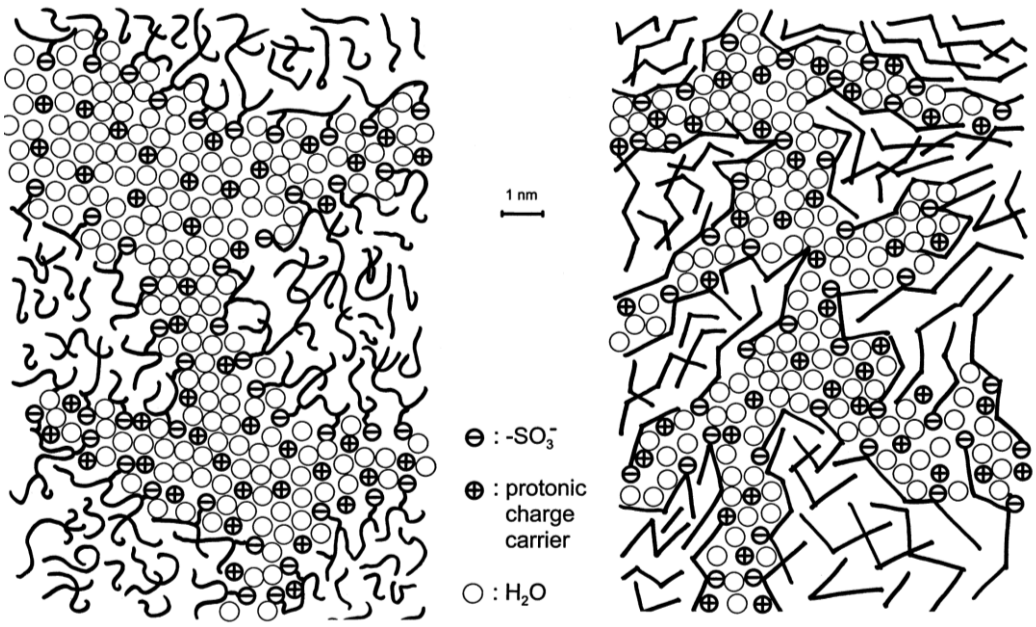

Figure 2.5: Schematic representation of the microstructures of Nafion® and a sulfonated poly(ether ether ketone ketone) by Kreuer.[34]

When these structures are compared, it can be understood that in wet systems proton transport as well as fuel crossover in Nafion® are high, and in case of poly(arylene ether ketone) these characteristics are low. A comparison study was done by Xue and Yin to compare methanol permeability and proton conductivity of sPEEK with *DS* between 59 and 93% to Nafion.[126] Methanol permeability strongly depends on the *DS* and increased in that range from $27 \cdot 10^{-8}$ to $154 \cdot 10^{-8}$ cm^2 s^{-1}. The lowest permeability was 6.5 times lower than for Nafion®, while this factor for proton conductivity was just 2.4. These results were obtained at 22 °C.

Modifications of Nafion® for usage in DMFC at relatively low temperatures were mainly focused on reducing the fuel crossover (**Section 2.1**). The fuel crossover of

poly(arylene ether ketone)s membranes is already relatively low, but membrane modifications should lead to further decrease in fuel crossover while maintaining or improving the proton conductivity. Obviously, the stability features (e.g., swelling, mechanical) should be optimal to obtain good performance in fuel cell tests. Similar to the development of the PFSA section, general modifications of poly(arylene ether ketone) are presented and, subsequently, an in-depth review of poly(arylene ether ketone) based composite membranes is given for the application of these membranes in fuel cells.

2.2.2. Modified poly(arylene ether ketone) based membranes

Literature on modification of poly(arylene ether ketone) membranes is merely based on the improvement of bulk material rather than 'just' surface modification. Poly(arylene ether ketone), which contain a high *DS* and, therefore, high proton conductivity, generally lacks proper stability. Xing et al.[127] described the *impregnation* of sPEEK into microporous PTFE to reduce the swelling properties of the sPEEK membrane. The mechanical strength and swelling properties were improved, but the fuel cell tests showed higher resistance and the performance was inferior to both sPEEK and Nafion®.

Crosslinking is an alternative method to limit fuel crossover and excess water uptake. Photochemical crosslinking with a combination of benzophenone and triethylamine as photo-initiator together with UV was studied by Zhong et al.[128] They found a better hydrolytic stability, reduced methanol crossover, but also a reduction in proton conductivity. These effects were more pronounced with longer irradiation times. Another type of crosslinking was described by Mikhailenko et al.[129] Alcohols, e.g., glycol and glycerine, were used for thermally activated bridging of the polymer chains. The bridging was done by reacting the crosslinking agents with the sulfonic acid groups of sPEEK, resulting in a decrease in proton conductivity. Crosslinking was effective to improve the mechanical strength and liquid uptake.

Another modification type frequently described in literature is *polymer blending*. Wu et al. reported on polymer blends of sPEEK with poly(ethersulfone) (PES),[130] poly(amide imide) (PAI),[131] and poly(vinylpyrrolidone) (PVP)[132] for possible application in DMFC. This was done with the purpose to stabilize the sPEEK structure. The blend sPEEK/PES membranes with various compositions showed a non-linear behavior in water uptake, proton conductivity and methanol permeability. All blends were homogeneous and a good miscibility and specific interaction between sPEEK and PES was shown with DSC data. Diagrams of methanol permeability and proton conductivity as a function of PES content showed similar non-linear developments when the PES content was more than 40%. Wilhelm et al.[122] studied similar blends for ionic transport in ion permeable membranes. sPEEK content in the blend ranging from 50 to 80% appeared to be the most suitable. Below that, not all ion exchange groups were available for ion transport due to the high PES content. Above that range, the PES content was too low to provide the physical crosslinking required for a reduction in water content. In case of sPEEK/PAI polymer blend, similar observations were done. The decrease in methanol permeability was similar to the sPEEK/PES blended polymers, though the proton conductivity was lower. sPEEK with different sulfonation degrees were blended with various PVA contents by Yang.[133] PVA exhibits high methanol resistance and the large quantities of hydroxyl groups in PVA might interact with sulfonic acid groups of sPEEK. The uptake of blend membranes in water increased with the increasing PVA content, while the absorption of blend membranes in methanol solution showed a decrease upon the PVA content, which can minimize the swelling ratio of electrolyte membrane in DMFC applications. The *IEC* was considerably lower than the theoretical *IEC* according to the mixing rule. The sPEEK/PVP polymer blends showed acid-base interactions. sPEEK with a sulfonation degree of 69% blended with PVP showed decreasing proton conductivity with increasing amount of PVP. The water and methanol uptake showed best values when the PVP content was between 20% and 30%. DMFC tests with a sPEEK/PVP membrane (ratio of 4) showed better performance than Nafion®. Pasupathi et al.[134]

reported on the sPEEK-PBI acid-base polymer blend. sPEEK/PBI membranes were studied with DMFC tests and their performance was found to be considerably better than that of commercial Nafion®117 membranes. These polymer blends were found to be extremely stable under DMFC operating conditions up to 60 °C. An extensive review about ionomer blend with various interactions, e.g., covalently crosslinking, hydrogen-bridge and acid-base interactions, is given by Kerres.[62]

2.2.3. Poly(arylene ether ketone) based composite membranes

Poly(arylene ether ketone) based organic-inorganic hybrid materials are reviewed in this section similar as is done in **Section 2.1.2**. Membranes with various inorganic materials and prepared via various routes have been described in literature, mainly for application in DMFC systems. These materials will be described in this section, because the DMFC technology is further developed than DEFC and the functioning is similar.

Inorganic phase prepared by sol-gel processing

The formation of an inorganic phase with sol-gel chemistry based on silicon-, zirconium- and titanium-based precursors was studied by Nunes et al.[135] Modification of the ZrO_2- and TiO_2-based inorganic systems appeared to be difficult because of the inert surface of those particles. Modified silica systems led to a decrease in methanol permeability values. An approach to bind a functional silane covalently to the sulfonic acid groups of sPEK was given. This was done via the reaction of 1,1'-carbonyl-diimidazole followed by the addition of aminopropylsilane. This system was combined with tetraethoxysilane or 1-(3-triethoxysilylpropyl)-4,5-dihydro-imidazole to obtain silica based composite membranes. The prepared composite membranes showed improved incorporation of silica in the polymeric matrix. An improvement with respect to methanol permeability, but significant decrease in proton conductivity was achieved using the functional silanes bearing a basic group.

Tchicaya-Bouckary et al.[136] prepared the inorganic phase with various combinations of aminophenyltrimethoxysilane and TEOS. They suggested that the small and well-dispersed particles, preferentially localized in hydrophilic domains of the polymer, maximize the interface region between the organic and inorganic components. Therefore, the proton conductivity is maintained or enhanced with associated advantage of better mechanical strength. sPEEK composite systems with non-functionalized and sulfonic acid functionalized silica prepared with TEOS and 3-mercaptopropyltrimethoxysilane respectively were studied by Sambandam et al.[137] No remarkable enhancement in proton conductivity was obtained due to the large agglomerate size of the inorganic phase.

Commercial particles

Gomes et al.[138] extensively studied the functionalizing of Aerosil®R380 particles. Silanization onto the fumed silica surface was done by bromophenyltrimethoxysilane. Then, sulfonated bishydroxy aromatic compounds were chemically attached by nucleophilic substitution reactions. All tested composite membranes contained 5% functionalized silica. The membrane consisting of silica with sulfonated hydroxytelechelic containing 1,3,4-oxadiazole units had higher proton conductivity values in a temperature range of 40 °C to 140 °C than the membrane containing only the plain electrolyte polymer, while the methanol permeability determined by pervaporation experiment was unchanged. Carbone et al.[139] built in commercial 3-aminopropyl functionalized particles with 1 mmol g^{-1} NH_2 loading. sPEEK matrixes with a degree of sulfonation of 35% and 52% were used. The silica contribution reduced the membrane swelling through interactions between sulfonic and amino groups. This effect is highlighted in membranes with 52% *DS*, where the reduction of water uptake and swelling does not interfere with the proton conduction.

Various silicates

Layered silicates

Chang et al.[140] prepared sPEEK based composite polymer membranes by embedding layered silicates, laponite and montmorillonite (MMT) into sPEEK membranes for fuel-cell applications. They found a reduction in swelling and methanol permeability. H_2-O_2 fuel cell tests were performed, and the composite membrane was slightly better than the pure sPEEK membrane but was inferior to Nafion®. In addition to laponite and MMT, Karthikeyan also investigated magadiite.[141] Composite system with laponite and magadiite showed similar methanol behavior and proton conductivity. The proton conductivity of the MMT was about a factor of two lower than the other composite systems. The permeability reduction in the composite membranes was discussed using Maxwell's model and a modified Maxwell's model. Maxwell's model does not take particle size and shape into account and is valid for inorganic volume fractions smaller than 10%. These shortcomings are compensated in the modified Maxwell's model. Experimental deviations from the theoretical models were addressed to the inhomogeneity of composite system and the dense top layer because of sedimentation of particles during membrane preparation. Gaowen et al.[142] added organically modified MMT to sPEEK with a *DS* of 65%. Hexadecyltrimethyl-ammonium ions have been used to replace Na^+. They showed that sPEEK intercalated into MMT and that the organic modification of MMT is a necessary step to incorporate nanosized MMT in the sPEEK matrix. The reduction in methanol permeability was more pronounced than the decrease in proton conductivity. Gosalawit et al.[143] reported on the incorporation of sulfonated MMT (sMMT) into sPEEK. MMT was sulfonated with 3-aminopropyltriethoxysilane as a coupling agent to immobilize 4-sulfophthalic acid onto MMT layers. Proton conductivity of the hybrid membranes with sMMT was significantly higher than the membranes with non-sulfonated MMT. The methanol permeation remained low, resulting in DMFC performance remarkably better than Nafion® and pure sPEEK.

Zeolites

Erce et al.[144] prepared zeolite based sPEEK nanocomposites with various silica/alumina compositions. The proton conductivity of the composite membrane consisting of zeolite beta fillers into sPEEK was a factor of two higher than the plain sPEEK membrane. Among the zeolite beta/sPEEK composite membranes, the best conductivity results were achieved with zeolite beta containing 10% loading and having a SiO_2/Al_2O_3 ratio of 50. The composite membranes could further be stabilized by blending sPEEK with sPES, resulting in better fuel cell performance.

Karthikeyan et al.[145] compared laponite, also a synthetic layered silicate, with a mesoporous molecular sieve, MCM-41, spherical Aerosil®380 particles, and *in situ* generated silica. The inorganic particles were modified by organo silanes, imidazole glycidoxypropyl triethoxysilane (IGPTES), and 3-2-imidazolin-1-yl-propyltrimethoxy-silane. The *in situ* generated network was formed by a sol-gel process with aminopropyltrimethoxysilane and IGPTES. The silica network was more effective in decreasing the methanol permeability, whereas the modified particles showed higher proton conductivity. The imidazole modified Aerosil® membrane exhibited the best combination of low methanol permeability and high proton conductivity.

Precipitation

Zirconium phosphate

Tchicaya-Bouckary et al.[136] described the *in situ* precipitation of ZrP in sPEEK membranes. Protonated membranes were first immersed in a $ZrOCl_2{\cdot}8H_2O$ aqueous solution followed by phosphoric acid treatment. A composite membrane with 25% loading was compared to sPEEK and both membranes showed similar proton conductivity and fuel cell tests results. Composite membranes with various zirconium phosphate and zirconia combined composition were described by Nunes et al.[135] Two types of polymer were investigated, sPEEK and sPEK. It was shown that the zirconia present in the polymer matrix had an amorphous structure leading to a well

associated network. A good balance of high conductivity and low water and methanol permeability was possible with a mixed zirconia-zirconium phosphate inorganic phase. DMFC performance was not improved by these composite membranes.[146] A notable reduction of methanol crossover in the fuel cell test system was measured, and these data correlated well with the data obtained with pervaporation experiments. Better chemical stability with improved DMFC efficiency was obtained when the ZrP was pretreated with n-propylamine and polybenzimidazole before mixing the ZrP solution with sPEEK.[146,147]

A zeolite-ZrP incorporated inorganic system in a sPEEK matrix was studied by Tripathi et al.[148] The sPEEK solution contained the surfactant, cetyl pyridinium chloride, to increase the porosity of the sPEEK membranes. Swollen sPEEK membranes were soaked in a zeolite, NaX, suspension containing fine particles. Subsequently, this system was loaded with ZrP with the procedure described above. With increasing amount of ZrP, the methanol permeability was reduced and the proton conductivity enlarged, leading to good selectivities of proton conductivity to methanol permeability.

Heteropolyacids

Zaidi et al.[149] prepared nanocomposite membranes based on sPEEK with commercial heteropolyacids: molybdo- and tungstophosphoric acid (MoPA resp. TPA). Both HPA-sPEEK composite membranes were stable over a period for 9 months. This was verified by proton conductivity measurements before and after this period. The proton conductivity of TPA was higher than MoPA. It is remarkable, that the same group reported on the loading of TPA onto the pores of the molecular sieve MCM-41 to prevent leaching out the membrane several years later.[150,151] These membranes showed promising results, because of the high characteristic factor defined as the ratio of proton conductivity and methanol permeability. No further stability characteristics were given. Ponce et al.[152] studied the incorporation of heteropolyacids combined with an inorganic phase consisting zirconia or silica

containing imidazole-groups. Both inorganic networks were prepared by sol-gel. The additional inorganic phase was to prevent HPA to leach out of the membrane and to reduce methanol permeability. Two commercial HPAs, TPA and MoPA, were tested and compared to non-commercial HPAs. The polymeric matrix was sPEK obtained from Fumatech with a sulfonation degree between 40% and 50%. Best results, with highest reduction of methanol flux across the membrane without diminishing proton conductivity, were obtained by modifying the heteropolyacid with the silane and using also the silane as precursor for the inorganic network. Tungstosilicic acid was loading on silica-alumina mixtures with various compositions by Ismail et al.[153] Promising results in terms of selectivity of proton conductivity to methanol permeability were obtained with high HPA loading and high silica content in the inorganic composition.

2.2.4. Membranes for DEFC

Literature focused on membranes particular for DEFC applications is relatively scarce. Tan et al.[37] studied composite membranes with a sPEEK/PES blend as organic phase and silica with HPA as inorganic phase. Addition of HPA led to higher proton conductivity in comparison to the sPEEK/PES blend. A more profound study about the membrane design for DEFC is given by Fu et al.[36] Hybrid proton conducting membranes with an interpenetrating polymer network structure were prepared. In these membranes, glutaraldehyde crosslinked PVA were interpenetrated with the copolymer of 2-acrylamido-2-methyl-propanesulphonic acid and 2-hydroxy-ethyl methacrylate crosslinked by poly(ethylene glycol) dimethacrylate. Silica obtained from the *in situ* sol-gel hydrolysis of TEOS was uniformly dispersed in the polymer matrix. PVA based membranes exhibited lower swelling behavior with increasing alcohol concentration, whereas the swelling in methanol was higher than in ethanol. Alcohol permeability decreased with increasing silica content in the membrane. The characteristic factor was in all cases better than Nafion®. Another publication dealing with membranes for application in DEFC comes from our

group.[154] Here, the behavior of proton conductive sPEEK membranes in ethanol-water environments is described. This work is also (more profoundly) described in Chapter 4.

2.2.5. Summary of non-fluorinated membranes

Many non-fluorinated specialty polymers have been functionalized, characterized and tested for application in direct alcohol fuel cells. A promising polymer type are the poly(arylene ether ketone)s. Sulfonation of these polymers lead to structures which can nanoseparate similar to Nafion®. Sulfonation degree has a significant impact on swelling behavior, fuel crossover, and proton conductivity. sPEEK is applicable with sulfonation degrees ranging from 40 to 90%. Modifications are mainly based on reinforcement of the membrane of high sulfonated sPEEK or making low sulfonated sPEEK more proton conductive. Various modifications are described like fabric supporting, crosslinking and polymer blending. The main focus lies on inorganic-organic mixed-matrix systems. The presence of an inorganic phase resulted in nearly all cases in a reduction in alcohol crossover. Similar to PFSA modifications, inorganic materials used by various groups are metal oxides, prepared by sol-gel or commercially obtained, layered silicates, zeolites, and zirconium phosphates. Heteropolyacids are mainly used in combination with an inorganic phase to prevent leaching out. Modification of the inorganic phase is preferable to increase the membrane stability. Basic modification by means of basic polymers or basic silanes appeared to be promising for this property. The bulk of membrane developments are based on the direct methanol fuel cell, whereas few studies are known about membrane development for direct ethanol fuel cells.

Chapter 3

Methodology

In this chapter, the methods and procedures are presented, which were used to characterize the polymers and membranes. Methodology is divided in three main domains: i) material analysis (**Section 3.1**), ii) membrane characterization (**Section 3.2**), and iii) fuel cell tests (**Section 3.3**).

Membrane characterization is subdivided in two sections: proton conductivity and membrane behavior in water-ethanol systems. The latter involves static measurements, like liquid uptake and sorption, and dynamic measurements to obtain information about the transport of permeating components through the membrane.

3.1. Material analysis

3.1.1. Acid-base titration

Titration is an often applied technique to determine the *ion exchange capacity* (*IEC*). In case of proton exchange materials containing sulfonic acid groups, the equivalence point of the acid-base titration is at a pH of 7. The following titration procedure is standard for all studied materials.

About 0.2 g of polymer/membrane were freshly protonated in 1 M HCl for 20 h. Then the polymer/membrane was rinsed extensively with deionized DI water. After that, the polymer/membrane was air-dried followed by drying in a vacuum oven (80 °C/ <100 mbar/16-20 h). The dry weight was determined before transferring the polymer/membrane into 2 M NaCl and stirring for 20 h to exchange the protons with

the sodium cations. Back titration was performed with 0.05 M NaOH automatically with a titroprocessor (Metrohm). The measurement was performed in duplicate.

The ion exchange capacity is defined as:

$$\mathrm{IEC} = \frac{\text{ion exchange active groups}}{\text{dry mass of the membrane}} \qquad \textit{Eq. 3.1}$$

The *degree of sulfonation* (*DS*) of the polymers and the polymeric membranes (already defined in **Section 2.2.1**) is related to the ion exchange capacity by:[119,122]

$$DS = \frac{M_{w,p} IEC}{1 - M_{w,f} IEC} \quad \rightarrow \quad IEC = \frac{DS}{M_{w,p} + DS \cdot M_{w,f}} \qquad \textit{Eq. 3.2}$$

where $M_{w,p}$ is the molecular weight of the non-functional polymer repeat unit (288.29 g mol^{-1}) and $M_{w,f}$ the molecular weight of the functional group with the counter ion (-SO_3H; 81.06 g mol^{-1}). The *DS* is 100% when all the monomers bear a sulfonic acid group. The maximum *IEC* of sPEEK with single sulfonated monomers is 2.71 mmol g^{-1}.

<u>Accuracy</u>

The accuracy of the titration method is determined by i) the mass determination with a precision balance; ii) the titration volume and iii) the concentration of the NaOH-solution. The concentration of the NaOH solution (titer) was determined by titrating a 0.1000 ± 0.0003 M HCl-solution. The relative error in *IEC* is calculated with the *propagation of error* method and is 0.6%.

3.1.2. ^{1}H nuclear magnetic resonance spectroscopy (NMR)

The ^{1}H-NMR spectroscopy is used to quantify the sulfonic acid groups in the copolymer. The presence of the sulfonic acid groups accounts for a significant down-field shift of the proton on the position next to this group. The fundamentals of the characterization of sulfonated polymers by NMR is given by Nolte et al.[111] This technique is nowadays a common method for verifying the degree of sulfonation.[119,126,130,155] The equation for determining the *DS* from the integrals of the NMR peaks is:

$$\frac{DS}{12-2DS} = \frac{AH_E}{\sum AH_{A,\,A',\,B,\,B',\,C,\,D}} \qquad \textit{Eq. 3.3}$$

The nomenclature of the aromatic protons is given in **Figure 3.1**.

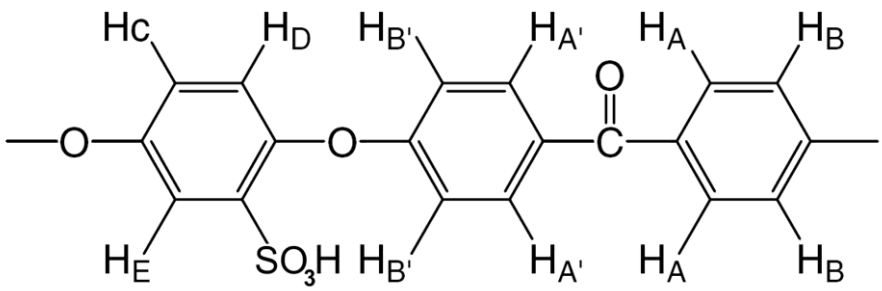

Figure 3.1: Nomenclature of the aromatic protons for the sPEEK repeat unit.

The ^{1}H-NMR spectra were recorded on a Bruker Advance DPX 250 NMR spectrometer at a resonance frequency of 250.13 MHz. Polymer solutions between 0.5 and 5% were prepared in dimethylsulfoxide-d_6 (DMSO-d_6), and tetramethylsilane (TMS) was used as the internal standard.

3.1.3. Gel permeation chromatography (GPC)

Gel permeation chromatography is a separation technique where molecules are separated based on differences in molecular size. GPC is performed in an organic mobile phase in which the polymer is solved. Dimethylacetamide (DMAc) was used because of the good solubility of sPEEK in this organic solvent. The sample is passed through a porous media, where the smaller molecules passing a longer path as the larger molecules.

Samples were prepared by solving 20 mg of polymer in 6 ml DMAc. These samples (injection volume of 100 µl) passed through the PLgel mixed column (Latek Labortechnik GmbH., inner diameter 7.5 mm and length 60 cm) by means of a DMAc mobile phase. The volume flow was 800 µl min^{-1} and the system temperature was 60 °C. Detection was done by a Knauer refractive index detector. The system was calibrated with polystyrene standards (PSS: PS25019; PS9039; PS30039; PS26058; PS19117C; PS30121).

3.1.4. Thermogravimetric analysis (TGA)

Thermogravimetric analysis determines the thermally induced weight change of a sample as a function of temperature. The apparatus used was TGA Q500 V6.7 Build 203 (Universal V4.1D TA Instruments). A 5 mg sample was heated in air with 20 K min^{-1} till 900 °C where the temperature was kept constant for 10 min. The mass of the remaining inorganic matter was compared to the dry mass of the starting material. The membrane contained absorbed water and, therefore, the inorganic loading was determined by:

$$L_{TGA} = \frac{m_{200\,°C} - m_{900\,°C}}{m_{900\,°C}} \cdot 100\% \qquad \textit{Eq. 3.4}$$

3.1.5. Wavelength dispersive X-ray fluorescence (WDXRF)

Wavelength dispersive X-ray fluorescence is used for quantitative analysis of broad range of elements. This technique involves the measurement of the wavelength spectrum of the emitted radiation, e.g., by using a diffraction grating or crystal.

Samples with a mass of 250 mg were dried at 110 °C for determining the dry weight of the sample. After that, the sample was ashed till a mass equilibrium was reached followed by Borax digestion from which a glass disc was prepared. The content of the selected element in the samples was measured with a Philips PW 1220 WDXRF spectrometer.

3.2. Membrane characterization

3.2.1. Scanning electron microscopy (SEM)

Scanning electron micrographs were taken with a scanning electron microscope (LEO 1530VP) to investigate the membrane morphology. The samples were prepared by fractioning in liquid nitrogen and sputtering with platinum with a Bal-tec MED 020 apparatus.

3.2.2. Density of dry membranes

The density of dry membranes was calculated by means of the dry mass, diameter and thickness of membranes. To this, at least two membrane samples of the same membrane batch were taken with a diameter of approximately 25 mm. Before determining the dry mass and dimensions, the samples were dried in a vacuum oven (80 °C/<100 mbar/16-20 h). The diameter was determined in threefold with 60° rotation in between. Membrane thickness was determined eightfold, four times in the inner circle and four times in the outer circle. These membranes were also used in the swelling experiments at RT (**Section 3.2.4.1**).

Accuracy

The error in dry density is determined by the *propagation of error method*. The deviation in i) dry mass is set at 0.5% (precision balance), ii) dry diameter at 1% (ruler bar, three points), and iii) thickness (2% micrometer, eight points). Maximum deviation in dry density of the membranes was 2.3%.

3.2.3. Proton conductivity

The proton conductivity was measured by AC impedance spectroscopy using an electrochemical workstation, IM6 (Zahner, Kronach). The measurements were carried out in potentiostatic mode over the frequency range typically between 1 Hz – 1000 Hz with an oscillating voltage of 5 mV.

Two different setups were used to determine the in-plane proton conductivity. Proton conductivity of the membranes at RT and in wet condition in water or ethanol-water mixtures was determined with the spring tips configuration (STC) (**Figure 3.2**, right).[156-158] This setup consisted of four spring tip electrodes (spring probes, P19-2221, Harwin). Circular shaped membranes with a diameter of 25 mm were first pretreated in 1 M HCl for 20 h. After excluding the acid by thoroughly rinsing, the membranes were stored in the liquid (typically water, 2 M or 4 M ethanol) for another 20 h before measuring the proton conductivity. The proton conductivity, $\sigma_{H^+}(STC)$, was calculated with:[157]

$$\sigma_{H^+}(STC) = \frac{\ln 2}{\pi} \frac{1}{\ell \cdot |Z|_{-2^\circ<\varphi<2}} \cdot \frac{1}{f_1 \cdot f_2} \qquad \textit{Eq. 3.5}$$

The proton conductivity is inversely proportional to the membrane thickness (ℓ) and the average impedance ($|Z|_{-2^\circ<\varphi<2^\circ}$). The latter is the average impedance of three frequency series where the phase is between -2° and 2°.[158] In this area, it was assumed that the impedance equals the membrane resistance. This measurement was repeated with two other membranes of the same membrane batch to exclude

errors. The two correction factors f_1 and f_2 are the finite thickness and the finite width correction respectively.[156,159]

Another setup was used to determine the proton conductivity as a function of temperature and relative humidity. This platinum wire configuration (PWC) was based on the setup proposed by Zadowzinski[160] and is repeatedly described in

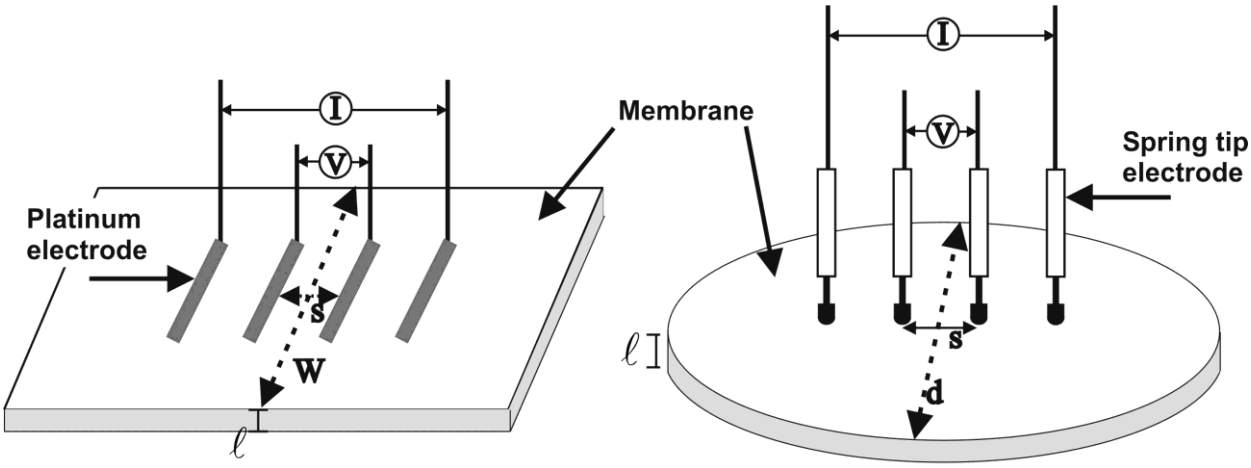

Figure 3.2: Schematic representation of the platinum wire configuration (PWC) (left) and the spring tips configuration (STC) (right).

literature.[161,162] The setup consisted of four platinum wires (diameter of 0.5 mm) with 15 mm length and 17 mm distance between them (**Figure 3.2**, left). The dimensions of the membrane sample were 50 mm by 100 mm. The electrodes were pressed on the membrane with 2 kg cm^{-2} and the measurements were performed in a climate chamber (ESPEC). Again the membranes were pretreated in 1 M HCl for 20 h followed by extensive rinsing with DI water. The membranes were equilibrated for each measurement for 10 h at the measuring temperature and humidity. The proton conductivity, $\sigma_{H^+}(PWC)$, was calculated as follows:[161]

$$\sigma_{H^+}(PWC) = \frac{s}{|Z|_{-2°<\varphi<2} \cdot W \cdot \ell} \qquad \textit{Eq. 3.6}$$

The membrane cross-sectional surface is the product of the membrane thickness by the width of the membrane sample (W), and s is the distance between the inner electrodes. $|Z|_{-2°<\varphi<2°}$ is the average impedance of five frequency series recorded with a time interval of 5 min.

Accuracy

The average impedance obtained with the STC and the PWC method is typically determined by averaging 250 to 800 and 200 to 500 measuring points respectively. The relative error in membrane thickness is 4%. In case of the PWC, the relative errors in width of the membrane sample and the distance between the electrodes are 1% and 3% respectively. The accuracy is mainly determined by the standard deviation of the impedance results. This results in relative errors for both methods varying typically between 4% for low proton conductivities (< 10 mS cm^{-1}) and 12% for high proton conductivities (> 70 mS cm^{-1}).

3.2.4. Membrane behavior in water-ethanol systems

3.2.4.1. Liquid uptake and swelling degree

Room temperature

Liquid uptake determination was performed in water and ethanol-water mixtures with various ethanol concentrations at RT. The diameter of the dry membrane samples was 25 mm. The dry weight, diameter, and thickness (m_{dry}, d_{dry} and ℓ_{dry} respectively) were determined after a drying procedure (80 °C/<100 mbar/16-20 h). After 1 day of immersion, the weight, diameter and thickness of the swollen membrane were measured (m_{wet}, d_{wet} and ℓ_{wet} respectively). This measurement was repeated several times at different days (typically three times in ten days). These longer incubation times led only to small deviations (< 3.5%). The wet weight was determined after removing the surface liquid by placing the membrane between dust-free cloths and gently pressing with 28.5 N cm^{-2}. The diameter and thickness of the membrane was

measured in total wet condition. The diameter was determined in threefold with 60° rotation in between, and the membrane thickness was determined fourfold in the inner circle of the membrane. Afterwards, the dry weight and dry dimensions were determined again to see if there were any irreversible changes. The liquid uptake of the membrane was calculated with:

$$Uptake = \frac{m_{wet} - m_{dry}}{m_{dry}} \cdot 100\% \qquad \textit{Eq. 3.7}$$

The swelling degree in surface area is determined with:

$$SD_{surface\ area} = \frac{\frac{\pi}{4} d_{wet}^2 - \frac{\pi}{4} d_{dry}^2}{\frac{\pi}{4} d_{dry}^2} \cdot 100\% = \frac{d_{wet}^2 - d_{dry}^2}{d_{dry}^2} \cdot 100\% \qquad \textit{Eq. 3.8}$$

The swelling degree based on the volume increase due to wetting is calculated with:

$$SD_{volume} = \frac{d_{wet}^2 \ell_{wet} - d_{dry}^2 \ell_{dry}}{d_{dry}^2 \ell_{dry}} \cdot 100\% \qquad \textit{Eq. 3.9}$$

<u>Various temperatures</u>

Liquid uptake and swelling degree in water as a function of temperature were performed with membranes with a diameter of 16 mm. The weight and membrane dimensions were measured after the drying procedure (80 °C/<100 mbar/16-20 h). The soaking time in water for each temperature was 45 min and the water temperature was 40 to 90 °C with 10 °C interval. The wet weight and wet membrane dimensions were determined as described in the previous section. The liquid uptake and swelling degree in surface area were calculated with **Eq. 3.7** and **Eq. 3.8** respectively.

Accuracy

Liquid uptake and swelling in surface area and volume are average values of at least three measurements performed at different days. The error in uptake is compiled of the error in the precision balance and the drying of the wet membrane during the measurement. The deviation of the dry and wet measurement is set at 0.5% and 1% respectively. This results in a relative error in uptake of 9%. The relative error in swelling in surface area is determined similarly. It should be noted, that the surface is proportional to square of its diameter. When the error in diameter is set at 1%, the error in swelling in $SD_{surface\ area}$ determined by the *propagation of error method* is 2%. In case of the swelling in volume, the surface area has to be multiplied by membrane thickness, which has a relative error of 4%. The relative error in SD_{volume} is, therefore, 10%.

3.2.4.2. Sorption behavior

Sorption experiments were done to determine the equilibrium concentration of water and ethanol in the membrane. The experiment was similar to that described in literature.[163,164] Membrane samples of 1.5 - 3 g, dependent on the *IEC* of the membrane, were immersed in 2 M ethanol for 1 day. The sample was taken out of the liquid and surface liquid was removed as described in **Section 3.4.1**. The membrane was placed in a glass tube and desorption under vacuum was performed. The evaporated gas was collected in a cold-trap in liquid nitrogen. The mass of the sample was compared to the mass decrease of the membrane sample. The ethanol concentration of the sample was determined with a refractometer (A. Krüss Optronic, DR301-95). The sorption selectivity was determined by:

$$\text{Sorption selectivity} = \frac{w_{i,\ membrane} / w_{j,\ membrane}}{w_{i,\ sorption\ liquid} / w_{j,\ sorption\ liquid}} \qquad \textit{Eq. 3.10}$$

w is the weight fraction of component *i* or *j* in the desorbed liquid and the initial ethanol-water mixture given by the subscipts *membrane* and *sorption liquid* respectively.

Accuracy

The sorption selectivity is mainly determined by the accuracy of the concentration determination. Based on a 3% error in concentration, the relative error in sorption selectivity is 6%.

3.2.4.3. Ethanol permeability

Ethanol permeability is determined in two different systems: i) liquid-liquid (L-L) system and ii) liquid-gas (L-G) system. These systems differ in driving force and concomitant fluxes of the measuring components (water and ethanol). Concentration difference is the driving force in the L-L system, resulting in opposite flux directions. Partial pressure is the driving force in the L-G system (also called pervaporation), and the fluxes are in the same direction. Both methods will be applied to describe the permeation behavior through the membrane, because water and ethanol transport through the membrane is not fully unambiguous in direct alcohol fuel cells.

Liquid-liquid systems

Ethanol permeability was determined in a diffusion cell as shown in **Figure 3.3**. The cell consisted of a water (1) and an ethanol (2) compartment (compartment W and E respectively). The membrane (3) was placed between two perforated metal supports (5) and was sealed with O-rings (4). The effective membrane surface was 14.7 cm^2. Both compartments were stirred magnetically to provide agitation. A pipette (6) was placed on the water compartment to monitor the volume change during time interval Δt. A syringe (7) was used to collect samples of 0.25 ml. In the ethanol compartment, the ethanol solution was circulated by means of a pump (8) to assure a constant

concentration on the ethanol side. The temperature of the supply (~400 ml) (9) was regulated with a water bath (10). Heating channels in the diffusion cell were connected to the water bath to assure a constant temperature in the whole system.

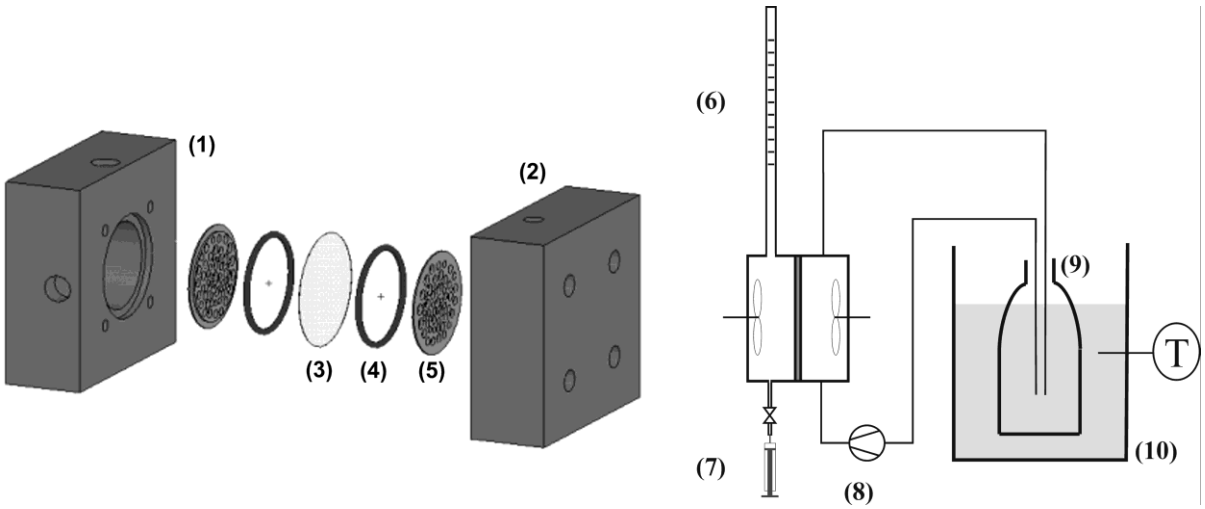

Figure 3.3: Schematic representation of the diffusion cell (left) and the setup (right).

Prior to testing, the membranes were pretreated for at least 16 h in an ethanol-water mixture with the same ethanol concentration as used on the ethanol side with the measurement. The ethanol concentration in the ethanol compartment was typically 2 M or 4 M ethanol and assumed constant during the measurement, because of the ten times larger volume in comparison to the water side (concentration decline < 7.5%). The ethanol concentration was determined with a refractometer (A.Krüss Optronic, DR301-95) and the measurements were performed at 25, 40, 50 and 60 °C.

Besides the ethanol permeability, the water permeability can also be monitored. The flux directions however are in opposite directions. The permeability coefficients of ethanol and water ($P_{ethanol}$ and P_{water} respectively) are determined based on Fick's diffusion equation:

$$\frac{C_{W,ethanol}(t_i)V_{W,ethanol}(t_i)}{\left(C_{E,ethanol}(t_i)-C_{W,ethanol}(t_i)\right)}\frac{\ell}{A}=P_{ethanol}\left(t_i-t_{i-1}\right) \qquad \text{Eq.3.11}$$

$$\frac{C_{W,water}(t_i)V_{W,water}(t_i)}{\left(C_{W,water}(t_i)-C_{E,water}(t_i)\right)}\frac{\ell}{A}=-P_{water}\left(t_i-t_{i-1}\right) \qquad \textit{Eq. 3.12}$$

The concentration difference over the membrane is in the denominator in left hand side of equations **Eq. 3.11** and **Eq. 3.12**. The molar increase in ethanol (**Eq. 3.11**) or decrease in water (**Eq. 3.12**) in time interval (t_i - t_{i-1}) is determined with the concentration and volume of both substances at the start and end of the measurement. A and ℓ are the membrane area and thickness respectively. The permeability coefficients are obtained by plotting the left hand side of **Eq. 3.11** and **Eq. 3.12** against time.

Accuracy

The error in permeability coefficient is determined from the standard deviation of the slope. The accuracy of the L-L permeation system is caused by errors in concentration determination, membrane dimensions, and time interval. These errors are all lumped in the double value of the standard deviation of the slope and are determined for each measurement separately. Relative errors for the permeability coefficient are typically in the range from 6% for low permeability coefficients (< $15 \cdot 10^{-8}$ cm^2 s^{-1}) to 12% for high permeability coefficients (> $100 \cdot 10^{-8}$ cm^2 s^{-1}).

Liquid-gas systems

The setup to examine membranes in a L-G system is presented schematically in **Figure 3.4**. A circular membrane (1) with an area of 40.7 cm^2 was built into a pervaporation cell (2). The membrane was put on a sintered metal support (pore size: 10 µm) and sealed with an O-ring. The cell was continuously stirred by a built-in stirrer. The membrane was pretreated for at least 16 h in an ethanol solution with the same molarity as was used during the measurement. Before building the membrane in the cell, the membrane thickness was measured at eight positions to obtain an average membrane thickness. During the measurement, the temperature on the feed

side was kept constant by connecting a water bath to the cell. Measurements were performed with an ethanol-water mixture (ethanol concentrations typically 2 M and 4 M) (3) on the feed side at 40 °C. The permeate pressure was maintained at 13 ± 1 mbar by means of a vacuum pump (4) and permeate sample was condensed with liquid nitrogen in a glass cold trap (5). Permeate was weighed and the ethanol concentration was determined with a refractometer (A.Krüss Optronic, DR301-95). Permeate between measurements was condensed in a second cold trap (6). The system was equilibrated for one hour before the measurement started. At least five measuring points were taken for an average value.

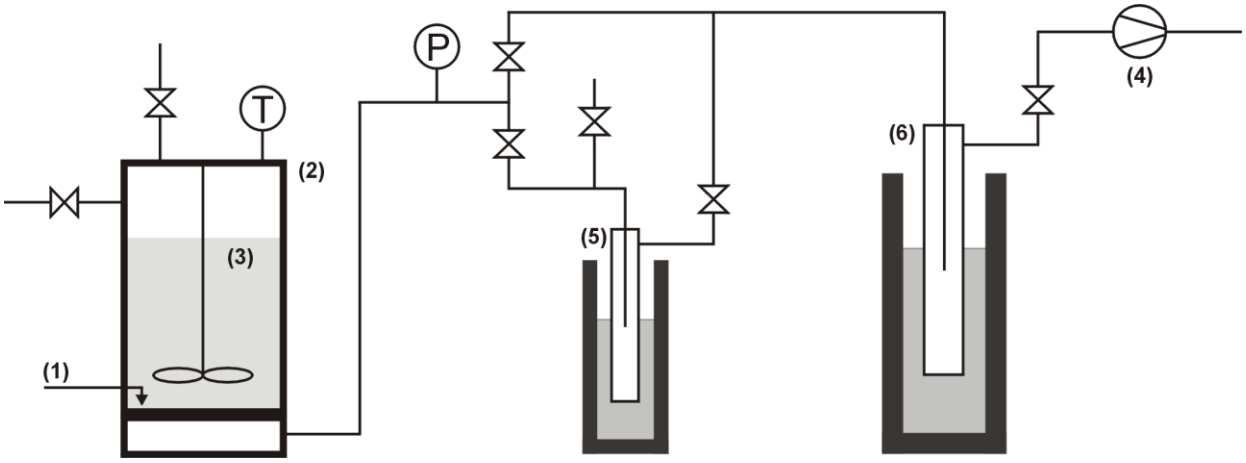

Figure 3.4: Schematic representation of the pervaporation setup (L-G system).

The partial fluxes were determined by:

$$J_i^{L-G} = \frac{w_i \, m_{tot}}{A \, \Delta t} \qquad \textit{Eq. 3.13}$$

w_i is the weight fraction in the permeate of component i collected in time interval Δt and A is the surface area.[135,163,165] The membrane permeability coefficient of component i, F_i, is given by:

$$F_i = \frac{J_i^{L-G}{}_{\ell}}{\left(x_i \gamma_i p_i^{sat} - y_i p^p\right)} \qquad \textit{Eq. 3.14}$$

x and y are the molar fractions in the liquid and gas phase respectively, γ is the activity coefficient which are determined by extrapolating the data given by Verhoef et al.[166] The activity coefficient of water and ethanol in ethanol-water mixtures with various ethanol concentrations as a function of temperature are given in **Figure 3.5**.

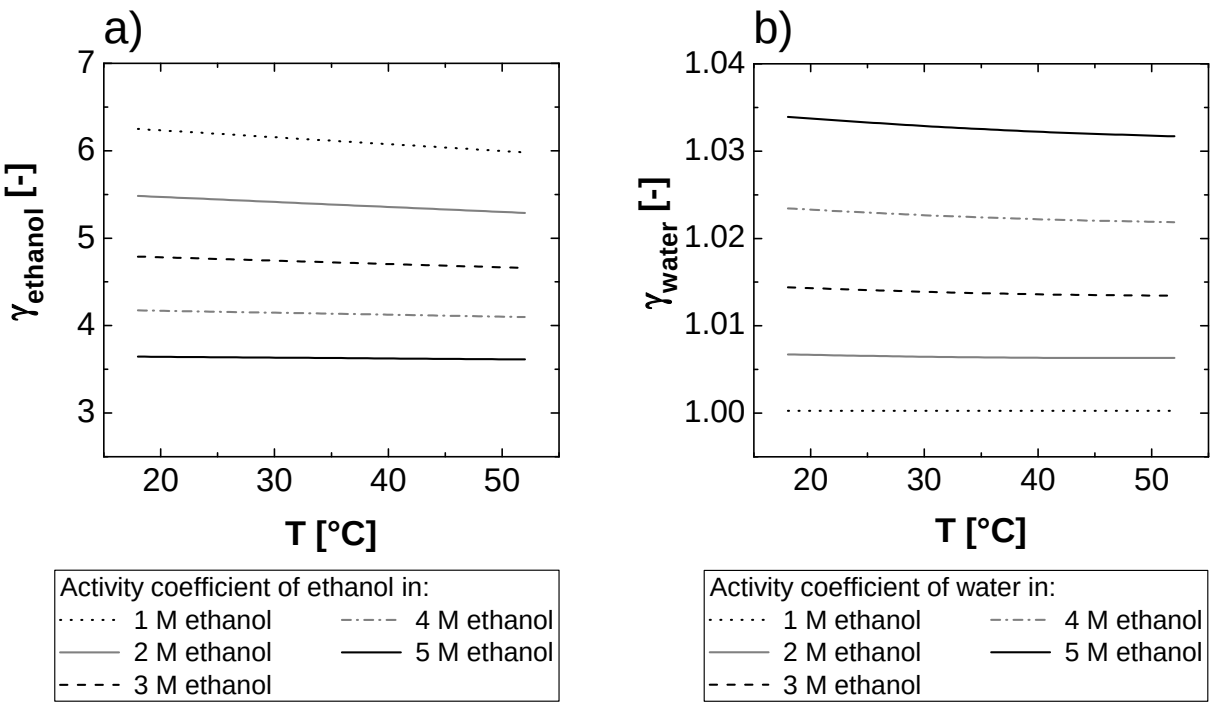

Figure 3.5: Activity coefficients for a) ethanol and b) water in ethanol-water mixtures with various ethanol concentrations as a function of temperature.

The permeate pressure is p^p and saturation pressure, p^{sat}, is calculated with the Antoine equation:[167]

$$\log p^{sat} = A - \frac{B}{T + C} \qquad \textit{Eq. 3.15}$$

In this equation the dimensions of p^{sat} and T are bar and K respectively and the Antoine constants are given in the **Table 3.1**.

Table 3.1: Antoine constants for water and ethanol for a certain temperature range.[167]

Component	Antoine Constants			Temperature range
	A	B	C	[K]
Water	5.40221	1838.675	-31.737	273 - 303
	5.20389	1733.926	-39.485	304 - 333
	5.07608	1657.793	-45.854	334 - 363
Ethanol	5.24677	1598.673	-46.424	293 - 366

The permeability coefficient divided by the membrane thickness is called the permeance. This is an often used term in pervaporation processes. The (ideal) membrane selectivity is defined by the ratio of permeability coefficients of component *i* and *j*:

$$S_{i/j} = \frac{F_i}{F_j} \qquad \textit{Eq. 3.16}$$

The separation factor is the selectivity over the whole system, which includes the transport through the membrane and component properties under certain measurement conditions, and is defined as:

$$\alpha_{i/j} = \frac{y_i / y_j}{x_i / x_j} \qquad \textit{Eq. 3.17}$$

For the membranes in this study, *i* stands for water and *j* for ethanol, since water is the preferentially permeating component.

Accuracy

The accuracy of this method is determined by the propagation in errors. The relative errors in the variables are given in **Table 3.2**. The relative error in ethanol and water permeability coefficient is 9.9%. The relative errors in relative permeability coefficient and ideal membrane selectivity are both 14.0%. The relative error in separation factor is 6.0%.

Table 3.2: Pervaporation variables and their relative errors.

Variable	Symbol	Apparatus	Relative error [%]
Concentration	w_i; x_i; y_i	Refractometer	3
Mass	m_{tot}	Balance	0.2
Membrane thickness	ℓ	Micrometer	4
Membrane diameter	d	Ruler	1
Time interval	Δt	Stopwatch	0.7
Permeate pressure	p^p	Pressure gauge	7.7

3.3. Fuel cell tests

Fuel cell tests were performed externally by Fraunhofer Institute for Chemical Technology (ICT) and Fraunhofer Institute for Solar Energy Systems (ISE). The membrane electrode assemblies (MEAs) were prepared at Fraunhofer ICT.

3.3.1. MEA preparation

PEM type MEAs were prepared by hotspraying an ink of the catalyst with appropriate amounts of Nafion dispersion and double distilled water (less than 0.05 mS cm^{-1}) onto

the membrane. As catalyst 40% Pt_3Sn/C (BASF Fuel Cells Inc.) and 60% PtRu/C (HiSPEC 10000, Johnson Matthey) were used for the anode and a precommercial PtCo/C catalyst was used for the cathode.[32] The catalyst ink was prepared by mixing at RT followed by ice-cooled ultrasonic treatment for 10 min. After that, the catalyst ink was stirred for 72 h at RT.

The membrane was pretreated in 1 M HNO_3 at RT followed by profoundly washing in water for 8 h. Subsequently, the membranes were dried and fixated in a metal frame. Spraying of the ink onto the membrane was performed between 50 and 60 °C. Multiple layers were prepared with drying in between and the metal frame was rotated over 90° before the next spray process started. Fixation of the MEA was performed at 130 °C in a drying oven, followed by calandering of the MEA with 1 kN cm^{-2} at 130 °C. The ionic binder content in the final electrode layers was 37 -38 wt-%.

Accuracy

The accuracy of catalyst determination in the electrode layers is estimated at 0.1 mg cm^{-2}. Furthermore, no further specifications were given.

3.3.2. Fuel cell setup and measurements

Fuel cell tests at Fraunhofer Institute for Chemical Technology (ICT)

Fuel cell measurements were performed in a set-up comprising a balticFuelCells GmbH. quick connect fixture qFC 25/100 for fuel cell MEAs with 25 cm^2 geometrical surface area and an Autolab PG302 potentiostat by Ecochemie connected with a 20 A booster module. The anolyte (fuel) of the cell could be directed through a home-made membrane inlet set (developed at ICT) on top of a Balzers QMS 200 mass spectrometer. Commercial gas diffusion electrodes were obtained from Acta S.p.A. Electrodes and membrane were assembled in the cell of the qFC 25/100 and fixed at a pressure of 3 bar.

The flow of 1 M ethanol at the anode was 2 ml min^{-1} and the air flow at the cathode was 500 ml (STP) min^{-1}. The measuring procedure consisted of I-V measurements at 30 °C, 40 °C and 50 °C taking three I-V loops per temperature. I-V loops were recorded at a scan rate of 1 mV s^{-1} in the voltage intervals: 0.8 V → 0.2 V → 0.8 V.

Fuel cell tests at Fraunhofer Institute for Solar Energy Systems (ISE)

Fuel cell measurements were performed in a test cell of balticFuelCells GmbH. Gas diffusion layers, Toray TGP-H-090, with a thickness of 280 µm were applied on both sides of the MEA. Gold coated stainless steel flow fields comprising 5x5 cm^2 geometrical surface area were used and the contact pressure was 2.5 bar. Current and voltage taps were separated to exclude current-dependent deviations by means of Ohmic losses with voltage measurements. Fuel cell voltages were imposed by means of a potentiostat, Solartron 1286 electrochemical interface. The 10 kHz impedance was recorded with a frequency response analyzer, Solartron 1255 HF. The readout was done with a data logger, Agilent 34907A. Control and data storage was enabled by an in-house developed Labview program. Ethanol-water mixture was supplied to the fuel cell by a PF200 pump, Ingenieurbüro Cat Zipperer GmbH., and the oxygen flow was regulated with mass flow controllers, Bronkhorst High-Tech. Oxygen was saturated with water by means of a bubble humidifier. The flow of ethanol-water mixtures (1 M; 2 M and 3 M ethanol concentration) at the anode was 5 ml min^{-1} and the oxygen flow at the cathode was 100 ml (STP) min^{-1}. All measurements were performed at 25 °C. I-V diagrams were recorded stepwise in a voltage range between 800 mV to 250 mV with 50 mV steps with duration of 180 s.

Accuracy

No specifications related to the fuel cell measurement accuracy were given. Further analysis is not possible due to the limited number of fuel cell measurements per membrane/MEA.

Chapter 4

Polymeric proton exchange membranes

In this chapter, the functionalization of PEEK, sPEEK membrane preparation, and the polymer and membrane characterization are reported. The chemical structure of sulfonated PEEK copolymer with a certain degree of sulfonation (*DS*) is presented in **Figure 4.1**. The behavior of these proton conductive membranes in aqueous-

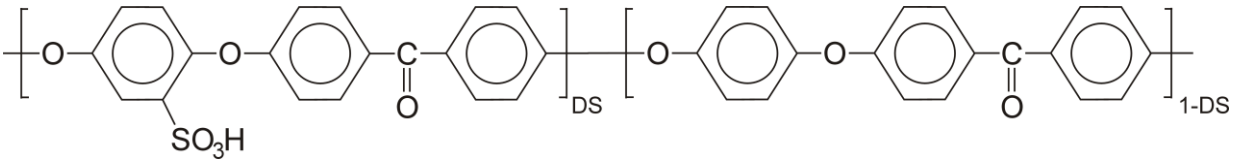

Figure 4.1: Chemical structure of sulfonated poly(ether ether ketone) with a sulfonation degree denoted as DS.

ethanolic environments is discussed. A model for the application of sPEEK membranes in these environments is given in **Figure 4.2**. In aqueous systems, the polymer swells due to the hydration of the hydrophilic sulfonic acid groups. Liquid uptake results in swelling of the polymer structure with a concomitant increase in free volume. This swelling behavior influences the proton diffusion as well as the diffusion of water and ethanol. Polymers with various sulfonation degrees are prepared by regulating the sulfonation time or sulfonation temperature. Liquid uptake and swelling characteristics of the polymer membranes are investigated at room temperature. Membrane stability as a function of temperature (up to 80 °C) is tested only in water. The proton conducting properties of the membranes are investigated with impedance spectroscopy in water and water-ethanol systems. The ethanol and water transport

through the membrane is studied in liquid-liquid and liquid-gas systems, because the unclarity of transport mechanism in the actual DEFC.

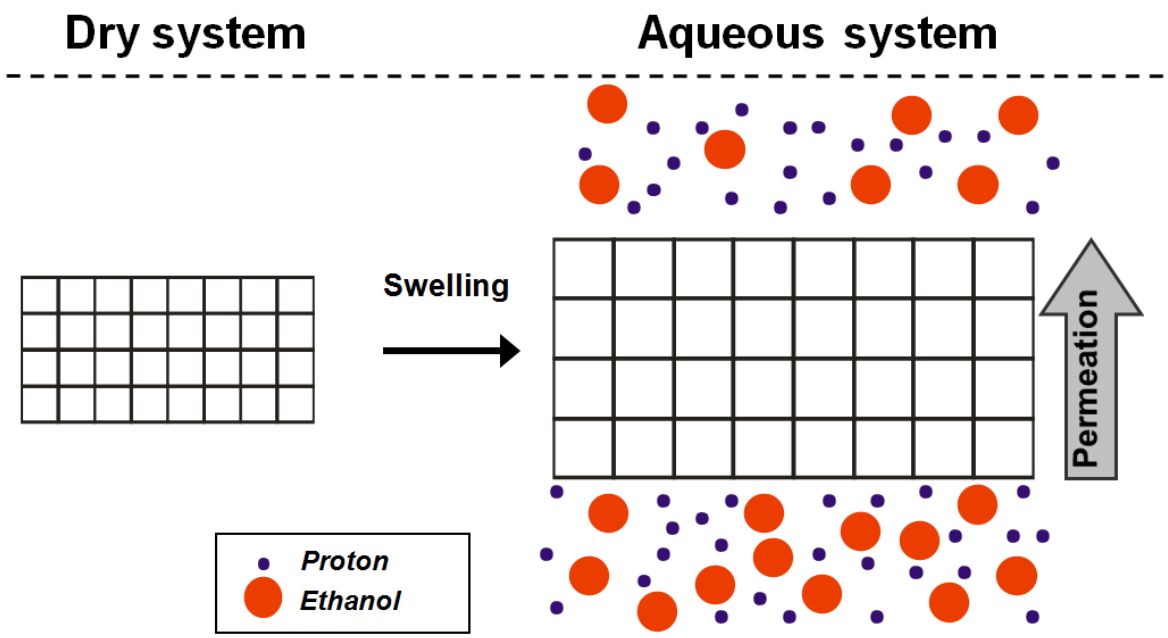

Figure 4.2: Model for the application of a proton conductive sPEEK membrane in ethanolic-aqueous system.

4.1. Membrane preparation

4.1.1. Chemicals

Poly(ether ether ketone) (PEEK, 450G, pellets) was obtained from Victrex® and sulfuric acid (95 - 97%) from Fluka. N-methyl-2-pyrrolidone (NMP, 99.8%) and hydrochloric acid (HCl, 25%) were obtained from Roth. All chemicals were used as received without further purification.

4.1.2. Sulfonation of PEEK

The degree of sulfonation of sPEEK is mainly dependent on sulfonation time ($t_{sulfonation}$) and sulfonation temperature ($T_{sulfonation}$).[116,119,121] Both parameters are

studied in this chapter, and differences in sulfonation procedure are given in the following sections.

4.1.2.1. DS($t_{sulfonation}$)

The sulfonation of PEEK was performed similar to the procedures given in the literature.[119,155] The sulfonation was carried out in a 1 liter jacketed flat bottom flask fitted with a mechanical stirrer. Sulfuric acid was tempered at 35 °C for one hour. Subsequently PEEK pellets were added to obain a 1/20 (weight/volume) mixture. The pellets were solved and concomitant sulfonation of the polymer occurred. After a certain sulfonation time, $t_{sulfonation}$, typically 16, 19, and 22 hours, the solution was cooled below 15 °C in 45 min to arrest the reaction. The viscous solution was quenched in ice water and washed several times until the pH was higher than 6. The polymer was wrung out and transferred into a 60 °C drying oven for 6 h. After that, the polymer was transferred to a vacuum oven (80 °C/<100 mbar) for 20 h.

4.1.2.2. DS($T_{sulfonation}$)

The sulfonation procedure was similar to the one described above, but now the sulfonation temperature was varied. To this PEEK was dissolved in sulfuric acid for 16 hours at 25 °C. Then the solution was heated to a certain temperature between 35 °C and 60 °C (typically 35 °C, 40 °C, 45 °C, 50 °C, 55 °C, or 60 °C) and kept at this temperature for 5 h. The solution was cooled below 15 °C in 45 min to arrest the reaction. The post treatment was identical to DS($t_{sulfonation}$).

4.1.3. Membrane formation

A polymer solution was prepared by dissolving sPEEK in NMP in a ratio of 0.12 (weight/volume). The solution was stirred at room temperature for at least three days. In case of poorly dissolving polymers (low degree of sulfonation), the solution was heated to 120 °C for 3 h. Polymer membranes were prepared by a casting and

solvent evaporation process.[145] Before casting, a glass plate was cleaned with NMP followed by acetone. Then, a film of polymer solution was cast with a 0.6 mm doctor blade. The solvent was evaporated by drying in an oven at 70 °C for 20 h followed by drying in a vacuum oven (100 °C/<100 mbar) for 20 h. The membranes, which adhered to the glass plates, were soaked in a deionized water (DI water) bath for 2 h. In this step, the remaining solvent was eliminated and the membranes were peeled off from the glass plate. Protonation was carried out in 1 M HCl for 1.5 h followed by soaking the membranes again in DI water for 2 h. The membranes were air dried and stored until further characterization. The thickness of the membranes varied between 30 and 40 µm.

4.2. Results and discussion

In this section, results are presented and discussed of the polymers and membranes prepared with different sulfonation routes. Membrane behavior in aqueous-ethanolic environment is studied as a function of *DS* as well as the proton conductive properties.

4.2.1. Ion exchange capacity and degree of sulfonation

The ion exchange capacity and the degree of sulfonation of the polymers and the membranes are determined by titration. In addition the *DS* of the polymers is measured by NMR.

DS($t_{sulfonation}$)

Various batches are prepared with this sulfonation procedure. The amount of batches together with the average values of *IEC* and *DS* are presented in **Table 4.1**.

Table 4.1: Average values for IEC and DS for DS($t_{sulfonation}$).

$t_{sulfonation}$ [-]	# Batches [-]	IEC [mmol g^{-1}]	DS [%]
16	8	1.388 ± 0.024	45.1 ± 0.9
19	6	1.667 ± 0.016	55.6 ± 0.6
22	4	1.791 ± 0.009	60.4 ± 0.4

Huang et al.[119] reported a kinetic study on the sulfonation of PEEK. *DS* was related to sulfonation time with:

$$-\ln(1-DS) = k \cdot C_{H_2SO_4} \cdot t_{sulfonation} \qquad \textit{Eq. 4.1}$$

This was valid with the assumption that the sulfonation is a second order reaction and that at first all monomers must be sulfonated (*DS* = 1) before further substitution on the sulfonated monomers can take place. The concentration of sulfuric acid in the solution is obviously much higher than the concentration of PEEK and is 18.0 M (assumption: 96 % H_2SO_4). When -ln(1-*DS*) is plotted against sulfonation time, a linear dependency must be found according to **Eq. 4.1**. These data are presented in **Figure 4.3**. The reaction rate coefficient is $3.13 \cdot 10^{-3}$ L mol^{-1} h^{-1}. Huang et al. found $5.05 \cdot 10^{-3}$ L mol^{-1} h^{-1} (at 36 °C) with the sulfonation of PEEK (Victrex, 38.400 g mol^{-1}, powder). They first solved the PEEK powder in 1 h at 22 °C and found an intercept with the y-axis at -ln(1-*DS*) = 0. The presented experimental data are obtained with PEEK pellets, where a longer dissolving time is expected in comparison to PEEK powder (presented in literature). The intercept with the x-axis in **Figure 4.3** is 5.1 h. representing the practical dissolving time for PEEK pellets at 35 °C.

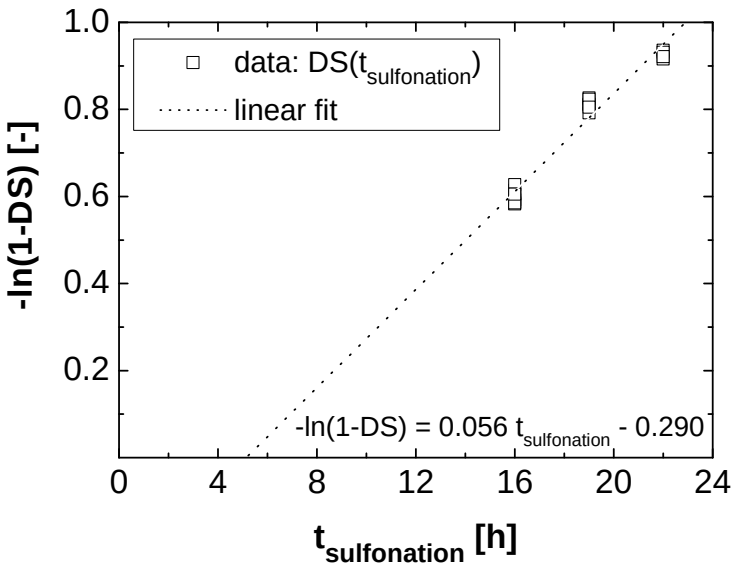

Figure 4.3: Determination of the reaction rate coefficient.

DS($T_{sulfonation}$)

The sulfonation proceeds with dissolving PEEK in sulfuric acid at 25 °C followed by sulfonation at a certain sulfonation temperature. This is a similar approach as described by Do et al.[120] In the dissolving step, sulfonation takes place to a small extent. The amount of ion exchangeable groups is measured with titration and is 0.177 mmol g^{-1}. *DS* and *IEC* of the final membranes as a function of the sulfonation temperature are shown in **Figure 4.4**. There is a linear relationship in that temperature interval and the *DS* can be well controlled or predicted. In all cases the values measured by NMR are slightly higher. With a different titration method Huang et al.[119] determined values which are consistent with the presented results. It is remarkable, that they also observed a constant difference between both methods, but in all cases the titration values were slightly higher. For all further calculations, the titration values are used. Reasons for this are:

- A lower measureable *DS* limit with titration and, therefore, avoiding difficulties of dissolving low sulfonated polymers in case of NMR sample preparation.
- Time, effort and expenses, because the NMR-measurements are performed externally and the titration measurements in our own laboratory.

- Expected complications when these polymers should be compared to inorganic-organic hybrid materials, where dissolving in a solvent in case of NMR sample preparation is complicated or not possible.

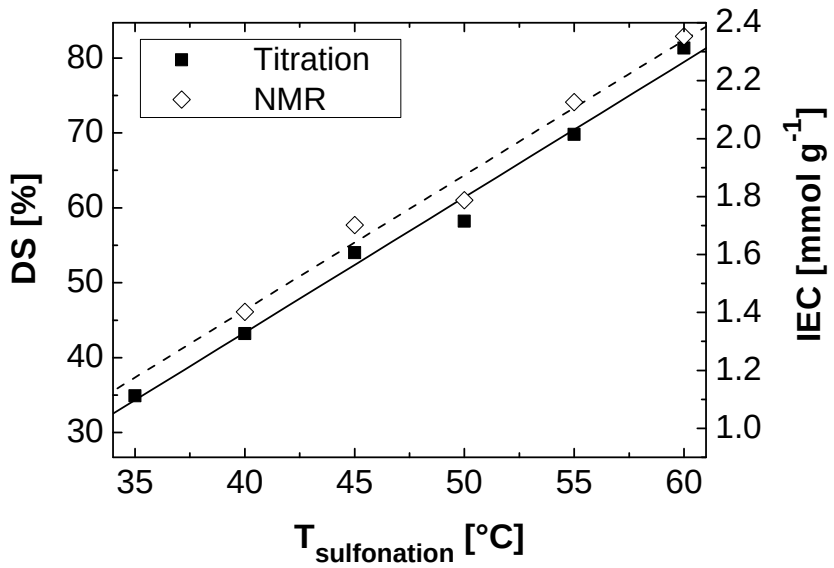

Figure 4.4: Ion exchange capacity (IEC) and degree of sulfonation (DS) as a function of sulfonation temperature determined by titration and ^{1}H-NMR.

The reaction rate coefficient is dependent on temperature and therefore described by the Arrhenius equation:

$$k = k_0 e^{-\frac{E_a}{RT}} \rightarrow \quad \ln k = \ln k_0 - \frac{E_a}{RT} \qquad \textit{Eq. 4.2}$$

The reaction rate coefficient for each sulfonation temperature is calculated with **Eq. 4.2**. To this, the *DS* is corrected by subtracting the initial sulfonation (0.177 mmol g^{-1}). The Arrhenius plot is given in **Figure 4.5**. The sulfonation time is 5 h and the sulfuric acid concentration is again 18 M. The activation energy is 43.5 kJ mol^{-1} and the pre-exponential factor (k_0) is 9.4·10^4 L mol^{-1} h^{-1}. In this case, the

activation energy for sulfonation is lower and the pre-exponential factor is about 6 orders of magnitude lower in comparison to the values of Huang et al.[119] (E_a = 18.8 kCal mol^{-1} (71.1 kJ mol^{-1}); k_0 = 1.31·10^{11} L mol^{-1} h^{-1} respectively). These differences can be explained by the determination of the reaction rate constant. Huang et al. determined this rate constant with different sulfonation times at a certain temperature. The rate constant determined in this work is determined by the slope obtained from the sPEEK characteristics and the zero point. The reaction rate coefficient at 35 °C obtained with the results of DS($t_{sulfonation}$) and DS($T_{sulfonation}$) are 3.13·10^{-3} L mol^{-1} h^{-1} and 4.04·10^{-3} L mol^{-1} h^{-1} respectively.

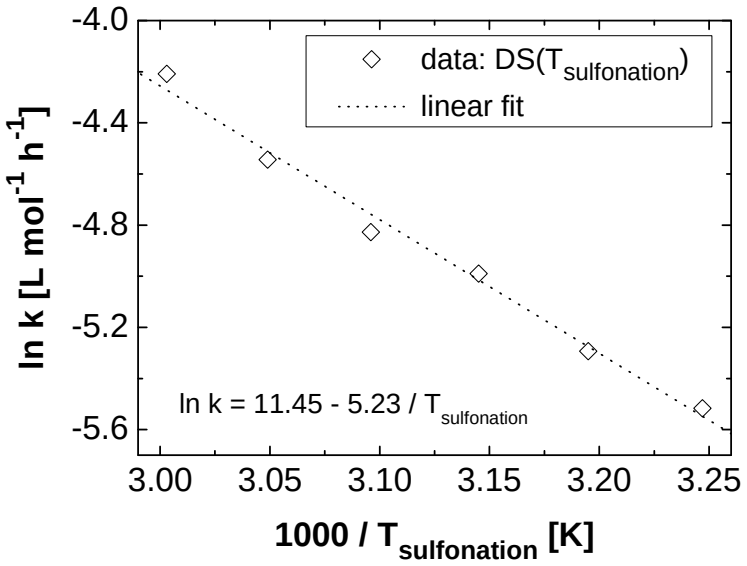

Figure 4.5: Dependence of reaction rate constant of the sulfonation reaction on temperature.

4.2.2. Molecular weight and polydispersity

This technique is applied to characterize the polymer with respect to molecular mass and homogeneity. The gel permeation chromatography (GPC) results of sPEEK polymers of the DS($T_{sulfonation}$)-series are presented in **Figure 4.6** and **Table 4.2**. Polystyrene (PS) standards are used to calibrate the GPC apparatus. Differences in chemical structure and behavior between sPEEK and PS result in a deviation of the

absolute molecular masses. Polydispersity defined as the M_w/M_n ratio is a quantification of the molar weight distribution. Results of sPEEK among one another are comparable.

Molecular weight and polydispersity of sPEEK polymers below 1.73 mmol g^{-1} are similar (Table 4.2). Lower molar masses of sPEEK with an *IEC* of 1.15 mmol g^{-1} are attributed to the poorer solubility. At *IEC*s higher than 2 mmol g^{-1}, molar weight distribution broadens and a bimodal distribution is observed (**Figure 4.6**). It is remarkable, that the result of the polymer with the highest *IEC* shows a larger molar mass and lower polydispersity than the polymer with an *IEC* of 2 mmol g^{-1}. This phenomenon is attributed to coincidental deviation because of the limited measured samples. Obviously, the polymer deteriorates to a large extent when the sulfonation temperature is equal to or more than 55 °C (in 5 hours sulfonation time). It is expected, that all polymers with an *IEC* of 1.73 mmol g^{-1} or lower have a monomodal distribution with a polydispersity around 2.5.

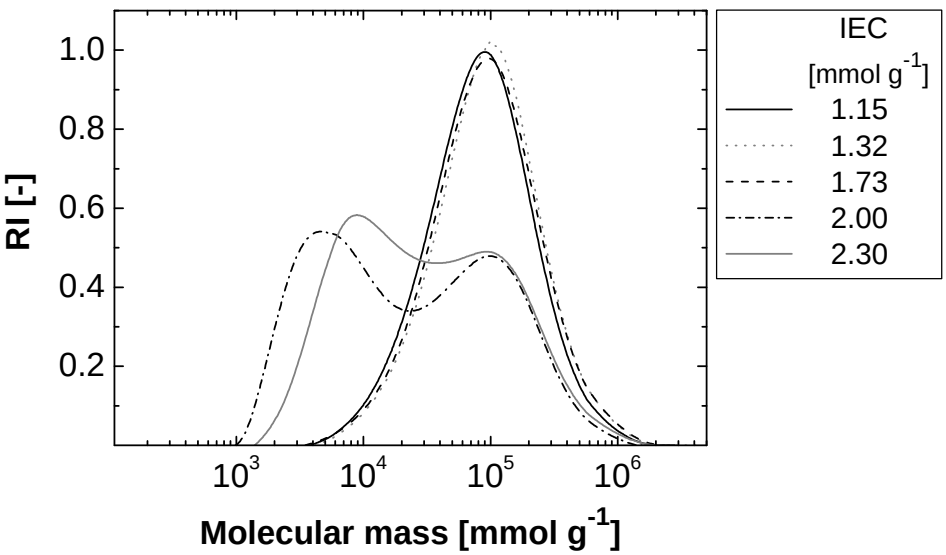

Figure 4.6: GPC diagrams of sPEEK polymers with various sulfonation degrees.

Notable is, that experiments to relate the *IEC* of sPEEK with the molar weight and polydispersity determined with GPC, are not found in literature. Wu et al.[168] measured the weight-average molar weight with GPC and also used PS standards for

calibration. They found a M_w of 256000 g mol^{-1} for sPEEK with a *DS* of 64%. Xing et al.[121] measured a weight-average molar mass of 34100 g mol^{-1} with sPEEK with a *DS* of 79 %. GPC results have to be treated critically. Ion-containing sPEEK can have a size-excluding effect due to the interaction between ionic groups. Interactions between sPEEK and various GPC columns can have an impact on the molar weights and polydispersity as well.

Table 4.2: Weight-average and number-average molar masses and heterogeneity index of sPEEK polymers of the DS($T_{sulfonation}$)-series.

IEC [mmol g^{-1}]	DS [%]	M_w [g mol^{-1}]	M_n [g mol^{-1}]	M_w/M_n ratio
1.15	35	$1.29 \cdot 10^5$	$5.20 \cdot 10^4$	2.48
1.32	43	$1.46 \cdot 10^5$	$5.91 \cdot 10^4$	2.47
1.73	58	$1.44 \cdot 10^5$	$5.55 \cdot 10^4$	2.58
2.00	70	$7.14 \cdot 10^4$	$8.38 \cdot 10^3$	8.52
2.30	81	$8.27 \cdot 10^4$	$1.36 \cdot 10^4$	6.10

4.2.3. Liquid uptake, swelling degree and sorption

Liquid uptake and swelling characteristics of sPEEK membranes as a function of *IEC* are given in **Figure 4.7**. Both liquid uptake and swelling in surface area increase exponentially with increasing *IEC*, whereby uptake and swelling of the membranes in 2 M ethanol always exceed the water values. Up to an *IEC* of 1.8 mmol g^{-1}, the differences are below 20%. Considerably higher uptake and swelling in 2 M ethanol in comparison to water are observed when the *IEC* exceeds this value. For instance, the membrane with *IEC* of 2.3 mmol g^{-1}, not given in **Figure 4.7**, exhibit a water uptake more than 100%, and the uptake in 2 M ethanol is even sevenfold higher. The increase of *IEC* implies an increase of hydrophilicity. More liquid is absorbed and, therefore, the polymer structure swells. For shorter storage times (< 24 h), Li and

coworkers found a linear increase for water uptake as a function of *IEC* up to an *IEC* of 2.0 mmol g^{-1} followed by a rapid increase in water uptake with higher *IEC*.[169] This increase was also observed by Xue and coworkers but started at 1.76 mmol g^{-1}.[126] In this range of *IEC*, a shift is observed in the hydrophobicity-hydrophilicity balance. The hydrophobic regions, which assure stability, are separated by the hydrophilic regions. The further increase in water volume fraction occurs as a second water phase resulting inexcessive swelling.[170] In our work, this behavior is more pronounced in ethanolic solutions, because aside from the hydrophilic interactions of the water and the hydrophilic part of ethanol with the polymer, also hydrophobic interactions between the hydrophobic part of ethanol and the polymer take place.

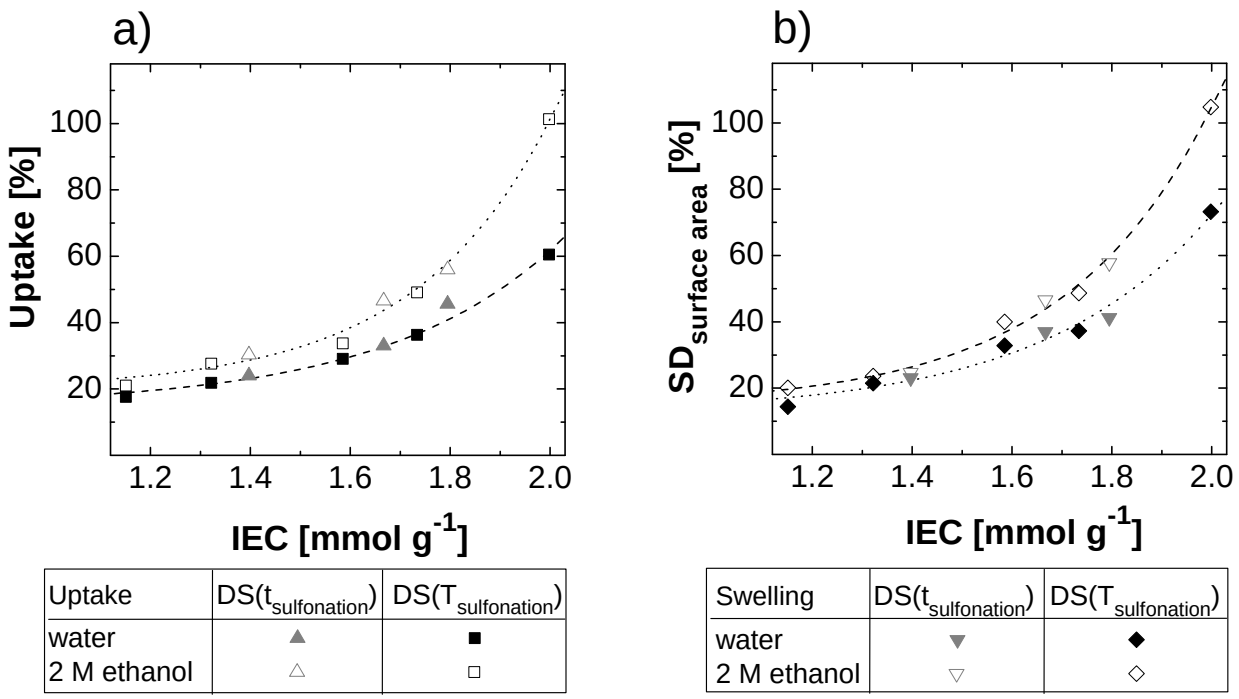

Figure 4.7: Water and 2 M ethanol uptake (a) and swelling (b) as a function of IEC.

The uptake after one day immersion is also verified. For all membranes with an *IEC* lower than 2 mmol g^{-1}, the uptake deviation between 1 and 12 days is below 3.5%. The deviation for the highest sulfonated membrane (*IEC* = 2.30 mmol g^{-1}, not given in **Figure 4.7**) is larger, 7.2%. The application of this sPEEK material is less relevant due to the extreme structural changes under the tested conditions. So this short time

is chosen to precondition the membrane for other characterization methods like proton conductivity and ethanol permeability measurements.

A parameter that to some extent describes the hydrophilicity is the water number. The water number is the ratio of the molar amount of water, n_{water}, to the molar amount of sulfonic acid groups present in the membrane, n_{-SO_3H} .

$$\lambda_{water} = \frac{n_{water}}{n_{-SO_3H}} = \frac{uptake}{IEC \cdot M_{w,water}} \qquad Eq.\ 4.3$$

The uptake is defined dimensionless and $M_{w,water}$ is the molar mass of water. Similar to the water number determined with **Eq. 4.3**, the water and ethanol numbers can be calculated based on the 2 M ethanol uptake and the ethanol concentration in the membrane. This concentration is determined with sorption experiments, also described by Huang et al.[163] for isopropanol and water in sPEEK membranes. In **Figure 4.8**, the decrease in sorption selectivity as a function of *IEC* is shown. For similar conditions, but in an isopropanol-water mixture, Huang and coworkers found

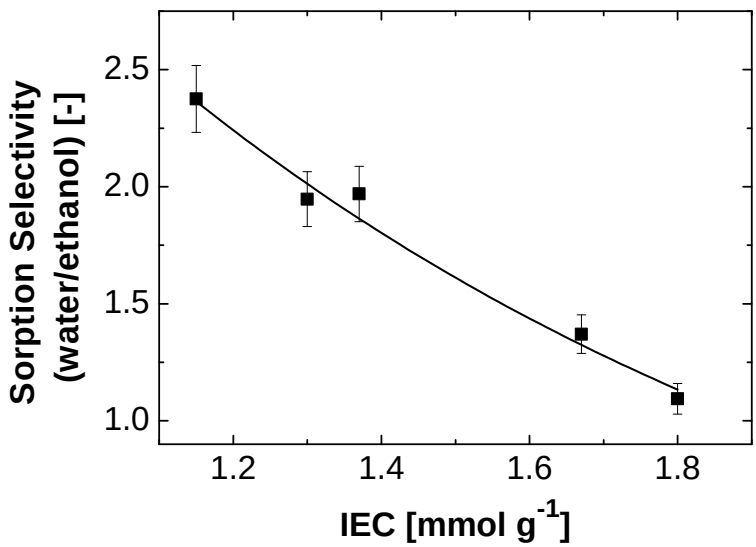

Figure 4.8: Water to ethanol sorption selectivity as a function of IEC.

significantly higher sorption selectivity (= 4) in a similar *IEC* range. These differences are addressed to solubility characteristics of ethanol-water and isopropanol-water systems and interaction with the sPEEK membrane.[171]

The molar ratio of water or ethanol to the sulfonic acid groups, λ'_{water} and $\lambda'_{ethanol}$ respectively, is given in **Figure 4.9**. Up to an *IEC* of 1.7 mmol g^{-1}, both water numbers λ_{water}, and λ'_{water} are relatively constant. Water numbers in the ethanol-water system are in all cases higher than water numbers in the pure water system. The increase in ethanol and water number is more pronounced than the water number in the pure water system when the *IEC* of the membranes were larger than 1.7 mmol g^{-1}. Difference between both water numbers increases at higher *IEC*. The water uptake and the structural deformation of the membrane are affected by ethanol present in the membrane in the static measurements, and are also expected to affect the permeation behavior in the dynamic measurements.

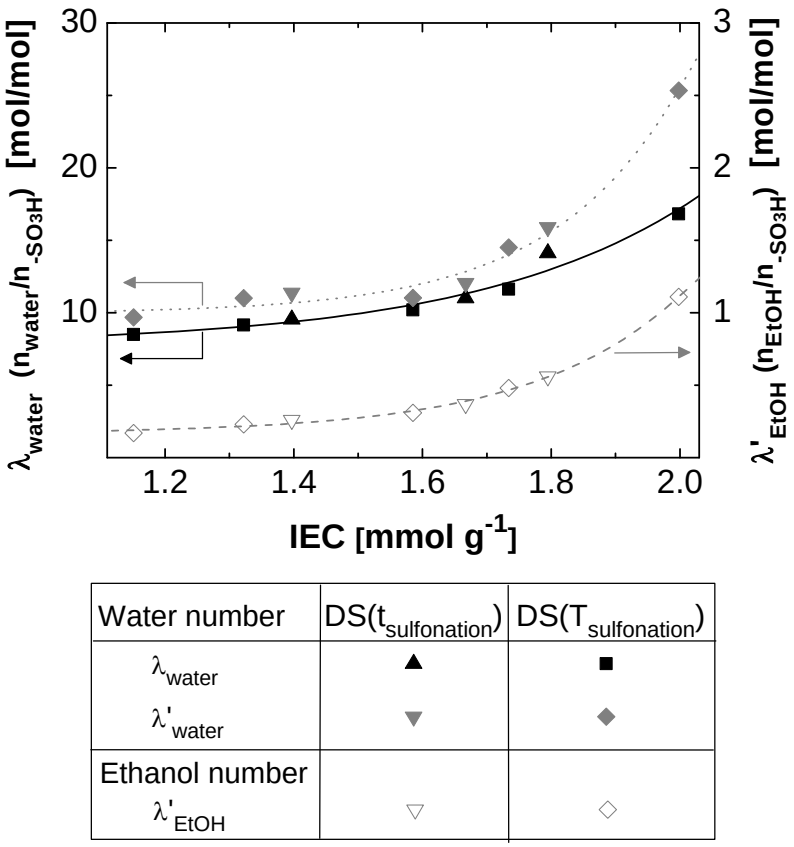

Figure 4.9: Water numbers determined from the water and 2 M ethanol uptake (λ_{water} and λ'_{water} respectively) and the ethanol number, λ'_{EtOH}.

Swelling in surface area in water as a function of temperature is given in **Figure 4.10**. The swelling increases with temperature. The membrane with an *IEC* of 1.15 mmol g^{-1} is just slightly deformed in the temperature range. The membranes with high *IEC* (> 1.7 mmol g^{-1}) swell excessively so that the measuring range up to 80 °C could not be completed due to the fragile structure of the membrane or partial dissolution in the heated liquid.

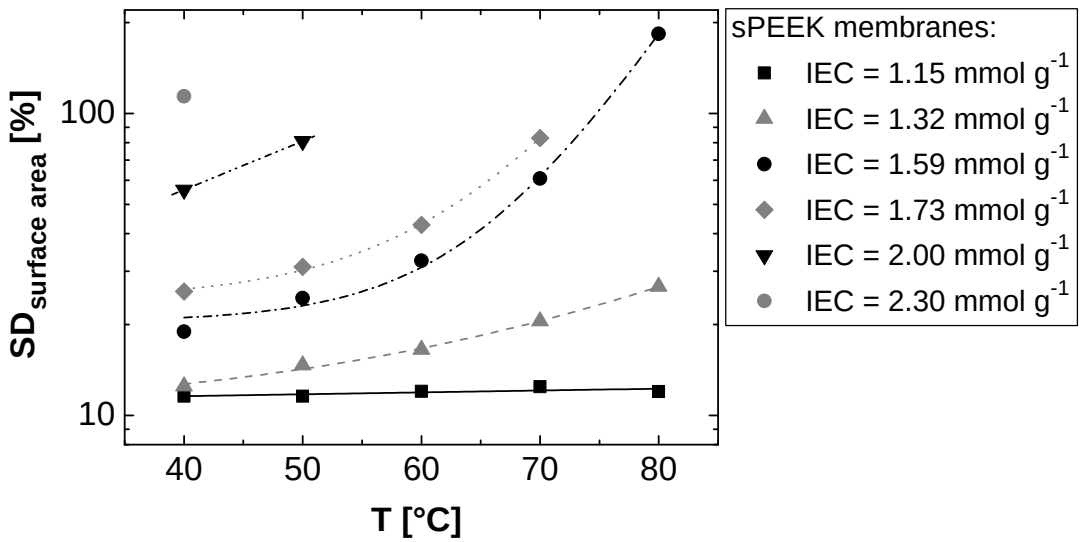

Figure 4.10: Membrane swelling in water as a function of temperature for sPEEK membranes of the DS($T_{sulfonation}$)-series.

In this section, it is shown that the application of pure sPEEK membranes is limited based on swelling characteristics and that swelling of the membrane is a function of *IEC* and temperature. In addition, the swelling medium (water or ethanol-water mixture) clearly has an impact on the swelling behavior. Swelling can roughly be subdivided into three regions:

- *IEC* < 1.4 mmol g-1: low swelling
- 1.4 < *IEC* < 1.8 mmol g-1: intermediate swelling
- *IEC* > 1.8 mmol g-1: high swelling

It is expected, that swelling of the membrane is directly related to permeation behavior of water and ethanol, and that high fuel crossover will negatively affect the fuel cell performance. High swelling behavior of the membrane also complicates the preparation of membrane electrode assemblies, which is undesirable with respect to reproducibility and costs.

4.2.4. Proton conductivity

Proton conductivity is measured using two different in-plane configurations as described in **Section 3.2.1**. The comparison of both methods is performed with sPEEK membranes of the DS($T_{sulfonation}$)-series and is done to obtain information about the reliability of the measurements. The proton conductivity in water measured with the platinum wire configuration (PWC) is similar but always higher than the values measured with the spring tips configuration (STC) (**Figure 4.11**). The average value of the absolute difference between both methods is 4.6 ± 0.6 mS cm^{-1}. This deviation is dedicated to differences in experimental setup and membrane geometries.

The proton conductivity of sPEEK membranes with various *IEC*s wetted in water and 2 M ethanol measured with the STC is given in **Figure 4.11a**. The proton conductivity in both systems is similar in the region where the uptake in water and 2 M ethanol remains low (< 1.7 mmol g^{-1}). From that point, proton conductivity in the 2 M ethanol system increases significantly due to the higher uptake resulting in excessive swelling. These results agree with the water numbers shown in **Figure 4.9**. Therefore, the water number is given as a function of *IEC* in **Figure 4.11b** (left y-axis), to see how the conductivity relates with the water content in the membrane. This time, the proton conductivity measured with the PWC is given. The water number increases slightly from 8.5 to 10.2 within the *IEC* range of 1.1 to 1.6 mmol g^{-1}. The proton conductivity tripled in this area from 10 to 30 mS cm^{-1}. A further increase in *IEC* results in an exponential increase in water number and conductivity. In that *IEC*-

range, membrane instability is observed with liquid uptake and swelling measurements. Water content in the membrane becomes higher due to the larger amount of hydrophilic sulfonic acid groups on the polymer chains. This behavior was also found in the works of, amongst others, Jiang et al.[172] and Xue et al.[126]

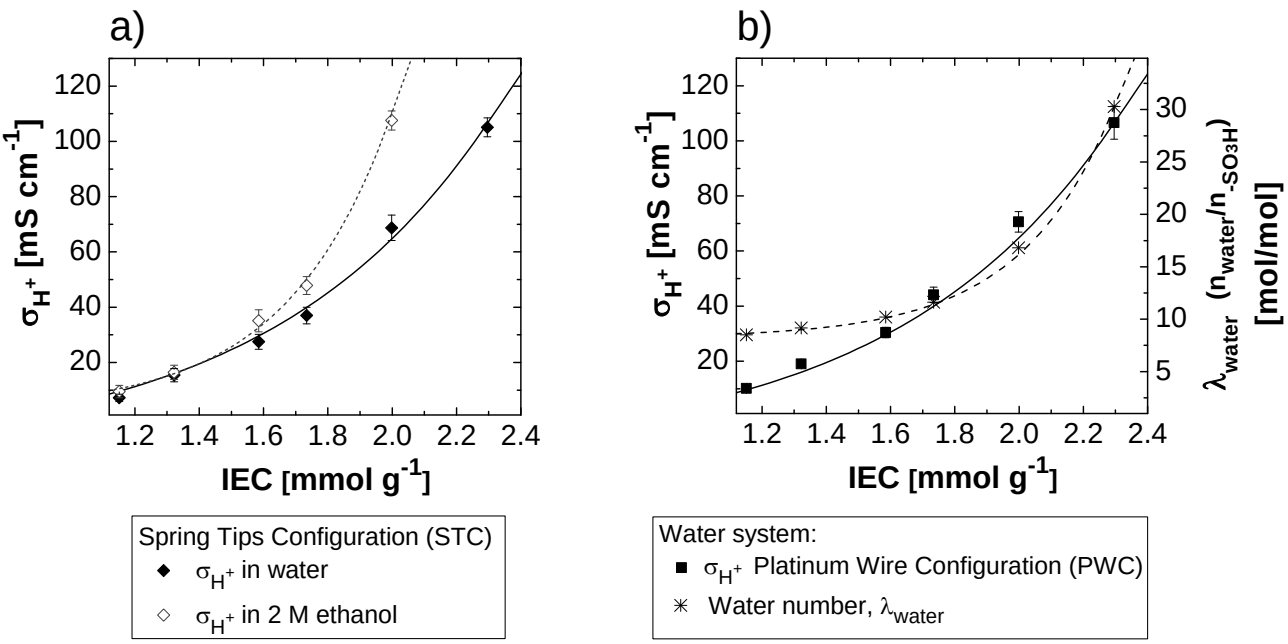

Figure 4.11: a) Proton conductivity measured with the spring tip configuration (STC) in water and 2 M ethanol as a function of IEC and b) proton conductivity measured with the platinum wire configuration (PWC) and the water number as a function of IEC.

Proton conductivity results of sPEEK membranes of the DS($t_{sulfonation}$)-series are given in **Table 4.3**. Again, proton conductivity determined with the STC is always lower than the PWC values. This deviation is also described with the DS($T_{sulfonation}$)-series. The

Table 4.3: Proton conductivity results of the DS($t_{sulfonation}$)-series; conditions: wetted in water and measured at RT.

IEC [mmol g^{-1}]	σ_{H^+} (STC) [mS cm^{-1}]	σ_{H^+} (PWC) [mS cm^{-1}]
1.40	14.6 ± 2.2	19.8 ± 1.2
1.66	36.3 ± 2.3	40.8 ± 2.5
1.79	42.9 ± 3.8	45.1 ± 2.6

proton conductivity values as a function of *IEC* fit well with the results obtained with the DS($T_{sulfonation}$)-series. No notable difference in proton conductive behavior between both sPEEK sulfonation methods is found.

The proton diffusion coefficient (D_σ) is calculated from the proton conductivity (σ_{H^+}) based on the Nernst-Einstein relationship:

$$\sigma_{H^+} = \frac{D_\sigma C_{fg} F^2}{RT} \rightarrow D_\sigma = \frac{RT\sigma_{H^+}}{C_{fg} F^2} \qquad \textit{Eq. 4.4}$$

F is the Faraday constant and C_{fg} is the concentration of functional groups in the membrane and is calculated with *IEC*, density of the dry membrane and volume swelling ratio:

$$C_{fg} = \frac{IEC \cdot \rho_{m,dry}}{(SD_{volume} + 1)} \qquad \textit{Eq. 4.5}$$

The final equation for determining the proton diffusion coefficient from experimental data is:

$$D_\sigma = \frac{\sigma_{H^+} RT (SD_{volume} + 1)}{IEC \, \rho_{m,dry} F^2} \qquad \textit{Eq. 4.6}$$

The proton diffusion coefficient is dependent on the water content in the membrane.[34,131,173] The calculated proton diffusion coefficient is plotted against the water number in **Figure 4.12a**. This is done for the water system (D_σ - λ_{water}) and the 2 M ethanol system (D'_σ - λ'_{water}). Three different regions are observed: 1) $\lambda_{water} < 10$:

D_σ strongly dependent on λ_{water}; 2) λ_{water} > 14: D_σ slightly dependent on λ_{water} and 3) 10 < λ_{water} < 14: a transition region.

At low water numbers, the excess protons tend to be more localized in the vicinity of the sulfonic acid groups. In this region, the dissociation of the protons and the fixed anions becomes easier with increasing water number.[34] The dominating transport mechanism is based on the diffusion of the protons by the vehicle mechanism. In the second region, the proton diffusion coefficient is less dependent on the water number. The sulfonic acid groups are completely hydrated and the dissociation is complete (similar to diluted acid solutions). In this region, Grotthuss hopping is the dominating transport mechanism.[174]

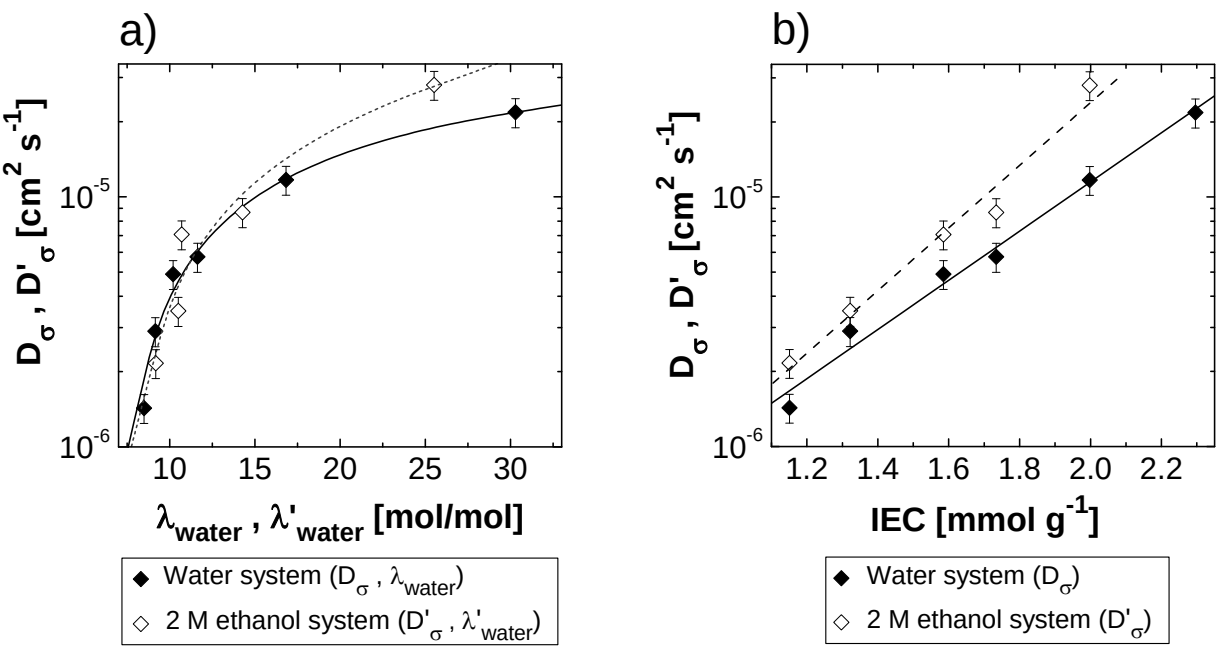

Figure 4.12: Proton diffusion coefficient as a function of water number, in water and 2 M ethanol systems as function of a) water number and b) IEC.

In **Figure 4.12a,** it is shown that the presence of ethanol accelerates the proton diffusion because of the larger liquid phase present in the membrane. A transition region is around λ_{water} of 12 where both mechanisms account for the proton transport (coupled motion). These results are in good agreement with the shift of the

hydrophobicity-hydrophilicity-balance and the formation of a bulky water phase observed with the uptake and surface swelling experiments. The diffusion coefficients of a water molecule and a proton in water are $2.3 \cdot 10^{-5}$ cm^2 s^{-1} and $9.3 \cdot 10^{-5}$ cm^2 s^{-1} respectively.[13] The largest proton diffusion coefficient in this study is $2.2 \cdot 10^{-5}$ cm^2 s^{-1} with a water number of 30. The diffusion coefficient of a proton in water is not reached, which is also expected because of the barrier function of the membrane. Compared to Kreuer similar results were obtained.[34]

The proton diffusion coefficient as a function of *IEC* is presented in **Figure 4.12b**. This relation is exponential, which is expected because of the exponential relationship between *IEC* and water number, as shown in **Figure 4.9**.

4.2.5. Ethanol permeability

The permeation behavior of ethanol and water in ethanolic-aqueous systems is measured with two different systems: i) liquid-liquid (L-L) system and ii) liquid-gas (L-G) system. With the L-L systems, the membrane separates two liquid phases. The transport of ethanol and water occurs in opposite directions and permeation of ethanol as well as water can be experimentally determined. In the L-G system, ethanol and water permeates through the membrane because of the applied vacuum on the permeate side of the membrane. This technique is also called pervaporation. The transport direction of both permeating species is the same. In this section, permeation results through sPEEK membranes obtained with both methods are presented and compared.

4.2.5.1. Liquid-liquid systems

The permeability of ethanol and water is determined in an L-L diffusion cell as described in **Section 3.2.4**. On both sides of the membrane, a liquid phase is present and the driving force is based on concentration difference. Permeability coefficients of water and ethanol are low in the case of low sulfonated membranes (see **Figure**

4.13). With higher sulfonated membranes, the membrane swells excessively and more free volume is created for transport of both components through the membranes, so the permeability increases exponentially. Due to membrane instability, it was not practicable to obtain reliable results at 25 °C with membranes having an *IEC* higher than 1.73 mmol g^{-1}. This limit was 1.67 mmol g^{-1} in case of measurements at 40 °C. The water permeability of this membrane was $367 \cdot 10^{-8}$ cm^2 s^{-1} and is not given in **Figure 4.13b** because of the y-axis scaling. In all cases, the water permeability coefficients exceed the ethanol permeability coefficients. In L-L systems, it is not possible to speak of selectivity based on the ratio of permeability coefficients of water and ethanol because the transport is in opposite directions.

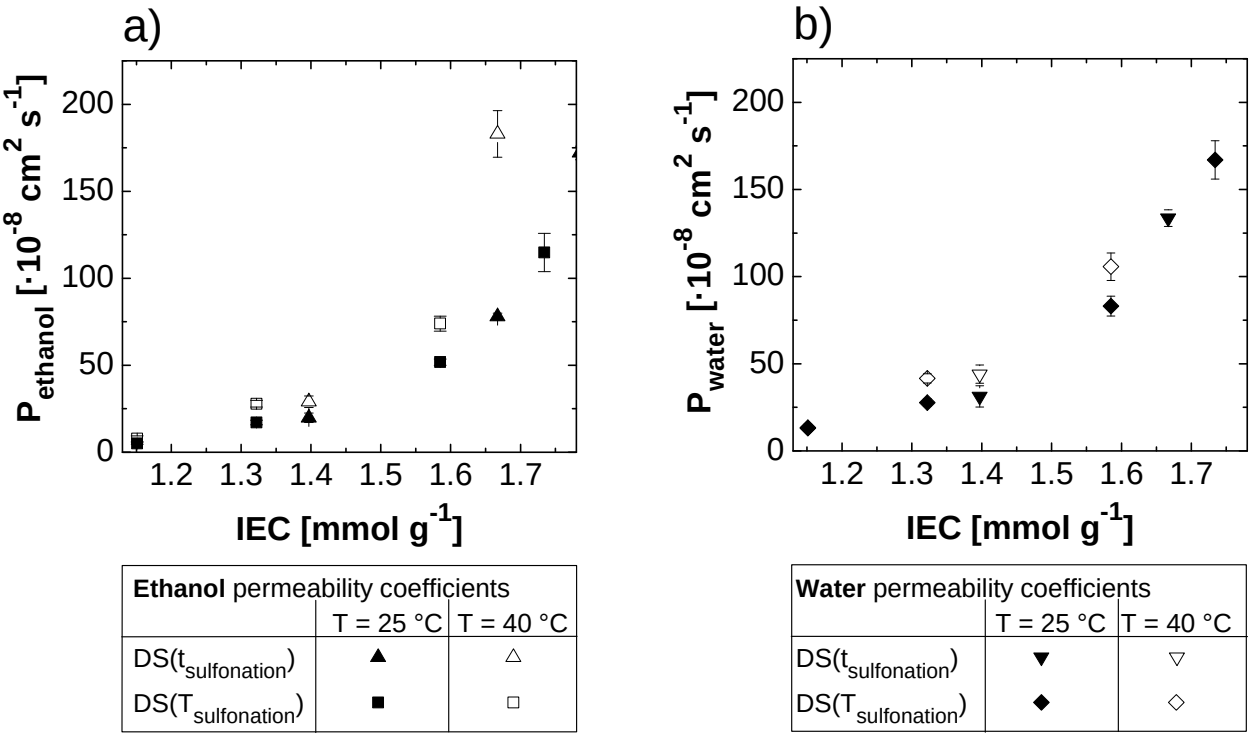

Figure 4.13: Ethanol permeability (a) and water permeability (b) as a function of IEC measured in a diffusion cell with an ethanol concentration difference of 4 M.

In **Figure 4.14**, the permeability is given as a function of the reciprocal temperature to see if the ethanol permeation shows Arrhenius behavior. Membranes with low *IEC* can be measured over the whole temperature interval. Membranes with an *IEC* of

1.6 and 1.8 mmol g^{-1} can just be measured up to a temperature of 40 °C. Extreme swelling of the membrane hindered reliable measurements at higher temperatures. Ethanol permeability did not show Arrhenius behavior. The increase in permeability between 25 °C and 40 °C is relatively low in comparison to the increase in the other temperature intervals. In this temperature interval, the membrane structure is stable and liquid transport remains low. The increase in ethanol permeability in the temperature range from 40 °C to 60 °C is exponential, which suggests a relationship with swelling in aqueous-ethanolic systems. This is the reason why measurements at different temperatures do not show Arrhenius behavior. The Arrhenius equation is valid for stationary systems. The membrane swelling is dependent on temperature. The altering of free volume in the membrane system results in a deviation of Arrhenius behavior.

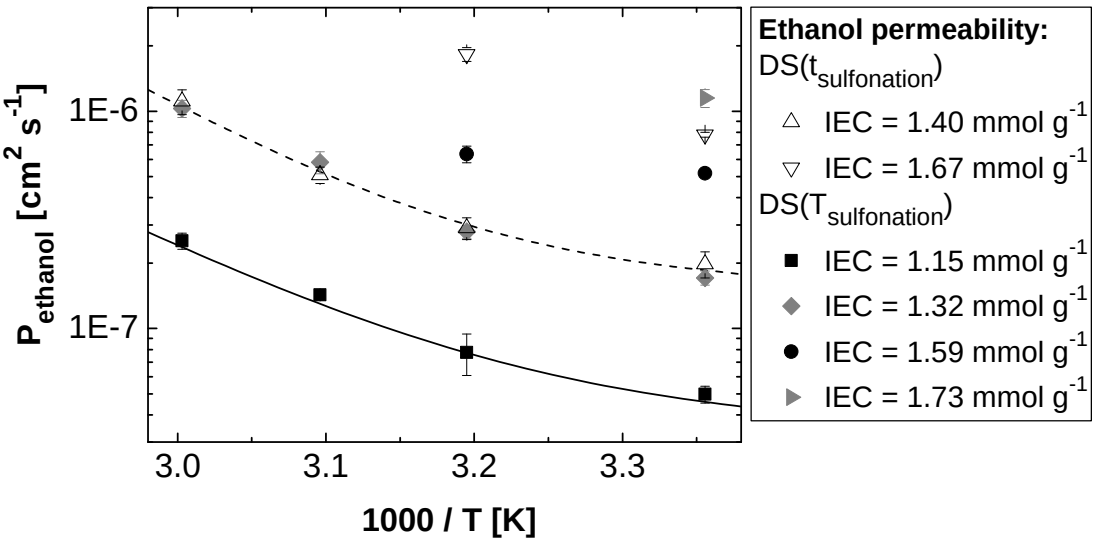

Figure 4.14: Arrhenius plot of the ethanol permeability for various sPEEK membranes.

4.2.5.2. Liquid-gas systems

The transport of ethanol and water through the membrane is examined in liquid-gas systems by means of pervaporation. In the pervaporation process, the transport of all species is in the same direction. The pervaporation results as a function of *IEC* are given in **Figure 4.15**. The ethanol and water permeability coefficients increase

exponentially with *IEC*, while the selectivity decreases linearly. The increase in permeability accompanied with a decrease in selectivity is a well known and unwanted feature in pervaporation processes.

For transport of water and isopropanol in sPEEK membranes, a model is given by Huang and coworkers,[163] where the membrane was separated in hydrophilic and hydrophobic regions. The transport of both components was based on a random hopping mechanism. In case of large water uptake, the interaction between the water molecules dominated the interaction between the water molecules and sulfonic acid groups. This resulted in a decrease in sorption selectivity to water. The composition of the liquid in the membrane was independent of sulfonation degree. They proposed that the isopropanol transport took place due to coupled transport in the hydrophilic phase and that the transport in the hydrophobic phase could be neglected.

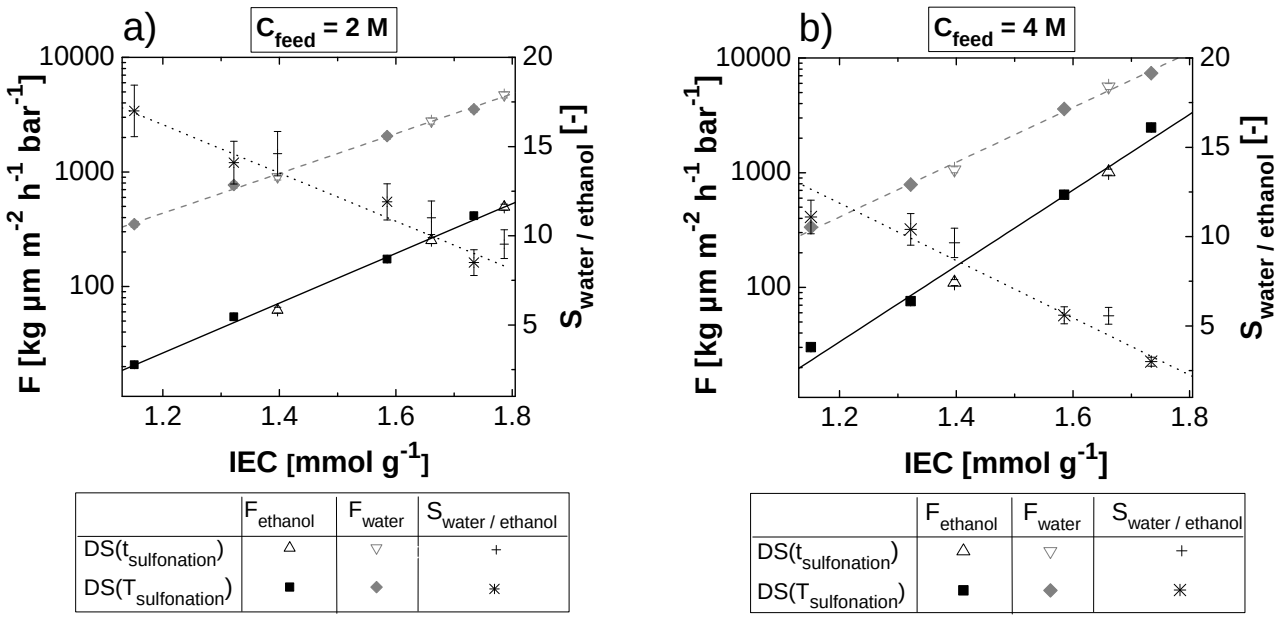

Figure 4.15: Ethanol and water permeability coefficients and ideal membrane selectivity of sPEEK membranes as a function of IEC measured with pervaporation (T: 40 °C; p^0: 13 mbar); a) ethanol feed concentration: 2 M; b) ethanol feed concentration: 4 M.

On the other hand, a simplified solution-diffusion model is given by Schaetzel and coworkers.[164] The model was validated with water-ethanol pervaporation with PVA-

based membranes. The model was based on molecular diffusion. The permeant diffusivity was given as a function of the total volume occupied by all solvent species. They found that the sorption of ethanol at high water concentrations was rather influenced by the water present in the membrane than with the ethanol-membrane interaction. This was similar to the findings of Huang and coworkers. The coupling effect of both components was found in the thermodynamic part (solubility). From then, the ethanol flux was only a function of the ethanol concentration gradient. The selectivity was, therefore, caused by sorption and less by coupled transport.

In our case, the swelling and, therefore, the membrane free volume increases with increasing *IEC*, and the sorption selectivity decreases from 2.4 to 1 in the *IEC* range of 1.15 to 1.8 mmol g^{-1}. The linear decrease in membrane selectivity is mainly caused by permeation of both components through hydrophilic domains of the membrane. The ethanol flux is highly dependent on the water transport in the membrane and coupled transport takes place. This means that with ethanol-water pervaporation of low ethanol concentration (e.g., 2 M and 4 M ethanol) the kinetic part dominates the thermodynamic part in the separation process. This also allows normalization to membrane thickness because the permeation is more dependent on diffusion than on solubility. According to Fick's law, diffusion is proportional to membrane thickness and results in good comparison opportunities between various kinds of membranes.

4.2.5.3. sPEEK in ethanol-water systems: Comparison of L-L and L-G systems

In this section, the L-L and L-G permeation systems are compared although the driving force for permeation is different in both systems. For comparison, the measurements at 40 °C are used. The presented data are based on the feed concentration of 2 M and 4 M with pervaporation and 4 M in the diffusion cell. The fluxes of both methods are converted to the same unity and presented in **Figure 4.16** as a function of *IEC*.

The ethanol and water flux in L-G systems increase significantly when the ethanol concentration of the feed solution was doubled from 2 M to 4 M. The ethanol and water flux show both an exponential increase with *IEC* when the ethanol feed side concentration is 2 M. The ethanol and water flux both increase more than exponentially with 4 M feed side concentration. Up to an *IEC* of 1.4 mmol g^{-1}, the water fluxes of both systems are similar. This implies that ethanol permeates due to its own driving force, independent from water transport through the membrane. A deviation in water permeation is observed with membranes with an IEC higher than 1.4 mmol g^{-1} when the pervaporation behavior with feed side concentrations of 2 M and 4 M are compared. Water permeation, as well as ethanol permeation, as a function of IEC increase more than exponential within the selected IEC region. This implies that apart from the sorption of ethanol and water in the membrane, also coupled transport takes place.

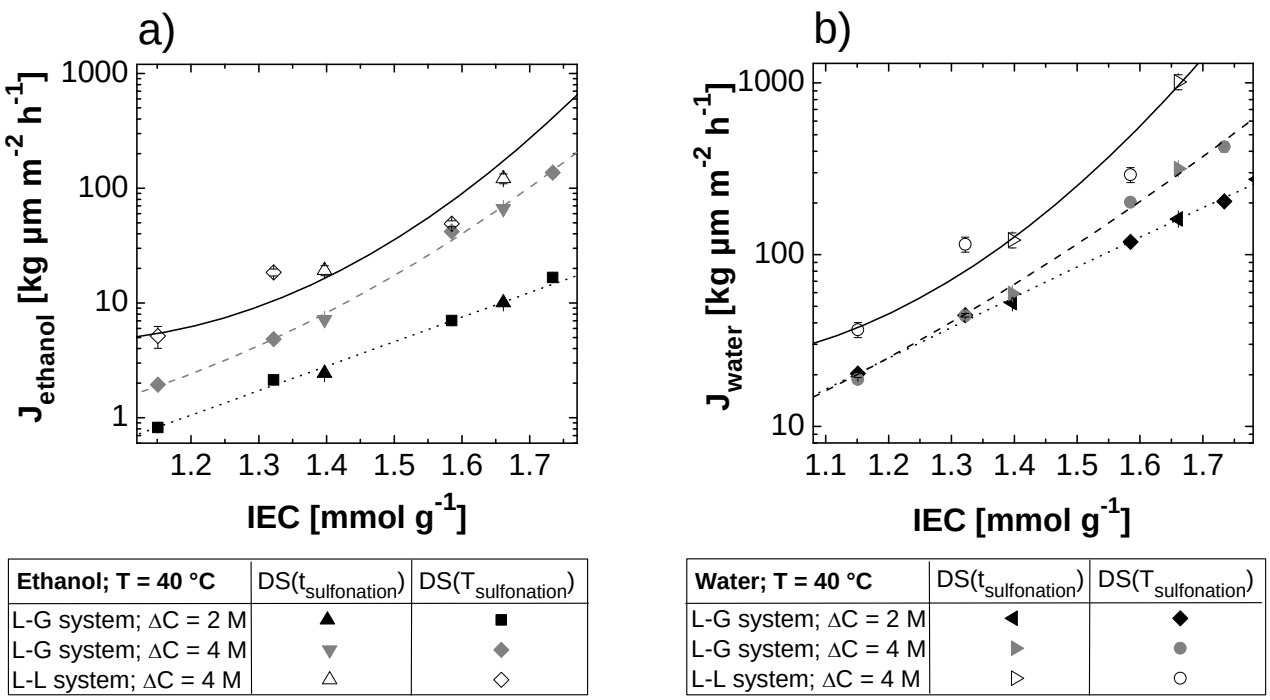

Figure 4.16: Comparison of the L-G and L-L permeation system; a) ethanol fluxes; b) water fluxes.

The enhancement in fluxes is a result of the increase in membrane swelling during the measurement as well. The ethanol flux measured with pervaporation is in the same direction as the water flux, whereas the fluxes in the diffusion cell are in contrary directions. It is expected that the ethanol flux is retarded by the opposite water flux. This is actually the case in the whole *IEC* range, and it is more pronounced for membranes with an *IEC* larger than 1.4 mmol g^{-1}. In case of the L-L system, water permeation as a function of *IEC* increases more substantial than the ethanol permeation, while in the L-G system this behavior is the opposite.

4.2.6. Differences between both sulfonation routes

As shown in previous sections, the sulfonation time and sulfonation temperature are the main parameters to control the sulfonation of PEEK in sulfuric acid. sPEEK polymer and membranes prepared with both sulfonation methods were reproducible and no remarkable differences in membrane properties are obtained up to an *IEC* of 1.8 mmol g^{-1}. Membranes prepared with DS($T_{sulfonation}$) exhibiting *IEC*s larger than 1.73 mmol g^{-1} results in poor membrane stability in ethanol-water mixtures. On the one hand, this is caused by polymer chain deterioration, observed with molecular weight studies. On the other hand, the chemical character changes with increasing amount of sulfonic acid groups. Cristallinity of the polymer is reduced which subsequently affects solubility.[169]

High swelling or partially dissolving of high sulfonated membranes are also reported by other researchers.[116,119,169] Do et al.[120] investigated the differences in membrane properties of homo- and heterogeneously sPEEK sulfonated at RT. In case of homogeneously sulfonation, PEEK was already dissolved (in methylsulfonic acid) before sulfonation in sulfuric acid took place. Simultaneous dissolving and sulfonation in sulfuric acid occurred with the heterogeneously sulfonation. These methods are comparable to DS($T_{sulfonation}$) and DS($t_{sulfonation}$) respectively. Membranes with ion exchange capacities varying from 1.4 to 2.4 mmol g^{-1} were prepared and characterized with respect to proton conductivity and methanol permeability. Results

of sulfonated membranes up to 1.8 mmol g^{-1} were similar. The preferred sulfonation route to prepare sPEEK for membrane modifications is DS($t_{sulfonation}$). A disadvantage of DS($T_{sulfonation}$) is the inevitable heating and cooling times. This is especially significant at higher temperatures. A practical advantage of DS($t_{sulfonation}$) is the scheduling, resulting in longer continuous washing period of the sulfonated polymer.

4.2.7. Comparison of sPEEK with Nafion®117

Nafion® is a common membrane material for benchmarking as already stated in literature review in **Chapter 2**. In this section, the sPEEK data are compared with the practically obtained data of Nafion®117. The ion exchange capacity of Nafion®117 is 0.909 mmol g^{-1}, which is also experimentally verified.

Liquid uptake and swelling characteristics of Nafion®117 in water and water-ethanol mixtures is presented in **Table 4.4**. Water uptake in Nafion®117 is relatively low, comparable with a sPEEK membrane with an *IEC* of 1.15 mmol g^{-1}. The liquid uptake in 2 M ethanol is much higher, comparable to a sPEEK membrane with an *IEC* of 1.59 mmol g^{-1}. The deformation determined by means of swelling in surface area for Nafion® is relatively high. In water and 2 M ethanol, swelling in surface area for Nafion® is comparable to sPEEK membrane with an *IEC* of 1.59 mmol g^{-1} and 1.73 mmol g^{-1} respectively. The increase in liquid uptake and swelling in surface area from 2 M to 4 M ethanol is in the range of 40% - 45% in case of Nafion®. For sPEEK with a relatively high sulfonation degree, *IEC* of 1.66 mmol g^{-1}, this increase is in the range of 110% - 120%. Reasons for the different swelling behavior between Nafion®

Table 4.4: Liquid uptake and swelling data of Nafion® 117 in water and 2 M and 4 M ethanol-water mixtures.

		water	2 M ethanol	4 M ethanol
Uptake	[wt-%]	18 ± 2	33 ± 3	48 ± 4
$SD_{surface\ area}$	[%]	31 ± 1	53 ± 1	74 ± 2

and sPEEK membranes can be found in the different morphologies and microstructure.[34] The Nafion® structure consists of wide water channels, a good connected percolated hydration structure, and no dead-end channels. In case of sulfonated polyetherketones, the hydrophilic/hydrophobic regions are less separated and water domains are highly branched with many dead ends.

Peculiar proton conductivity results are obtained with Nafion®117. The proton conductivity is determined with the spring tips configuration (STC) in longitudinal direction (**Table 4.5**). In contradiction to the sPEEK membranes, the proton conductivity decreases with increasing ethanol concentration, although the membrane swells and the liquid uptake increases. Proton diffusion coefficients in the water and 2 M ethanol systems are similar because the increase in swelling balances the decrease in proton conductivity (**Eq. 4.6**). Further swelling of the membrane in 4 M ethanol results in a higher proton diffusion coefficient in the 4 M ethanol system. Proton diffusion coefficients of sPEEK increase exponentially between $2.2 \cdot 10^{-6}$ and $28.0 \cdot 10^{-6}$ cm^2 s^{-1} as a function of *IEC* (**Figure 4.12b**).

Table 4.5: Proton conductivity determined with STC and proton diffusion coefficient of Nafion® 117 in water and 2 M and 4 M ethanol-water mixtures.

		water	2 M ethanol	4 M ethanol
σ_{H^+}	[mS cm^{-1}]	73.4 ± 2.5	58.4 ± 3.2	56.0 ± 3.0
D_σ	[$\cdot 10^{-6}$ cm^2 s^{-1}]	15.5 ± 2.1	15.2 ± 2.0	17.2 ± 2.3

The permeation characteristics of Nafion® determined in L-G system and L-L system are given in **Table 4.6** and **Table 4.7** respectively. It is remarkable, that the water permeability coefficient in the L-G system is lower with 4 M than 2 M ethanol feed side concentration. On the other hand, the ethanol permeability coefficient is 1.5 times higher. The membrane selectivity coefficients are low and the separation

factors show even selectivity towards ethanol. Pervaporation behavior with 4 M feed concentration of Nafion® is similar to sPEEK with an *IEC* of 1.73 mmol g^{-1}. When permeability and selectivity coefficients are compared, pervaporation characteristics of sPEEK membranes are significantly better than Nafion®.

Ethanol permeability could be determined over the whole temperature range (25 °C - 60 °C) in the L-L system. Membrane stability of Nafion®117 with respect to swelling was superior over sPEEK membrane with *IEC* higher than 1.4 mmol g^{-1}. The membrane thickness was also four times thicker than the sPEEK membranes. The ethanol permeability coefficients are significantly higher than the sPEEK membranes. For example, the ethanol permeability at 40 °C of Nafion®117 is nearly eight times higher than sPEEK with 1.4 mmol g^{-1}.

Table 4.6: Pervaporation results of Nafion® 117 with 2 M and 4 M ethanol feed concentration (pervaporation conditions: 13 mbar; 40 °C).

C_{feed} [M ethanol]	F [kg µm m^2 h^{-1} bar^{-1}]		$S_{water / ethanol}$	$\alpha_{water / ethanol}$
	ethanol	water		
2	1942 ± 192	9530 ± 943	4.9 ± 0.7	0.83 ± 0.05
4	3022 ± 300	8629 ± 854	2.9 ± 0.4	0.65 ± 0.04

Table 4.7: Ethanol permeability as a function of temperature with 2 M and 4 M ethanol concentration difference.

ΔC [M ethanol]	$P_{ethanol}$ [$\cdot 10^{-8}$ cm^2 s^{-1}]			
	25 °C	40 °C	50 °C	60 °C
2	157 ± 10	233 ± 21	363 ± 24	458 ± 36
4	215 ± 9	286 ± 12	N/A	N/A

N/A = not applicable

As presented in this section, the membrane properties of Nafion® and sPEEK are contrary with respect to the main electrolyte functions: proton conductivity and permeability. Nafion® exhibits high proton conductivity with concomitant high ethanol crossover, whereas sPEEK (dependent on *IEC*) exhibits lower proton conductivity with concomitant lower ethanol crossover. This leads to the strategy to further reduce the ethanol crossover while maintaining or increasing the proton conductivity.

4.2.8. Fuel cell prediction

A parameter to compare membranes with respect to possible application in direct ethanol fuel cells is the selectivity of proton conductivity to ethanol permeability.[36] The ethanol permeability should be as low as possible whereas proton conductivity should be high. This characteristic parameter is often used in literature with direct methanol fuel cells.[61,126] Although, the predictive value of this parameter should be treated critically according to Yildirim et al.[61]

In this work, the characteristic ratio is defined as the proton diffusion coefficient to the ethanol permeability coefficient determined with pervaporation $(D_\sigma / F_{ethanol})$. A good overview of the results is obtained when the proton diffusion coefficient is plotted against the ethanol permeability. Such a D_σ - $F_{ethanol}$ diagram is presented in **Figure 4.17**, where both quantities, D_σ and $F_{ethanol}$, are determined in 2 M ethanol systems. Nafion® exhibits high proton conductivity as well as high ethanol permeability. Based on the ratio of proton diffusion coefficient and ethanol permeability coefficient a curve can be plotted that separates the diagram in two areas. The characteristic slope of Nafion® in this 2 M ethanol system is determined by:

$$\text{Characteristic slope} = \frac{15.2}{1942} \; \frac{\cdot 10^{-6}\ \text{cm}^2\ \text{s}^{-1}}{\text{kg}\,\mu\text{m}\,\text{m}^{-2}\ \text{h}^{-1}\ \text{bar}^{-1}}$$

The area below this plot represents the area where the ethanol permeability is higher and/or the proton diffusion coefficient is lower than Nafion®. In this area, membrane

characteristics are inferior to those of Nafion® and, therefore, worse fuel cell behavior is expected as well. It should be stated that this slope does not represent the direct relationship between the proton diffusion coefficient and the ethanol permeability coefficient. This slope is given to compare different kinds of membranes with respect to the main electrolyte functions. Proton diffusion should be high (numerator) and ethanol permeability should be low (denominator) resulting in high ratios for promising membranes.

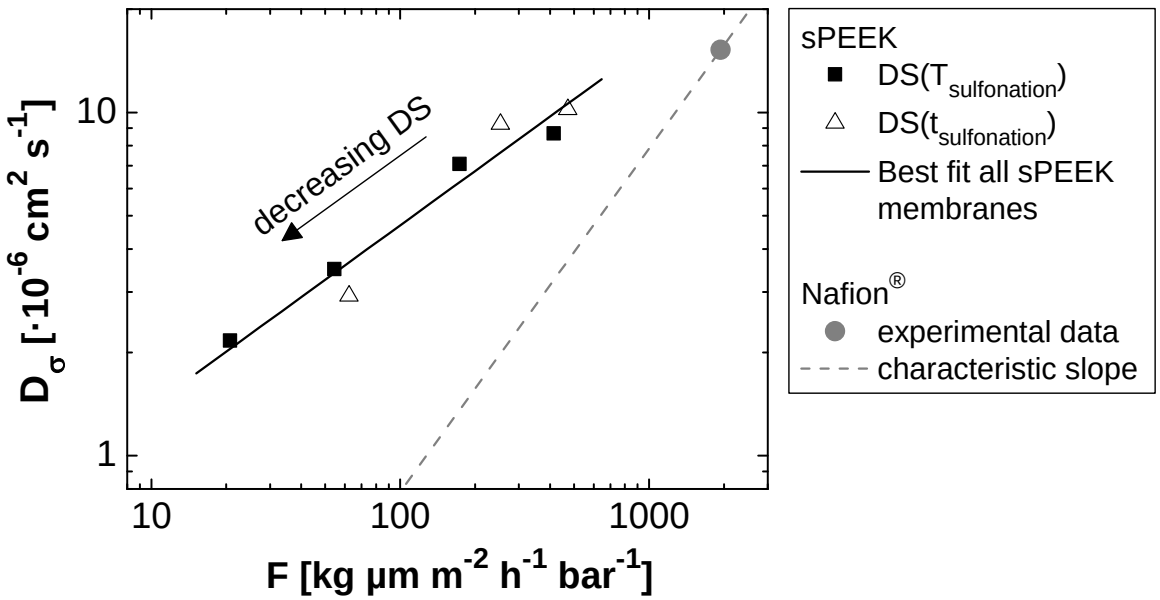

Figure 4.17: Proton diffusion coefficient (2 M ethanol; RT) versus ethanol permeability coefficient (L-G system; 2 M ethanol feed concentration; 40°C) for Nafion® 117 and various sPEEK membranes.

Experimental data of the sPEEK membranes are all located in the area above this characteristic slope of Nafion®, indicating that sPEEK is a promising polymer type for application in DEFCs. In addition to the sole data points, a best fit diagram is presented in **Figure 4.17** to observe a trend as a function of *DS*. The slope of this best fit is less steep respective to the characteristic slope of Nafion®. This implies that with low sulfonated sPEEK membranes more promising fuel cell performances are

expected than with high sulfonated membranes. The lowest sulfonated sPEEK is actually limited by practical considerations. The sPEEK polymer becomes insoluble in solvents when the sulfonation degree is below 30% (*IEC* of approximately 1 mmol g^{-1}).[122] With polymers containing a *DS* lower than 30%, membranes cannot be prepared by means of the applied evaporation procedure. On the other hand, another limitation is given for high sulfonated sPEEK membranes. Excessive swelling results in high ethanol permeation and membrane instability. The latter hampers the preparation of the membrane electrode assembly and will probably result in higher production costs. The highest sulfonated sPEEK membranes, presented in **Figure 4.17**, exhibit an *IEC* of 1.79 mmol g^{-1}. Ethanol permeation of membranes with higher *IEC*s could not be measured in a 2 M ethanol system due to excessive swelling (sPEEK with 2.0 mmol g^{-1}) or partial dissolution (sPEEK with 2.3 mmol g^{-1}).

Chapter 5

Silica based mixed-matrix membranes

In this chapter, the formation of an interconnected inorganic phase in a non-fluorinated organic phase is studied. The concept of a particle loaded and interconnected mixed-matrix membrane is presented in **Figure 5.1**. In the field of nanocomposite membranes, particle loaded membranes are mostly described in literature. In this work, the inorganic particles are hydrophilic fumed silica particles (Aerosil®380). The new aspect is to interconnect these particles by means of partial hydrolysis and polycondensation of a silicon alkoxide. In this way, the free volume of the polymeric matrix will be filled with particles, but the formed inorganic network between these particles will assure additional stability. With this strategical step, it is expected that membranes containing an interconnected inorganic phase exhibit reduced swelling behavior and lower ethanol crossover. Hydrophilic inorganic components are chosen because of the interaction with water molecules leading to an improved water household in the membrane during application.

As presented in **Section 2.1.2** and **Section 2.2.3** and their references, the majority of the nanocomposite systems consists of an inorganic content less than 10%. In this chapter, inorganic-organic hybrid membranes are investigated with higher inorganic loadings. It is expected, that higher inorganic loading improves the blocking of permeating species. The hydrophilic nature of the inorganic phase should especially retain the more hydrophobic ethanol, leading to higher water to ethanol selectivities.

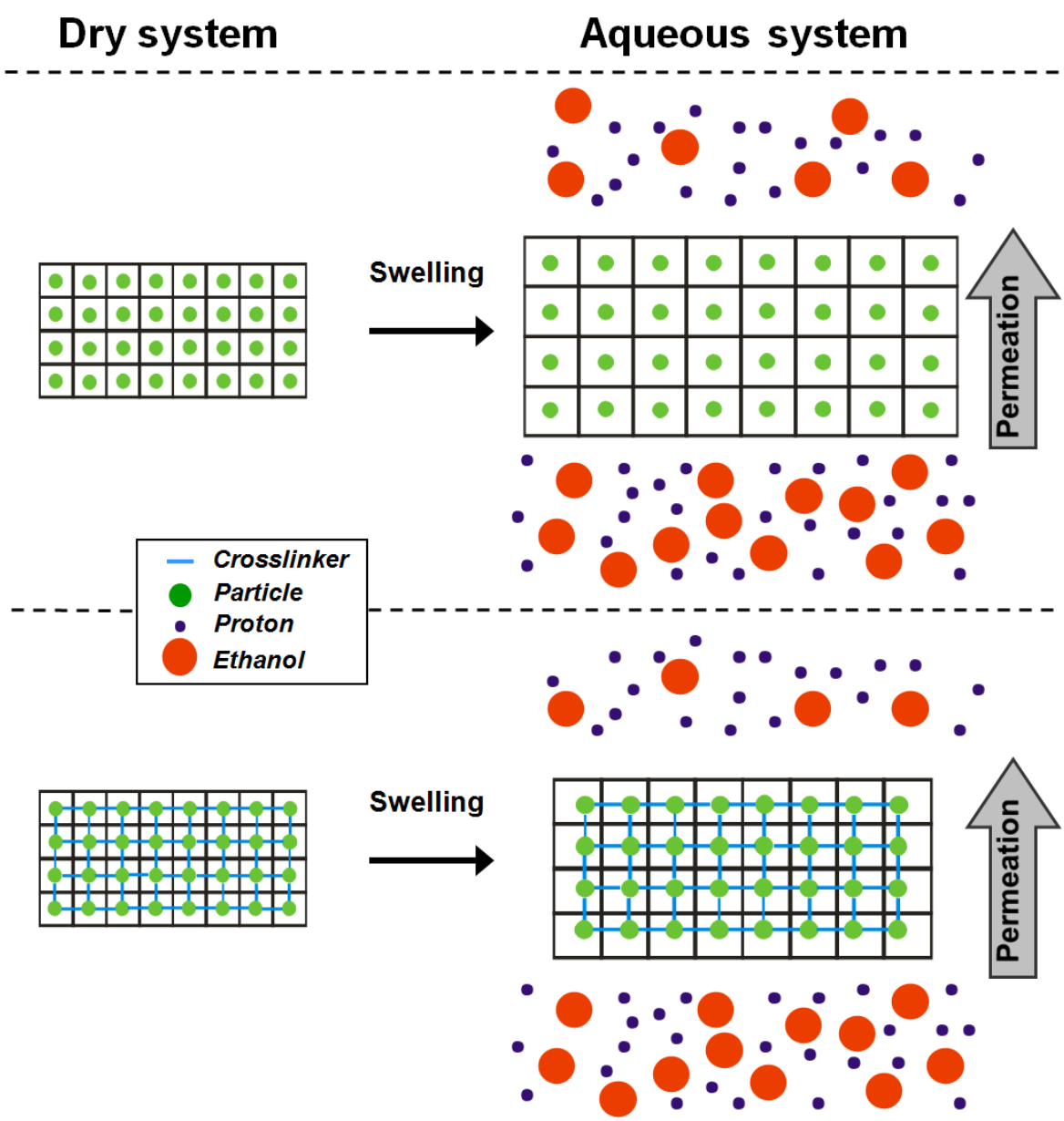

Figure 5.1: Schematic representation of particle loaded mixed-matrix membrane (top) and interconnected mixed-matrix membrane (bottom).

Tetraethoxysilane (TEOS) is used in this study because it is widely studied and the reactions are relatively slow and controllable.[67] Partial hydrolysis occurs when the molar amount of water is less than the amount of ligand groups on the silicon atom. The partial hydrolysis reaction in its general form is:

$$Si(OR)_4 + n\ H_2O \rightarrow Si(OR)_{4-n}(OH)_n + n\ ROH \qquad R.\ 5.1$$

Possible condensation reactions are:

$2\ Si(OR)_{4-n}(OH)_n \rightarrow (OH)_{n-1}(OR)_{4-n}Si\text{-}O\text{-}Si(OR)_{4-n}(OH)_{n-1} + H_2O$ *R. 5.2*

$2\ Si(OR)_{4-n}(OH)_n \rightarrow (OH)_n(OR)_{3-n}Si\text{-}O\text{-}Si(OR)_{4-n}(OH)_{n-1} + ROH$ *R. 5.3*

$\mathbf{P}\text{-}OH + Si(OR)_{4-n}(OH)_n \rightarrow P\text{-}O\text{-}Si(OR)_{4-n}(OH)_{n-1} + H_2O$ *R. 5.4*

Here, **P** is denoted for a particle and the -OH is the hydroxyl group on the particle surface. The network can be built of those partial hydrolyzed segments due to polycondensation. This network can be attached to the particle surface and interconnect these particles. Also branching and interconnecting of the chains can occur. Water which is formed during the condensation steps can be used for hydrolysis of the unreacted silicon alkoxide or further hydrolysis of the partial hydrolyzed and condensed network. The partially hydrolyzed and condensed TEOS network will be abbreviated with $TEOS_{H/C}$ to make a distinction between the reacted and unreacted TEOS.

Hybrid materials with various amounts of inorganic loading and different inorganic compositions are prepared and characterized. Next to proton conductivity, the behavior in ethanol-water systems is investigated by means of swelling and ethanol permeability measurements. The ethanol transport through the membrane is studied in liquid-liquid and liquid-gas systems (L-L diffusion and pervaporation respectively).

5.1. Membrane preparation

5.1.1. Chemicals

In addition to the chemicals presented in **Section 4.1.1**, tetraethoxysilane (99%, TEOS) was obtained from ABCR (Germany). Hydrophilic fumed silica, Aerosil®380, was provided by Evonik Degussa (Germany). According to the producer, Aerosil®380 primary particles have an average size of 7 nm. The SiO_2 content, based on ignited

material, is larger than 99.8 wt-%. The specific surface area (BET) is 380 ± 30 $m^2 g^{-1}$ and the pH of a 4% dispersion is between 3.7 – 4.7. Particle size measurements of Aerosil®380 in water resulted in an average particle or agglomerate size of 72.7 nm. All chemicals were used as received without further purification.

Sulfonation of PEEK

Sulfonation of PEEK was performed according to the DS($t_{sulfonation}$) procedure given in **Section 4.1.2**. The sulfonation time was set at 19 hours at 35 °C to obtain sPEEK with an IEC of 1.67 mmol g^{-1}.

5.1.2. Polymer solution and composite precursor dispersion

The concentration of the polymer solution for the preparation of the reference membrane was 0.12 g polymer per ml NMP. Three series of organic-inorganic nanocomposite systems with different inorganic loadings and inorganic compositions were prepared: i. Aerosil®380 (A-system), ii. TEOS-based inorganic network (T-system), and iii. a mixture of Aerosil®380 and hydrolyzed and polycondensed TEOS (AT-system). The serial and membrane names and the compositions of the Aerosil®380 and $TEOS_{H/C}$ pure and mixed nanocomposite systems are presented in **Table 5.1**.

Two different series of Aerosil®380 and $TEOS_{H/C}$ mixed systems were prepared with mass ratios of Aerosil®380 to sPEEK of 0.125 and 0.25. The ratio of Aerosil®380 to $TEOS_{H/C}$ are given in the membrane names (A*X*T*Y* means Aerosil®380 to $TEOS_{H/C}$ is *X*:*Y*). Loading, *L*, is defined as the mass of inorganic matter to the total solid mass:

$$L = \frac{m_{inorganic}}{m_{polymer} + m_{inorganic}} \qquad \textit{Eq. 5.1}$$

$$L = \frac{m_{TEOS,\,H/C} + m_{particles}}{m_{polymer} + m_{TEOS,\,H/C} + m_{particles}}$$

$$L = \frac{\left(m_{TEOS,\,H/C} / m_{particles}\right) + 1}{\left(m_{polymer} / m_{particles}\right) + \left(m_{TEOS,\,H/C} / m_{particles}\right) + 1}$$

Table 5.1: Serial and membrane names as well as with compositions and theoretical loadings of Aerosil®380 and TEOS based composite systems (A- and T-system) and of the AT-composite system.

Serial name	Membrane name	Polymer [wt-%]	Aerosil®380 [wt-%]	$TEOS_{H/C}$ [wt-%]	Loading [wt-%]
A	11A	88.9	11.1	0	11.1
	20A	80.0	20.0	0	20.0
	27A	72.7	27.3	0	27.3
0.125AT	16A2T1	84.2	10.5	5.3	15.8
	20A1T1	80.0	10.0	10.0	20.0
	27A1T2	72.7	9.1	18.2	27.3
	33A1T3	66.7	8.3	25.0	33.3
0.25AT	27A2T1	72.7	18.2	9.1	27.3
	33A1T1	66.7	16.7	16.7	33.3
	43A1T2	57.1	14.3	28.6	42.9
	50A1T3	50.0	12.5	37.5	50.0
T	11T	88.9	0	11.1	11.1
	20T	80.0	0	20.0	20.0
	27T	72.7	0	27.3	27.3

Mixed-matrix membranes (MMM) consisting of sPEEK/Aerosil®380 were prepared by dispersing the Aerosil®380 particles in NMP followed by ice-cooled ultrasonic treatment for 60 min. Then, the dispersion was stirred at room temperature (RT) for 3 h and subsequently the polymer was added. Composite membranes based on

sPEEK and TEOS were prepared by adding TEOS to NMP. After stirring for 30 min, MilliQ-water was added (n_{water}/n_{TEOS} = 2). Polymer was added after stirring the mixture for 3 h. The preparation of the membrane solutions of the AT-system started with dispersing the Aerosil®380 particles in NMP followed by ice-cooled ultrasonic treatment for 60 min. After 30 min, TEOS was added to the dispersion. MilliQ-water was added after 30 min to partially hydrolyze TEOS (n_{water}/n_{TEOS} = 2). This solution was stirred for 3 h at RT and then sPEEK was added. In all cases, after addition of the polymer the solution was stirred again for three days. The ratio of polymer to solvent was equal in all solutions.

5.1.3. Membrane formation

Membrane formation was based on the casting-solvent evaporation process as described in **Section 4.2.3**. A pure polymeric sPEEK membrane consisting of the same polymer as used in the preparation of mixed-matrix membranes was used as a reference membrane. All membranes were homogeneous and transparent, and the thickness varied between 50 and 60 µm. Mixed-matrix membranes with an inorganic loading higher than 40% became brittle. The membrane 50A1T3 (L = 50%) cracked during the membrane preparation and will not be further discussed in the results.

5.2. Results and discussion

5.2.1. Ion exchange capacity

The ion exchangeable groups present in the polymer and composite systems are determined by titration. The *IEC* of the pure polymeric matrix was 1.67 mmol g^{-1}. The *IEC* of the mixed-matrix systems is expressed as a function of loading and as a function of mass ratio of $TEOS_{H/C}$ to Aerosil®380 (**Figure 5.2**). The *IEC* as a function of loading is given by:

$$IEC_{MMM} = \frac{IEC_{polymer}\ m_{polymer}}{m_{MMM}} = (1-L)\ IEC_{polymer} \qquad Eq.\ 5.2$$

The subscripts polymer and MMM stand for the polymeric and mixed-matrix membrane respectively. The slope and the intersection with the y-axis represent *IEC* of the polymer used as an organic matrix in the nanocomposite systems (**Figure 5.2a**).

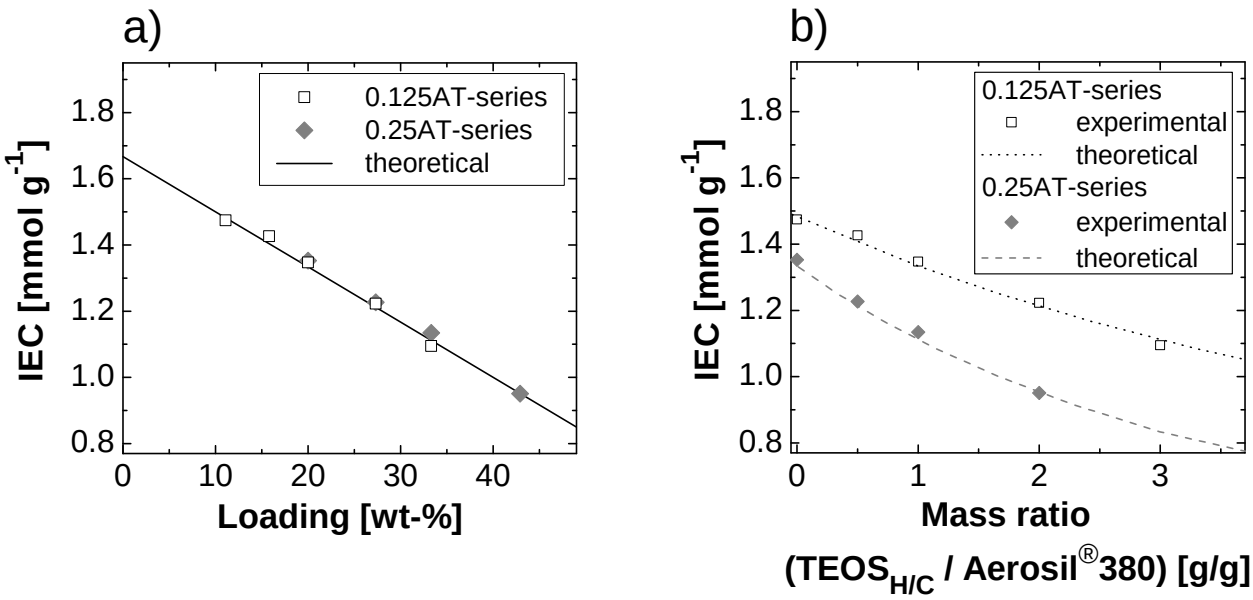

Figure 5.2: IEC as a function of a) inorganic loading and b) $TEOS_{H/C}$ to Aerosil®380 mass ratio. Experimental and theoretical data for two different Aerosil®380 to polymer mass ratios.

Two different Aerosil®380 to polymer mass ratios were prepared, namely 0.125 and 0.25. When **Eq. 5.1** is substituted in **Eq. 5.2**, the *IEC* as a function of $TEOS_{H/C}$ to Aerosil®380 mass ratio is obtained. The theoretical *IEC* was calculated by the sulfonic acid groups present in the mixed-matrix system and the ion exchangeability of the inorganic matter could be neglected. **Figure 5.2b** shows, that the calculated and practically determined *IEC*s are similar. The yield of the incorporation of inorganic compounds, based on the theoretical and experimental *IEC*, is in all cases larger than 98%. This means that the inorganic matrix added during membrane preparation remained nearly completely in the membrane and that the ion exchangeable groups

are the sulfonic acid groups of sPEEK. The same was valid for the pure A and T systems (data not shown).

5.2.2. Silica content

Thermogravimetrical analysis (TGA) is performed to determine the silica content in the composite material according to the procedure presented in **Section 3.1.4**. The spectra of all composite membranes are similar (**Figure 5.3**). The samples did not undergo a pretreatment step to eliminate the absorbed water in the material. In the temperature range RT till 200 °C, a decrease in mass is observed. This means that the absorbed water is evaporated. The absorbed water in the measured membranes varies between 2 and 3 wt-%. Subsequently, a plateau is obtained till 300 °C. From there, the degradation of the sulfonic acid groups starts. Just over 500 °C, a steep decrease is observed. The polyaromatic matrix decomposes and finally the inorganic matter (SiO_2) remains. A TGA measurement with the same conditions with pure sPEEK was performed by Jiang et al.[172] and a similar degradation behavior was observed.

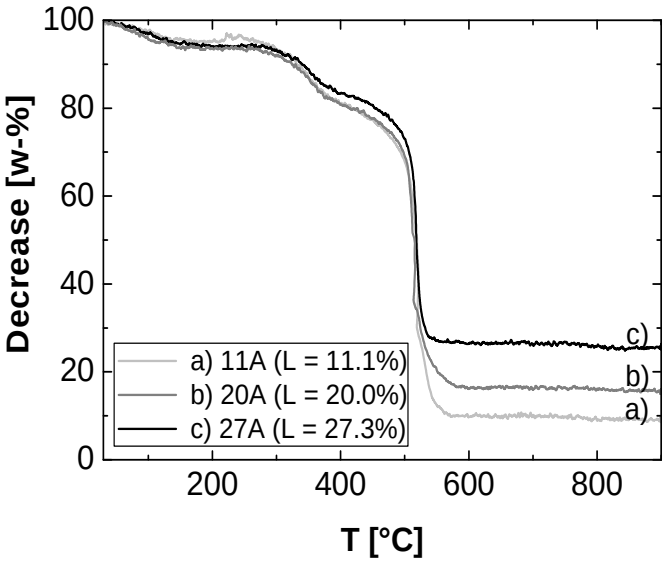

Figure 5.3: TGA curves for nanocomposite membranes of the A-system (Aerosil® 380).

All TGA results are shown in **Table 5.2** together with the theoretical loadings. Especially with membrane A11 (low loading), the results found with this method are significantly lower. In this table, the results of the wavelength dispersive X-ray fluorescence (WDXRF) measurements after digestion are also presented (**Section 3.1.5**). About 50 times more material is used in comparison to the TGA measurement (250 mg and 5 mg respectively), and the measured silica contents in the membrane are very similar to the theoretical silica contents. In accordance with the *IEC* measurements, the loss of silica during the membrane preparation seems to be marginal and the conversion of TEOS to silica is complete.

Table 5.2: Theoretical inorganic loading in comparison to inorganic content determined with TGA and WDXRF.

Name	Loading [wt-%]		
	Theoretical	TGA	WDXRF
11A	11.1	9.6	11.0
20A	20.0	16.7	19.9
27A	27.3	27.4	27.6
20A1T1	20.0	17.9	19.1
27A2T1	27.3	26.1	28.3

5.2.3. Density of dry membranes

In **Figure 5.4**, the density of the dry membrane is given for various composite systems. This density is experimentally determined with the procedure described in **Section 3.2.2**. The density of amorphous fumed silica particles is assumed to be 2.2 g ml^{-1} as frequently reported for fumed silica.[175,176] The same density is assumed for $TEOS_{H/C}$. The calculated density of a dry membrane is determined with:

$$\rho_{m,dry} = \left(\frac{1-L}{\rho_{polymer}} + \frac{L}{\rho_{inorganic}} \right)^{-1} \quad \text{with } 0 \leq L \leq 1 \qquad \textit{Eq. 5.3}$$

Dry densities of membranes of the AT-system correspond to the calculated values except for the membrane 43A1T2. Also membranes of the A-system and T-system exhibit lower density than the calculated ones. In case of the Aerosil®380 filled membranes and membranes 20A1T1 and 27A2T1, it is shown that the inorganic loading in the membranes are similar to the theoretical loading. Deviations in densities are assigned to a more voluminous structure due to the interstitial spaces between the polymer and inorganic matter.

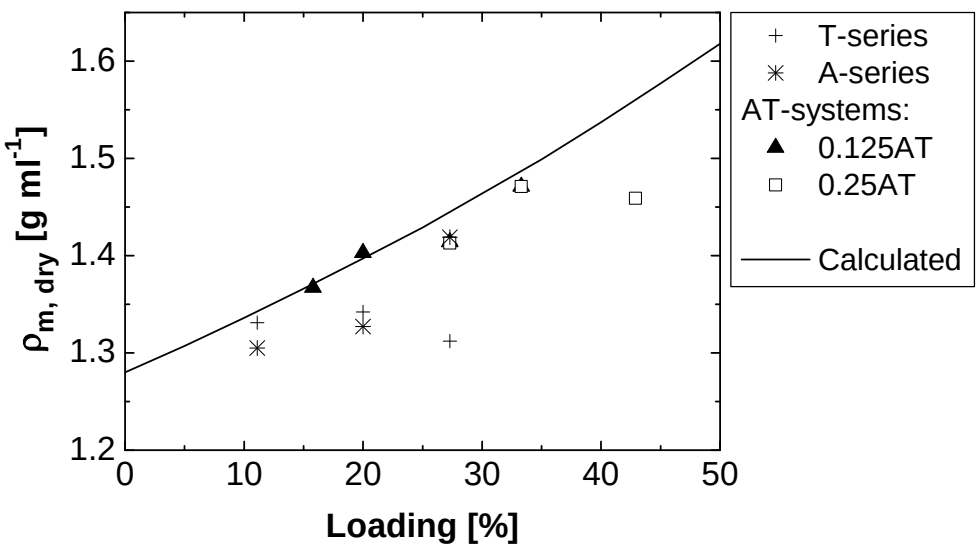

Figure 5.4: Densities of the dry membranes as a function of loading.

5.2.4. Morphology of composite systems

In this section, the morphology of the composite systems and the polymeric reference is discussed. The polymeric reference and the composite membranes with a silica loading of 11.1% are presented in **Figure 5.5**. Composite membranes with a loading

of 20.0% and 27.3% with different inorganic compositions are presented in **Figure 5.6** and **Figure 5.7** respectively.

The cross sectional structure of a pure sPEEK membrane was smooth and dense, giving no viable morphological information (**Figure 5.5a**). In contradiction to this, a ragged structure was found with the membrane exhibiting the lowest TEOS concentration (11T) (**Figure 5.5b**). No particles are observed and the inorganic phase was well dispersed in the polymeric matrix. The structure is obviously changed by the addition of TEOS. In the membrane with the lowest Aerosil®380 concentration (11A), particles were homogeneously distributed in the polymer matrix (**Figure 5.5c**).

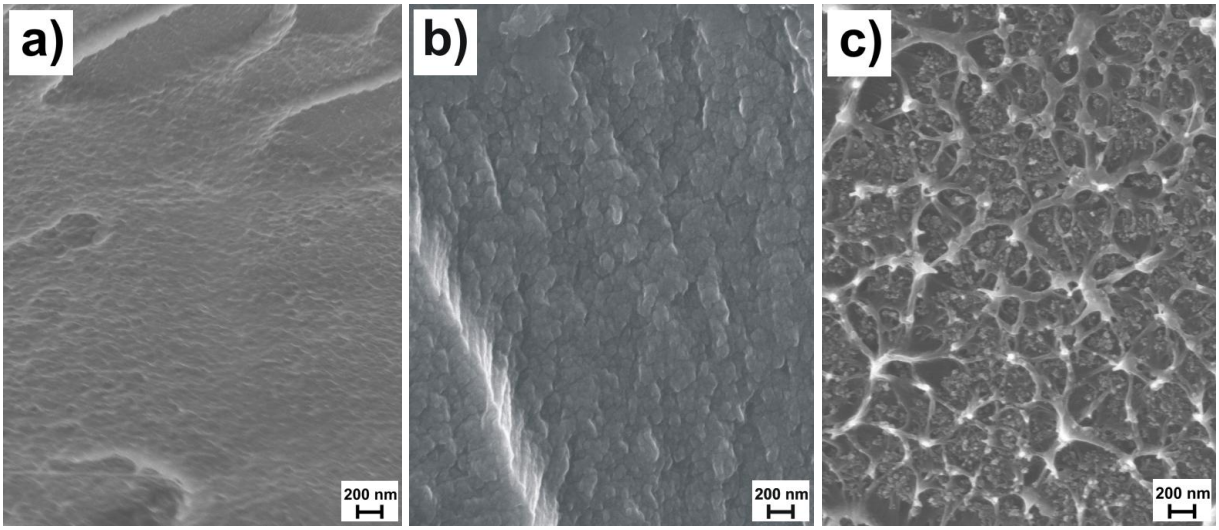

Figure 5.5: SEM pictures of a) sPEEK, and composite membranes with 11.1% silica loading: b) 11T; c) 11A.

The pure TEOS based composite system, 20T (**Figure 5.6a**) exhibited a ragged structure similar to membrane 11T, but now additional small particles are observed (high specific surface). The Aerosil®380-TEOS composite system, 20A1T1, showed a homogenous distribution, but agglomerated regions appeared (**Figure 5.6b**). When the inorganic phase consists of pure Aerosil®380 (20A), the particles were distributed homogeneously (**Figure 5.6c**). The concentration of Aerosil®380 particles is clearly increased in comparison to 11A.

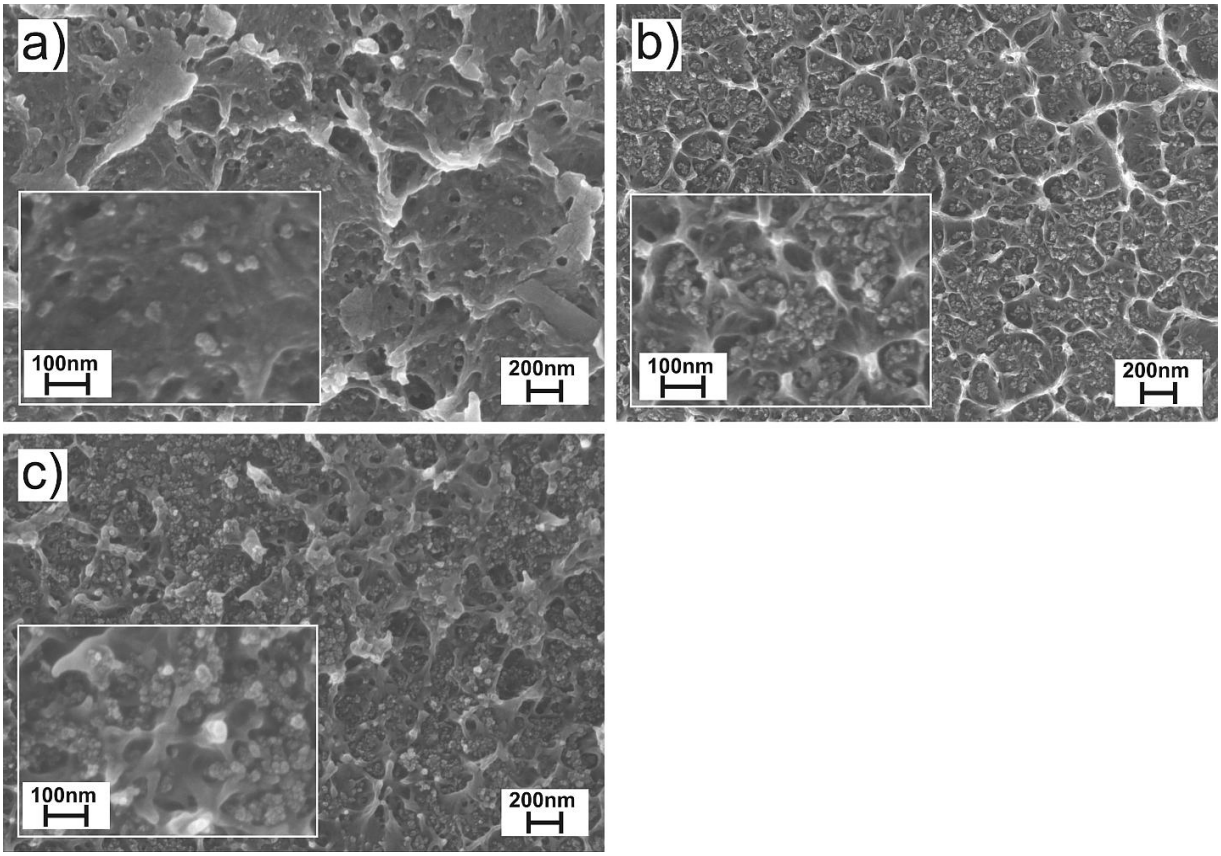

Figure 5.6: SEM pictures of composite membranes with 20.0% silica loading: a) 20T; b) 20A1T1; c) 20A.

An increase in TEOS concentration from 20% to 27.3% loading (20T to 27T) caused a complete change in cross sectional morphology (**Figure 5.7a**). The higher concentration of TEOS during the membrane preparation resulted in a composite membrane with large particles (approximately 100nm, low specific surface). When double the amount of $TEOS_{H/C}$ is added in comparison to Aerosil®380 (27A1T2), the agglomerates consisted of small particles and this structure seemed to be connected (**Figure 5.7b**). The composite system with the other mixed inorganic matrix (27A2T1) consisted of smaller particles (**Figure 5.7c**) and more aggregated and connected regions appeared. These cauliflower structures are typical for Aerosil-$TEOS_{H/C}$ combined inorganic phases. In case of the pure Aerosil®380 composite membrane (27A), the particles remained small and again homogeneously distributed in the polymer matrix (**Figure 5.7d**). The structure was similar to 20A, but the inorganic phase was more concentrated.

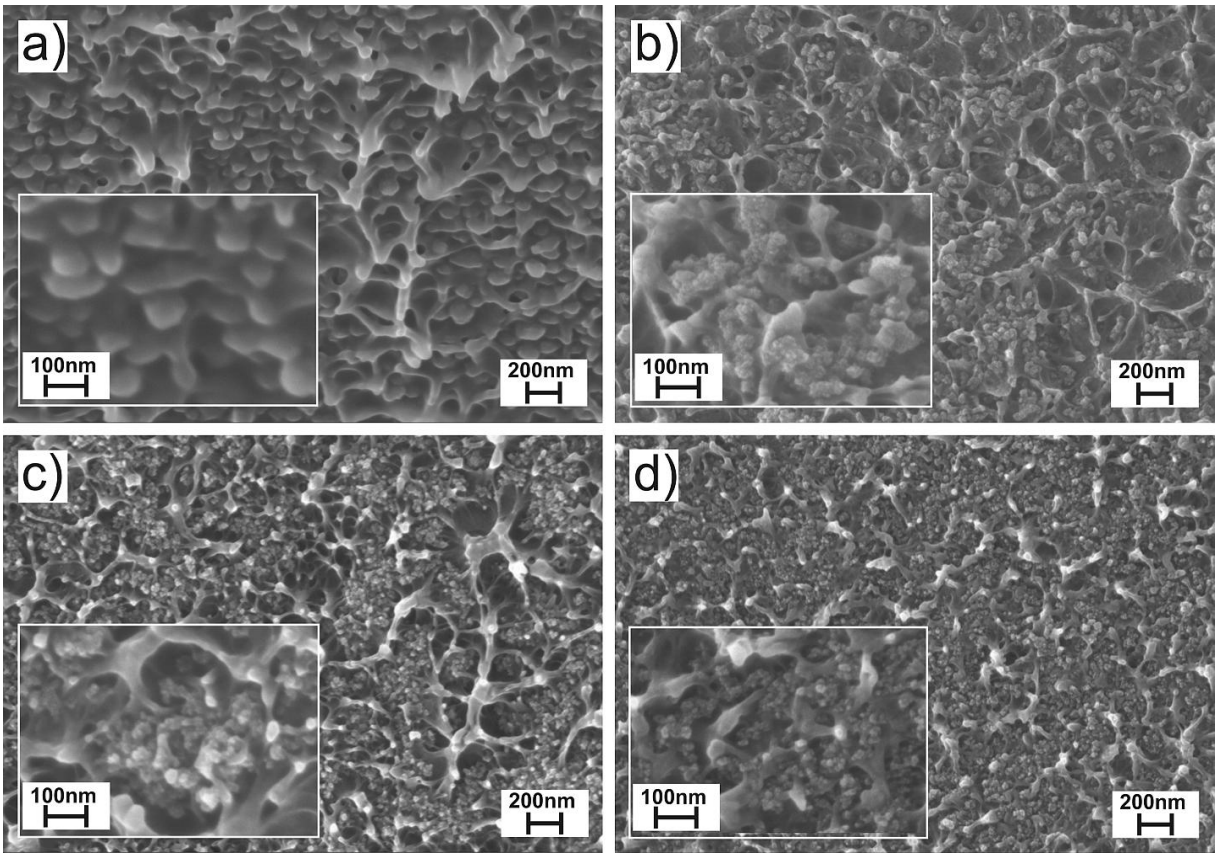

Figure 5.7: SEM pictures of composite membranes with 27.3% silica loading: a) 27T; b) 27A1T2; c) 27A2T1; d) 27A.

5.2.5. Liquid uptake and swelling

Liquid uptake and swelling in surface area and volume are determined with all membranes. Similar to the findings presented in **Section 4.2.3**, the uptake and swelling characteristics follow the same trend. To minimize the amount of data, only the liquid uptake results are presented.

Liquid uptake of pure Aerosil®380 and pure TEOS composite systems are given in **Figure 5.8a**. Water uptake of the T-series shows a modestly reducing trend with increasing $TEOS_{H/C}$ loading. For the lowest concentration (11T) no particles are observed with SEM and $TEOS_{H/C}$ probably exists in low molecular weight, partially condensed TEOS clusters randomly and homogeneously distributed in the material. The high amount of silanol groups respective to the $TEOS_{H/C}$ mass leads to a high water uptake. Increasing the TEOS content leads to larger particles and, therefore, to

a lower specific surface area with less active silanol groups per mass $TEOS_{H/C}$. A slightly reduced water uptake is measured. An additional effect is the decrease in concentration of hydrophilic sulfonic acid groups in the MMM with increasing loading.

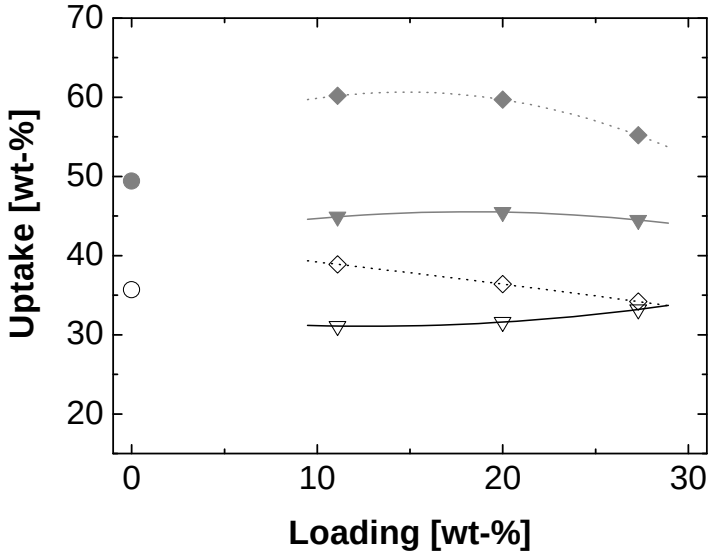

	sPEEK-REF	A-series	T-series
Water uptake	○	▽	◇
2 M EtOH uptake	●	▼	◆

Figure 5.8: Water and 2 M ethanol uptake of the mixed-matrix membranes: A-series (Aerosil® 380) and T-series (TEOS based). The sPEEK reference is denoted with circular symbols.

A remarkable increment respective to the polymeric reference is measured in 2 M ethanol. These observations can be explained by the various structures observed with SEM. A distinct inorganic phase is not observed in the structure of membrane 11T. $TEOS_{H/C}$ was well dispersed in the polymer, but the concentration is probably too low to form a network. Water, as well as ethanol, diffuses into the composite structure, where water prefers the hydrophilic regions. Ethanol interacts with the hydrophobic regions of the polymer and destabilizes the polymeric phase. On this, the composite structure swells, but is not stabilized by the inorganic phase. A similar argumentation can be given for membrane 20T. In case of membrane 27T, the

interaction between the large particles and the polymer is weaker than the other two membranes. This is, because the inorganic phase is more localized (large particles) and less distributed in the polymer matrix. Due to this feature, the hydrophobic backbone is less accessible to ethanol and less interrupted. The hydrophobic parts remain to a large extent intact resulting in lower 2 M ethanol uptake. In comparison to the polymeric reference, the membrane structure of the T-membranes is in all cases worsened, because the membranes are more susceptible to ethanol.

Liquid uptake of the membranes of the A-series shows a relatively constant course in the measured loading domain and these values are in all cases lower than the membranes of the T-series (**Figure 5.8**). The weight percentage of the polymer, and therefore also concentration of sulfonic acid groups in the mixed-matrix material, is reduced with increasing loading content. Based on purely the polymeric properties, less hydrophilic domains and, therefore, lower water uptake is expected. Simultaneously, the content of Aerosil®380 particles with high specific surface is increased. No remarkable structure changes are observed with SEM, implying that the enlargement of Aerosil®380 indulges in a higher specific surface as a function of particle mass. This results in additional water storage capacity in the MMM. The lowering of sulfonic acid concentration is therefore compensated by the higher proportion of hydrophilic particles, resulting in a similar water uptake for all membranes of the A-series. The water phase in these swollen membranes of the A-system is approximately 30% respective to the dry membrane material. With liquid uptake in 2 M ethanol, the ethanol diffuses into the composite structure along with water and this diffusion is driven by concentration difference inside and outside the membrane. The more hydrophobic ethanol molecules interact with the hydrophobic backbone of the polymer, inducing additional swelling and coexistent liquid uptake. The movement of the polymer chains is hampered due to the inorganic particles and an apparent equilibrium (stationary state) is reached.

Summarizing the results of the T-series and A-series, it is found that $TEOS_{H/C}$ clusters or small particles (< 5 nm) demolish the membrane structure on molecular

level. Large particles (100 nm) do not show much interaction with the polymer matrix, resulting in 'macro-effects'. The Aerosil®380 particles of approximately 10 nm appear to be the best size to fill the free volume of the polymer and stabilize the polymer matrix.

Figure 5.9 presents the uptake of the Aerosil®380-TEOS mixed-matrix systems. Two series with Aerosil®380 to polymer mass ratios of 0.125 and 0.25 are measured. In both series a maximum is observed at a $TEOS_{H/C}$ to Aerosil®380 ratio of 1. The curvature is mainly determined by the TEOS content leading to a higher total inorganic loading. At low content, liquid uptake increases due to increasing silanol groups. At higher contents, the interconnectivity of the inorganic network is enhanced and the movement of the polymer chains restrained due to the enlargement of the inorganic phase. The ability for liquid absorption decreases. The material becomes less flexible with increasing $TEOS_{H/C}$ content due to the higher total inorganic loading. This is observed by practical handling of these membranes.

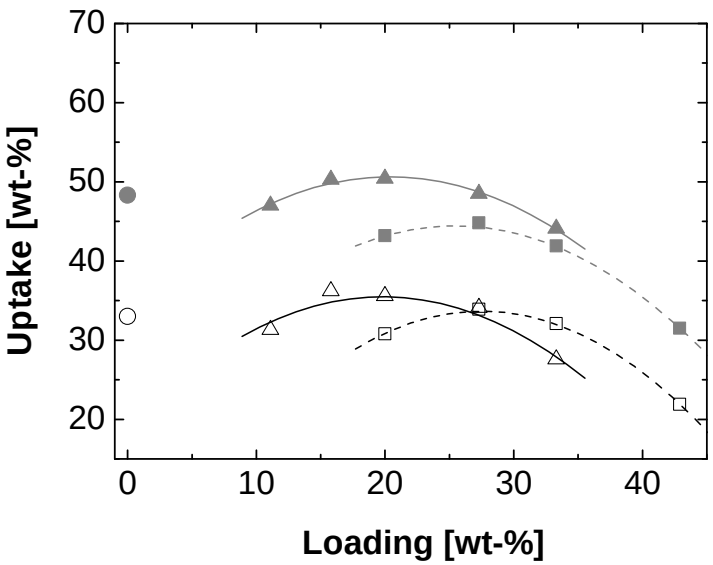

	sPEEK REF	0.125AT-series	0.25AT-series
Water uptake	○	△	□
2M EtOH uptake	●	▲	■

Figure 5.9: Water and 2 M ethanol uptake of the mixed-matrix membranes: AT-series, various inorganic loading consisting of different $TEOS_{H/C}$ to Aerosil®380 mass ratios. The sPEEK reference is denoted with circular symbols.

Uptake of water, 2 M and 4 M ethanol of membranes with an inorganic loading of 27.3% with different inorganic compositions is given in **Figure 5.10**. The water uptake is similar for all mixed-matrix systems. This is due to opposite effects. On the one hand, TEOS affects the hydrophilicity (higher water uptake) and on the other hand, TEOS enhances the interconnectivity of the inorganic phase (lower water uptake). These effects result in a water uptake similar to the polymeric reference. 2 M ethanol uptake decreases with increasing mass ratio of Aerosil®380 to inorganic matter. The 2 M ethanol uptake of the 27T membrane is even higher than the pure polymer reference. The excessive swelling is caused by the weak interaction between the silica particles and the polymeric matrix, as discussed before. Membrane 27A1T2 shows similar 2 M ethanol uptake as the polymeric reference. The interconnected inorganic phase should decrease the uptake, but the hydrophilic character of the TEOS results in similar absorption as the reference membrane. The membranes 27A2T1 and 27A show lower uptake values. The inorganic phase is homogeneously distributed and the inorganic phase acts as a barrier for chain movement of the

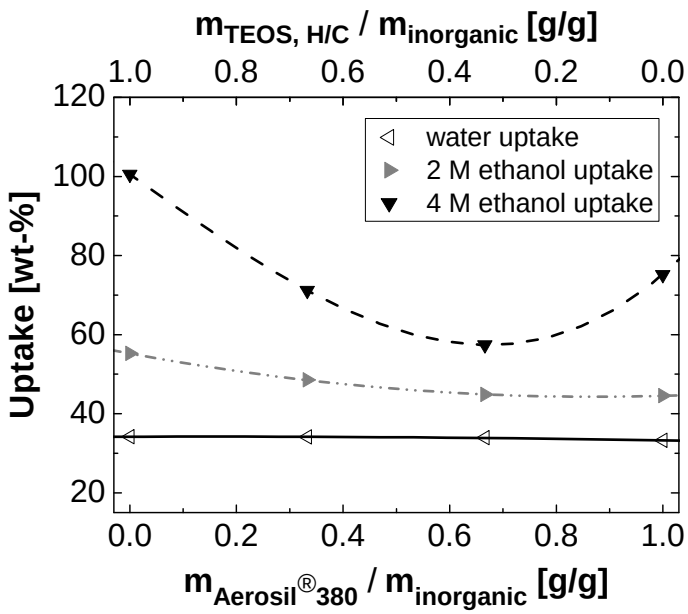

Figure 5.10: Water, 2 M and 4 M ethanol uptake of composite membranes with 27.3% loading consisting of different inorganic compositions. Uptake of the sPEEK reference in water, 2 M and 4 M ethanol were 36%, 49% and 98% respectively.

polymer. Liquid uptake and concomitant swelling remain lower than the polymeric reference. The stability is even more pronounced when the uptake measurement is performed in 4 M ethanol. The uptake of the polymeric reference is in this case 98% and the uptake of membrane 27T is similar. The pure Aerosil®380 membrane 27A is higher than both membranes of the AT-system. This implies less interaction between particles and less influence on the swelling behavior than the AT-system. Within the AT-system an inorganic network can be developed. Consequently, this results in less uptake due to the compact membrane structure. Lowest uptake is obtained with membrane 27A2T1, where the uptake is reduced by 40% in comparison to the polymeric reference.

5.2.6. Proton conductivity

Proton conductivity is strongly related to the liquid content in the membrane as presented in **Section 4.2.4** and is measured with the spring tips configuration (STC) as described in **Section 3.2.1**. Proton conductivity of the mixed-matrix systems as a function of *IEC* is given in **Figure 5.11a**. In addition, the sPEEK data from **Section 4.2.4** are implemented to make a direct comparison. The solid line in **Figure 5.11a** represents the fit of these sPEEK results. The proton conductivity of the polymeric reference used as polymeric matrix in the MMMs is emphasized.

The proton conductivity curves of the MMMs (**Figure 5.11a**) show similar development as the water uptake curves (**Figure 5.8** and **Figure 5.9**). This confirms the relationship between absorbed water and proton conductivity. The membranes of the T-series show a decrease in proton conductivity with decreasing IEC (increasing loading), which is consistent to the liquid uptake (**Figure 5.8**). The lowering in specific surface (active silanol groups) respective to the $TEOS_{H/C}$ mass results in less storage and less distribution of the water phase. The resistance for the proton flow increases. The membranes in the A-series, with a homogeneous distribution and similar aggregate size of Aerosil®380, show relatively constant proton conductivity. On the

one hand, the sulfonic acid groups in the composite material become less concentrated with increasing loading. On the other hand, the high specific hydrophilic surface increases the water absorption. Maxima obtained with the Aerosil®380-$TEOS_{H/C}$ mixed-matrix systems are at the same positions for water uptake as well as for proton conductivity. In the latter case, the maxima are more pronounced. This behavior has been explained previously.

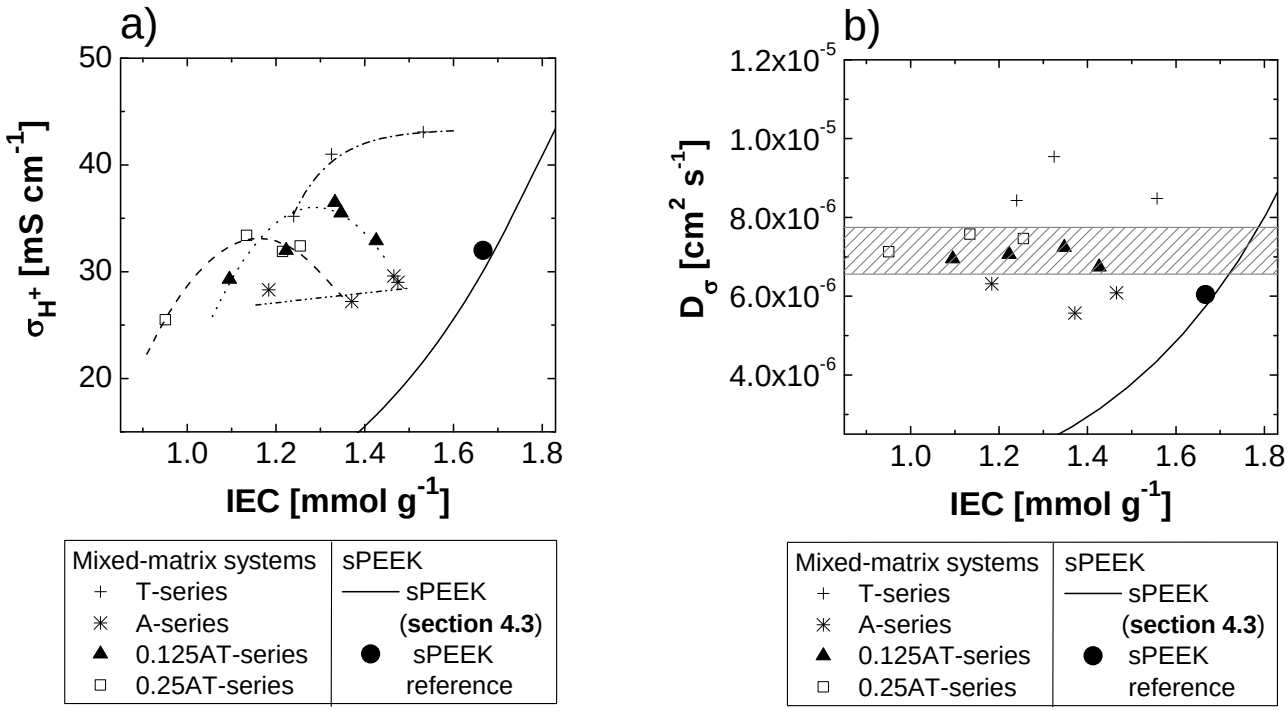

Figure 5.11: a) Proton conductivity and b) proton diffusion coefficient as a function of IEC for various mixed-matrix membranes in comparison to sPEEK membranes with different IEC.

The proton diffusion coefficient (D_σ) is calculated from the proton conductivity based on the Nernst-Einstein relationship (**Section 4.3.4**). The proton diffusion coefficient as a function of *IEC* is given in **Figure 5.11b**. The advantage of using D_σ is that the water content is integrated in this parameter by means of swelling in volume of the membrane and the concentration of functional groups in the wet membrane. Therefore, a better comparison between membranes can be made than with the

proton conductivity values, which strongly relates to the water content in the membrane.

The sPEEK curve is again the best fit of sPEEK membranes with *IEC* between 1.15 and 2 mmol g^{-1} presented in **Section 4.2.4** and again the sPEEK reference is emphasized. Notable are the constant D_σ values for the AT-membranes, in the marked area in **Figure 5.11b**. This implies that the proton diffusion coefficient is independent of the Aerosil®380-$TEOS_{H/C}$ system which is used. In all cases, a higher proton diffusion coefficient is obtained with lower *IEC* respective to the polymeric reference. In case of the A-system and T-system, proton diffusion coefficients show a similar development as water uptake and proton conductivity.

5.2.7. Ethanol permeability

5.2.7.1. Liquid-liquid systems

Ethanol permeability of MMMs with a loading of 20.0% and 27.3% measured in the L-L diffusion system with 2 M ethanol concentration difference at 25 °C and 40 °C are presented in **Figure 5.12a**. High ethanol permeability of the pure T-system membranes is expected based on the liquid uptake results (**Figure 5.8**). Membranes of the A-series and AT-series show similar results and the inorganic content does not seem to affect the permeability under these conditions. These MMMs have ethanol permeability coefficients significantly lower than the polymer reference. In case of the 40 °C measurement, this is more pronounced than with the measurement preformed at 25 °C. No considerable difference between the membranes of the AT-system with 20.0% and 27.3% loading is observed.

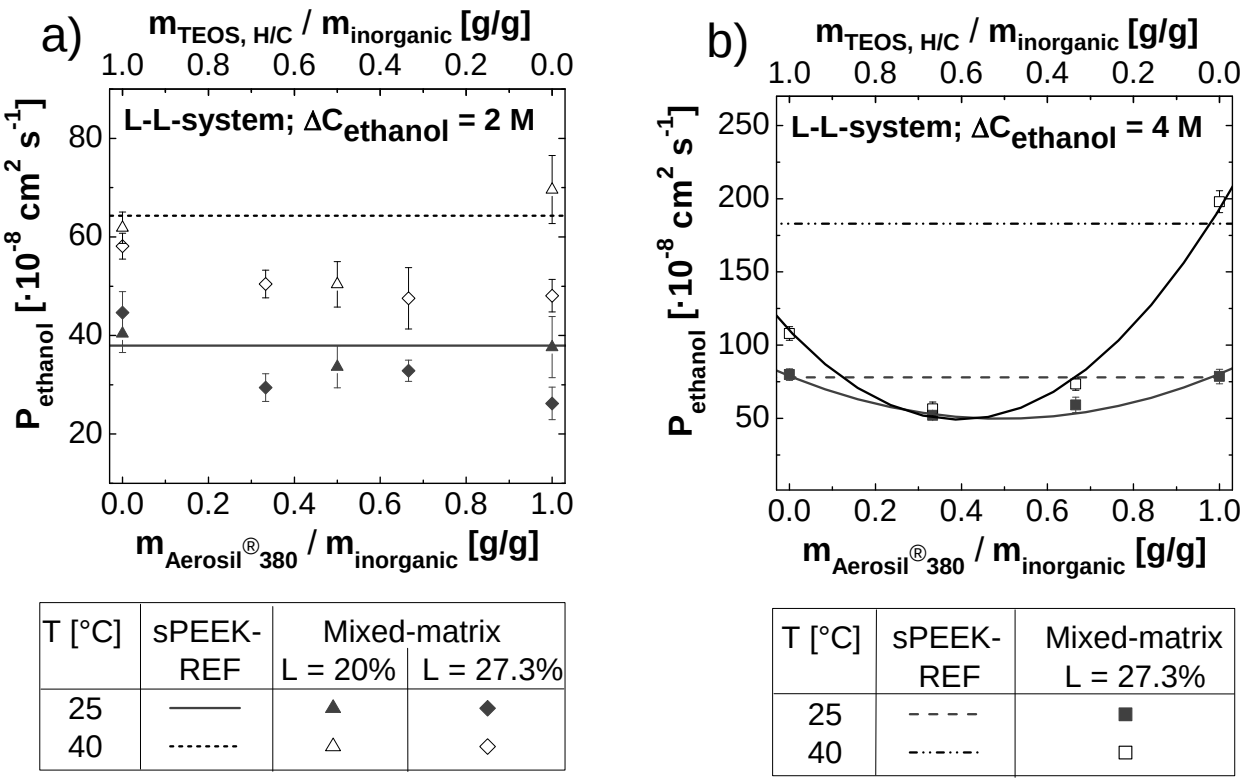

Figure 5.12: Ethanol permeability coefficients of various mixed-matrix membranes with various silica compositions at 25 °C and 40 °C measured with L-L diffusion. a) 2 M feed concentration; b) 4 M feed concentration.

The measurements with 4 M ethanol concentration difference show significant distinction between the membranes with different inorganic compositions (**Figure 5.12b**). In this case, just membranes with 27.3% loading are studied. Remarkable reduction in ethanol permeation is obtained with membranes of the AT-system. The ethanol permeability coefficients are reduced by a factor of 2 and 3 for the measurements at 25 °C and 40 °C respectively. This reduction is not achieved when the inorganic filler consisted of pure $TEOS_{H/C}$ or pure Aerosil®380. Static liquid uptake measurements of membrane 27T result in the highest uptake values (**Figure 5.10**). In this dynamic measurement under these conditions, it is found that large $TEOS_{H/C}$ particles hindered the movement of the polymer chains resulting in a more stable membrane system in comparison to membrane 27A. This pure Aerosil®380 mixed-matrix membrane consists of small, homogeneously distributed particles (**Figure 5.7**).

At 25 °C the permeability coefficient is similar to that of the T-system. At 40 °C the membrane completely lost stability, even worse than membrane 27T. In this mixed-matrix structure the particles do not show a strong interaction with each other or with the polymer. The remarkable high permeability coefficient is not expected based on the uptake data (**Figure 5.10**).

Lowest ethanol permeability coefficients are obtained with the membranes of the AT-system. The stabilizing effect and the reduction in ethanol permeability are best observed under relatively severe conditions. The low ethanol permeability coefficients indicate that an interconnected inorganic phase stabilizes the composite structure. This is not observed under milder conditions (2 M ethanol concentration), where not much diversity in permeability coefficient is observed.

5.2.7.2. Liquid-gas systems

Ethanol and water permeability and other separation characteristics are also determined with L-G system (pervaporation). Results of the MMMs with 27.3% loading are presented in **Figure 5.13**. Permeability coefficients of ethanol and water of MMMs containing an Aerosil®380-$TEOS_{H/C}$ combined inorganic matrix are modestly lower than the sPEEK reference membrane. Aerosil®380 and $TEOS_{H/C}$ filled membranes (A-system and T-system) exhibit higher permeability coefficients. The increase in ethanol permeability coefficient is 1.3 times and 1.8 times higher than the sPEEK membrane. Ideal membrane selectivity for all membranes varies between 10 and 12.

Pervaporation behavior as a function of loading is tested with the A-series, T-series and the MMMs with 20% inorganic loading. In case of the A-series, all ethanol permeability coefficients are between 280 and 330 kg µm m^{-2} h^{-1} bar^{-1}, slightly higher as the polymeric reference (250 kg µm m^{-2} h^{-1} bar^{-1}). Ethanol permeability coefficients of the T-series are even higher (between 390 and 520 kg µm m^{-2} h^{-1} bar^{-1}). Membranes with 20% loading show permeability coefficients between 320 and

400 kg µm m^{-2} h^{-1} bar^{-1}. Ideal membrane selectivity for all these membranes is approximately 10 (average value: 10.2 ± 0.4). Separation factors of these membranes vary between 1.6 and 1.8.

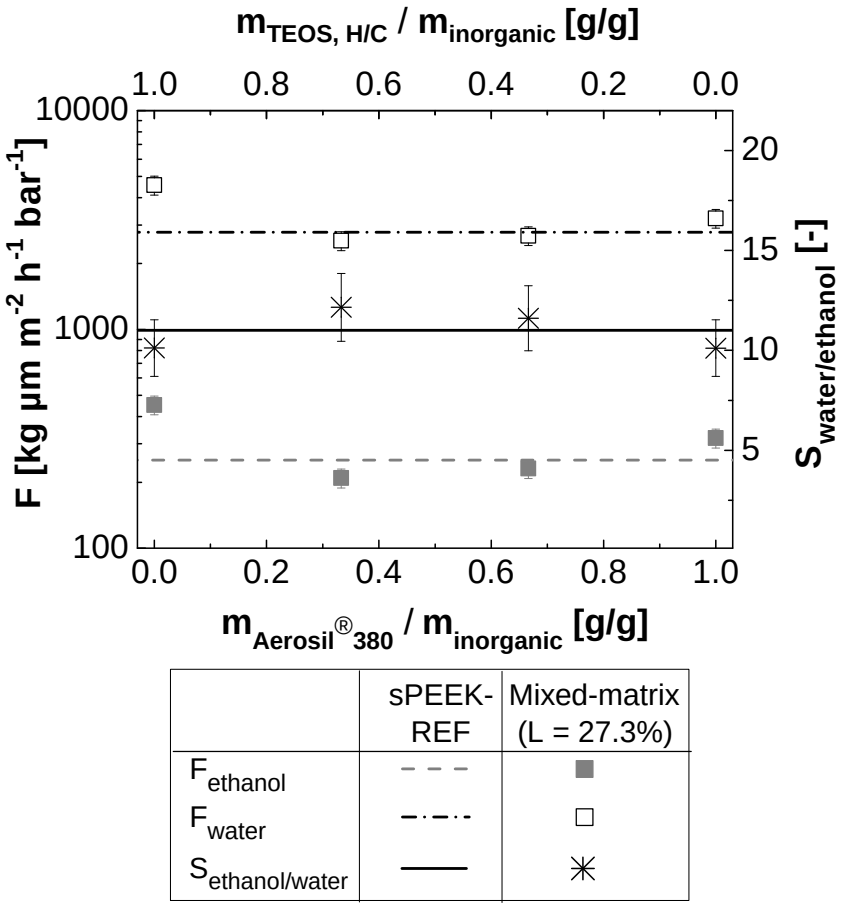

Figure 5.13: Permeability coefficients of water and ethanol (left axis) and ideal membrane selectivity (water / ethanol) (right axis) determined with pervaporation of mixed-matrix membranes with a total loading of 27.3% and various silica compositions measured with pervaporation (feed concentration: 2 M; T: 40 °C; p^0: 13 mbar).

The ideal water to ethanol selectivity is barely influenced by the loading of the inorganic matrix or its composition. Best selectivity coeffients are obtained with the Aerosil®380-$TEOS_{H/C}$ combined MMMs with 27.3% inorganic loading ($S_{water/ethanol}$ ≈ 12). All other membranes are modestly lower ($S_{water/ethanol}$ ≈ 10), even lower as the sPEEK reference ($S_{water/ethanol}$ = 11). The influence of the hydrophilic inorganic matrix is therefore marginal. The composition of the inorganic matter, consisting of

hydrophilic silica particles and/or a hydrophilic silica network, rather influences the swelling of the membrane and (L-L) permeation behavior than the water to ethanol selectivity. It is expected that the hydrophilic polymer regions and the hydrophilic interconnected inorganic network is able to absorb water to such an extent that transport of ethanol will occur via this water phase by its own driving force. This second water phase, as described by Kreuer,[34] can easily be stored in this mixed-matrix material, because there is no interaction between the polymeric and inorganic network.

5.2.7.3. Comparison of L-L and L-G systems

As described in **Section 4.2.5.3**, a comparison between L-L and L-G systems is not completely straightforward, because the driving force and the transport mechanism in both systems are different. It is remarkable, that the ethanol permeability of the MMMs with a Aerosil®380-$TEOS_{H/C}$ combined inorganic phase is clearly lower than the sPEEK reference membrane in L-L systems. This difference is more demonstrative in 4 M ethanolic systems than in 2 M systems. In case of ethanol permeability coefficients determined in L-G systems, these differences between the MMMs and sPEEK reference membrane are rather modest.

The absolute fluxes (expressed in kg µm m^2 h^{-1}, data not presented) measured in L-G systems are again much lower than the absolute fluxes in L-L systems, similar to the presented data in **Figure 4.16** (*IEC* = 1.67 mmol g^{-1}). It is expected, that this is mainly due to the different swelling behavior in both systems. In the L-L system, the membrane is unsupported with a liquid on both sides. In the L-G system, the membrane is supported and pressed by a hydrostatic pressure of the liquid on the support. Additionally, the applied vacuum on the permeate side draws this membrane towards the support. Less swelling of the membrane material is expected because it is wetted on just on side, and the permeating species are continuously removed by means of the applied vacuum.

5.2.8. Summary and outlook

The presence of the interconnected inorganic phase leads to improved membrane properties in comparison to the polymeric reference. Addition of an interconnected inorganic matrix induces improved swelling behavior and lower fuel crossover, especially in higher concentrated ethanol systems, with higher proton diffusion coeffients. An influence of $TEOS_{H/C}$ concentration on stationary liquid uptake and proton conductivity is shown. The influence of inorganic composition is rather marginal with respect to dynamic ethanol permeability measurements, because both inorganic components are hydrophilic. The large inner silica surface, obtained by the high loading in the composite structure, can be used for further improvement of membrane properties by means of functional silanes. It was expected, that the mixed-matrix composition improved the swelling behavior and water to ethanol selectivity because of hydrophilic nature of the inorganic phase. The swelling properties of the investigated MMMs are not optimal, because the inorganic and organic matrices are not connected. Applying appropriate silanes, this connection can be established. This should lead to more compact and stable membrane structures with reduced swelling behavior.

Chapter 6

Modified silica based mixed-matrix membranes

In **Chapter 5**, the formation of an interconnected inorganic phase in a non-fluorinated organic phase is proposed. The inorganic phase consisted of hydrophilic fumed silica particles (Aerosil®380) interconnected by partially hydrolyzed and condensed tetraethoxysilane ($TEOS_{H/C}$). This modestly affected the swelling and permeation behavior of the membranes, while maintaining the proton conductivity in low concentrated ethanol-water mixtures. At higher ethanol concentrations, an improvement with respect to these properties in comparison to the pure polymeric membrane was observed.

In this chapter, membranes are studied where this inorganic phase is modified with silanes bearing basic groups. This strategic step is done to establish a connection between the organic and inorganic network by means of acid-base interactions. The modified interconnected mixed-matrix membrane is schematically represented in **Figure 6.1**. It is expected, that these modified mixed-matrix systems result in low swelling materials with low fuel crossover, even in higher concentrated ethanolic systems. Higher concentrated feed stocks in DEFC are desirable, because of the better fuel cell performance.

In the first part of this chapter (**Section 6.1**), various modifiers with different basic groups and/or spacer lengths are investigated. The modifier concentration is kept constant and these membranes are mutually compared. In addition, these membranes are also compared to the polymeric reference and the unmodified mixed-

matrix membrane. The main membrane parameters like liquid uptake, permeation behavior, and proton conductivity are used for this purpose. Based on these results a modifier is selected.

The membrane modification with this functional silane is studied in detail and is presented in the second part of this chapter (**Section 6.2**). A membrane series is prepared whereby the modifier concentration is varied. The influence of modifier concentration on membrane properties is studied in ethanol-water systems, in comparison to the unmodified mixed-matrix membrane and the polymeric reference. Liquid uptake is measured in water and ethanol-water mixtures with various ethanol concentrations at room temperature and in water as a function of temperature. Dynamic ethanol and water permeability measurements are performed by means of pervaporation (L-G system) and L-L diffusion (L-L system). The proton conductivity is investigated as a function of ethanol concentration and as a function of temperature.

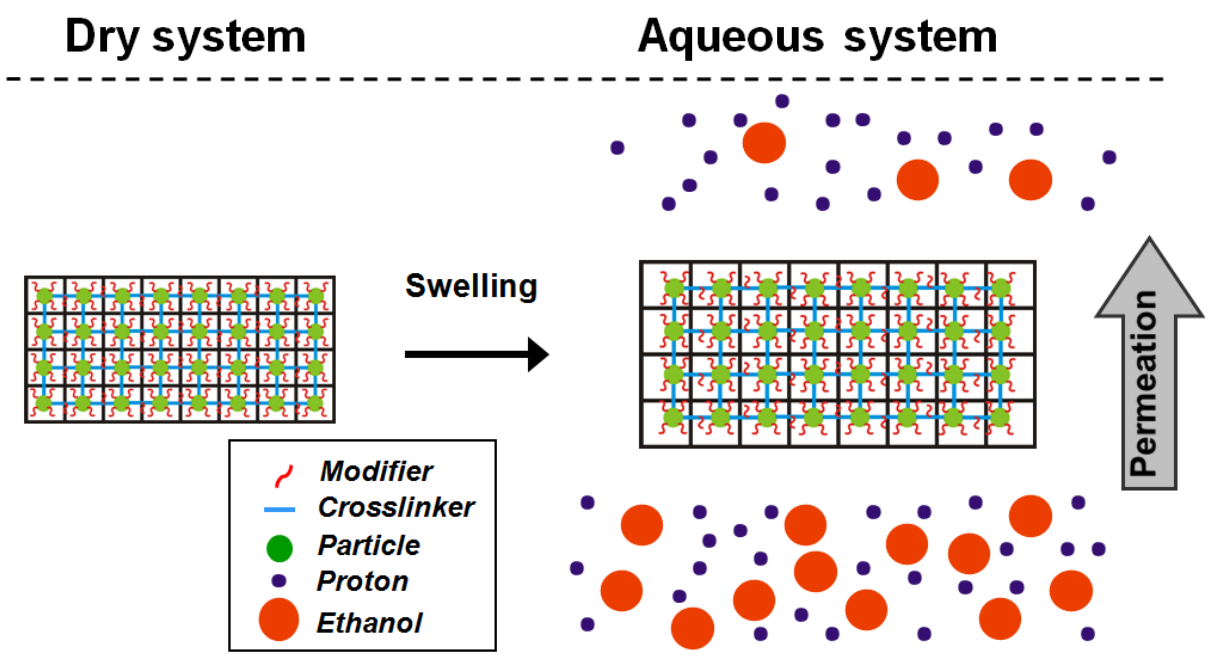

Figure 6.1: Schematic representation of a modified interconnected mixed-matrix membrane.

6.1. Modifier screening for mixed-matrix membrane modification

6.1.1. Membrane preparation

6.1.1.1. Chemicals

In addition to the chemicals presented in **Section 4.1.1** and **Section 5.1.1**, functional silanes bearing basic groups (**Table 6.1**) were obtained from ABCR (Germany). All chemicals were used as received without further purification.

Sulfonation of PEEK

The sulfonation of PEEK was performed according to the DS($t_{sulfonation}$) procedure given in **Section 4.1.2**. The sulfonation time was set at 22 hours at 35 °C to obtain sPEEK with an *IEC* of 1.79 mmol g^{-1}. This higher *IEC*, in comparison to the polymeric matrix material chosen in **Chapter 5**, is chosen because of its excessive swelling behavior and high ethanol permeability as shown in **Section 4.2.5**. Respective to these properties, improvements should be observed best, and the impact of various modifiers should be easily differentiated than when an instable matrix is used.

6.1.1.2. Functional silanes bearing basic groups

N-[3-(triethoxysilyl)propyl]-4,5-dihydroimidazole (*DHIM*) and 3-aminopropyltriethoxy-silane (*APTES*) are functional silanes bearing a dihydroimidazole group and a primary amine group respectively. Markowitz et al.[177] prepared silica particles with amino and dihydroimidazole surface groups by means of a modified Stöber process. In addition to TEOS, functional silanes were added to a water-in-oil emulsion. They found that dihydroimidazole-modified silica has a greater amount of surface basicity with stronger basic sites than amino-modified silica, since dihydroimidazoles contain

Table 6.1: Chemical structure and properties of functional silanes bearing basic groups.[178]

Functional silane	Abbr.	$T_{boiling}$ [°C]	M_w [g mol^{-1}]	$M_{w,\ hydrolyzed}$ [g mol^{-1}]
N-[3-(triethoxysilyl)propyl]-4,5-dihydroimidazole 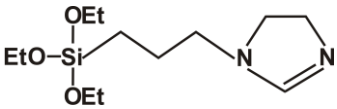	DHIM	134	274.43	190.34
3-Aminopropyltriethoxysilane 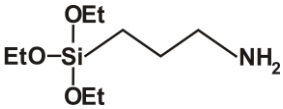	APTES	122-3	221.37	137.27
Bis(trimethoxysilylpropyl)amine 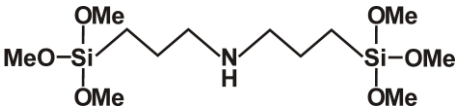	TMSPA	152	341.56	257.46
N-(2-aminoethyl)-3-amino propyltrimethoxysilane 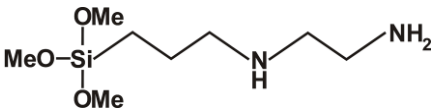	AEAPTMS	140	226.36	180.31
N-(6-aminohexyl)amino-propyltrimethoxysilane 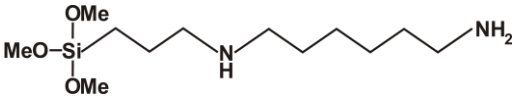	AHAPTMS	160-5	292.49	236.42

two nitrogen groups. Linker length is a measurement for the distance between the silicon atom and the organic functionality. This linker length is identical in case of DHIM and APTES. Bis(trimethoxysilylpropyl)amine (*TMSPA*) is a dipodal coupling agent and should have an impact on substrate bonding and hydrolytic stability of the composite system.[178] The functional group is a secondary amine in the centre of the molecule with two alkoxysilypropyl groups with equivalent linker length to DHIM and APTES. N-(2-aminoethyl)-3-aminopropyltrimethoxysilane (*AEAPTMS*) and N-(6-

amino-hexyl)aminopropyltrimethoxysilane (*AHAPTMS*) are diamine functional silanes with different linker length. Differences in linker lengths have an impact on hydrophobicity and mobility of the functional groups, and a longer linker length can extent further from the inorganic substrate. This has an influence on the reactivity of the functional groups. The presence of two amino groups could theoretically lead to the formation of two acid-base pairs.

Base dissociation constants

Unfortunately, base dissociation constants of functional silanes were not available. These dissociation constants are determined with titration. To this, 250 µl of modifier is added to 50 ml MilliQ-water, and during titration with 0.1 M HCl the pH is monitored. These water reactive modifiers are instantly hydrolyzed to $-Si(OH)_3$ and probably condensed when getting in contact with water. Titration curves and results are presented in **Figure 6.2** and **Table 6.2** respectively. The basicity of the monofunctional groups decreased in the order:

APTES > DHIM > TMSPA

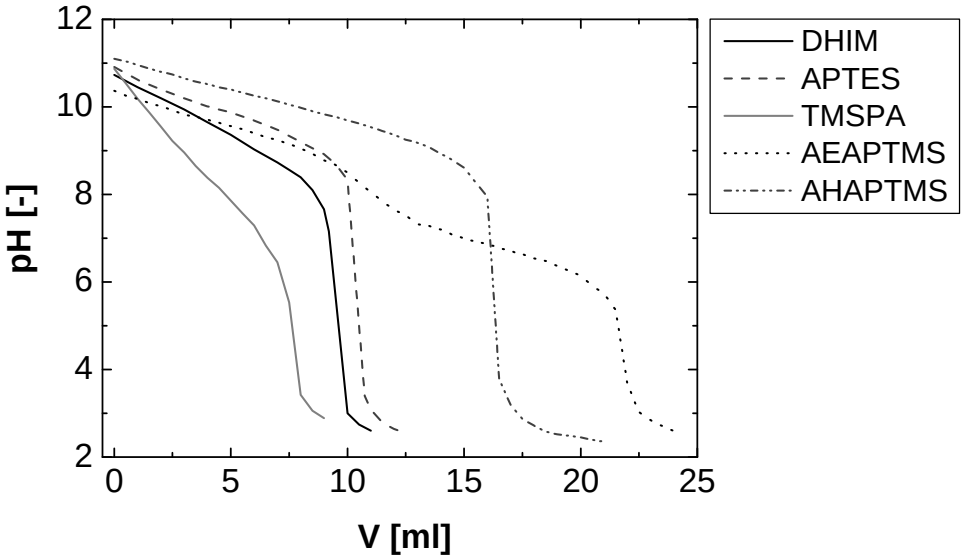

Figure 6.2: Titration curves of various modifiers.

Table 6.2: Titration results of various modifiers.

Modifier	$n_{modifier}$ [mmol]	$\#_{basic\ groups}$	$pH_{initial}$		n_{H^+} (EP) [mmol]		EP		pK_b
DHIM	0.92	1	10.7		0.96		5.1		4.6
APTES	1.07	1	10.9		1.03		5.9		4.2
TMSPA	0.76	1	10.9		0.78		4.6		5.5
AEAPTMS	1.14	2	10.4	1:	1.15	1:	7.9	1:	4.6
				2:	1.03	2:	4.4	2:	7.4
AHAPTMS	1.00	2	11.1		1.66		5.2		4.1

EP: equivalence point

The higher pK_b value of the primary amine respective to the dihydroimidazole is in contradiction to the findings of Markowitz et al.[177] In **Table 6.3**, dissociation constants of basic compounds in aqueous solutions are presented.[179] These compounds are similar to the functional groups present in the silanes, but they do not contain the alkoxysilyl groups. They are given to make a comparison to the practically determined values. The pK_b values of the monoamines vary between 3.1 and 3.5, whereas the pK_b values determined with titration varied between 4.1 and 5.5. These higher pK_b values can be explained by the acidic character of the $Si(OH)_3$-groups. TMSPA is a dipodal silane containing two alkoxysilyl groups on the secondary amine. The higher amount of acidic silanol groups within the modifier results in a higher pK_b value in comparison to DHIM and APTES. The molar amounts of basic groups of these monofunctional silanes are similar to the amount of added protons at the equivalence point (EP) (**Table 6.2**). This implies good accessibility of the functional groups in the water-modifier mixture.

Comparison of the pK_b of DHIM with imidazole and 2,4-dimethylimidazole is less meaningful because of the different chemical characters. Imidazole is an aromatic compound with various resonance structures resulting in an amphoteric substance.

The presence of two methyl groups on positions 2 and 4 increases basicity. In case of DHIM, the alkoxysilylpropyl group is present on position 1 of the imidazole ring. The ring is no conjugated system anymore, resulting in stronger basicity because of free electron pairs on both nitrogen atoms.

Table 6.3: Base dissociation constants of organic basis in aqueous solution.[179]

		pK_b	T [°C]
ethylamine		3.19	20
propylamine		3.29	20
n-hexylamine		3.44	25
dimethylamine		3.27	25
ethylenediamine	1:	3.29	0
	2:	6.44	
hexamethylenediamine	1:	2.14	0
	2:	3.24	
imidazole		7.05	25
2,4-dimethylimidazole		5.64	25

The chemical structure of AEAPTMS and AHAPTMS varies just in linker length. With the titration of AEAPTMS, two EPs are found, whereas one EP is found with AHAPTMS. Mutual interaction between the two amino-groups, separated by an ethylene group, causes two different pK_b values. In case of AHAPTMS, the separating group is a hexamethylene group. Both amines do not interact anymore because of the large interspacing, which results in similar pK_b values. These two pK_b values could not be distinguished by this titration procedure, leading to one pK_b value for AHAPTMS. This explanation is supported by the pK_b values for the similar basic substances, ethylenediamine and hexamethylenediamine. The pK_b values of ethylenediamine differ by three *pH* units, whereas hexamethylenediamine by just

one. Another significant observation in **Table 6.2** is the amount of acid added to reach the EP (n_{H^+}). In case of AEAPTMS, the molar amount of protons is similar to the theoretical amount of basic groups (2.18 mmol to 2.28 mmol). Just 1.66 mmol of protons are added to reach the EP of AHAPTMS interacting with just 83% of the theoretically available basic groups. Reasons for this are, on the one hand, the stronger basic character. AHAPTMS is the strongest base among the tested modifiers (pK_b of 4.1). The amino groups interact more strongly and irreversibly with acidic silanol groups, reducing the available basic groups. On the other hand, the longer flexible linker accounts for intermolecular interaction. Preferably, the amino groups i) are hydrogen-bonded or ii) interact with silanols.[180]

6.1.1.3. Polymer solution and composite precursor dispersion

The concentration of the polymer solution for the preparation of the reference membrane was 0.12 g polymer per ml NMP. The inorganic phase of the reference mixed-matrix membrane consisted of Aerosil®380 and partially hydrolyzed and polycondensed TEOS (AT-System). This composition was similar to membrane 20A1T1 described in **Section 5.1.2**. This was apparently not the optimal inorganic composition, because the unmodified MMM investigations (**Chapter 5**) and modifier screening were (partially) performed simultaneously.

The precursor dispersion was prepared by dispersing Aerosil®380 particles in NMP followed by ice-cooled ultrasonic treatment for 60 min. After 30 min, TEOS was added to the dispersion. MilliQ-water was added after 30 min to partially hydrolyze TEOS (n_{water}/n_{TEOS} = 2). In case of modification with functional silanes, the silane was added after another 30 min. The modifier concentration was 1 mmol modifier respective to the mass of inorganic phase and the molar ratio of modifier to TEOS ($n_{modifier}/n_{TEOS}$) was 0.12. This solution was stirred for 3 h at RT and subsequently sPEEK was added. In all cases, after addition of the polymer, the solution was stirred for three days, and the ratio of polymer to solvent was equal in all solutions. The

mass ratio of Aerosil®380 to sPEEK was 0.125, and the mass ratio of Aerosil®380 to $TEOS_{H/C}$ was one, resulting in a total inorganic loading of 20% (excluding the modifier).

6.1.1.4. Membrane formation

Membrane formation was based on the casting-solvent evaporation process as described in **Section 4.2.3**. A pure polymeric sPEEK membrane consisting of the same polymer as used in the preparation of composite membranes was used as a reference membrane. All membranes were homogeneous and transparent and the thickness varied between 50 and 60 µm.

6.1.2. Results and discussion

The sPEEK polymer chosen for modifier screening in modified mixed-matrix systems has an *IEC* of 1.79 mmol g^{-1} (equivalent to 60% sulfonation). The usage of this polymer as pure polymeric membranes in DEFC is critical because of its excessive swelling behavior and high ethanol permeability as shown in **Section 4.2.5**. This polymer is chosen to study various modifiers to functionalize the inorganic matrix in mixed-matrix membranes (MMM), because expected improvements of this instable matrix should be observed best. Basic functional groups of the silanes can interact with the sulfonic acid groups of the polymer matrix to form ion pairs. This interaction should improve the membrane stability. The formation of ion pairs results in a reduction in liquid uptake, and consequently, a reduction in proton conductivity is expected. Modifier screening is based on the macroscopic properties of the modified mixed-matrix membranes. Firstly, the membrane behavior in ethanol-water systems, subdivided in static and dynamic measurements, is discussed. Secondly, proton conductive behavior is investigated. Finally, these results are linked together by means of the characteristic ratio, the selectivity of proton diffusion respective to

ethanol permeability. This ratio is used to compare membranes and is also described in **Section 4.2.8**.

6.1.2.1. Membrane behavior in water-ethanol systems

Liquid uptake and swelling in surface area in water and 2 M ethanol is done with the modified MMMs, the unmodified MMM and the polymeric reference (**Figure 6.3**). The same trend is observed with both methods. Membrane properties of the polymeric reference and the unmodified MMM are similar. Liquid uptake of the unmodified MMM is even higher than the polymeric membrane because of the hydrophilic inorganic content in the membrane.

Modification with functional silanes bearing basic groups resulted in all cases in a reduction of liquid uptake and coherent swelling. It can be seen that the DHIM modified membrane exhibits lower swelling properties than the membrane containing APTES. Next to the interaction with the sulfonic acid groups, sterical reasons can also be brought forward as an argument to explain this difference. It is likely, that the dihydroimidazole group shields the sulfonic acid more than the amino group. This leads to inhibition of the hydration.

Another comparison of monofunctional silanes is based on primary and secondary amines, APTES and TMSPA, respectively. TMSPA is a dipodal coupling agent resulting in a good substrate coupling, e.g., on the Aerosil®380 particles. This silane can also be built in the silica network or can have a crosslinker function by connecting, e.g., particles and $TEOS_{H/C}$ network. Liquid uptake is lower in case of the TMSPA modified membrane in comparison to the APTES modified membrane. Twice as much alkoxysilypropyl linker groups are present in the chemical structure of TMSPA respective to APTES making the modified membrane more hydrophobic. Next to the water repellant nature, hydrophobic interaction may also take place between these hydrophobic parts of the silane and the hydrophobic parts of the polymer. The alignment of both phases can be improved resulting in a more stable structure. In addition, the weight proportion of TMSPA is expected to be nearly twice

as that of APTES based on the hydrolyzed molar weight (**Table 6.1**). This results in a concomitant higher volume fraction of TMSPA present in the free volume of the polymer restraining the polymer chain movements. Due to these reasons, less liquid is absorbed in the TMSPA modified MMM resulting in less swelling.

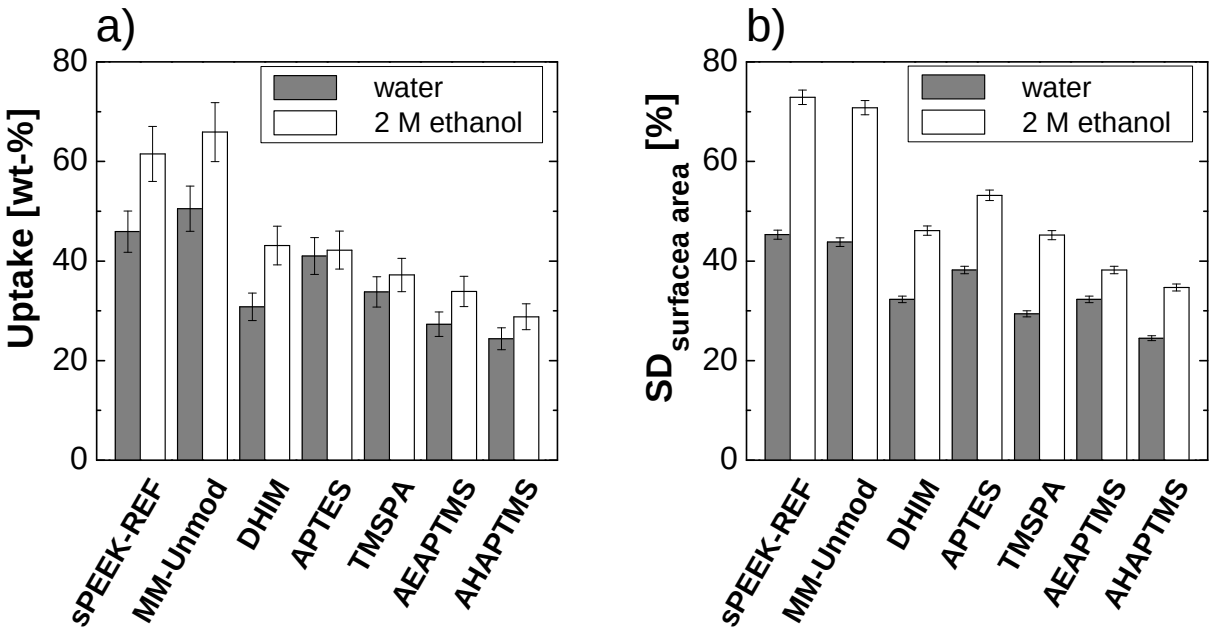

Figure 6.3: a) Liquid uptake and b) swelling degree in surface area at RT of modified mixed-matrix membranes in comparison to the sPEEK and unmodified mixed-matrix membrane. IEC_{sPEEK} is 1.79 mmol g^{-1}; silica loading is 20%; modifier concentration ($n_{modifier}$ / m_{silica}) is 1 mmol g^{-1}.

AEAPTMS and AHAPTMS are both diamine functional silanes. AHAPTMS contains a hexamethylene group between both amino groups, whereas AEAPTMS contains an ethylene group. The longer linker length of AHAPTMS is more mobile and flexible, and both amino groups are equally basic and stronger basic than AEAPTMS. This results in a more stable composite structure. In addition, the longer and more hydrophobic linker of AHAPTMS also makes the MMM more hydrophobic. Similar to the TMSPA and APTES comparison, these hydrophobic parts can be compactly arranged with the hydrophobic parts of the polymer. Also the volume proportion of AHAPTMS is larger than AEAPTMS. Liquid uptake and swelling is therefore to a larger extent reduced compared to the AEAPTMS modified MMM.

Ethanol permeability coefficients of this membrane series determined in the *L-L system* (diffusion cell) are given in **Figure 6.4**. The unmodified MMM shows inferior permeation behavior to the pure polymeric reference. The interconnected inorganic matrix does not interact with the polymer. This network cannot stabilize the excessive swelling of the polymer matrix and may even worsen it by its hydrophilic character. The presence of functional silanes in the mixed-matrix accounts for interaction between the inorganic matrix and the sPEEK polymer. Ethanol permeation is significantly reduced respective to the polymeric reference in the following order:

APTES > DHIM ≥ TMSPA > AEAPTMS > AHAPTMS

Highest $P_{ethanol}$ … … … … … … lowest $P_{ethanol}$

Reasons why this order is obtained are similar to the reasons given in the discussion of liquid uptake and swelling results.

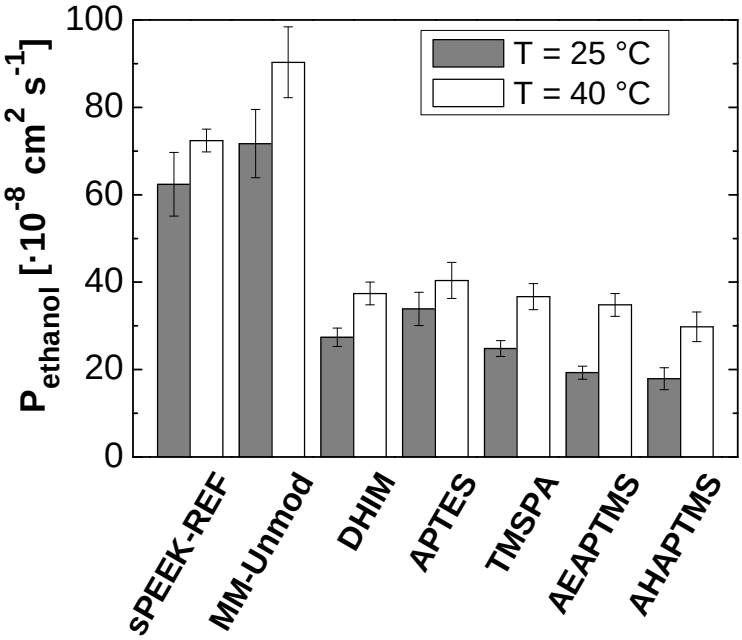

Figure 6.4: Ethanol permeability coefficients determined with L-L diffusion cell (conditions: ΔC is 2 M; T is 25 °C and 40 °C) of modified mixed-matrix membranes in comparison to the sPEEK and unmodified mixed-matrix membrane. IEC_{sPEEK} is 1.79 mmol g^{-1}; silica loading is 20%; modifier concentration ($n_{modifier}$ / m_{silica}) is 1 mmol g^{-1}.

Ethanol permeability coefficients determined in the *L-G system* (pervaporation) reveal a similar trend as with the L-L system (**Figure 6.5**), except for the DHIM and TMSPA. DHIM modified MMM exhibits lower ethanol permeability than the TMSPA modified MMM. A more significant difference is observed with the water to ethanol ideal membrane selectivity. The DHIM modified MMM has a selectivity of water to ethanol of 21, higher than all other membranes. Worst selectivity is 14 and is obtained with the TMSPA modified MMM. Ideal water to ethanol selectivity coefficients of APTES, AHAPTMS, and AEAPTMS modified membranes are 15, 18, and 20 respectively, resulting in the following order:

TMSPA < APTES < AHAPTMS < AEAPTMS < DHIM

Lowest $S_{water/ethanol}$ ... ... Highest $S_{water/ethanol}$

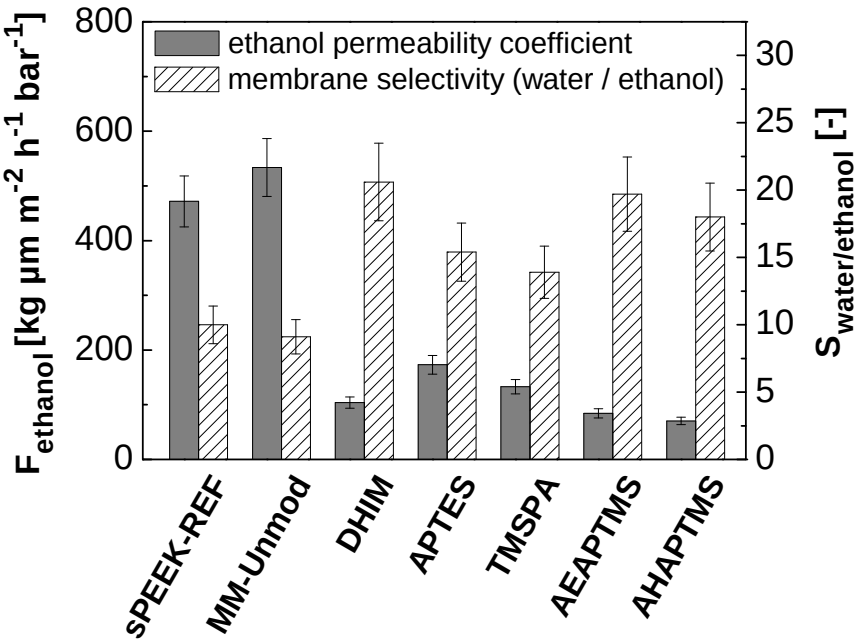

Figure 6.5: Ethanol permeability coefficients and ideal membrane selectivity coefficients (water to ethanol) determined with pervaporation (conditions: C_{feed} = 2 M; T_{feed} = 40 °C and p^{perm} = 13mbar) of modified mixed-matrix membranes in comparison to the sPEEK and unmodified mixed-matrix membrane. IEC_{sPEEK} is 1.79 mmol g^{-1}; silica loading is 20%; modifier concentration ($n_{modifier}$ / m_{silica}) is 1 mmol g^{-1}.

The lower ethanol permeability and the lower water to ethanol selectivity of TMSPA respective to APTES, and AHAPTMS respective to AEAPTMS, are explained by the higher modifier volume fraction in the modified mixed-matrix system, and the more hydrophobic nature of the modifiers respectively. The higher volume fraction accounts for enhanced blocking of the permeating species. Due to the more hydrophobic nature of these silanes, the transport of hydrophobic ethanol is enhanced, whereas the transport of water is inhibited. Obviously, this results in lower water to ethanol selectivity. Based on the low ethanol fluxes, it is unlikely that ethanol permeates through the hydrophobic regions of the polymer. This is in agreement with Huang et al.[163] They described similar findings with the separation of isopropanol and water by means of pervaporation.

The high water to ethanol selectivity of DHIM is most likely due to the more hydrophilic nature of the dihydroimidazole group in comparison to the amino groups of APTMS and TMSPA. Hydrolyzed molecular weights and total fluxes through the membrane coincide, indicating a relation between weight fraction (and accordingly volume fraction) and inhibition of total flux:

Modifier		APTMS		DHIM		TMSPA
$M_{w,\ hydrolyzed}$	[g mol^{-1}]	137.27	<	190.34	<	257.46
J_{total}	[kg µm m^{-2} h^{-1}]	160	>	128	>	113

This relation does not include the permeation of both species separately, because the water to ethanol selectivity is dependent on the hydrophobicity of the applied silanes. High water to ethanol selectivity is favored, because next to lowering of ethanol crossover a water rich phase should be maintained to assure proton mobility.

6.1.2.2. Proton conductivity

Proton mobility is the other important parameter with respect to membrane investigation for fuel cells. Proton conductivity and proton diffusion coefficients for this membrane series are given in **Figure 6.6**. Proton conductivity of the unmodified MMM is lower than the polymeric membrane, while the proton diffusion coefficient is higher. This is due to *IEC* and swelling properties of the membranes. With DHIM and APTES modified membranes similar values are obtained. These values are lower than the references, because the basic groups interact with the sulfonic acid groups. The hydrophilic character of the membrane is reduced which affects the hydration of the membrane. The membrane containing TMSPA, bearing a secondary amine, exhibits lower proton conductivity than the other monofunctional silanes. This is explained by its more hydrophobic nature. Highly stable membranes are obtained with the diamine modified MMM. Theoretically, interactions with double the amount of sulfonic groups

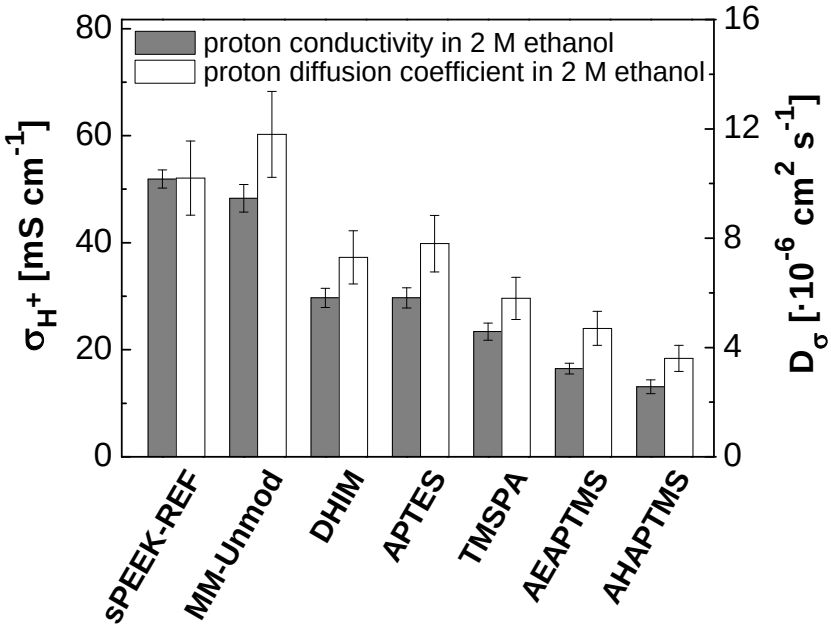

Figure 6.6: Proton conductivity (left y-axis) and proton diffusion coefficient (right y-axis) in 2 M ethanol at RT of modified mixed-matrix membranes in comparison to the sPEEK and unmodified mixed-matrix membrane. IEC_{sPEEK} is 1.79 mmol g^{-1}; silica loading is 20%; modifier concentration ($n_{modifier}$ / m_{silica}) is 1 mmol g^{-1}.

are possible in comparison to monofunctional silanes. Therefore, less sulfonic acid groups are available and less water can be absorbed. The hydrated network is then probably less connected in these stabilized composite membranes. In case of AHAPTMS, this effect is more pronounced than with AEAPTMS. This is attributed to the stronger basic character and the more hydrophobic nature of the silane. The positive impact as described with the swelling and permeation characteristics evolves into a negative effect on proton mobility.

6.1.2.3. Fuel cell prediction

Mixed-matrix membranes with various modifiers are compared by means of the characteristic ratio, the selectivity of proton diffusion respective to ethanol permeability. In addition to the ratio of proton diffusion coefficient to ethanol permeability coefficient determined with pervaporation (D_σ / $F_{ethanol}$) as described in **Section 4.2.8** (**Figure 6.7a**), the ratio respective to the ethanol permeability coefficient determined in the L-L system (D_σ / $P_{ethanol}$) is presented as well (**Figure 6.7b**). Ethanol permeability coefficients are used of the measurement with 2 M ethanol feed concentration at 40 °C (pervaporation) and 2 M ethanol concentration difference at 25 °C (L-L diffusion). Proton conductivity is determined in 2 M ethanol at RT.

Differences in characteristic ratio are more pronounced in case of D_σ / $F_{ethanol}$ than with D_σ / $P_{ethanol}$. Selectivity coefficients of the polymeric reference and the unmodified MMM are nearly identical. D_σ / $F_{ethanol}$, as well as D_σ / $P_{ethanol}$, show best values for the DHIM modified membrane. Membranes modified with the primary and secondary amine, APTES and TMSPA, have similar selectivity coefficients. The difference between functional silanes containing two amino groups, AEAPTMS and AHAPTMS, is mainly based on the difference in proton diffusion coefficient. D_σ / $F_{ethanol}$ of both membranes is higher than the other amine-based modified MMMs, because of the significantly lower ethanol pervaporation.

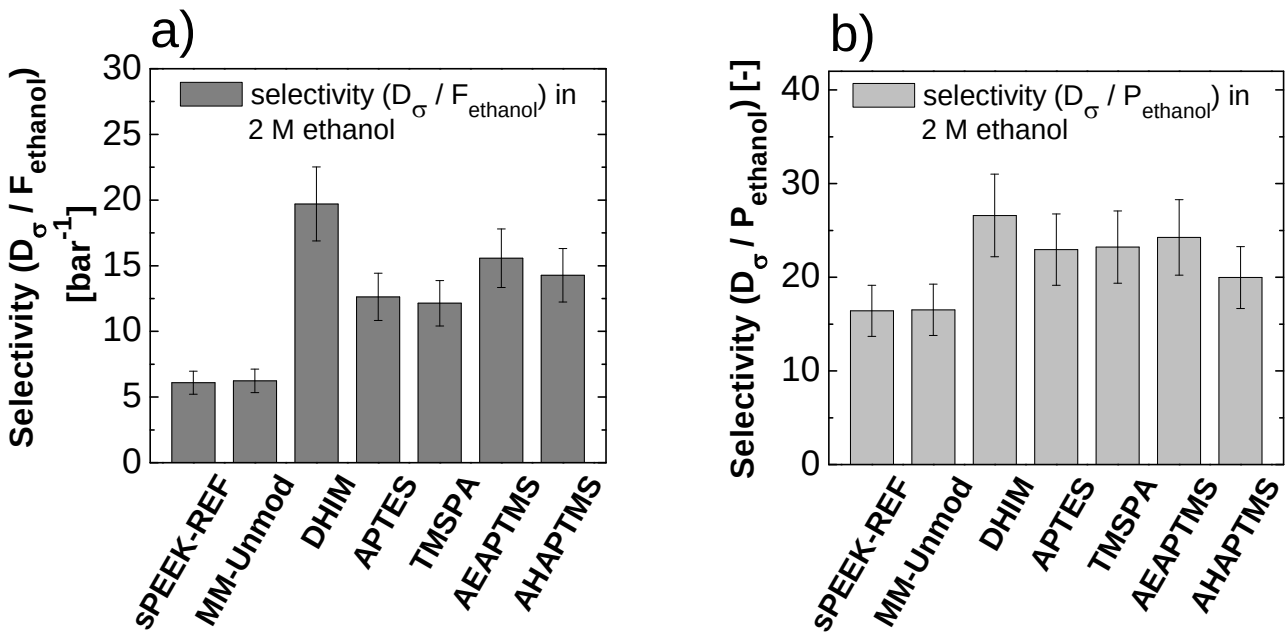

Figure 6.7: Selectivity of proton diffusion respective to ethanol permeability in 2 M ethanol systems of modified mixed-matrix membranes in comparison to the sPEEK and unmodified mixed-matrix membrane. Ethanol permeability determined in a) L-G system: (D_σ / $F_{ethanol}$) and b) L-L system: (D_σ / $P_{ethanol}$). IEC_{sPEEK} is 1.79 mmol g^{-1}; silica loading is 20%; modifier concentration ($n_{modifier}$ / m_{silica}) is 1 mmol g^{-1}.

6.1.2.4. Modifier selection for further investigation

Mixed-matrix membranes modified with various functional silanes bearing basic groups have been compared by means of liquid uptake, swelling properties, ethanol permeability, and proton mobility. Membrane stability and coherent reduction in ethanol permeability were improved compared to the polymeric reference and unmodified mixed-matrix membrane. The acid-base interaction resulted in a connected organic-inorganic network. Less sulfonic acid groups were available to form and connect the hydration network and, therefore, the proton conductivity of the modified membranes was in all cases lower. All tested functional silanes had these membrane features in common.

Membranes containing monoamine groups (primary and secondary amine) showed similar selectivity of proton diffusion to ethanol permeability. Differences in membrane

properties were mainly caused by differences in hydrophilicity and weight fraction of the modifier in the mixed-matrix system. Membranes containing diamine functional groups showed remarkable low ethanol permeation. Ethanol permeability of the modified membrane with longer linker was even lower than the silane containing shorter linker length. This is attributed to the stronger basic character and the mobility of the functional end groups. The more hydrophobic nature of the AHAPTMS caused lower water to ethanol selectivity than AEAPTMS. Extreme reduction in proton conductivity makes these silane types less favorable for proton conductive membranes.

The functional silane which is selected for profound investigation of modified mixed-matrix membranes is N-[3-(triethoxysilyl)propyl]-4,5-dihydroimidazole (DHIM). The membrane containing dihydroimidazole groups studied in this section exhibited low ethanol permeability with an acceptable decrease in proton conductivity. This membrane showed highest water to ethanol selectivity coefficient as well as highest proton diffusion to ethanol permeation selectivity coefficients.

6.2. Dihydroimidazole modified mixed-matrix membranes

6.2.1. Membrane preparation

Chemicals used in the membrane preparation of the dihydroimidazole modified mixed-matrix membranes are described in **Section 6.1.1.1**. The sulfonation of PEEK was performed according to the DS($t_{sulfonation}$) procedure given in **Section 4.1.2**. The sulfonation time was set at 19 hours at 35 °C to obtain sPEEK with an *IEC* of 1.66 mmol g^{-1}. This *IEC* is similar to the polymer used in **Chapter 5**, where it was shown that this polymer exhibited acceptable swelling properties, ethanol permeability, and proton conductivity. The *IEC* is lower than the polymer used in **Section 6.1** which was too high for applicable DEFC membranes.

6.2.1.1. Polymer solution and composite precursor dispersion

The concentration of the polymer solution for the preparation of the reference membrane was 0.12 g polymer per ml solvent. The mixed-matrix membranes were prepared as described in **Section 5.1.2** (membrane type: 27A2T1). This composition is favored because the unmodified mixed-matrix membrane showed low swelling characteristics (up to 4 M ethanol) in combination with low permeation and acceptable proton diffusion properties.

The inorganic phase of the MMM consisted of Aerosil®380 particles interconnected with partially hydrolyzed and condensed TEOS ($TEOS_{H/C}$). The following procedure to obtain composite precursor dispersion solutions was followed. Aerosil®380 particles were dispersed in NMP followed by ice-cooled ultrasonic treatment for 60 min. After 30 min, TEOS was added to the dispersion. MilliQ-water was added after 30 min to partially hydrolyze TEOS (n_{water} / n_{TEOS} = 2). In case of modification with N-(3-triethoxysilylpropyl)-4,5-dihydroimidazole, DHIM, the silane was added after another 30 min. This solution was stirred for 3 h at room temperature (RT) and subsequently sPEEK was added. In all cases, after addition of polymer, the solution was stirred for three days. The ratio of polymer to solvent was equal in all solutions. The mass ratio of Aerosil®380 to sPEEK was 0.25 and the mass ratio of Aerosil®380 to $TEOS_{H/C}$ was 2 resulting in a total inorganic loading of 27.3% (excluding the modifier). The composition of the membranes and other characteristic ratios are given in **Table 6.4**. The ratio, $n_{modifier} / m_{silica}$, represents the concentration of modifier related to the silica phase. The ratio, $n_{modifier} / n_{SO_3H}$, is the base-acid ratio and represents the amount of possible interactions between the basic modifier and the acidic polymer by means of salt bridges.

6.2.1.2. Membrane formation

Membrane formation was based on the casting-solvent evaporation process as described in **Section 4.1.3**. A polymeric sPEEK membrane consisting of the same

polymer as used in the preparation of mixed-matrix membranes was used as a reference membrane. All membranes were homogeneous and transparent and the thickness varied between 50 and 60 µm.

Table 6.4: Composition and characteristic ratios of the reference (sPEEK-REF) and inorganic-organic mixed-matrix (MM) membranes with various dihydroimidazole (DHIM) modifier concentrations.

Membrane	Composition [wt-%]				$n_{modifier}/m_{silica}$	$n_{modifier}/n_{-SO3H}$
	sPEEK	Aerosil®380	$TEOS_{H/C}$	Modifier	[mmol g^{-1}]	[-]
sPEEK-REF	100	0	0	0	-	-
MM-DHIM-0	72.7	18.2	9.1	0	0	0
MM-DHIM-0.25	71.8	17.9	9.0	1.3	0.25	0.06
MM-DHIM-0.5	70.9	17.7	8.9	2.5	0.50	0.11
MM-DHIM-0.75	70.0	17.5	8.8	3.7	0.75	0.17
MM-DHIM-1.0	69.1	17.3	8.7	4.9	1.00	0.23

6.2.2. Results and discussion

In this section, the results are presented and discussed of membranes with varying dihydroimidazole concentrations in comparison to a sPEEK and unmodified mixed-matrix membranes. A material based study is given followed by membrane behavior in ethanol-water mixtures (static and dynamic) and proton conductive properties in similar environments. Finally, results are linked together by means of a characteristic factor expressed in the selectivity of proton diffusion to ethanol permeability.

6.2.2.1. Ion exchange capacity

The ion exchange capacity of sPEEK is 1.66 mmol g^{-1} and is equal to a degree of sulfonation of 55%. This polymer forms the organic matrix in the MMM. This polymer is chosen because membranes using polymer with this sulfonation degree (polymer and mixed-matrix) exhibited acceptable swelling properties, ethanol permeability, and proton conductivity as shown in **Chapter 5**. These properties should be further improved by DHIM modification to make them promising for application in DEFC.

Molar quantities of basic and acidic functional groups in the prepared modified membranes are calculated per gram of dry membrane (**Figure 6.8**). Subtracting the basic groups from the acidic groups results in the theoretical *IEC* of the MMM with different modifier concentrations. When the basic modifier interacts stoichiometrically with sulfonic acid groups, the *IEC* of modified MMM, $IEC_{MM\text{-}DHIM}$, can be predicted with:

$$IEC_{MM-DHIM} = \left(1 - \frac{n_{\text{modifier}}}{n_{-SO_3H}}\right) IEC_{MM-DHIM-0} = (1-L)\left(1 - \frac{n_{\text{modifier}}}{n_{-SO_3H}}\right) IEC_{polymer} \qquad \textit{Eq. 6.1}$$

Where L is the silica loading of the unmodified MMM and $n_{modifier}/n_{-SO3H}$ is the base-acid ratio (**Table 6.4**). $IEC_{MM\text{-}DHIM\text{-}0}$ and $IEC_{polymer}$ are the *IEC*s of the unmodified MMM and of the sPEEK polymer respectively.

In **Figure 6.8**, it is shown that experimentally determined *IEC*s are consistent with the theoretical values. This indicates that the unmodified and modified silica phase was successfully built in the nanocomposite structure. The intercept of the y-axis as well as the slope of the linear function represents the *IEC* of the unmodified MMM (**Eq. 6.1**). The base-acid ratio (lower x-axis) and the concentration of modifier (upper x-axis) cohere via the *IEC* of the polymer, the dry membrane mass and silica loading. In this work, the concentration of modifier is preferred over the base-acid ratio to relate the modification of the inorganic matrix to various parameters.

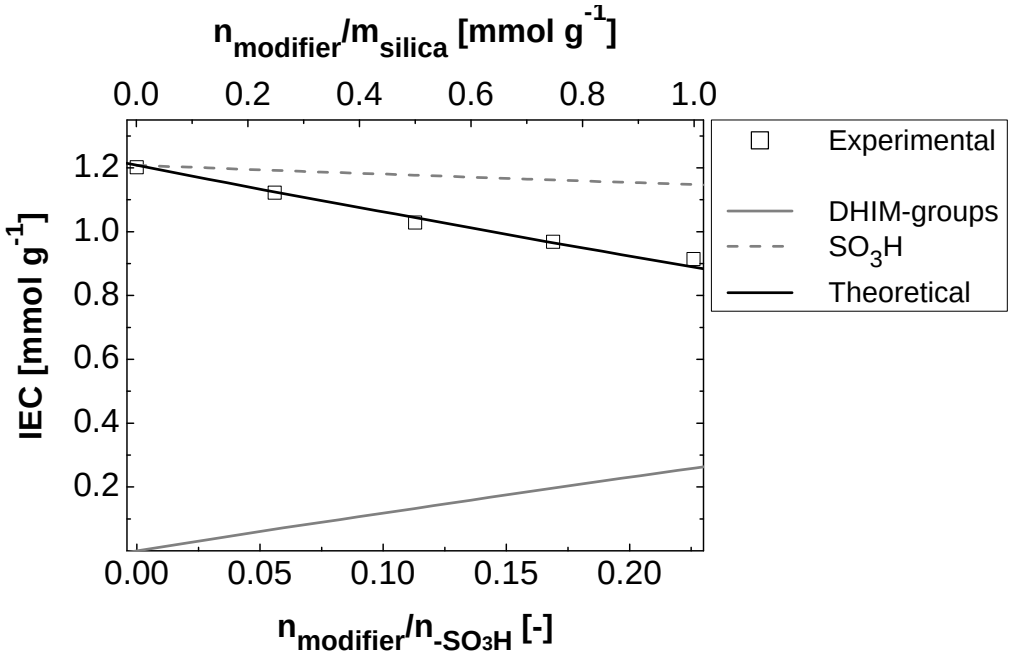

Figure 6.8: Experimental and calculated data of ion exchange properties of the mixed-matrix membranes ($IEC_{polymer}$ = 1.66 mmol g^{-1}).

6.2.2.2. Morphology of composite systems

The morphology of all mixed-matrix membranes is studied with SEM. SEM pictures of the cross section of unmodified MMM and MM-DHIM-0.75 are presented in **Figure 6.9**. It can be seen that the particles in the DHIM modified membrane are smaller and more homogeneously distributed than the unmodified MMM. Particles are better distributed due to interaction with the polymer. Cross sections of all modified MMMs are observed but the morphology was similar.

6.2.2.3. Liquid uptake and swelling

Liquid uptake of the MMM is studied in water and ethanol-water mixtures with various ethanol concentrations, 1 M, 2 M and 4 M (**Figure 6.10**). Next to the weight increase, the swelling in surface area is also monitored. These data are not shown, but an identical trend is observed. Water uptake results in a slight decrease with increasing

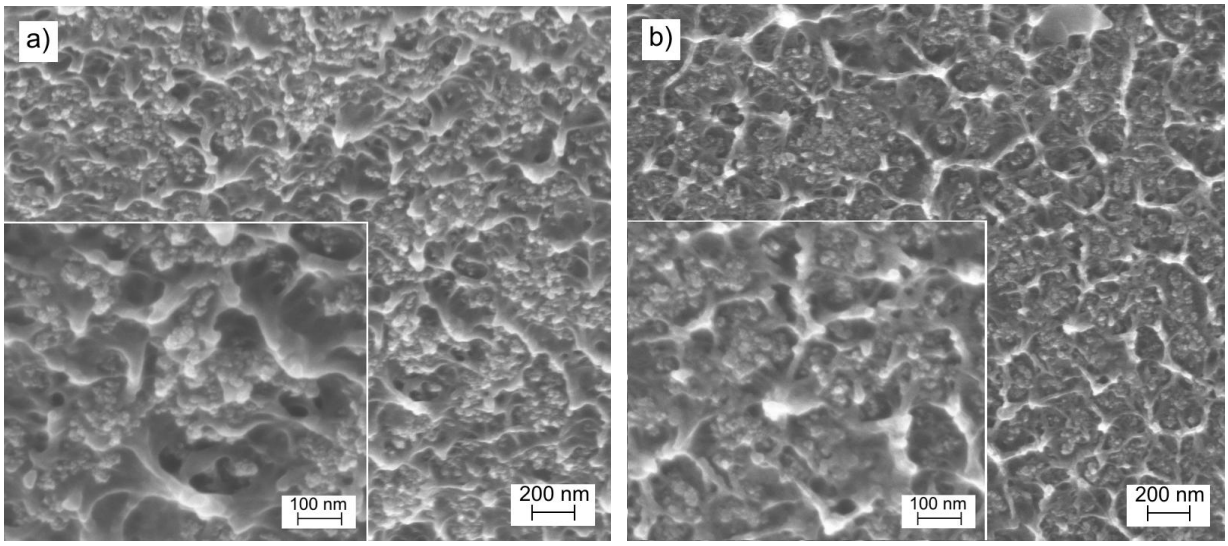

Figure 6.9: SEM picures of a) the unmodified mixed-matrix membrane, and b) the dihydroimidazole modified membrane $n_{modifier} / m_{silica}$ = 0.75 mmol g^{-1}.

modifier content. Liquid uptake of these membranes differentiates more when they are investigated in ethanol-water mixtures. Uptake of an unmodified membrane in 1 M ethanol is a factor of 1.4 higher than the modified MMM with the highest modifier concentration. In 4 M ethanol, this factor is 2. In comparison to the pure polymer membrane, uptake of this modified MMM is a factor of 3 lower in the same system. Liquid uptake results in expansion and, therefore, structural deformation of the membrane. The weight and membrane dimensions before and after the measurement with concentrations lower than 4 M ethanol were similar, which is an indication of the reversibility of the membrane structure. When the ethanol concentration was 4 M or higher, the membranes afterwards were more brittle and turbid. Especially the membranes with high swelling characteristics, e.g., polymeric reference and unmodified MMM, suffer these alterations in membrane structure.

Liquid uptake represents stability in aqueous media. The presence of an unmodified interconnected inorganic matrix results in a modest decrease in liquid uptake and concomitant swelling of the material (**Section 5.2.5**). Modification of the inorganic matrix leads to enhanced membrane stability in liquid media resulting in a further decrease in uptake and a reduction in swelling behavior. This stability improves with increasing modifier concentration. Reasons for this are: i) the formation of ion pairs

leading to a connected inorganic-organic network, ii) the acid-base interaction accounts for hindrance to hydration of the hydrophilic sulfonic acid groups, iii) higher modifier volume (and total inorganic volume fraction) in the MMM, and iv) presence of modifier can reduce the amount of hydrophilic silanol groups on the silica phase.

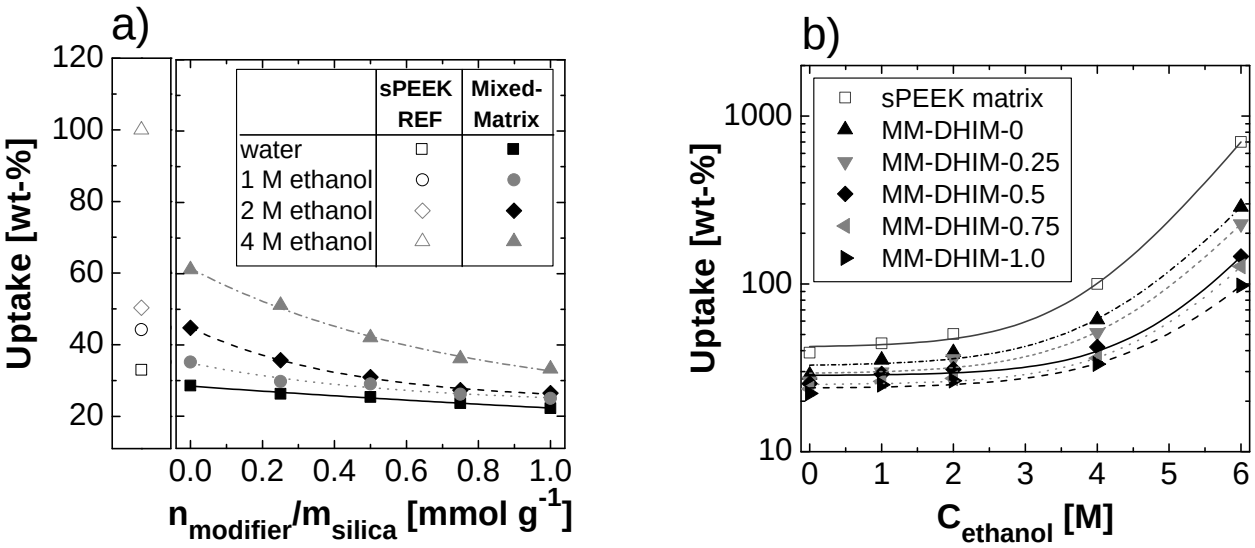

Figure 6.10: Liquid uptake results at RT of unmodified and modified mixed-matrix membranes in comparison to the polymeric reference in water and ethanol-water mixtures as a function of a) modifier concentration and b) molarity of ethanol of the liquid.

Water uptake as a function of temperature is measured up to 90 °C (**Figure 6.11a**). Membrane stability is promoted by the sol-gel silica network, the attachment of the functional silanes and the base-acid interaction. This experiment is done to study of the membranes with various modifier concentrations remain stable under these conditions. Uptake values exceeding 200% are not shown. The sPEEK reference shows similar behavior as the unmodified MMM and hence is not presented.

The membranes MM-DHIM-0 and MM-DHIM-0.25 show similar development, whereby uptake values of MM-DHIM-0 always exceed those of MM-DHIM-0.25. Above 70 °C, both membranes become instable resulting in high water uptake (> 200 wt-%) and coherent excessive swelling. Membrane MM-DHIM-0.5 shows also a steep increase in uptake after 70 °C, but the membrane is not as deformed as the

previous described membranes. Membranes with higher modifier content, MM-DHIM-0.75 and MM-DHIM-1.0, are more stable, but deteriorate in water hotter than 80 °C.

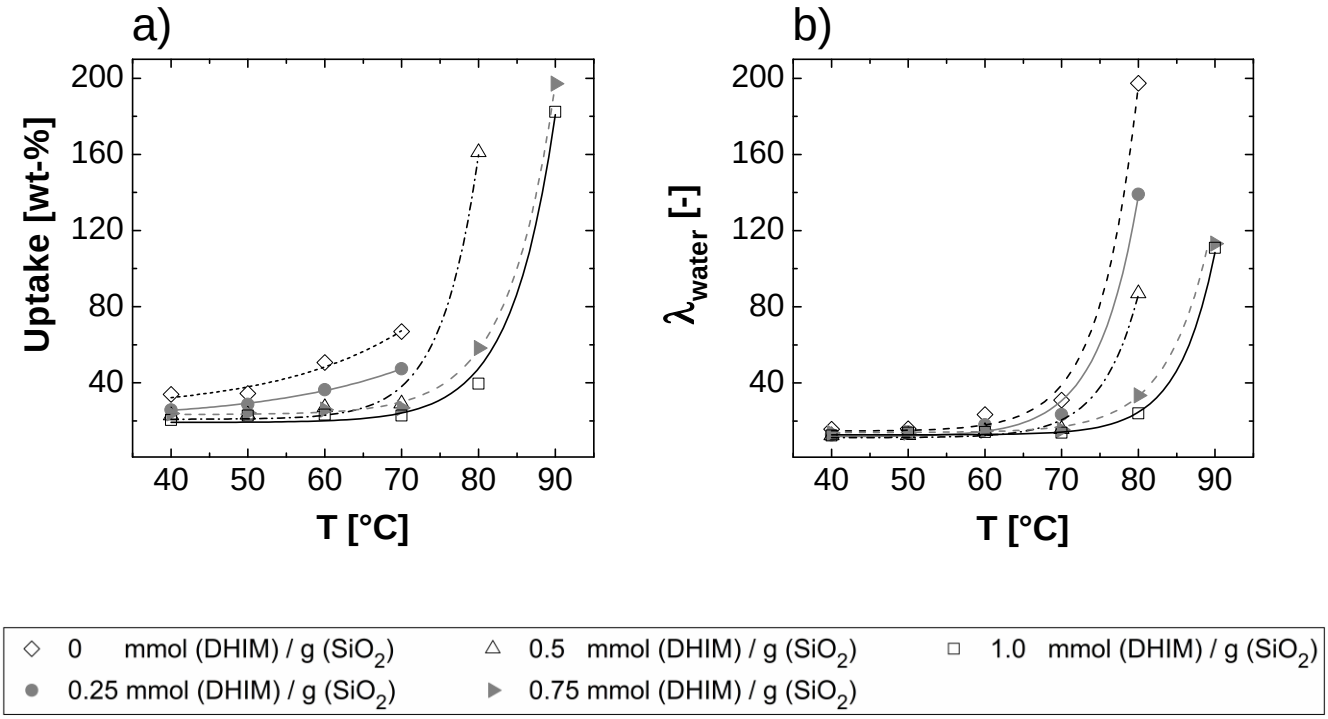

Figure 6.11: a) Water uptake and b) water number as a function of temperature of the mixed-matrix membranes.

Membrane stability is therefore related to acid-base interactions which results in an interaction between the organic and inorganic phase. Deterioration of the mixed-matrix material is accounted to swelling of the organic phase and dissociation of the acid-base pairs. Swelling of the organic phase results in tension between the organic and inorganic phase which are connected by the acid-base pairs. When the acid-base pair breaks, rapid hydration of the sulfonic acid groups occur. This inhibits the re-formation of this pair forming, leading finally to a stationary system in the liquid at a certain temperature. Higher modifier content in the MMM results in more acid-base bridges. The membrane is more stable because higher tension is needed to break up these acid-base interactions.

In **Figure 6.11b**, water numbers are plotted against water temperature. Water numbers are introduced in **Section 4.2.3** and are calculated with **Eq 4.3**. Water

numbers of the sPEEK membrane are lower than the water numbers of the unmodified MMM up to 60 °C. Water numbers are identical between 60 and 80 °C. Above 80 °C, both membranes deteriorate in water. MMMs with DHIM concentrations between 0.5 and 1.0 mmol g^{-1} exhibit low water uptake up to 70 °C. Water numbers slightly increase from 12 and 15. The impact of DHIM content in the membrane on water uptake expressed in terms of water number is best compared at 80 °C. With increasing DHIM content, the water number decreases from 200 wt-% (MM-DHIM-0) to 24 wt-% (MM-DHIM-1.0). The membranes, MM-DHIM-0.75 and MM-DHIM-1.0, show similar development and water numbers between 110 and 115 are obtained at 90 °C, whereas all membranes with lower modifier concentration are unstable under these conditions.

Modification of the mixed-matrix membrane with DHIM leads to stable materials with reduced swelling behavior. This enlarges the flexibility of fuel cell operation conditions. Higher concentrated ethanol feed stocks and higher application temperature can improve the fuel cell performance. Alteration in the membrane structure is little with modified mixed-matrix membranes and can be controlled by modifier concentration. These stable membranes induce less mechanical stress in the fuel cell and are beneficial for irregular application.

6.2.2.4. Ethanol permeability

Ethanol permeability is investigated with pervaporation and L-L diffusion and will be discussed in that order. With pervaporation, the liquid feed was an ethanol-water mixture with 2 M and 4 M ethanol respectively tempered at 40 °C. Permeability coefficients for ethanol and water determined with 2 M and 4 M feed concentration are presented in **Figure 6.12**. Both diagrams show an exponentially decreasing trend in permeability coefficient for ethanol as well as for water with increasing modifier content in the membrane. In all cases, the ethanol permeability coefficient is lower than that of the sPEEK reference.

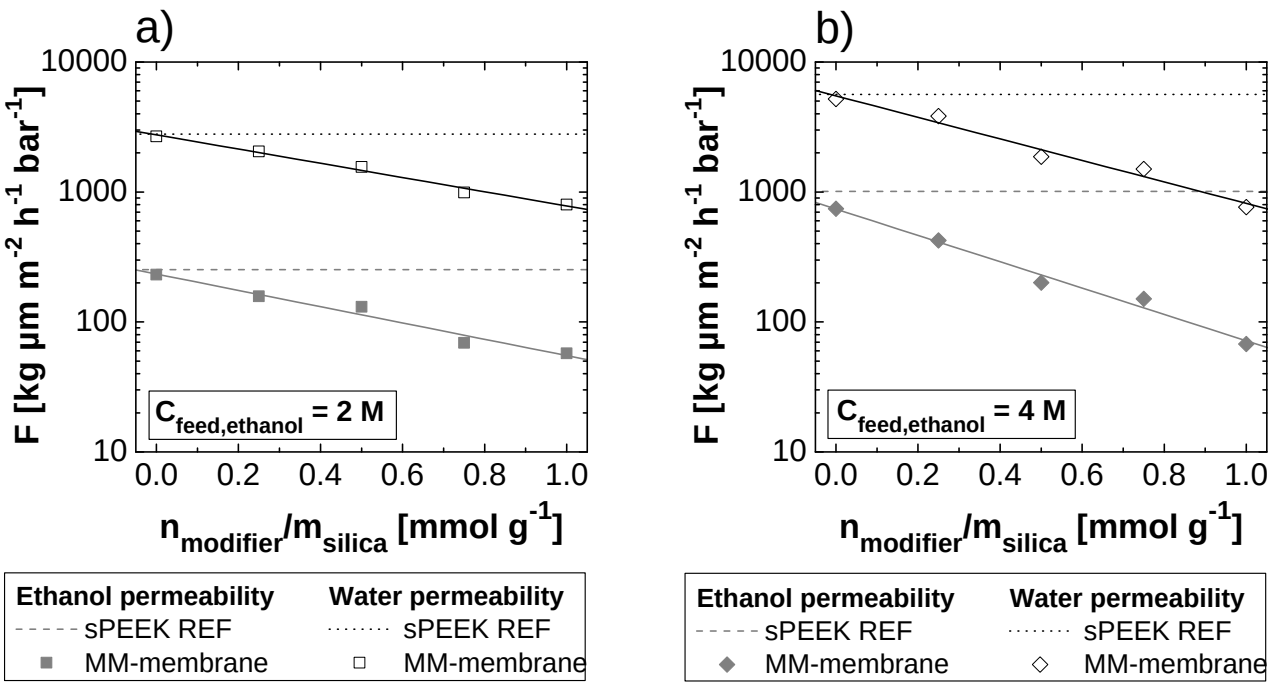

Figure 6.12: Ethanol permeability coefficients of the mixed-matrix membrane series in comparison to the polymeric reference measured with pervaporation (T is 40 °C; p^0 is 13 mbar; a) feed concentration is 2 M; b) feed concentration is 4 M.

When the permeability coefficients are normalized to the reference, the relative permeability coefficient is obtained:

$$F'_{rel} = \frac{F_{membrane}}{F_{sPEEK}} \cdot 100\% \qquad \textit{Eq. 6.2}$$

In **Table 6.5**, the relative permeability coefficients of water and ethanol are presented. The relative ethanol permeability coefficients with 4 M ethanol feed concentration are always lower than the relative permeability coefficients determined with 2 M feed concentration. These results cohere with the static liquid uptake results presented **Figure 6.10**. The effect of DHIM modification is observed best under more severe conditions. Even low concentrations of modifier in the membranes result in significantly lower ethanol permeability coefficients.

Table 6.5: Permeability coefficients of the mixed-matrix membranes relative to the sPEEK reference.

Membrane	$C_{feed,ethanol}$ = 2 M		$C_{feed,ethanol}$ = 4 M	
	$F'_{rel,ethanol}$ [%]	$F'_{rel,water}$ [%]	$F'_{rel,ethanol}$ [%]	$F'_{rel,water}$ [%]
MM-DHIM-0	91.4	96.3	73.6	92.1
MM-DHIM-0.25	62.3	73.8	41.9	68.0
MM-DHIM-0.5	51.8	56.0	19.8	33.1
MM-DHIM-0.75	27.3	35.5	14.9	26.7
MM-DHIM-1.0	22.7	28.7	6.7	13.6

Ethanol and water transport both decrease with increasing modifier concentration. This implies a better blocking mechanism for both species due to the modified inorganic matrix, because with increasing modifier content, the total inorganic content increases as well. Reduction in ethanol permeation is more pronounced than water permeation resulting in a change in ideal water to ethanol membrane selectivity (**Figure 6.13**). This selectivity is an important parameter, because it reveals the reduction in ethanol permeation, whereas the water household is maintained. The water content is significant for proton transfer through the membrane. The reduction in ethanol permeability is always lower than the water permeability indicating promising properties for fuel cell applications (**Table 6.5**).

The selectivity for measurements with 2 M ethanol feed concentration varies between 12 and 15 for the DHIM-modified membranes, higher as the sPEEK reference (11.0). The same trend is observed with measurements performed with 4 M ethanol feed concentration. With the same membranes, water to ethanol selectivity coefficients between 9 and 11.5 are obtained in comparison to 5.6 for the sPEEK reference.

The hydrophilic nature of the modifier plays an important role in the water to ethanol selectivity (**Section 6.1.2.1**). Higher modifier concentration results in a more compact

mixed-matrix structure. Transport is then determined by the hydration of the hydrophilic groups. In case of the unmodified MMM, a water network is built within the membrane and ethanol permeates through this water phase by its own driving force. In contradiction to this, the water network in modified MMM with high modifier concentrations is less voluminous and ethanol permeation through this water phase is retarded. Hence, ethanol and water permeability are strongly related to the liquid uptake and swelling of the membrane during the measurements. Differences in liquid uptake and coherent membrane swelling between the 2 M and 4 M ethanol systems are already presented in **Figure 6.10** and have a significant impact on the permeation behavior in dynamic systems.

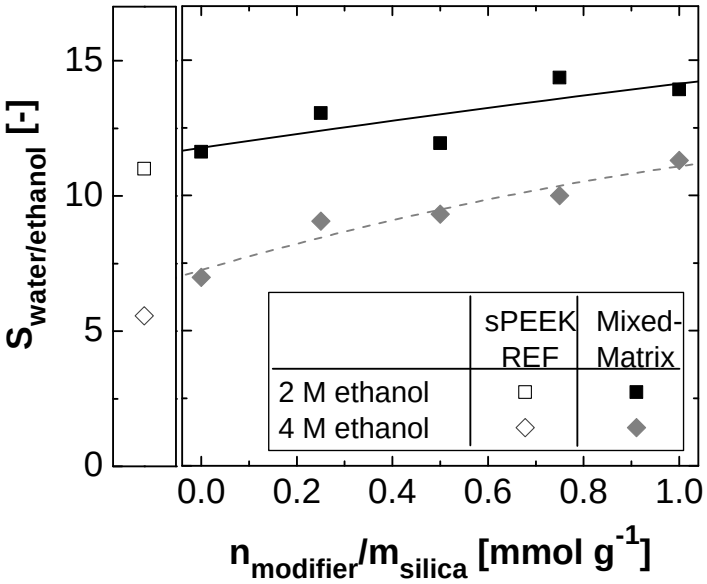

Figure 6.13: Ideal membrane selectivity coefficients (water to ethanol) of the mixed-matrix membranes in comparison to the polymeric reference determined with pervaporation and feed side concentrations of 2 M and 4 M.

Ethanol and water permeability coefficients are also determined by means of a L-L diffusion cell. These permeability coefficients of the sPEEK reference and the MMMs obtained with measurements at 25, 40 and 50 °C and 2 M ethanol concentration difference are presented in **Figure 6.14**. The scale on the y-axis in the diagram of

water permeability respective to the ethanol permeability differs by a factor of two. A linear dependency on DHIM concentration is obtained for measurements at 25 °C and 40 °C. This is unexpected based on the nonlinear decrease of 2 M ethanol uptake presented in **Figure 6.10**. From these results, curve developments similar to the 50 °C measurements are expected. Measurements at 60 °C are also performed, but just ethanol and water permeability coefficients of DHIM modified MMMs could be obtained. Ethanol permeability coefficients as a function of DHIM content decrease exponentially from $253 \cdot 10^{-8}$ cm^2 s^{-1} (MM-DHIM-0.25) to $49 \cdot 10^{-8}$ cm^2 s^{-1} (MM-DHIM-1.0). Water permeability coefficients decrease from $356 \cdot 10^{-8}$ cm^2 s^{-1} (MM-DHIM-0.25) to $94 \cdot 10^{-8}$ cm^2 s^{-1} (MM-DHIM-1.0).

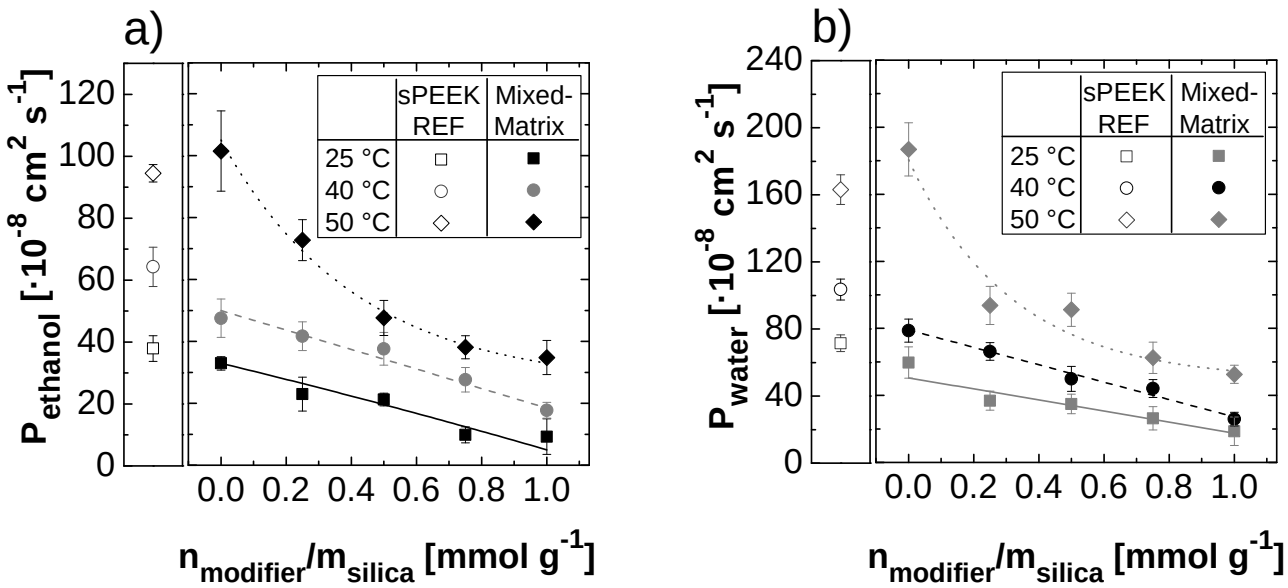

Figure 6.14: a) Ethanol permeability coefficients and b) water permeability coefficients determined with L-L diffusion cell (conditions: ΔC is 2 M; T is 25 °C, 40 °C and 50 °C).

6.2.2.5. Proton conductivity

Proton conductivity is measured at room temperature under wet conditions in water and water-ethanol mixtures with 2 M and 4 M ethanol concentration. The in-plane proton conductivity is measured by means of the spring-tips configuration (STC). Results show a decreasing trend with increasing modifier concentration (**Figure**

6.15a). In contradiction to pervaporation results, this trend is linear instead of exponential. Proton conductivity is dependent on liquid content in the membrane. Liquid content in the membrane increases as a function of ethanol concentration. A quantity where the proton conductivity, swelling, and ion exchangeable groups of the membrane are related is the proton diffusion coefficient, D_σ (**Section 4.2.4**). Proton diffusion coefficients in water, 2 M and 4 M ethanol are given as a function of modifier concentration in **Figure 6.15b**. Again, a linear dependence is obtained in this modifier concentration interval. In comparison to these values, the diffusion coefficients of a water molecule and a proton in water are $2.3 \cdot 10^{-5}$ cm^2 s^{-1} and $9.3 \cdot 10^{-5}$ cm^2 s^{-1} respectively.[13] The presented values are of course lower because of the hindrance of proton transport by the membrane material.

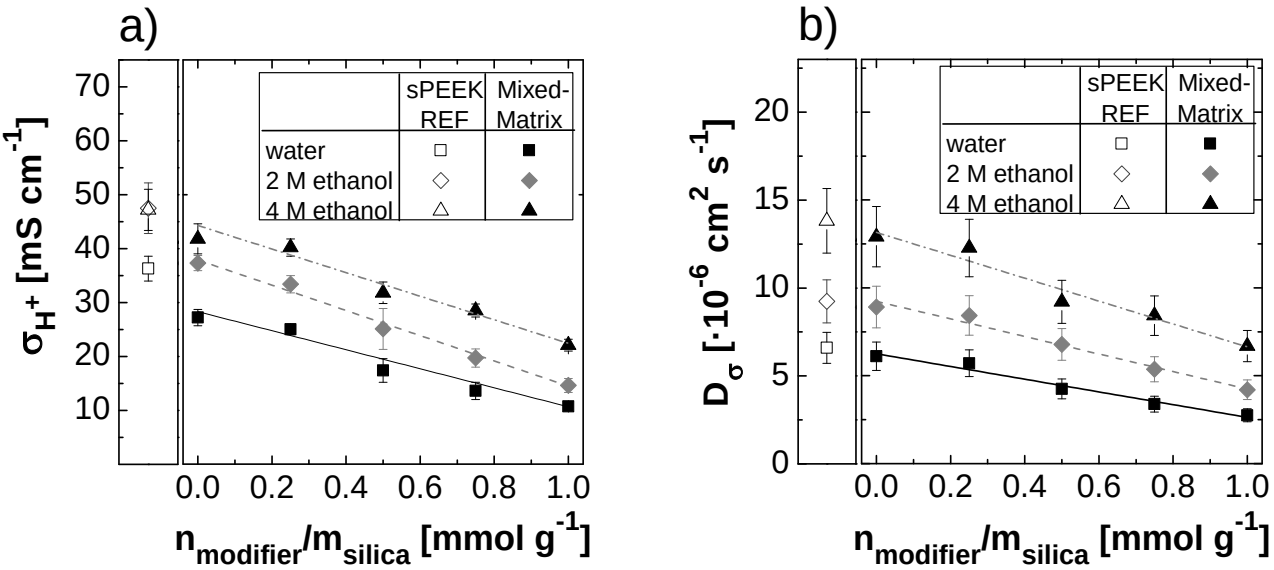

Figure 6.15: a) Proton conductivity and b) proton diffusion coefficients of the sPEEK reference and the mixed-matrix membranes at RT in water, 2 M and 4 M ethanol.

The effect of temperature on the proton conductivity of the membranes is studied as well. For this a platinum wire configuration (PWC) is used. Measurements are performed in a climate chamber and the humidity was set at 85%RH. The temperature dependency can be described by the following Arrhenius equation:

$$\sigma_{H^+} = \sigma_{H^+,0} \exp\left(-\frac{E_a}{RT}\right) \qquad \textit{Eq. 6.3}$$

In **Figure 6.16**, results are presented of the polymer reference, the unmodified MMM, and the modified MMMs: MM-DHIM-0.5 and MM-DHIM-1.0. The other two modified membranes were measured as well, but these results are excluded to give a better overview. The proton conductivity decreases in the following order:

sPEEK > MM-DHIM-0 > MM-DHIM-0.25 > MM-DHIM-0.5 > MM-DHIM-0.75 > MM-DHIM-1.0

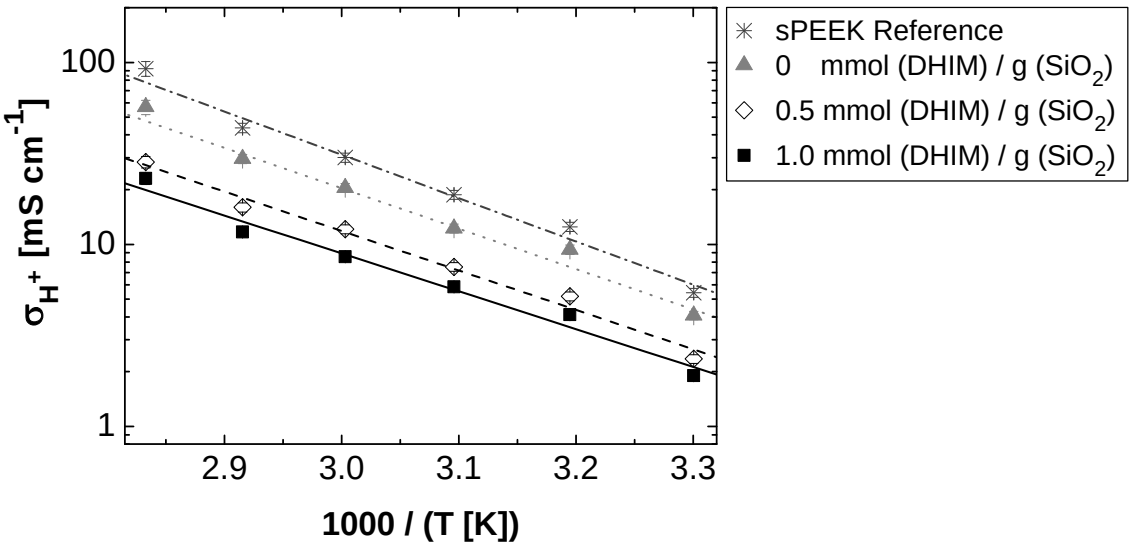

Figure 6.16: Arrhenius plot of proton conductivity of the sPEEK reference and the mixed-matrix membranes measured at temperatures between 303 K and 353 K (30 °C and 80 °C) with 85%RH.

Slopes of these Arrhenius plots are all similar, implying that the inorganic matrix, with or without basic modification, does not influence the activation energy. The activation energy for sPEEK (*IEC* = 1.66 mmol g^{-1}) in the temperature interval of 30 °C to 80 °C is 46.8 kJ mol^{-1}. The average value of the activation energy for the MMMs in the same temperature interval is slightly lower:

E_a = 43.9 ± 2.6 kJ mol^{-1}

Much lower proton conductivities at low temperatures are obtained with 85%RH in comparison to measurement of wet membranes. The difference is a factor of 5 which is due to the large difference in water sorption of the membranes in wet and humid environments, also known as the Schroeder's paradox.[181,182] The activation energy depends on the water content in the membrane. Therefore, the presented activation energies do not necessarily fit for the actual DEFC under operating conditions, where the water content may be higher.

6.2.2.6. Fuel cell prediction

The characteristic ratio is defined as the proton diffusion coefficient to the ethanol permeability coefficient, similar as is given in **Section 6.1.2.3.** Ethanol permeability coefficients are determined either with pervaporation or with L-L diffusion resulting in the ratios (D_σ / $F_{ethanol}$) and (D_σ / $P_{ethanol}$) respectively. In case of D_σ / $F_{ethanol}$, the permeability coefficients are converted to the unity cm^2 s^{-1} bar^{-1}. On the one hand, the proton diffusion coefficient determined in 2 M ethanol is related to the ethanol permeability coefficient obtained with 2 M ethanol feed concentration. On the other hand, proton diffusion coefficient and ethanol permeability coefficient of the 4 M ethanol systems are related.

The results are presented in **Figure 6.17a**. The dotted and dashed lines are modeled from the best fit values of the linear decrease in proton diffusion coefficient and the exponential decrease of the ethanol permeability coefficient, both as a function of modifier concentration. At low modifier concentrations, the relatively high ethanol permeability dominates the proton diffusion. At high DHIM concentrations in the membrane, ethanol permeability is low and little changes in ethanol permeability are obtained when the modifier concentration in the membrane is increased. The selectivity is therefore dominated by proton diffusion. The intersection of the 2 M and

4 M curve in **Figure 6.17a** reveal the point where the selectivity is dominated by proton conductivity. This is because the ethanol permeation coefficients in both systems are similar (**Figure 6.12**).

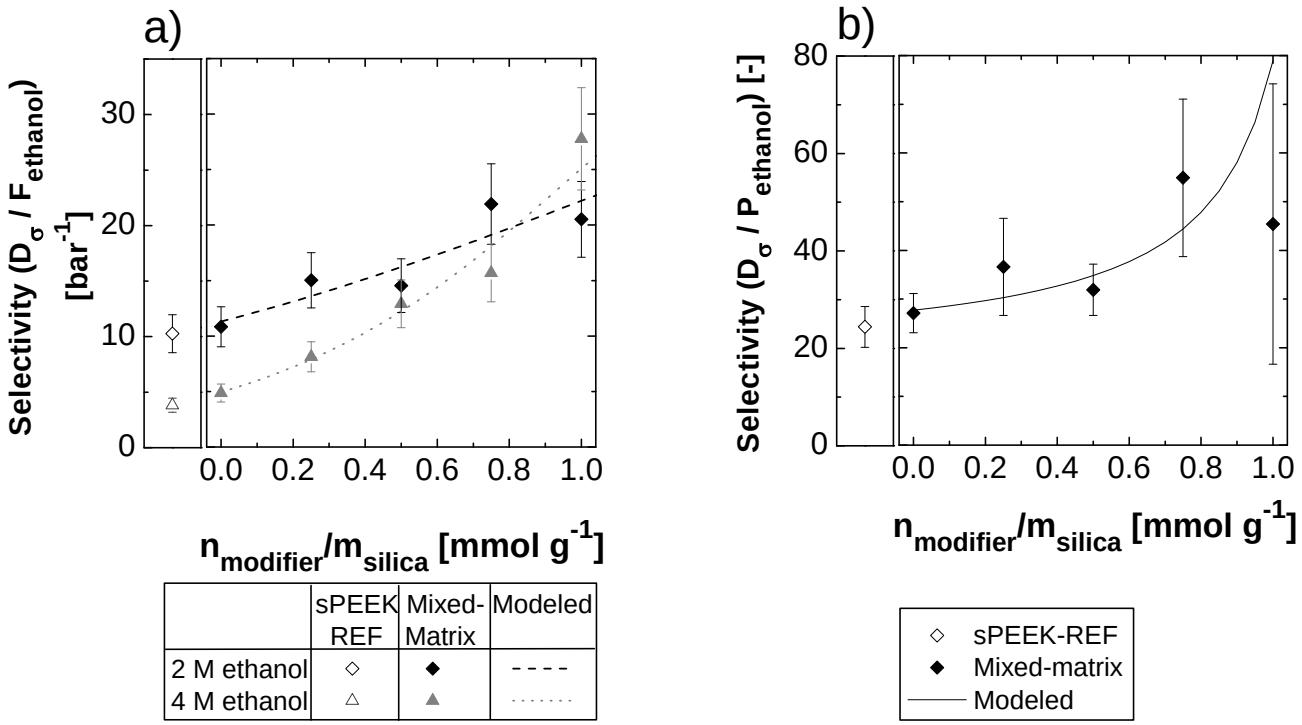

Figure 6.17: Characteristic ratio: a) D_σ / $F_{ethanol}$ in 2 M and 4 M ethanol system and b) D_σ / $P_{ethanol}$ in 2 M ethanol system as a function of modifier concentration of various mixed-matrix membranes in comparison to the sPEEK reference.

In **Figure 6.17b**, D_σ / $P_{ethanol}$ is plotted against the modifier concentration. The modeled curve is again obtained from best fit values of the linear decrease in proton diffusion coefficient and the linear decrease of the ethanol permeability coefficient, both as a function of modifier concentration. The scattering of the practically obtained data points is mainly due to variation in ethanol permeability coefficient and the relatively large deviation in low ethanol permeability coefficients. A strong increase in selectivity is obtained with the modeled curve. This can be addressed to the very low ethanol permeability coefficient at high modifier concentrations. When the ethanol permeability tends to zero, the characteristic ratio should go to infinity.

Systematic fuel cell measurements must be performed to give evidence to what parameter is more significant on the direct ethanol fuel cell performance. Is there a limiting value of proton conductivity, and how can the proton flow and fuel crossover be best balanced? To answer these questions, just the membrane compositions must be varied while keeping other influences (e.g., catalyst loading, binder content and electrode porosity) constant. Up to now, there is no standard measuring environment available to investigate these membrane properties, because within this DEFC project all other components are still under development as well.

6.2.2.7. Fuel cell tests

The most applied and significant method to characterize fuel cells is the recording of the current-voltage polarization plot. This can be recorded in potentiostatic or galvanostatic mode leading to a response of fuel cell current or voltage respectively. Cell voltage is plotted against the current or current density. Based on these quantities the power plot can be generated. This plot is generally presented directly in addition to the current-voltage plot and describes the performance of the fuel cell. Open-circuit voltage (OCV) is the fuel cell voltage under the equilibrium conditions, i.e., the voltage when no reactions occur inside the fuel cell and no current is flowing. The equilibrium cell voltage of the DEFC is 1.14 V (**Section 1.1**). Polarization of a fuel cell is the voltage drop from equilibrium cell voltage as a result of irreversible losses. These losses can occur due to four main sources:[183]

1. Mixed potential at the electrodes
2. Catalytic activity limitations
3. Internal resistance (Ohmic losses)
4. Mass transfer limitations

Comparability of the polarization curves is ensured when i) the MEA and fuel cell manufacturing and ii) the operating conditions are comparable. In this section, mixed-matrix membranes are tested under certain operating conditions. In the first part, the fuel cell properties as a function of modifier concentration in the MMM are investigated at temperatures between 30 °C and 50 °C. In the second part, the influence of ethanol feed stock concentration is studied at constant temperature.

The measurements are performed and kindly provided by associates of Fraunhofer ICT and Fraunhofer ISE (**Section 3.3.2**). These tests were not performed under optimized conditions (flow rates, ethanol feed stock concentration etc.). The results are based on sole measurements and are not statistically verified. In contradiction to membrane characterization, it was not possible to take full responsibility of the MEA preparation and DEFC measurements.

<u>Influence of modifier concentration of mixed-matrix membranes</u>

Mixed-matrix membranes are measured according to the fuel cell test procedure described in **Section 3.3.2** (fuel cell tests at Fraunhofer ICT). Fuel cell characteristics at 30 °C, 40 °C, and 50 °C are gathered during five successive measurement days. The tested membrane electrode assemblies (MEAs) are prepared by means of a hotspraying technique with the consequence that the catalyst loading in the electrode layers were not identical (**Table 6.6**). Current density and power density are usually expressed respective to the MEA geometrical surface area (A cm^{-2} and W cm^{-2} respectively). The electrode layers are often well defined commercial electrodes. This is not the case with the tested MEAs for membrane comparison. These variations in catalyst loading are excluded by dividing the fuel cell data with the total catalyst loading per surface area, $L_{catalyst,total}$ ($mg_{catalyst}$ cm^{-2}). Therefore, the current and power are expressed in terms of total weight of catalyst (A $mg_{catalyst}^{-1}$ and W $mg_{catalyst}^{-1}$ respectively).

Table 6.6: Cathode and anode metal loading in the electrode layers of membrane electrode assemblies with various mixed-matrix membranes.

Membrane	Catalyst loading [mg cm^{-2}]		
	Cathode PtCo/C	Anode Pt_3Sn/C+ PtRu/C	Total
MM-DHIM-0	2.6	3.7	6.3
MM-DHIM-0.25	2.4	3.5	5.9
MM-DHIM-0.5	2.5	3.5	6.0
MM-DHIM-0.75	2.6	3.9	6.5
MM-DHIM-1.0	2.2	3.8	6.0

To illustrate the significance of expressing the fuel cell data in terms of catalyst loading, the maximum power density at 40 °C for five successive measuring days is presented (**Figure 6.18**). The maximum power density is expressed in terms of total mass of catalyst (**Figure 6.18a**) and geometrical surface area (**Figure 6.18b**). No comprehensive order can be distinguished and no comparison can be made based on the fuel cell data expressed in terms of fuel cell area, whereas the fuel cell data expressed in terms of catalyst loading show a certain trend. This will be discussed more profoundly in the remaining section.

Unfortunately, membrane comparison is solely based on the mixed-matrix membrane which means that the polymeric reference membrane is not measured. In **Section 6.3**, a comparison will be made with a lower sulfonated sPEEK membrane as well as a Nafion® membrane. Polarization and power plots of the MMMs at three temperatures determined on the first and fifth day are presented in **Figure 6.19**. The development of cell voltage and power density under load at a current density of 2, 3 and 4 mA $mg^{-1}_{catalyst}$ at 30, 40, and 50 °C respectively are presented in **Figure 6.20**. These current densities are selected arbitrarily and are solely meant for comparing

the fuel cell data at a given temperature. Scaling of the x-axis and y-axis of diagrams determined at different temperatures are, therefore, not equal.

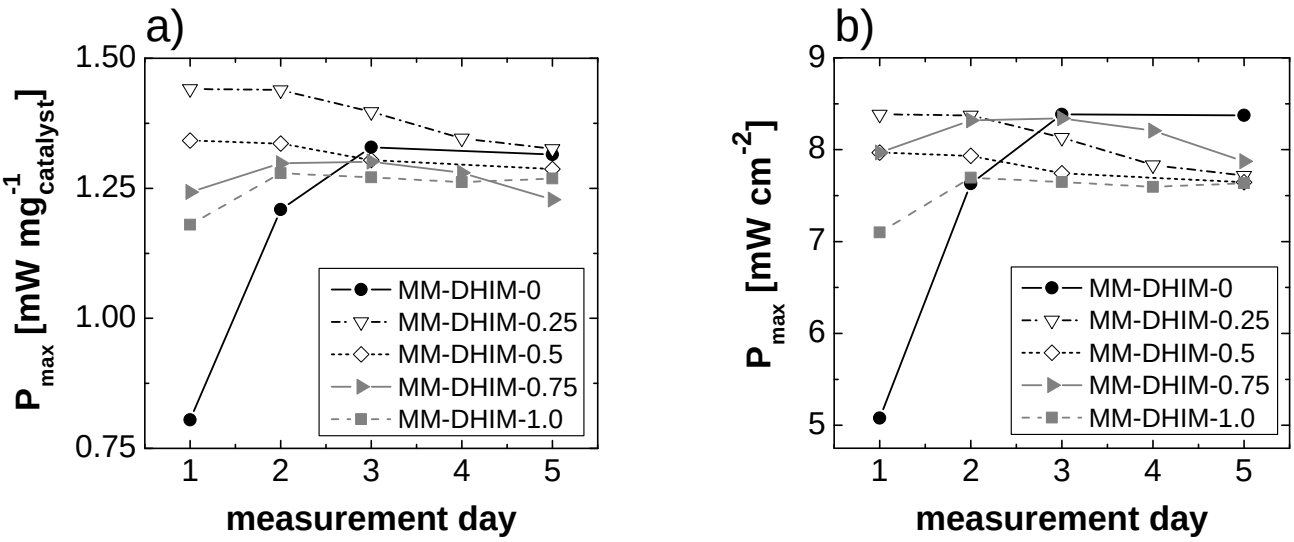

Figure 6.18: Development of the maximum power density of the mixed-matrix membranes over a period of five successive measurement days. P_{max} expressed in terms of a) catalyst weight and b) surface area.

Fuel cell performance improves with increasing temperature. This is obvious, because catalytic processes and proton conductivity increase exponentially with temperature.[11] The increasing ethanol permeation as a function of temperature should have a negative effect on the fuel cell performance. Mixed potential at the electrodes arise from the unavoidable parasitic reactions, particularly caused by crossover of the fuel through the electrolyte.[14] This leads to lowering of the cell voltage under no-current conditions with respect to equilibrium cell voltage (DEFC: 1.14 V). A clear trend respective to modifier concentration in the MMMs is observed. The OCV is in all cases between 760 and 830 mV and increase as follows:

MM-DHIM-0.25 < MM-DHIM-0 < MM-DHIM-0.5 < MM-DHIM-0.75 < MM-DHIM-1.0

This order corresponds to the ethanol permeability data presented in **Section 6.2.2.4**, except for the unmodified MMM and MM-DHIM-0.25. No clear reason is given for this

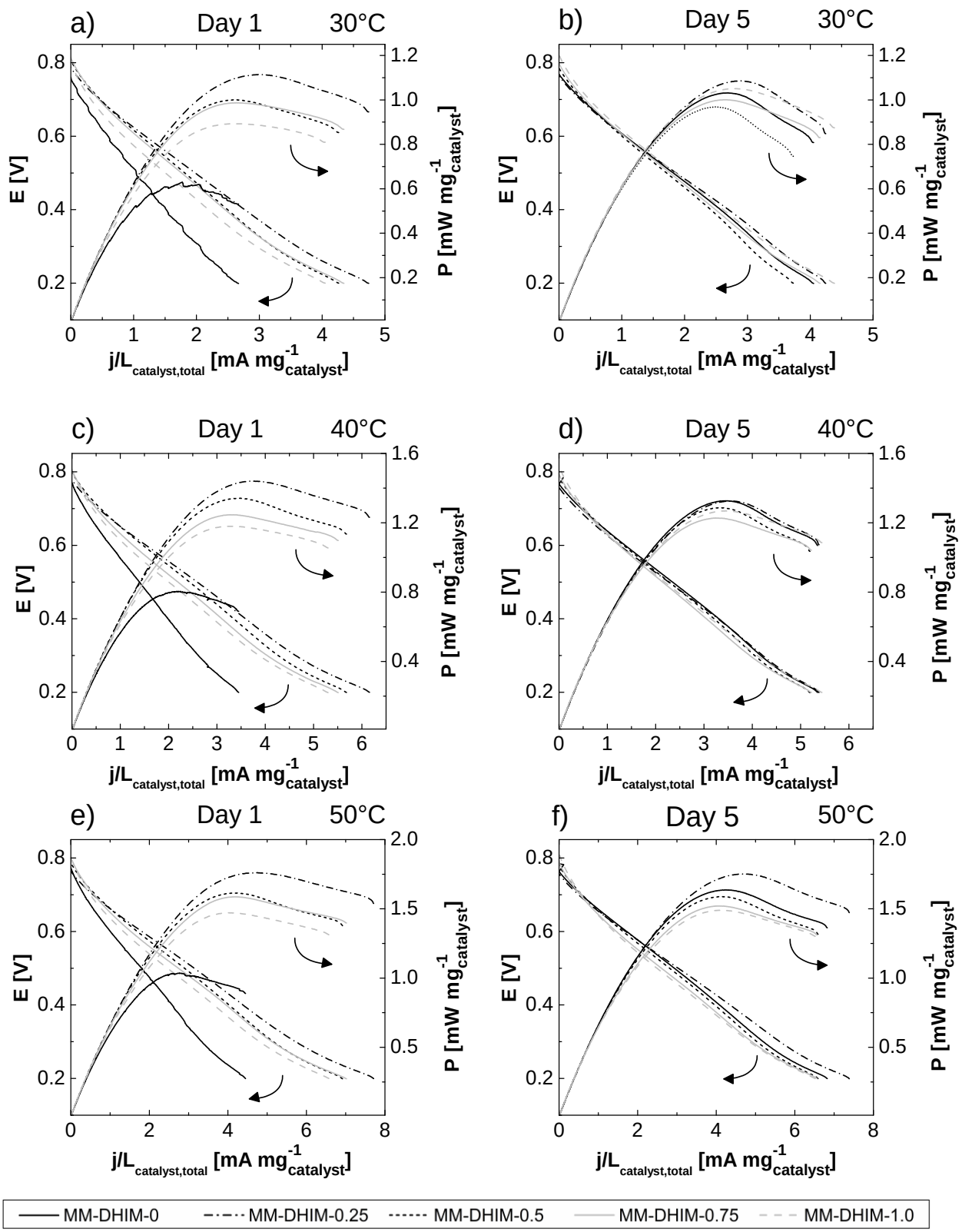

Figure 6.19: Polarization curves (left y-axis) and power plots (right y-axis) of the modified mixed-matrix membranes in comparison to the unmodified mixed-matrix membrane, a) first day, 30 °C; b) fifth day, 30 °C; c) first day, 40 °C; d) fifth day, 40 °C; e) first day, 50 °C; f) fifth day, 50 °C. Conditions: anode: $C_{ethanol}$ is 1 M, flow is 2 ml min^{-1}; cathode: air, 500 ml (STP) min^{-1}.

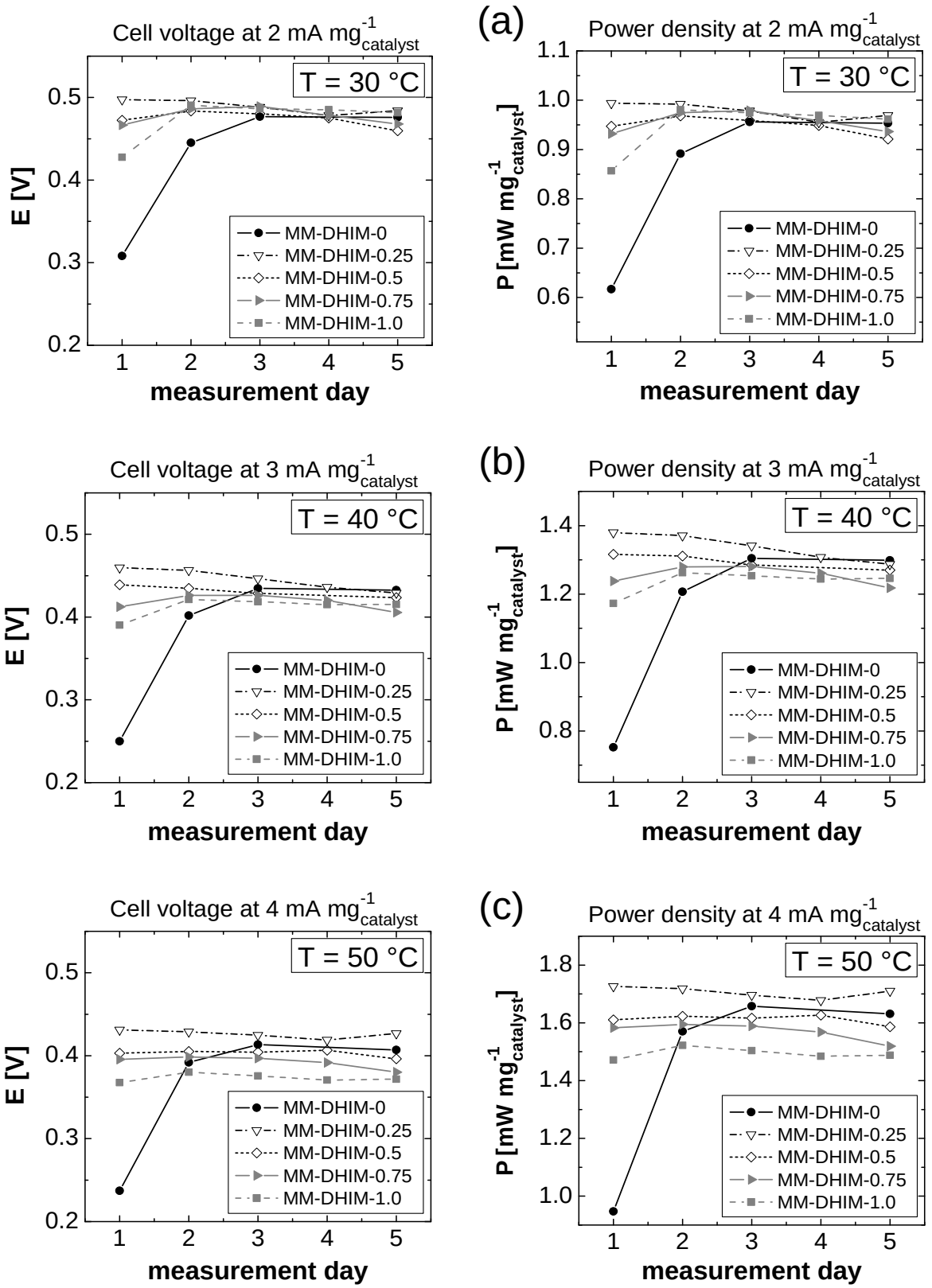

Figure 6.20: Development of cell voltage (left diagram) and power density (right diagram) of the mixed-matrix membranes over a period of five successive measurement days determined at a) 30 °C and 2 mA $mg^{-1}_{catalyst}$; b) 40 °C and 3 mA $mg^{-1}_{catalyst}$; c) 50 °C and 4 mA $mg^{-1}_{catalyst}$.

observation. Sluggish catalytic oxidation and reduction kinetics are generally observed in the lower current density region. By means of half-cell measurements, the anode and cathode kinetics can be separated. Unfortunately, these measurements were not accomplished. The activation of these reactions and electrical work performed by the cell correspond to the lowering of cell voltage respective to the equilibrium cell voltage. In the intermediate current density region, ohmic losses determine the (linear) development of the polarization curve. These losses arise from resistive losses in the electrolyte, electrode, and coherent interfaces. Mass transfer limitations could not be observed in **Figure 6.19**, probably due to the steep decrease in cell voltage as a function of current density which overshadows these mass transfer limitations.

The difference of the unmodified MMM fuel cell measurements on the first and the fifth day is remarkable. The higher resistance in the fuel cell on the first day results in a more negative slope than on the fifth day. Subsequently, the performance on the first day is also much lower. This behavior is observed at all measuring temperatures.

In case of modified MMMs, its high performance is directly obtained on the first day. This is an important feature of the modified MMMs, because fast activation and immediate functioning of the DEFC is requested. A feasible explanation is that the basic functional groups on the membrane surface interact with the Nafion® binder present in the electrode layer. The sulfonic acid groups of Nafion® exhibit stronger acidity than the sulfonic acid groups of sPEEK. This could improve the bonding between the membrane and electrode interfaces.

Some significant differences between various modifier concentrations are observed. In **Figure 6.20**, it can be seen that the differences in fuel cell behavior for various membranes are more pronounced with increasing measuring temperature.

- T = 30 °C: Differences in fuel cell behavior are especially significant on the first measurement day. In all cases, an increase in cell voltage and power density is observed from the first to the second day, except for MM-DHIM-0.25. This membrane directly starts at its maximum and, from then, the performance

slightly reduces. Small variations in cell voltage and power density at 2 mA $mg_{catalyst}^{-1}$ between the modified MMMs are observed from the second day to the fifth day. The membrane with the highest modifier concentration shows the most stable fuel cell behavior over the measuring time interval. Another important observation is done in **Figure 6.19**. In the current density range of 3 mA $mg_{catalyst}^{-1}$ and higher, the performance reduction as a function of current density is more pronounced for MM-DHIM-0, MM-DHIM-0.25 and MM-DHIM-0.5 than for MM-DHIM-0.75 and MM-DHIM-1.0. This performance reduction is expressed in a more negative slope resulting in a narrower peak of the power plot. This means that application area is broader in case of MM-DHIM-0.75 and MM-DHIM-1.0.

- T = 40 °C: The membranes MM-DHIM-0.25 and MM-DHIM-0.5 show a decreasing performance development over the whole measuring period, but in all cases, the performance is higher than the other modified MMMs. MM-DHIM-0.75 and MM-DHIM-1.0 show an increase from the first to the second day again. From that point, membrane MM-DHIM-1.0 shows constant fuel cell behavior, whereas the performance of MM-DHIM-0.75 slightly decreases after the third day. Polarization curves of all MMMs on the fifth day were nearly identical.

- T = 50 °C: Just membrane MM-DHIM-1.0 shows an increase from the first to the second day. All other modified MMMs exhibit constant fuel cell performance over the period of five days. This time a clear distinction in fuel cell performance is obtained with the modified membranes when the fuel cell data at 4 mA $mg_{catalyst}^{-1}$ are observed. Fuel cell performance reduces in the following order:

MM-DHIM-0.25 > MM-DHIM-0 > MM-DHIM-0.5 > MM-DHIM-0.75 > MM-DHIM-1.0

Concentration of ethanol feed stock

The modified mixed-matrix membrane, MM-DHIM-0.5, is measured according to the fuel cell test procedure described in **Section 3.3.2** (fuel cell tests at Fraunhofer ISE). The catalyst loading at the cathode was 2.72 mg cm^{-2} and 39 wt-% Nafion® was present as proton conductive binder material. The catalyst loading at the anode was 5.51 mg cm^{-2} with 37 wt-% Nafion®. The influence of ethanol concentration of the anode feed stock on the DEFC performance at 25 °C is investigated. The used ethanol concentrations were 1 M, 2 M and 3 M. Polarization curves as well as the power plots are presented in **Figure 6.21**. OCVs of these three measurements were similar: 0.85 ± 0.02 V. The fuel cell performance increases with increasing ethanol concentration. This is a major advantage because it is shown that DHIM modification of the MMMs increase membrane stability in higher concentrated ethanol-water mixtures. This allows fuel cell application with higher ethanol concentrations leading to higher performances. These data are not directly comparable to the previous fuel cell data. Reasons for this are differences in: i) fuel cell setup, ii) measuring conditions (i.e., flow rates, temperature), and iii) anode catalyst loading.

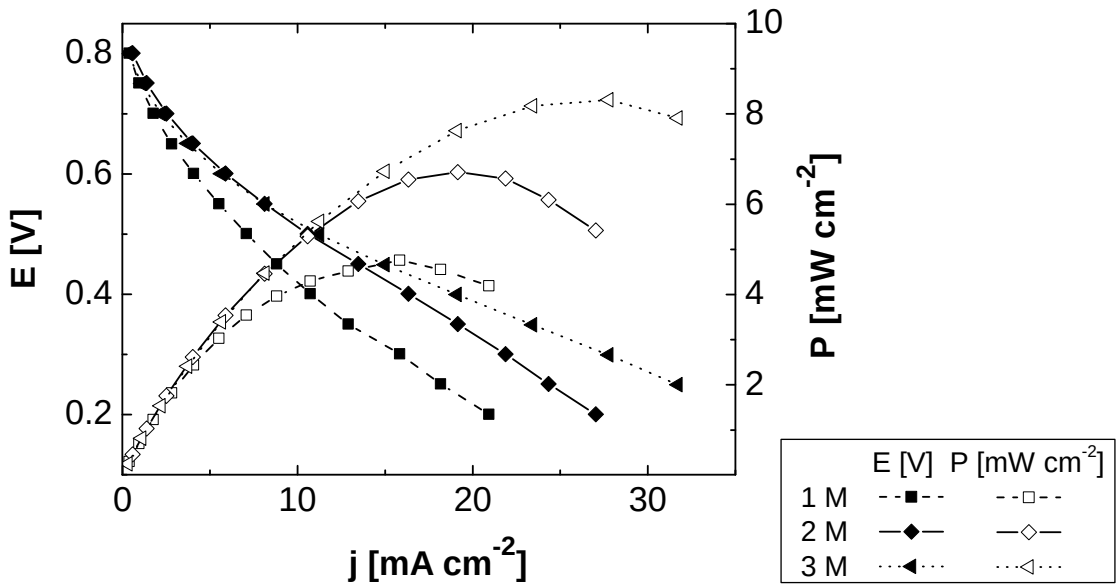

Figure 6.21: Cell voltage (left y-axis) and power density (right y-axis) as a function of current density. Influence on ethanol feed stock concentration. Membrane: MM-DHIM-0.5, T is 25 °C; anode: 5 ml min^{-1}; cathode: air, 100 ml (STP) min^{-1}.

Evaluation of fuel cell measurements

The OCVs at higher modifier concentration in the mixed-matrix membrane are an indication of the lower fuel crossover, which is also verified with the dynamic ethanol permeation experiments. The fuel cell performance of the lowest and higher modifier concentration, MM-DHIM-0.25 and MM-DHIM-1.0, are similar at 30 °C, whereas a significant difference is obtained 50 °C. At higher temperatures the catalytic reactions, proton conductivity, and fuel crossover are enhanced. This implies that the proton conductivity had a stronger influence on fuel cell performance than the reduction in ethanol permeability when the ethanol concentration on the anode side was low (1 M ethanol).

Based on the results obtained with membrane studies in water-ethanol mixtures, fuel cell predictions are not fully consistent with the actual fuel cell measurements. An improvement in fuel cell properties is expected with higher modifier content in the mixed-matrix membrane (**Figure 6.17**). This trend does not explicitly come back in the fuel cell data. A reason for this is the overshadowing effect of several performance determining factors. These factors are the resistances of various other layers (i.e., electrode layers, gas diffusion layers), the complexity of layer assembly with its different interfaces, as well as the sluggish catalytic reactions during application. Fuel cell predictions are made with membrane data obtained from measurements in 2 M and 4 M ethanol systems. Ethanol and water permeability are strongly related to the ethanol concentration in the measuring system, and permeation behavior is more pronounced in higher concentrated systems (**Section 6.2.2.4**). Fuel cell tests are performed with 1 M ethanol concentration in the anode feedstock. Modest differences in ethanol crossover are expected based on the liquid uptake data (**Section 6.2.2.3**), which is also a feasible explanation why the fuel cell prediction does not agree with the actual DEFC measurements.

Higher ethanol concentration in the anode feed stock resulted in improved fuel cell performance. Unfortunately, no comparison data are obtained with unmodified, low, and high modifier concentrations. A distinct difference in fuel cell performance is

expected based on the improved membrane stability as a function of modifier concentration in the mixed-matrix membrane. The goal of the DEFC project was to achieve a power density of 10 mW cm^{-2} at 40 °C. The best DEFC performance at 40 °C presented in this chapter is 8.4 mW cm^{-1} with 1 M ethanol feed stock concentration. The increase in power density at 25 °C from 1 M to 2 M and from 1 M to 3 M ethanol feed stock concentration is a factor of 1.40 and 1.75 respectively. Extrapolating the DEFC performance at 40 °C and 1 M ethanol anode feed concentration with these factors indicates that the application of MMMs as electrolyte in low temperature DEFCs are promising, especially at higher ethanol concentrations.

6.3. Overall membrane comparison

In this section, Nafion®, pure sPEEK with various degrees of sulfonation, and mixed-matrix membranes are mutually compared. The membrane characteristics and some selected membrane properties of various polymeric and mixed-matrix membranes, which are described in this thesis, are presented in **Table 6.7**. Since proton transport is one of the main requirements for proton exchange membranes, a comparison is made between the reported membranes. A convenient parameter for this comparison is the activation energy (**Eq. 6.3**). Subsequently, all membranes described in this thesis, are compared with respect to proton diffusion and ethanol permeability. Finally, Nafion®, pure sPEEK, and mixed-matrix membranes are compared with respect to fuel cell characteristics.

In addition, it is attempted to make a comparison with literature data. A straightforward comparison of absolute values is often difficult, because of differences in setups and measuring conditions used in the determination of proton conductivity or alcohol permeability. In case of proton conductivity, two or four electrode configurations are often used and the measuring conditions, e.g., wetting liquid, humidity or temperature, are not uniformly established. Alcohol permeability is normally measured with a diffusion cell or with pervaporation. In DAFC publications,

methanol-water is the most frequently studied system. This complicates a direct comparison with ethanol-water systems. Furthermore, the concentrations and measuring temperatures are often not comparable or the practical information is insufficient.

Table 6.7: Summarizing table of sPEEK (P), Nafion® 117 (N), unmodified and DHIM modified mixed-matrix membranes (uMM and mMM respectively).

Membrane characteristics					Membrane properties				
Membrane type	$IEC_{polymer}$ [mmol g^{-1}]	Loading [%]	Mass ratio Aerosil®380/$TEOS_{H/C}$	$n_{modifier}$ / m_{silica} [mmol g^{-1}]	σ_{H^+} [mS cm^{-1}]	D_σ [$\cdot 10^{-6}$ cm^2 s^{-1}]	$F_{ethanol}$ [kg µm m^{-2} h^{-1} bar^{-1}]	$P_{ethanol}$ [$\cdot 10^{-8}$ cm^2 s^{-1}]	D_σ / $F_{ethanol}$ [bar^{-1}]
N	0.91	0	-	-	58.4	15.2	1942.0	232.8	2.2
P	1.32	0	-	-	16.5	3.5	54.4	27.9 *	18.0
P	1.66	0	-	-	47.5	9.2	252.7	64.3	10.3
P	1.79	0	-	-	51.9	10.2	471.7	72.4	6.1
P	2.00	0	-	-	107.6	28.0	N/A	N/A	N/A
uMM	1.66	27.3	2	0	37.3	8.9	230.9	47.5	10.8
uMM	1.66	20	1	0	35.5 §	7.3 §	358.5	50.4	5.7 §
uMM	1.79	20	1	0	48.3	11.8	533.6	90.3	6.2
mMM	1.66	28.2	2	0.25	33.4	8.4	157.5	41.7	15.0
mMM	1.66	29.1	2	0.5	25.1	6.8	130.8	37.6	14.5
mMM	1.66	30.0	2	0.75	19.7	5.4	68.9	27.6	21.9
mMM	1.66	30.9	2	1	14.6	4.2	57.4	17.7	20.5
mMM	1.79	22.9	1	1	29.7	7.3	104.1	37.4	19.7

σ_{H^+}, D_σ, D_σ / $F_{ethanol}$: 2 M ethanol environments (§ : σ_{H^+}, D_σ in water)

$F_{ethanol}$: C_{feed} = 2 M ethanol and T = 40 °C

$P_{ethanol}$: ΔC = 2 M ethanol and T = 40 °C (* : ΔC = 4 M ethanol)

N/A: not applicable

Proton conductivity as a function of temperature is measured with the platinum wire configuration at 85%RH in a climate chamber. These data are presented in **Figure 6.22**. Obviously, Nafion® exhibits highest proton conductivity amongst all measured membranes. The slope is less steep than the sPEEK based membranes, revealing the lowest activation energy for proton transport (E_a = 17.3 kJ mol^{-1}). As pointed out in **Section 6.2.2.4**, the activation energy of sPEEK (1.66 mmol g^{-1}) is modestly higher than the unmodified and modified MMMs (46.8 kJ mol^{-1} versus 43.9 ± 2.6 kJ mol^{-1}). The highest activation energy is found for the sPEEK membrane with an *IEC* of 1.15 mmol g^{-1} (E_a = 58.5 kJ mol^{-1}). The very low proton conductivity at 30 °C could not even be determined, because of measuring limitations below 1 mS cm^{-1}. Application of this sPEEK is limited by proton conductivity, although the high characteristic ratio ($D_\sigma / F_{ethanol}$), which represents promising fuel cell properties.

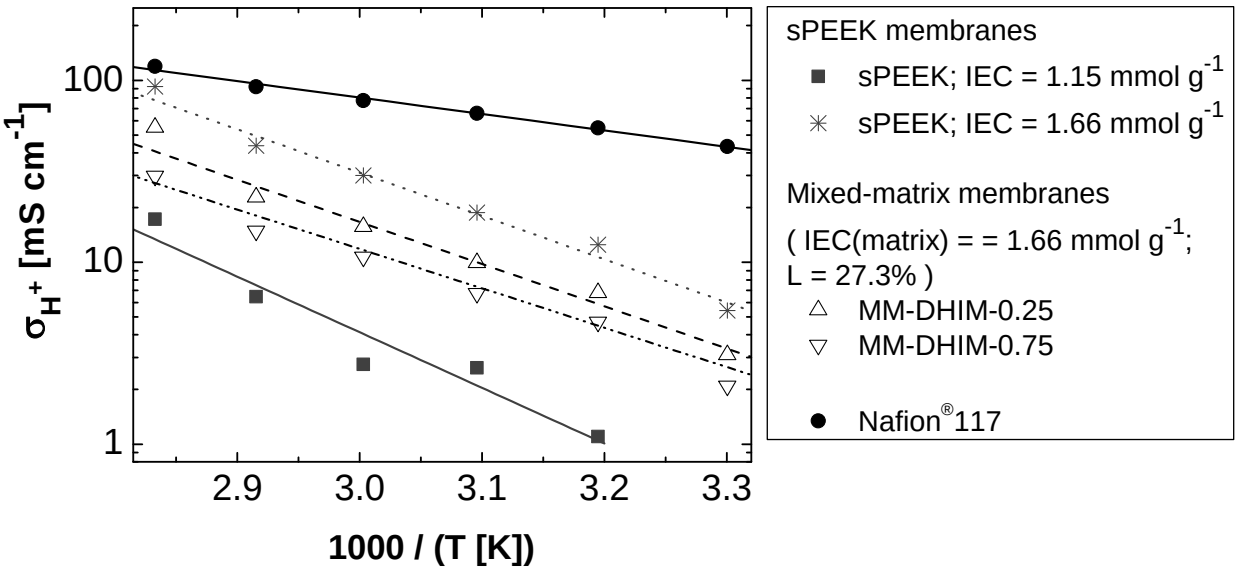

Figure 6.22: Proton conductivity Arrhenius plot for Nafion® 117, sPEEK and mixed-matrix membranes measured with platinum wire configuration (PWC) at temperatures between 30 °C and 80°C and 85%RH.

Comparable data of polymeric membranes were presented by Li et al.[169] They measured proton conductivity with a two-electrode setup and at 100%RH. They found a higher activation energy for the lower sulfonated sPEEK membrane, similar to the results described above. For sPEEK membranes with an IEC of 1.2 mmol g^{-1} and

1.4 mmol g^{-1}, they found 41.0 kJ mol^{-1} and 33.5 kJ mol^{-1} respectively. The activation energy of Nafion® was 9.0 kJ mol^{-1}, which was similar to the presented data of Shao et al.[95] (8.3 kJ mol^{-1}) and Goawen et al.[142] (10.8 kJ mol^{-1}). The activation energy for Nafion®117, presented in this thesis, is higher. This is probably due to the lower humidity. Di Vona et al.[173] compared activation energies determined with low and high humidities and found, indeed, a significant difference between these values.

Goawen et al.[142] prepared composite membranes with organically modified montmorillonite (layered silicate) with 5 wt-% and 10 wt-% loading. The activation energies of these composite systems were higher than the pure sPEEK membrane, which is the opposite of the results presented in this thesis. Here, the activation energies of the MMMs are lower than the polymeric reference, which suggests that the resistance to proton transfer is reduced due to the improved water household in the presented MMM.

The obtained proton diffusion coefficients and ethanol permeability coefficients of the membranes, studied in this thesis, are depicted in a D_σ - $F_{ethanol}$ plot (**Figure 6.23**). In **Section 4.2.8**, sPEEK membranes in comparison to Nafion® are already discussed. Higher characteristic ratios ($D_\sigma / F_{ethanol}$) of sPEEK membranes, led to the conclusion that sPEEK is a promising polymer type for application in DEFC. Unmodified MMMs show similar characteristics as their polymeric references. Significant improvements are found with DHIM modified MMMs. These membranes are marked in the oval area above the curve of the best fit of all sPEEK membranes (**Figure 6.23**). It should be noted that both scales in **Figure 6.23** are logarithmic, diminishing the positive effects to some extent.

The promising results of modified MMMs in comparison to pure sPEEK polymeric membranes are illustrated by means of two concrete examples. The ethanol permeability coefficients of sPEEK (IEC = 1.40 mmol g^{-1}) and MM-DHIM-0.75 are similar (62.3 versus 68.9 kg µm m^2 h^{-1} bar^{-1}), whereas the proton diffusion coefficient

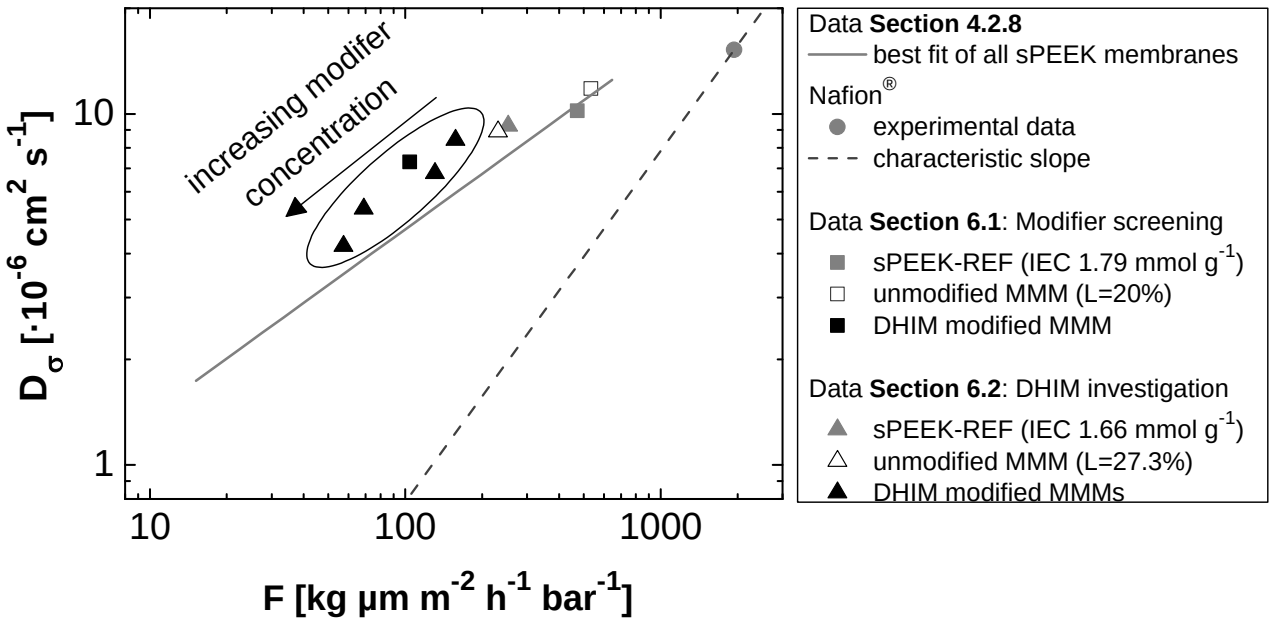

Figure 6.23: Proton diffusion coefficient (2 M ethanol; RT) versus ethanol permeability coefficient (L-G system; 2 M ethanol feed concentration; 40°C) for Nafion® 117, sPEEK and mixed-matrix membranes.

of the modified MMM is nearly twice the value of the sPEEK membrane ($5.4 \cdot 10^{-6}$ versus $2.9 \cdot 10^{-6}$ cm^2 s^{-1}). In case of sPEEK (*IEC* = 1.73 mmol g^{-1}) and MM-DHIM-0.25, the proton diffusion coefficients are similar ($8.7 \cdot 10^{-6}$ and $8.4 \cdot 10^{-6}$ cm^2 s^{-1} respectively). The ethanol permeability coefficients are 414 and 157 kg µm m^2 h^{-1} bar^{-1} respectively, which is a factor of 2.6. Based on the D_σ - $F_{ethanol}$ characteristics, DHIM modified mixed-matrix systems are promising electrolyte materials for the application in DEFCs.

Karthikeyan et al.[145] compared various organic-inorganic hybrid systems, amongst others, Aerosil® and *in situ* generated silica as inorganic filler (Section 2.2.3). In addition, they also used an imidazole-based silane and, therefore, these data are used for comparison with the data described in this thesis.

The published methanol and water permeability coefficients of sPEEK and the unmodified and modified Aerosil® membrane differed significantly. The loading of

Aerosil® composite membranes was 9 wt-% and 17 wt-%. When the proton conductivity was related to the methanol permeability, the sPEEK membrane and unmodified Aerosil® membranes were inferior to Nafion®, whereas the modified Aerosil® membranes exhibited a higher ratio. The ethanol permeability coefficients of Aerosil®380 filled membranes described in this thesis are similar to the sPEEK reference. The ethanol permeability can be further reduced by forming an interconnected inorganic network (**Section 5.2.7**). The ratio of proton conductivity to ethanol permeability is in all cases higher than Nafion® and is further improved by the addition DHIM to the mixed-matrix system.

In situ generated silica networks were prepared by sol-gel processing of aminopropyl-trimethoxysilane and imidazole glycidoxypropyl triethoxysilane.[145] The inorganic loading of these membranes was 10 wt-%. The pervaporation results were similar to the modified Aerosil® membranes. The membrane with the imidazole-consisting silica network exhibited identical proton conductivity values in comparison to the pure sPEEK membrane, but higher values than the membrane with the amine-consisting silica network. A few years before these findings, Nunes et al.[135], of the same research group, published data of a sPEK membrane with 33 wt-% DHIM-silane, which was the same silane as used in this thesis. The reduction in methanol permeability was a factor of 60 whereas the reduction in proton conductivity was nearly a factor of 200. This suggests that the selectivity of proton diffusion to alcohol permeability of this membrane is inferior to polymeric reference. The MMMs with unmodified or modified Aerosil®380-$TEOS_{H/C}$ combined inorganic matrix, described in this thesis, show distinct improvement in comparison to the pure polymer reference with respect to this selectivity.

Finally, a comparison is made between Nafion®, pure sPEEK, and mixed-matrix membranes with respect to fuel cell performances. The catalyst loading of the Nafion®115 based MEA and the sPEEK (1.35 mmol g^{-1}) based MEA are presented in **Table 6.8**. The fuel cell data are again expressed in terms of catalyst loading to make

a straightforward comparison between various membranes. The fuel cell test procedure is similar to the one described in **Section 3.3.2** (fuel cell tests at Fraunhofer ICT), but differs in the amount of measuring days. Unfortunately, this just allows the comparison of fuel cell data recorded on the first day.

Table 6.8: Cathode and anode metal loading in the electrode layers of membrane electrode assemblies with Nafion® 115 and sPEEK (1.35 mmol g^{-1}).

Membrane	Catalyst loading [mg cm^{-2}]		
	Cathode PtCo/C	Anode Pt_3Sn/C+ PtRu/C	Total
Nafion®115	2.3	3.6	5.9
sPEEK (1.35 mmol g^{-1})	1.8	3.3	5.1

Polarization plots recorded on the first day are presented in **Figure 6.24**. It is remarkable, that the OCVs of Nafion®115 as well as sPEEK (1.35 mmol g^{-1}) are lower than those of the mixed-matrix membranes. OCVs of the MMMs varies between 760-830 mV, whereas the OCV for the Nafion® and the sPEEK membrane are 700 mV and 650 mV respectively. This is an indication of a higher ethanol crossover.[184] No variation in OCV as a function of measuring temperature is found.

The cell voltage as a function of current density shows the steepest decrease with the unmodified MMM resulting in the lowest power densities. The polarization plots of sPEEK, Nafion® and MM-DHIM-0.25 run parallel in the following order:

sPEEK (1.35 mmol g^{-1}) < Nafion®115 < MM-DHIM-0.25

DEFC performance with the Nafion® membrane shows the strongest dependency on application temperature. The power density is very low at a measuring temperature of 30 °C (P_{max} = 0.8 mW $mg^{-1}_{catalyst}$). In addition, the power density plot is narrow, indicating a limiting application area. At 40 °C, the performance improves, but is still inferior to the modified MMM. At 50 °C, the polarization plot and coherent power

density plot is nearly identical to MM-DHIM-0.25. At higher temperatures, Nafion® will be the preferable membrane based on DEFC performance, because proton conductivity is the main determining quantity determining this performance. This modified mixed-matrix membrane shows remarkable fuel cell performances at 30 °C and 40 °C within the range of investigated membranes. This makes the modified mixed-matrix membrane suitable for application in low temperature operating DEFCs.

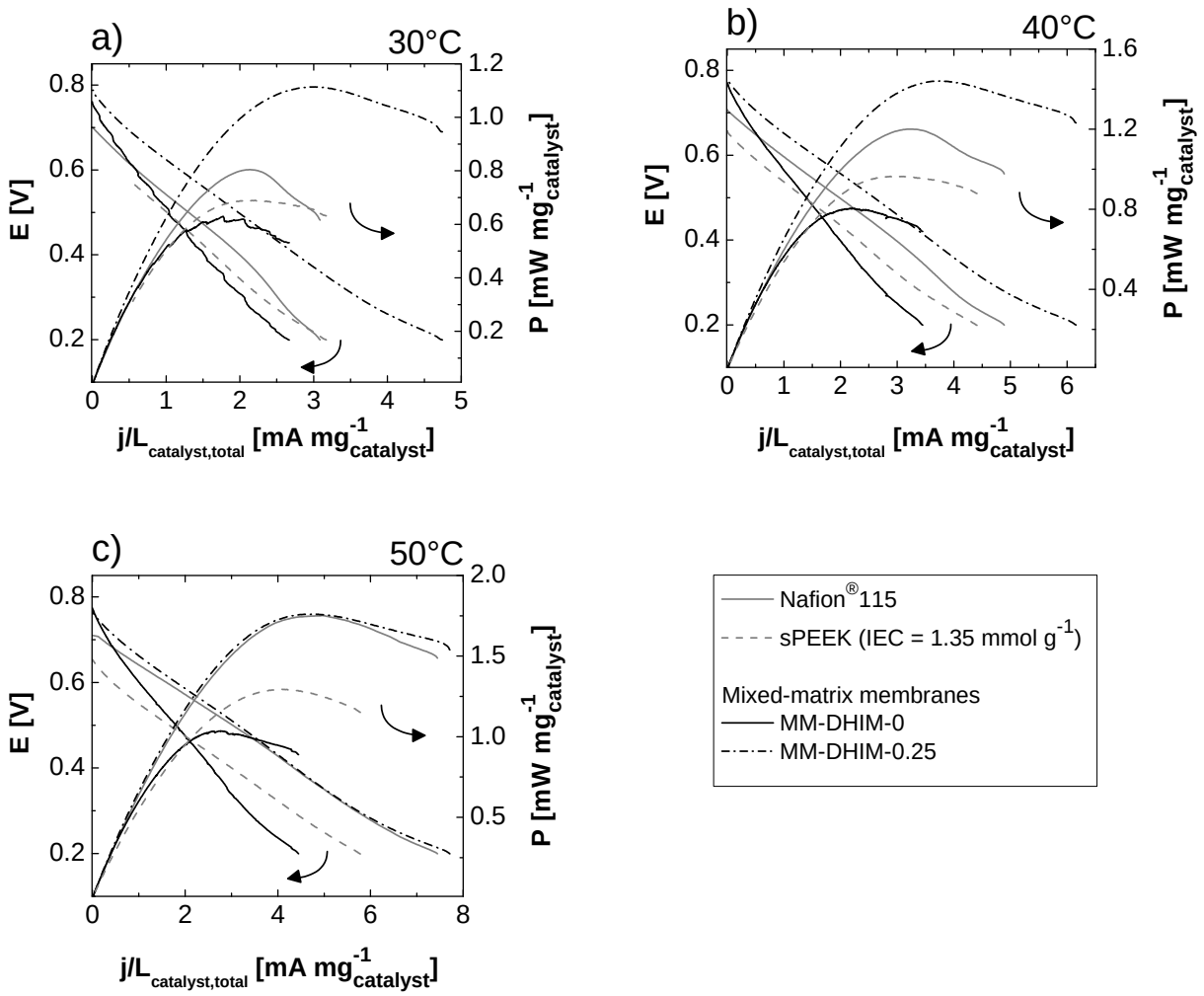

Figure 6.24: Polarization curves (left y-axis) and power plots (right y-axis) determined on the first measuring day of Nafion® 115 and sPEEK (1.35 mmol g^{-1}) in comparison to the mixed-matrix membranes, MM-DHIM-0 and MM-DHIM-0.25. a) 30 °C; b) 40 °C; c) 50 °C. Conditions: anode: 1 M ethanol concentration, 2 ml min^{-1}; cathode: air, 500 ml (STP) min^{-1} and for Nafion® 115, 1000 ml (STP) min^{-1}.

Chapter 7

Overall conclusions and outlook

<u>Pure sPEEK membranes</u>

The sulfonation of PEEK is reproducible and can be controlled by sulfonation time and temperature. The membrane properties, e.g., swelling, proton conductivity and permeability of ethanol and water, are strongly dependent on the degree of sulfonation. In comparison to Nafion®, improved fuel cell performance is predicted based on the ratio of proton diffusion coefficient to ethanol permeability. This makes sPEEK a promising polymer type for application in DEFCs. The main problem of sPEEK membranes is their stability features in aqueous-ethanolic environments in relation to their proton conductivity.

Low sulfonated membranes (*IEC* < 1.4 mmol g^{-1}) are stable and low ethanol permeability coefficients are obtained. Although the characteristic factor $(D_{\sigma} / F_{ethanol})$ is high for low sulfonated sPEEK membranes, the applicability is questioned because of the low proton conductivity. Membrane properties changes exponentially when the *IEC* exceeds 1.8 mmol g^{-1}. Due to its uncontrollable swelling properties in this *IEC* range, pure polymeric membranes cannot be applied. The most appropriate *IEC* range for applying sPEEK is between 1.4 and 1.8 mmol g^{-1}. Both ethanol crossover as well as proton conductivity are acceptable in this range. Further improvement of sPEEK membranes depends on possible modifications to stabilize the membrane in the higher conductive region, rather than on modifications to increase the proton conductivity in the more stable region.

Unmodified mixed-matrix membranes

To improve polymeric sPEEK membranes, an inorganic phase was added. This phase did not consist solely of hydrophilic fumed silica particles (Aerosil®380), but these particles were interconnected by means of partial hydrolysis and polycondensation of tetraethoxysilane. This interconnected inorganic matrix in a polymeric matrix was the strategic step to reduce swelling behavior and to lower ethanol crossover.

It is shown that the inorganic particles are homogeneously distributed, and TEOS is completely converted in the preparation of inorganic-organic mixed-matrix membranes. Liquid uptake experiments show that the stability improvements of interconnected inorganic phase are best observed in higher concentrated ethanol environments. Proton conductivity is dependent on water content in the membrane and the proton diffusion coefficients are similar for all Aerosil®380-$TEOS_{H/C}$ systems. These membranes exhibit lower *IEC* but higher proton diffusion coefficients than the polymeric reference. Reduction in ethanol permeability is more pronounced in the L-L system than in the L-G system. Membranes with an Aerosil®380-$TEOS_{H/C}$ based inorganic phase exhibit, in all cases, remarkable permeation reduction in the L-L system. Pervaporation results are less convincing, because the permeation behavior is similar to the polymeric reference. The ideal membrane selectivity is in all cases between 10 and 12, indicating that separation is not affected by the inorganic loading as well as the inorganic composition.

The presence of the interconnected inorganic phase leads to improved membrane properties in comparison to the polymeric reference. The addition of an interconnected inorganic matrix induced reduced swelling and lower fuel crossover, especially in higher concentrated ethanol systems, while maintaining or improving the proton conductivity. The large inner silica surface, obtained by the high loading in the composite structure, can be used for further improvement of membrane properties by means of functional silanes.

Modified mixed-matrix membranes

This strategic step is done to establish a connection between the organic and inorganic network by means of acid-base interactions. To this, various modifiers bearing basic groups have been compared. Basic group type, amount of basic groups, basicity, hydrophilicity and spacer lengths remarkably influence the mixed-matrix system. The mixed-matrix membrane modified with N-[3-(triethoxysilyl)propyl]-4,5-dihydroimidazole (DHIM) exhibits highest water to ethanol selectivity coefficient as well as highest proton diffusion to ethanol permeation selectivity coefficients and is studied more profoundly.

The ion exchange capacity of DHIM modified mixed-matrix membranes can be well predicted by means of the stoichiometrical interaction of the base-acid pairs. Liquid uptake as a function of ethanol concentration slightly increases up to 4 M and is strongly related to modifier concentration in the membrane. Liquid uptake increases significantly in a 6 M ethanol solution leading to excessive membrane swelling.

The presence of the modifier shows a significant effect on the permeation behavior of ethanol and water with pervaporation. An exponential decrease is observed for both components with increasing modifier concentration. Higher water to ethanol ideal membrane selectivity coefficients are obtained with higher modifier concentration. The strong dependency of ethanol permeation on application temperature is shown with the L-L diffusion system. Measurements performed at 25 °C and 40 °C showed a linear dependency respective to modifier concentration, whereas at 50 °C and 60 °C, this dependency was exponential.

Proton conductivity as well as the proton diffusion coefficient in water, 2 M and 4 M ethanol decrease linearly with increasing modifier content. Proton conductivity as a function of temperature reveals Arrhenius behavior, and the average activation energy of all mixed-matrix membranes was 43.9 ± 2.6 kJ mol^{-1}. Nafion® and sPEEK with the lowest *IEC* (1.15 mmol g^{-1}) exhibit the lowest and highest activation energy respectively (17.3 kJ mol^{-1} and 58.5 kJ mol^{-1}).

High proton diffusion to ethanol permeability selectivity coefficients are obtained with high modifier concentrations. At low modifier concentrations, this selectivity is determined by ethanol permeation and at high modifier concentrations by proton diffusion. The modified mixed-matrix membranes clearly demonstrate prosperous properties with respect to ratio of proton diffusion and ethanol permeability in comparison to Nafion® and pure sPEEK membranes.

Direct ethanol fuel cell tests

DEFC tests show that the presence of modifier in the MMM has a significant influence on the fast activation and immediate functioning of the DEFC. The open circuit voltage increases with increasing modifier concentration in the mixed-matrix membrane. The fuel cell performance is enhanced at higher temperatures, and differences in fuel cell behavior of the unmodified and modified mixed-matrix membranes are more pronounced at higher measuring temperatures. The highest power density at 40 °C and 50 °C is obtained with MM-DHIM-0.25. The most constant development in fuel cell characteristics in time at all temperatures is obtained with MM-DHIM-1.0. Higher ethanol concentration in the anode feed stock results in improved fuel cell performance. Nafion®115 exhibits highest increase in DEFC performance as a function of temperature, but is clearly inferior to the mixed-matrix membranes at 30 °C and 40 °C. The target of 10 mW cm^{-2} at 40 °C is not reached within the measuring conditions, but is predicted at a higher ethanol concentration (2 M or 3 M) in the anode feed stock.

Outlook

The functioning of a DEFC system is demonstrated within the DEFC project,[23] though commercialization is hampered due to the low power output of these systems. The major cause for this is probably the sluggish catalytic reactions especially taking place at the anode. As presented in **Chapter 1**, the intermediates and by-products are manifold and are formed in such a quantity, that they reduce the DEFC performance. Catalyst selection and development is a challenging topic, but is not subject in this thesis and was not the task of our institute in the DEFC project. Significant performance improvements are expected when the catalytic processes are enhanced.

The influence of membrane properties, e.g., swelling, proton conductivity, and ethanol and water permeation, on the DEFC performance is not clarified due to the restricted amount of DEFC measurements whereby certain interesting parameters should have been investigated more profoundly. Examples are ethanol concentration at anode side as well as its liquid flow, air flow at the cathode, and operation time.

The main membrane development parameters still remain proton conductivity, fuel crossover, and membrane stability. The ideal membrane exhibits no fuel (ethanol) crossover and high proton conductivity. In this work, stable membranes with low ethanol permeability are presented. Proton diffusion is enabled due to the water phase present in the membrane during application. This water phase can be controlled by applying functional silanes. The *ideal modifier* should i) interact with the polymer matrix, ii) be partially highly hydrophilic to assure hydration, but hamper the ethanol permeation, iii) be partially hydrophobic for an optimal inorganic-organic arranged structure. This *ideal modifier* consists of an acidic and basic group within one modifier molecule with a hydrophobic linker. This is nearly impossible, because of the possible inter- and intramolecular interactions. A possibility is a modifier with a basic group (secondary amine) connecting the alkoxysilyl group and an oxidizable endgroup (aldehyde group) by means of hydrophobic linkers with defined chain lengths. The basic group interacts with the polymeric matrix and the alkoxysilyl group

reacts (hydrolysis and condensation) and is implemented in the inorganic network. The oxidizable group can be converted into an acid group and, therefore, participates in the proton transferring. Another possibility, which is not investigated, is to apply mixtures of functional silanes or to treat a modified MMM afterwards in a precursor solution.

Proton conductivity will be the other parameter to improve the electrolyte function without diminishing the achieved membrane properties. Two approaches are i) blending low amounts of highly sulfonated sPEEK in the described stable membranes to obtain highly hydrophilic regions or ii) mixing in additional sulfonated silica particles to increase the amount of hydrophilic sulfonic acid groups.

Additional DEFC development potential lies in the membrane-electrode assembly. The MEAs described in this work consist of a Nafion® binder in the electrode layers. The incompatibility of non-fluorinated polymer with fluorinated polymer causes higher resistances at the electrode-membrane interfaces than when the polymers in the layers are similar. First developments have been achieved at our institute where MEAs were solely sPEEK-based. Challenges within this area are the solvent-free catalytic ink preparation and the MEA preparation process.

The approaches for obtaining stable proton conductive membranes can also be transferred to membrane processes where membranes are required with similar requirements. Next to fuel cells, other interesting membrane application areas for ion exchange membranes are dialysis, electrodialysis, and water splitting (bipolar membranes).[185] Fields of application are, for instance, food and biotechnology, waste water treatment and water purification, downstream processing of fermentation broths and the recovery of inorganics. Also other membrane processes, where dense membranes are required with tailor-made propertiesk, are of interest, e.g., gas separation, pervaporation and osmosis-driven processes.

The presented concept can be applied on various polymer types and inorganic materials. Filling the polymer free volume with an interconnected inorganic phase and

connecting this phase to a polymer phase improve the membrane stability. In addition, membrane properties like permeability and selectivity can be controlled by means of using modifiers selected out of the broad range of (commercially) available functional silanes.

References

1. I. Dincer, Renewable energy and sustainable development: a crucial review, *Renewable Sustainable Energy Rev.*, 4 (2), **2000**, 157.
2. P. Costamagna, S. Srinivasan, Quantum jumps in the PEMFC science and technology from the 1960s to the year 2000: Part II. Engineering, technology development and application aspects, *J. Power Sources*, 102 (1-2), **2001**, 253.
3. C.F. Schönbein, On the Voltaic Polarization of Certain Solids and Fluid Substances, *Philos. Mag.*, 14, **1839**, 43.
4. W.R. Grove, On a Gaseous Voltaic Battery, *Philos. Mag.*, 21, **1842**, 417.
5. L. Mond, C. Langer, A new Form of Gas Battery, *Proc. R. Soc. Lond.*, 46, **1889**, 144.
6. F.T. Bacon, Fuel Cells, Past, Presence and Future, *Electrochim. Acta*, 14 (7), **1969**, 569.
7. W.T. Grubb, L.W. Niedrach, Batteries with Solid Ion-Exchange Membrane Electrolytes, *J. Electrochem. Soc.*, 107, **1960**, 131.
8. W.T. Grubb, L.W. Niedrach, A High Performance Saturated Hydrocarbon Fuel Cell, *J. Electrochem. Soc.*, 110 (10), **1963**, 1086.
9. NASA, Gemini Project, *http://www.nasa.gov*, visited: 2008.
10. G.J. Schaeffer, *FUEL CELLS FOR THE FUTURE; A contribution to technology forecasting from a technology dynamics perspective*, **1998**, University of Twente.
11. EG&G Technical Services Inc., Fuel Cell Handbook, 7, 2004, U.S. Department of Energy.
12. J.-H. Wee, Applications of proton exchange membrane fuel cell systems, *Renewable Sustainable Energy Rev.*, 11 (8), **2007**, 1720.
13. P.W. Atkins, Physical Chemistry, 5th, 1994, Oxford University Press, Oxford, UK, New York.
14. L. Carrette, K.A. Friedrich, U. Stimming, Fuel Cells - Fundamentals and Applications, *Fuel Cells*, 1 (1), **2001**, 5.
15. C. Coutanceau, S. Brimaud, C. Lamy, et al., Review of different methods for developing nano-electrocatalysts for the oxidation of organic compounds, *Electrochim. Acta*, 53 (23), **2008**, 6865.
16. P.P. Edwards, V.L. Kuznetsov, W.I.F. David, et al., Hydrogen and fuel cells: Towards a sustainable energy future, *Energy Policy*, 36 (12), **2008**, 4356.
17. M. Conte, A. Iacobazzi, M. Ronchetti, et al., Hydrogen economy for a sustainable development: state-of-the-art and technological perspectives, *J. Power Sources*, 100 (1-2), **2001**, 171.
18. J.D. Holladay, J. Hu, D.L. King, et al., An overview of hydrogen production technologies, *Catalysis Today*, 139 (4), **2009**, 244.
19. M. Hugh, Fuel Cell Today: Portable Survey 2008, *www.fuelcelltoday.com*, visited: 2008.
20. C. Lamy, A. Lima, V. LeRhun, et al., Recent advances in the development of direct alcohol fuel cells (DAFC), *J. Power Sources*, 105 (2), **2002**, 283.
21. E. Antolini, Catalysts for direct ethanol fuel cells, *J. Power Sources*, 170 (1), **2007**, 1.

22. Departement of Defence, USA, *Technology Readiness Assessment (TRA) Deskbook*, http://www.dod.mil/ddre/doc/May2005_TRA_2005_DoD.pdf, **2005**, visited: 2009.
23. J. Tübke, Direkt Ethanol Brennstoffzelle, *8th f-cell symposium, Stuttgart*, **2008**.
24. U.B. Demirci, Direct liquid-feed fuel cells: Thermodynamic and environmental concerns, *J. Power Sources*, 169 (2), **2007**, 239.
25. J. Wang, S. Wasmus, R.F. Savinell, Evaluation of Ethanol, 1-Propanol, and 2-Propanol in a Direct Oxidation Polymer-Electrolyte Fuel Cell, *J. Electrochem. Soc.*, 142 (12), **1995**, 4218.
26. K. Yamada, K. Asazawa, K. Yasuda, et al., Investigation of PEM type direct hydrazine fuel cell, *J. Power Sources*, 115 (2), **2003**, 236.
27. B.H. Liu, Z.P. Li, Current status and progress of direct borohydride fuel cell technology development, *J. Power Sources*, 187 (2), **2009**, 291.
28. J.-H. Wee, Which type of fuel cell is more competitive for portable application: Direct methanol fuel cells or direct borohydride fuel cells?, *J. Power Sources*, 161 (1), **2006**, 1.
29. S.C.S. Lai, S.E.F. Kleyn, V. Rosca, et al., Mechanism of the Dissociation and Electrooxidation of Ethanol and Acetaldehyde on Platinum As Studied by SERS, *J. Phys. Chem. C*, 112 (48), **2008**, 19080.
30. S.C.S. Lai, M.T.M. Koper, Electro-oxidation of ethanol and acetaldehyde on platinum single-crystal electrodes, *Faraday Discuss.*, 140, **2009**, 399
31. G.A. Camara, T. Iwasita, Parallel pathways of ethanol oxidation: The effect of ethanol concentration, *J. Electroanal. Chem.*, 578 (2), **2005**, 315.
32. C. Cremers, D. Bayer, B. Kintzel, et al., Oxidation of Alcohols in Acidic and Alkaline Environments, *ECS Transactions*, 16 (2), **2008**, 1263.
33. J. Jagur-Grodzinski, Polymeric materials for fuel cells: concise review of recent studies, *Polym. Adv. Technol.*, 18 (10), **2007**, 785.
34. K.D. Kreuer, On the development of proton conducting polymer membranes for hydrogen and methanol fuel cells, *J. Membr. Sci.*, 185 (1), **2001**, 29.
35. V. Neburchilov, J. Martin, H. Wang, et al., A review of polymer electrolyte membranes for direct methanol fuel cells, *J. Power Sources*, 169 (2), **2007**, 221.
36. R.-Q. Fu, L. Hong, J.Y. Lee, Membrane Design for Direct Ethanol Fuel Cells: A Hybrid Proton-Conducting Interpenetrating Polymer Network, *Fuel Cells*, 8 (1), **2008**, 52.
37. A.R. Tan, L.M.d. Carvalho, F.G.d.R. Filho, et al., Nanocomposite Membranes Based on Sulfonated Poly(etheretherketone) Structured with Modified Silica for Direct Ethanol Fuel Cell, *Macromol. Symp.*, 245-246 (1), **2006**, 470.
38. K.S. Roelofs, T. Hirth, T. Schiestel, Sulfonated Poly(Ether Ether Ketone) based Silica Nanocomposite Membranes for Direct Ethanol Fuel Cells, *J. Membr. Sci.*, 346 (1), **2010**, 215.
39. D. Dunwoody, J. Leddy, Proton Exchange Membranes: The View Forward and Back, *Electrochem. Soc. Interface*, **2005**, 37.
40. J.A. Kerres, Development of ionomer membranes for fuel cells, *J. Membr. Sci.*, 185 (1), **2001**, 3.
41. K.-V. Peinemann, S.P. Nunes, Eds. Membranes for energy conversion, Chapter 1, Wiley-VCH Verlag: Weinheim, 2008.

42. R. Souzy, B. Ameduri, Functional fluoropolymers for fuel cell membranes, *Prog. Polym. Sci.*, 30 (6), **2005**, 644.
43. J.S. Lee, N.D. Quan, J.M. Hwang, et al., Polymer Electrolyte Membranes for Fuel Cells, *J. Ind. Eng. Chem.*, 12 (2), **2006**, 175.
44. Gore, www.gore.com, visited: 2009.
45. V. Arcella, C. Troglia, A. Ghielmi, Hyflon Ion Membranes for Fuel Cells, *Ind. Eng. Chem. Res.*, 44 (20), **2005**, 7646.
46. Fumatec, *http://www.fumatech.com*, visited: 2009.
47. K.A. Mauritz, R.B. Moore, State of Understanding of Nafion, *Chem. Rev.*, 104 (10), **2004**, 4535.
48. K. Schmidt-Rohr, Q. Chen, Parallel cylindrical water nanochannels in Nafion fuel-cell membranes, *Nat. Mater.*, 7 (1), **2008**, 75.
49. W.Y. Hsu, T.D. Gierke, Ion transport and clustering in nafion perfluorinated membranes, *J. Membr. Sci.*, 13 (3), **1983**, 307.
50. M. Eikerling, A.A. Kornyshev, U. Stimming, Electrophysical Properties of Polymer Electrolyte Membranes: A Random Network Model, *J. Phys. Chem. B*, 101 (50), **1997**, 10807.
51. H.G. Haubold, T. Vad, H. Jungbluth, et al., Nano structure of NAFION: a SAXS study, *Electrochim. Acta*, 46 (10-11), **2001**, 1559.
52. K.-D. Kreuer, S.J. Paddison, E. Spohr, et al., Transport in Proton Conductors for Fuel-Cell Applications: Simulations, Elementary Reactions, and Phenomenology, *Chem. Rev.*, 104 (10), **2004**, 4637.
53. S.J. Paddison, Proton Conduction Mechanisms at Low Degrees of Hydration in Sulfonic Acid Based Polymer Electrolyte Membranes, *Annu. Rev. Mater. Sci.*, 33 (1), **2003**, 289.
54. B. Bae, H.Y. Ha, D. Kim, Nafion®-graft-polystyrene sulfonic acid membranes for direct methanol fuel cells, *J. Membr. Sci.*, 276 (1-2), **2006**, 51.
55. D. Kim, M.A. Scibioh, S. Kwak, et al., Nano-silica layered composite membranes prepared by PECVD for direct methanol fuel cells, *Electrochem. Commun.*, 6 (10), **2004**, 1069.
56. Z.-G. Shao, X. Wang, I.M. Hsing, Composite Nafion/polyvinyl alcohol membranes for the direct methanol fuel cell, *J. Membr. Sci.*, 210 (1), **2002**, 147.
57. C.W. Lin, K.C. Fan, R. Thangamuthu, Preparation and characterization of high selectivity organic-inorganic hybrid-laminated Nafion 115 membranes for DMFC, *J. Membr. Sci.*, 278 (1-2), **2006**, 437.
58. Y. Lin, H. Li, C. Liu, et al., Surface-modified Nafion membranes with mesoporous SiO2 layers via a facile dip-coating approach for direct methanol fuel cells, *J. Power Sources*, 185 (2), **2008**, 904.
59. O. Savadogo, Emerging membranes for electrochemical systems: Part II. High temperature composite membranes for polymer electrolyte fuel cell (PEFC) applications, *J. Power Sources*, 127 (1-2), **2004**, 135.
60. J.H. Shim, I.G. Koo, W.M. Lee, Nafion-impregnated polyethylene-terephthalate film used as the electrolyte for direct methanol fuel cells, *Electrochimica Acta*, 50 (12), **2005**, 2385.
61. M.H. Yildirim, D. Stamatialis, M. Wessling, Dimensionally stable Nafion-polyethylene composite membranes for direct methanol fuel cell applications, *J. Membr. Sci.*, 321 (2), **2008**, 364.

62. J.A. Kerres, Blended and Cross-Linked Ionomer Membranes for Application in Membrane Fuel Cells, *Fuel Cells*, 5 (2), **2005**, 230.
63. N.W. DeLuca, Y.A. Elabd, Direct methanol fuel cell performance of Nafion®/poly(vinyl alcohol) blend membranes, *J. Power Sources*, 163 (1), **2006**, 386.
64. I.T. Kim, J. Choi, S.C. Kim, Blend membranes of Nafion/sulfonated poly(aryl ether ketone) for direct methanol fuel cell, *J. Membr. Sci.*, 300 (1-2), **2007**, 28.
65. R. Wycisk, J. Chisholm, J. Lee, et al., Direct methanol fuel cell membranes from Nafion-polybenzimidazole blends, *J. Power Sources*, 163 (1), **2006**, 9.
66. K.A. Mauritz, Organic-inorganic hybrid materials: perfluorinated ionomers as sol-gel polymerization templates for inorganic alkoxides, *Mater. Sci. Eng., C*, 6 (2-3), **1998**, 121.
67. C.J. Brinker, G.W. Scherer, Sol-Gel Science; the Physics and Chemistry of Sol-Gel Processing, 1990, Elsevier Science, San Diego, London.
68. R. Jiang, H.R. Kunz, J.M. Fenton, Composite silica/Nafion(R) membranes prepared by tetraethylorthosilicate sol-gel reaction and solution casting for direct methanol fuel cells, *J. Membr. Sci.*, 272 (1-2), **2006**, 116.
69. S. Ren, G. Sun, C. Li, et al., Organic silica/Nafion(R) composite membrane for direct methanol fuel cells, *J. Membr. Sci.*, 282 (1-2), **2006**, 450.
70. C. Li, G. Sun, S. Ren, et al., Casting Nafion-sulfonated organosilica nano-composite membranes used in direct methanol fuel cells, *J. Membr. Sci.*, 272 (1-2), **2006**, 50.
71. Y.J. Kim, W.C. Choi, S.I. Woo, et al., Proton conductivity and methanol permeation in Nafion(TM)/ORMOSIL prepared with various organic silanes, *J. Membr. Sci.*, 238 (1-2), **2004**, 213.
72. M. Lavorgna, L. Mascia, G. Mensitieri, et al., Hybridization of Nafion membranes by the infusion of functionalized siloxane precursors, *J. Membr. Sci.*, 294 (1-2), **2007**, 159.
73. N.H. Jalani, K. Dunn, R. Datta, Synthesis and characterization of Nafion®-MO2 (M = Zr, Si, Ti) nanocomposite membranes for higher temperature PEM fuel cells, *Electrochim. Acta*, 51 (3), **2005**, 553.
74. P. Dimitrova, K.A. Friedrich, B. Vogt, et al., Transport properties of ionomer composite membranes for direct methanol fuel cells, *J. Electroanal. Chem.*, 532 (1-2), **2002**, 75.
75. K.-V. Peinemann, S.P. Nunes, Eds. Membranes for energy conversion, Chapter 5, Wiley-VCH Verlag: Weinheim, 2008.
76. S. Pavlidou, C.D. Papaspyrides, A review on polymer-layered silicate nanocomposites, *Prog. Polym. Sci.*, 33 (12), **2008**, 1119.
77. M.-K. Song, S.-B. Park, Y.-T. Kim, et al., Characterization of polymer-layered silicate nanocomposite membranes for direct methanol fuel cells, *Electrochim. Acta*, 50 (2-3), **2004**, 639.
78. W. Lee, H. Kim, T.K. Kim, et al., Nafion based organic/inorganic composite membrane for air-breathing direct methanol fuel cells, *J. Membr. Sci.*, 292 (1-2), **2007**, 29.
79. Y.-F. Lin, C.-Y. Yen, C.-H. Hung, et al., A novel composite membranes based on sulfonated montmorillonite modified Nafion® for DMFCs, *J. Power Sources*, 168 (1), **2007**, 162.
80. X. Li, E.P.L. Roberts, S.M. Holmes, et al., Functionalized zeolite A-nafion composite membranes for direct methanol fuel cells, *Solid State Ionics*, 178 (19-20), **2007**, 1248.

81. V. Tricoli, F. Nannetti, Zeolite-Nafion composites as ion conducting membrane materials, *Electrochim. Acta*, 48 (18), **2003**, 2625.
82. S.C. Byun, Y.J. Jeong, J.W. Park, et al., Effect of solvent and crystal size on the selectivity of ZSM-5/Nafion composite membranes fabricated by solution-casting method, *Solid State Ionics*, 177 (37-38), **2006**, 3233.
83. C.T. Kresge, M.E. Leonowicz, W.J. Roth, et al., Ordered mesoporous molecular sieves synthesized by a liquid-crystal template mechanism, *Nature*, 359 (6397), **1992**, 710.
84. J.W. Park, Y.C. Kim, Y.J. Jeong, et al., Effects of organo-functionalization and sulfonation of MCM-41on the proton selectivities of MCM-41/Nafion composite membranes for DMFC, *Microporous Mesoporous Mater.*, 114 (1-3), **2008**, 238.
85. Y. Jin, S. Qiao, L. Zhang, et al., Novel Nafion composite membranes with mesoporous silica nanospheres as inorganic fillers, *J. Power Sources*, 185 (2), **2008**, 664.
86. F. Bauer, M. Willert-Porada, Microstructural characterization of Zr-phosphate-Nafion® membranes for direct methanol fuel cell (DMFC) applications, *J. Membr. Sci.*, 233 (1-2), **2004**, 141.
87. C. Yang, S. Srinivasan, A.B. Bocarsly, et al., A comparison of physical properties and fuel cell performances of Nafion and zirconium phosphate/Nafion composite membranes, *J. Membr. Sci.*, 237, **2004**, 145.
88. M. Eikerling, Y.I. Kharkats, A.A. Kornyshev, et al., Phenomenological Theory of Electro-osmotic Effect and Water Management in Polymer Electrolyte Proton-Conducting Membranes, *J. Electrochem. Soc.*, 145 (8), **1998**, 2684.
89. T. Thampan, S. Malhotra, H. Tang, et al., Modeling of Conductive Transport in Proton-Exchange Membranes for Fuel Cells, *J. Electrochem. Soc.*, 147 (9), **2000**, 3242.
90. H. Hou, G. Sun, Z. Wu, et al., Zirconium phosphate/Nafion115 composite membrane for high-concentration DMFC, *Int. J. Hydrogen Energy*, 33 (13), **2008**, 3402.
91. S. Hara, M. Miyayama, Proton conductivity of superacidic sulfated zirconia, *Solid State Ionics*, 168 (1-2), **2004**, 111.
92. Y. Zhai, H. Zhang, J. Hu, et al., Preparation and characterization of sulfated zirconia (SO_4^{2-}/ZrO_2)/Nafion composite membranes for PEMFC operation at high temperature/low humidity, *J. Membr. Sci.*, 280, **2006**, 148.
93. S. Ren, G. Sun, C. Li, et al., Sulfated zirconia-Nafion composite membranes for higher temperature direct methanol fuel cells, *J. Power Sources*, 157 (2), **2006**, 724.
94. U. Lavrencic Stangar, N. Groselj, B. Orel, et al., Proton-conducting sol-gel hybrids containing heteropoly acids, *Solid State Ionics*, 145 (1-4), **2001**, 109.
95. Z.-G. Shao, P. Joghee, I.M. Hsing, Preparation and characterization of hybrid Nafion-silica membrane doped with phosphotungstic acid for high temperature operation of proton exchange membrane fuel cells, *J. Membr. Sci.*, 229 (1-2), **2004**, 43.
96. H.-J. Kim, Y.-G. Shul, H. Han, Sulfonic-functionalized heteropolyacid-silica nanoparticles for high temperature operation of a direct methanol fuel cell, *J. Power Sources*, 158 (1), **2006**, 137.

97. Y.C. Kim, J.Y. Jeong, J.Y. Hwang, et al., Incorporation of heteropoly acid, tungstophosphoric acid within MCM-41 via impregnation and direct synthesis methods for the fabrication of composite membrane of DMFC, *J. Membr. Sci.*, 325 (1), **2008**, 252.
98. J. Roziere, D.J. Jones, Non-fluorinated polymer materials for proton exchange membrane fuel cells, *Annu. Rev. Mater. Sci.*, 33 (1), **2003**, 503.
99. H.R. Allcock, Recent developments in polyphosphazene materials science, *Curr. Opin. Solid State Mater. Sci.*, 10 (5-6), **2006**, 231.
100. Q. Guo, P. N. Pintauro, H. Tang, et al., Sulfonated and crosslinked polyphosphazene-based proton-exchange membranes, *J. Membr. Sci.*, 154 (2), **1999**, 175.
101. H. Tang, P.N. Pintauro, Q. Guo, et al., Polyphosphazene membranes. III. Solid-state characterization and properties of sulfonated poly[bis(3-methylphenoxy)phosphazene], *J. Appl. Polym. Sci.*, 71 (3), **1999**, 387.
102. Q. Li, J.O. Jensen, R.F. Savinell, et al., High temperature proton exchange membranes based on polybenzimidazoles for fuel cells, *Prog. Polym. Sci.*, 34 (5), **2009**, 449.
103. P. Staiti, F. Lufrano, A.S. Aricò, et al., Sulfonated polybenzimidazole membranes - preparation and physico-chemical characterization, *J. Membr. Sci.*, 188 (1), **2001**, 71.
104. K.-V. Peinemann, S.P. Nunes, Eds. Membranes for energy conversion, Chapter 3, Wiley-VCH Verlag: Weinheim, 2008.
105. H. Ghassemi, J.E. McGrath, Synthesis and properties of new sulfonated poly(p-phenylene) derivatives for proton exchange membranes. I, *Polymer*, 45 (17), **2004**, 5847.
106. T. Xu, D. Wu, L. Wu, Poly(2,6-dimethyl-1,4-phenylene oxide) (PPO)--A versatile starting polymer for proton conductive membranes (PCMs), *Prog. Polym. Sci.*, 33 (9), **2008**, 894.
107. K.-V. Peinemann, S.P. Nunes, Eds. Membranes for energy conversion, Chapter 2, Wiley-VCH Verlag: Weinheim, 2008.
108. X. Ye, H. Bai, W.S.W. Ho, Synthesis and characterization of new sulfonated polyimides as proton-exchange membranes for fuel cells, *J. Membr. Sci.*, 279 (1-2), **2006**, 570.
109. J.P. Quentin, 1973, US 3,709,841.
110. B.C. Johnson, I. Yilgör, C. Tran, et al., Synthesis and characterization of sulfonated poly(acrylene ether sulfones), *J. Polym. Sci., Polym. Chem. Ed.* , 22 (3), **1984**, 721.
111. R. Nolte, K. Ledjeff, M. Bauer, et al., Partially sulfonated poly(arylene ether sulfone) - A versatile proton conducting membrane material for modern energy conversion technologies, *J. Membr. Sci.*, 83 (2), **1993**, 211.
112. D.J. Jones, J. Roziere, Recent advances in the functionalisation of polybenzimidazole and polyetherketone for fuel cell applications, *J. Membr. Sci.*, 185 (1), **2001**, 41.
113. B. Smitha, S. Sridhar, A.A. Khan, Solid polymer electrolyte membranes for fuel cell applications--a review, *J. Membr. Sci.*, 259 (1-2), **2005**, 10.
114. K.-V. Peinemann, S.P. Nunes, Eds. Membranes for energy conversion, Wiley-VCH Verlag: Weinheim, 2008.
115. M.A. Hickner, H. Ghassemi, Y.S. Kim, et al., Alternative Polymer Systems for Proton Exchange Membranes (PEMs), *Chem. Rev.*, 104 (10), **2004**, 4587.

116. H.-H. Ulrich, G. Rafler, Sulfonated poly(aryl ether ketone)s, *Angew. Makromol. Chem.*, 263 (1), **1998**, 71.
117. X. Jin, M.T. Bishop, T.S. Ellis, et al., A sulphonated poly(aryl ether ketone), *Br. Polym. J.*, 17 (1), **1985**, 4.
118. M.T. Bishop, F.E. Karasz, P.S. Russo, et al., Solubility and properties of a poly(aryl ether ketone) in strong acids, *Macromolecules*, 18 (1), **1985**, 86.
119. R.Y.M. Huang, P. Shao, C.M. Burns, et al., Sulfonation of poly(ether ether ketone) (PEEK): Kinetic study and characterization, *J. Appl. Polym. Sci.*, 82 (11), **2001**, 2651.
120. K.N.T. Do, D. Kim, Comparison of homogeneously and heterogeneously sulfonated polyetheretherketone membranes in preparation, properties and cell performance, *J. Power Sources*, 185 (1), **2008**, 63.
121. P. Xing, G.P. Robertson, M.D. Guiver, et al., Synthesis and characterization of sulfonated poly(ether ether ketone) for proton exchange membranes, *J. Membr. Sci.*, 229 (1-2), **2004**, 95.
122. F.G. Wilhelm, I.G.M. Pünt, N.F.A.v.d. Vegt, et al., Cation permeable membranes from blends of sulfonated poly(ether ether ketone) and poly(ether sulfone), *J. Membr. Sci.*, 199, **2002**, 167.
123. M. Gil, X. Ji, X. Li, et al., Direct synthesis of sulfonated aromatic poly(ether ether ketone) proton exchange membranes for fuel cell applications, *J. Membr. Sci.*, 234 (1-2), **2004**, 75.
124. F. Wang, T. Chen, J. Xu, Sodium sulfonate-functionalized poly(ether ether ketone)s, *Macromol. Chem. Phys.*, 199 (7), **1998**, 1421.
125. R.T.S. Muthu Lakshmi, J. Meier-Haack, K. Schlenstedt, et al., Sulphonated poly(ether ether ketone) copolymers: Synthesis, characterisation and membrane properties, *J. Membr. Sci.*, 261 (1-2), **2005**, 27.
126. S. Xue, G. Yin, Methanol permeability in sulfonated poly(etheretherketone) membranes: A comparison with Nafion membranes, *Eur. Polym. J.*, 42 (4), **2006**, 776.
127. D.M. Xing, B.L. Yi, F.Q. Liu, et al., Characterization of Sulfonated Poly(Ether Ether Ketone)/Polytetrafluoroethylene Composite Membranes for Fuel Cell Applications, *Fuel Cells*, 5 (3), **2005**, 406.
128. S. Zhong, X. Cui, H. Cai, et al., Crosslinked sulfonated poly(ether ether ketone) proton exchange membranes for direct methanol fuel cell applications, *J. Power Sources*, 164 (1), **2007**, 65.
129. S.D. Mikhailenko, K. Wang, S. Kaliaguine, et al., Proton conducting membranes based on cross-linked sulfonated poly(ether ether ketone) (SPEEK), *J. Membr. Sci.*, 233 (1-2), **2004**, 93.
130. H.-L. Wu, C.-C.M. Ma, F.-Y. Liu, et al., Preparation and characterization of poly(ether sulfone)/sulfonated poly(ether ether ketone) blend membranes, *Eur. Polym. J.*, 42 (7), **2006**, 1688.
131. H.-L. Wu, C.-C.M. Ma, C.-H. Li, et al., Sulfonated poly(ether ether ketone)/poly(amide imide) polymer blends for proton conducting membrane, *J. Membr. Sci.*, 280 (1-2), **2006**, 501.
132. H.-L. Wu, C.-C.M. Ma, H.-C. Kuan, et al., Sulfonated poly(ether ether ketone)/poly(vinylpyrrolidone) acid-base polymer blends for direct methanol fuel cell application, *J. Polym. Sci., Part B: Polym. Phys.*, 44 (3), **2006**, 565.
133. T. Yang, Preliminary study of SPEEK/PVA blend membranes for DMFC applications, *Int. J. Hydrogen Energy*, 33 (22), **2008**, 6772.

134. S. Pasupathi, S. Ji, B. Jan Bladergroen, et al., High DMFC performance output using modified acid-base polymer blend, *Int. J. Hydrogen Energy*, 33 (12), **2008**, 3132.
135. S.P. Nunes, B. Ruffmann, E. Rikowski, et al., Inorganic modification of proton conductive polymer membranes for direct methanol fuel cells, *J. Membr. Sci.*, 203 (1-2), **2002**, 215.
136. L. Tchicaya-Bouckary, D.J. Jones, J. Rozière, Hybrid Polyaryletherketone Membranes for Fuel Cell Applications, *Fuel Cells*, 2 (1), **2002**, 40.
137. S. Sambandam, V. Ramani, SPEEK/functionalized silica composite membranes for polymer electrolyte fuel cells, *J. Power Sources*, 170 (2), **2007**, 259.
138. D. Gomes, I. Buder, S.P. Nunes, Sulfonated silica-based electrolyte nanocomposite membranes, *J. Polym. Sci., Part B: Polym. Phys.*, 44 (16), **2006**, 2278.
139. A. Carbone, R. Pedicini, A. Saccà, et al., Composite S-PEEK membranes for medium temperature polymer electrolyte fuel cells, *J. Power Sources*, 178 (2), **2008**, 661.
140. J.-H. Chang, J.H. Park, G.-G. Park, et al., Proton-conducting composite membranes derived from sulfonated hydrocarbon and inorganic materials, *J. Power Sources*, 124 (1), **2003**, 18.
141. C.S. Karthikeyan, S.P. Nunes, K. Schulte, Ionomer-silicates composite membranes: Permeability and conductivity studies, *Eur. Polym. J.*, 41 (6), **2005**, 1350.
142. Z. Gaowen, Z. Zhentao, Organic/inorganic composite membranes for application in DMFC, *J. Membr. Sci.*, 261, **2005**, 107.
143. R. Gosalawit, S. Chirachanchai, S. Shishatskiy, et al., Sulfonated montmorillonite/sulfonated poly(ether ether ketone) (SMMT/SPEEK) nanocomposite membrane for direct methanol fuel cells (DMFCs), *J. Membr. Sci.*, 323 (2), **2008**, 337.
144. S. Erce, H. Erdener, R.G. Akay, et al., Effects of sulfonated polyether-etherketone (SPEEK) and composite membranes on the proton exchange membrane fuel cell (PEMFC) performance, *Int. J. Hydrogen Energy*, 34 (10), **2009**, 4645.
145. C.S. Karthikeyan, S.P. Nunes, L.A.S.A. Prado, et al., Polymer nanocomposite membranes for DMFC application, *J. Membr. Sci.*, 254, **2005**, 139.
146. B. Ruffmann, H. Silva, B. Schulte, et al., Organic/inorganic composite membranes for application in DMFC, *Solid State Ionics*, 162-163, **2003**, 269.
147. V.S. Silva, S. Weisshaar, R. Reissner, et al., Performance and efficiency of a DMFC using non-fluorinated composite membranes operating at low/medium temperatures, *J. Power Sources*, 145 (2), **2005**, 485.
148. B.P. Tripathi, M. Kumar, V.K. Shahi, Highly stable proton conducting nanocomposite polymer electrolyte membrane (PEM) prepared by pore modifications: An extremely low methanol permeable PEM, *J. Membr. Sci.*, 327 (1-2), **2009**, 145.
149. S.M.J. Zaidi, S.D. Mikhailenko, G.P. Robertson, et al., Proton conducting composite membranes from polyether ether ketone and heteropolyacids for fuel cell applications, *J. Membr. Sci.*, 173 (1), **2000**, 17.
150. M. Bello, S.M.J. Zaidi, S.U. Rahman, Proton and methanol transport behavior of SPEEK/TPA/MCM-41 composite membranes for fuel cell application, *J. Membr. Sci.*, 322 (1), **2008**, 218.

151. S.M.J. Zaidi, M.I. Ahmad, Novel SPEEK/heteropolyacids loaded MCM-41 composite membranes for fuel cell applications, *J. Membr. Sci.*, 279 (1-2), **2006**, 548.
152. M.L. Ponce, L. Prado, B. Ruffmann, et al., Reduction of methanol permeability in polyetherketone-heteropolyacid membranes, *J. Membr. Sci.*, 217 (1-2), **2003**, 5.
153. A.F. Ismail, N.H. Othman, A. Mustafa, Sulfonated polyether ether ketone composite membrane using tungstosilicic acid supported on silica-aluminium oxide for direct methanol fuel cell (DMFC), *J. Membr. Sci.*, 329 (1-2), **2009**, 18.
154. K.S. Roelofs, A. Kampa, T. Hirth, et al., Behavior of sulfonated poly(ether ether ketone) in ethanol-water systems, *J. Appl. Polym. Sci.*, 111 (6), **2009**, 2998.
155. G.P. Robertson, S.D. Mikhailenko, K. Wang, et al., Casting solvent interactions with sulfonated poly(ether ether ketone) during proton exchange membrane fabrication, *J. Membr. Sci.*, 219 (1-2), **2003**, 113.
156. F.M. Smits, Measurement of sheet resistivities with the four-point probe, *Bell Syst. Tech. J.*, 37, **1958**, 711.
157. M.C. Benjamin, R.J. Hillard, J.O. Borland, Ultra-shallow junction (USJ) sheet resistance measurements with a non-penetrating four point probe, *Nucl. Instrum. Methods Phys. Res., Sect. B*, 237 (1-2), **2005**, 351.
158. B.D. Cahan, J.S. Wainright, AC impedance investigations of proton conduction in Nafion, *J. Electrochem. Soc.*, 140 (12), **1993**, L185.
159. Bridge Technology, Four-Point-Probes, Finite-size corrections for 4-point probe measurements, *http://four-point-probes.com/4-point.pdf*, visited: 2008.
160. T.A. Zawodzinski, M. Neeman, L. Sillerud, et al., Determination of Water Dlffusion Coefficients in Perfluorosulfonate Ionomeric Membranes, *J. Phys. Chem.*, 95, **1991**, 6040.
161. S. Kaliaguine, S.D. Mikhailenko, K.P. Wang, et al., Properties of SPEEK based PEMs for fuel cell application, *Catal. Today*, 82 (1-4), **2003**, 213.
162. X. Li, C. Zhao, H. Lu, et al., Direct synthesis of sulfonated poly(ether ether ketone ketone)s (SPEEKKs) proton exchange membranes for fuel cell application, *Polymer*, 46 (15), **2005**, 5820.
163. R.Y.M. Huang, P. Shao, X. Feng, et al., Pervaporation separation of water/isopropanol mixture using sulfonated poly(ether ether ketone) (SPEEK) membranes: transport mechanism and separation performance, *J. Membr. Sci.*, 192 (1-2), **2001**, 115.
164. P. Schaetzel, C. Vauclair, Q.T. Nguyen, et al., A simplified solution-diffusion theory in pervaporation: the total solvent volume fraction model, *J. Membr. Sci.*, 244 (1-2), **2004**, 117.
165. P. Shao, R.Y.M. Huang, Polymeric membrane pervaporation, *J. Membr. Sci.*, 287 (2), **2007**, 162.
166. A. Verhoef, A. Figoli, B. Leen, et al., Performance of a nanofiltration membrane for removal of ethanol from aqueous solutions by pervaporation, *Sep. Purif. Technol.*, 60 (1), **2008**, 54.
167. NIST, *National Institute of Standards and Technology*, http://webbook.nist.gov/, visited: 2008.
168. H.-L. Wu, C.-C.M. Ma, C.-C. Lin, et al., Effects and properties of poly(arylene ether benzonitrile)s of various molecular weights blended with sulfonated poly(ether ether ketone), *J. Appl. Polym. Sci.*, 107 (5), **2008**, 3236.

169. L. Li, J. Zhang, Y. Wang, Sulfonated poly(ether ether ketone) membranes for direct methanol fuel cell, *J. Membr. Sci.*, 226 (1-2), **2003**, 159.
170. K.D. Kreuer, On the development of proton conducting materials for technological applications, *Solid State Ionics*, 97 (1-4), **1997**, 1.
171. H.-L. Wu, C.-C.M. Ma, C.-H. Li, et al., Swelling behavior and solubility parameter of sulfonated poly(ether ether ketone), *J. Polym. Sci., Part B: Polym. Phys.*, 44 (21), **2006**, 3128.
172. R. Jiang, H.R. Kunz, J.M. Fenton, Investigation of membrane property and fuel cell behavior with sulfonated poly(ether ether ketone) electrolyte: Temperature and relative humidity effects, *J. Power Sources*, 150, **2005**, 120.
173. M.L. Di Vona, D. Marani, A. D'Epifanio, et al., Hybrid materials for polymer electrolyte membrane fuel cells: Water uptake, mechanical and transport properties, *J. Membr. Sci.*, 304 (1-2), **2007**, 76.
174. N. Agmon, The Grotthuss mechanism, *Chem. Phys. Lett.*, 244 (5-6), **1995**, 456.
175. J. Ahn, W.-J. Chung, I. Pinnau, et al., Polysulfone/silica nanoparticle mixed-matrix membranes for gas separation, *J. Membr. Sci.*, 314 (1-2), **2008**, 123.
176. D.A. Donatti, A.I. Ruiz, D.R. Vollet, Structural study of composites of aerosil fumed silica and tetraethoxysilane-derived sonogels, *J. Non-Cryst. Solids*, 351 (14-15), **2005**, 1226.
177. M.A. Markowitz, P.E. Schoen, P. Kust, et al., Surface acidity and basicity of functionalized silica particles, *Colloids Surf., A*, 150 (1-3), **1999**, 85.
178. Gelest, Silane Coupling Agents: Connecting Across Boundaries, *http://www.gelest.com*, visited: 2009.
179. R.C. Weast, Ed. Handbook of chemistry and physics, CRC press: BocaRaton, Florida, 1987-1988.
180. J.C. Hicks, C.W. Jones, Controlling the Density of Amine Sites on Silica Surfaces Using Benzyl Spacers, *Langmuir*, 22, **2006**, 2676.
181. M. Bass, V. Freger, Hydration of Nafion and Dowex in liquid and vapor environment: Schroeder's paradox and microstructure, *Polymer*, 49 (2), **2008**, 497.
182. C. Vallieres, D. Winkelmann, D. Roizard, et al., On Schroeder's Paradox, *J. Membr. Sci.*, 278 (1-2), **2006**, 357.
183. V. Ramani, Fuel Cells, *Electrochem. Soc. Interface*(spring), **2006**, 41.
184. V.S. Silva, J. Schirmer, R. Reissner, et al., Proton electrolyte membrane properties and direct methanol fuel cell performance; II. Fuel cell performance and membrane properties effects, *J. Power Sources*, 140, **2005**, 41.
185. R.K. Nagarale, G.S. Gohil, V.K. Shahi, Recent developments on ion-exchange membranes and electro-membrane processes, *Adv. Colloid Interface Sci.*, 119 (2-3), **2006**, 97.

Acknowledgement

The first contact between Thomas Schiestel and me arose at the end of 2005, because he had an available PhD position within the group '*Anorganische Grenzflächen und Membranen*'. Prof. Herwig Brunner gave me the opportunity to start my PhD thesis in March 2006. After the institute director change in 2007, Prof. Thomas Hirth took over the PhD supervision and I am very grateful for his interest, energy, scientific input and support. Additionally, I am honored, that Prof. Matthias Wessling managed to be my '*Zweitgutachter*'. Because of his membrane knowledge and activities, this is an added value to my promotion. And I want to thank Prof. Ulrich Nieken for being the chairman of the examination committee.

I owe Thomas Schiestel a lot of thanks for his motivation, guidance, creativity, trust, and critical eye. I am glad that we continue working together in the membrane field. Then, I want to thank my PhD colleagues, Marita Zipperle and Jessica Christel, for everything that good roomies do: supporting each other, discussing and having fun. During my studies, I became support from several *Diplom*-students, who made a direct or indirect contribution to this thesis. In chronological order: Nilesh Kothale, Christopher Hänel, Andreas Kampa, Johannes Radtke, Philipp Wursthorn. A special thanks goes out to Peter Holzhauer (2009, †) for constructing and builing setups, and sharing his *membrane* experiences with me. Furthermore, I want to thank my former and present colleagues: Annika, Chris, Christiane, Jenny, Mirjam and Tanja, and all the *Praktikanten & HIWI's*, with whom I had the pleasure to work together. I am grateful to the other colleagues of Fraunhofer IGB and Uni Stuttgart IGVT, for the motivating atmosphere, sharing (scientific) knowledge and experiences, and supporting the *flying dutchman* in Stuttgart.

In a project like this, it is impossible to do everything alone. Hereby, the persons are acknowledged (in random order) for their contribution to this thesis:

- Monika Riedl of Fraunhofer IGB: SEM investigations
- Mehdi Rathgeb of Fraunhofer IGB: GPC measurements
- Walter Vogt of Fraunhofer IGB: Setup construction and equipment building
- Melanie Dettling of Fraunhofer IGB and Malina Burcea of University of Stuttgart, IPOC: arranging and performing the NMR measurements
- Carsten Cremers and Florina Jung of Fraunhofer ICT: MEA preparation and DEFC measurements
- Julia Melke and Stefan Keller of Fraunhofer ISE: DEFC measurements
- Jutta Fink of Facility Services GmbH: TGA measurements
- Helmut W.E. Lüdemann, Labor für instrumentelle Analytik: WDXRF measurements

In addition, I want to thank all project partners of the Fraunhofer-team '*DEFC, the power of ethanol*' for their cooperation, discussions and social events.

A work like this can just be completed when everybody in the social environment is supporting you. Hereby, I thank all my Dutch and German friends for the good times, the distraction, and the most important thing: just being there for me.

My parents cannot be thanked enough for their never ending support and advice, anytime and in every way. To my dear family, and my brother, his wife and my nephew, Damon, in particular, thank you very much.

And last, but certainly not least, my dear Julia. Without your love, patience and support, this work was probably never finished. I am looking forward to new experiences and challenges with you, knowing that together we will manage everything! *Ich liebe dich!*

Kimball

Curriculum Vitae

Kimball Sebastiaan Roelofs was born on 21th of May 1978 in Zevenaar (the Netherlands). In July 1996, he received his VWO diploma from the Mozaïkcollege, division Thorbecke in Arnhem. Subsequently, he started his study Chemical Technology at the University of Twente in August. During his industrial training (2000/2001), he worked for four months at Membraflow Filtersysteme GmbH (Germany) on the development of ceramic membranes for pervaporation. He received his M.Sc. degree in January 2003. His Master thesis, completed at the Membrane Technology Group at the University of Twente, concerned module development for adsorption membranes used for downstream processing of fermentation processes. In 2003, he returned to Germany to work again for Membraflow Filtersysteme GmbH (since 01-10-2005 Westfalia Separator Membraflow GmbH, GEA Group). His main topics were the development and optimization of inorganic multiple layer systems for gas separation, nanofiltration and pervaporation. He started his PhD in March 2006 at the University of Stuttgart, Institute for Interfacial Engineering/Fraunhofer Institute for Interfacial Engineering and Biotechnology. His study on proton conductive mixed-matrix membranes for Direct Ethanol Fuel Cell applications is presented in this thesis.

List of Publications

K.S. Roelofs, B. Seling, H. Olapinski, Microporous Titania Membranes on Production Level, *Desalination*, 200(1-3), **2006**, 83.

T. Mathuraiveeran, K.S. Roelofs, D. Senftleben, T. Schiestel, Proton Conducting Composite Membranes with Low Ethanol Crossover for DEFC, *Desalination*, 200(1-3), **2006**, 662.

K.S. Roelofs, A. Kampa, T. Hirth, T. Schiestel, The Behavior of Sulfonated Poly(Ether Ether Ketone) in Ethanol-Water Systems, *J. Appl. Polym. Sci.*, 111(6), **2009**, 2998.

C. Cremers, F. Jung, B. Kintzel, K.S. Roelofs, T. Schiestel, J. Tübke, Development of Direct Ethanol Fuel Cell Membrane Electrode Assemblies Using Sulfonated Polyetheretherketone Mixed-Matrix Membranes, *ECS Trans.*, 25(1), **2009**, 1685.

K.S. Roelofs, T. Hirth, T. Schiestel, Sulfonated Poly(Ether Ether Ketone) Based Silica Nanocomposite Membranes for Direct Ethanol Fuel Cells, *J. Membr. Sci.*, 346(1), **2010**, 215.

K.S. Roelofs, T. Schiestel, SPEEK based Nanocomposites for Direct Ethanol Fuel Cell Applications, *Desalination*, 250(3), **2010**, 1051.

K.S. Roelofs, T. Hirth, T. Schiestel, Dihydrogenimidazole Modified Inorganic-Organic Mixed-Matrix Membranes for Direct Ethanol Fuel Cells, *J. Membr. Sci.*, submitted.

The decreasing availability of fossil fuels and the increasing impact of greenhouse gases on the environment lead to an extensive development of more efficient or renewable energy sources. The direct alcohol fuel cell (DAFC) as a portable energy source is a promising and fast growing technology which meets these demands. Up to now, methanol is mostly studied as a fuel for these devices, however, applying ethanol has some evident advantages over methanol. The major challenges in direct ethanol fuel cell (DEFC) research on component level are the catalyst development and the electrolyte membrane development.

The focus of this thesis lies on the development and characterization of proton conductive membranes for application in direct ethanol fuel cells (DEFC). Sulfonated poly(ether ether ketone) (sPEEK) based organic-inorganic mixed-matrix membranes are developed and, in addition, the inorganic phase is modified with functional silanes carrying basic groups. The membranes are characterized with respect to fuel crossover, proton conductivity, membrane stability and direct ethanol fuel cell tests.

ISBN 978-3-8396-0122-8

9 783839 601228